Basic Problems of Fibre-Reinforced Structural Components when Fibres Resist Bending

Ali Farag Farhat, MSc

Thesis submitted to The University of Nottingham

for the degree of Doctor of Philosophy

January 2013

Abstract

This thesis generates certain sets of analytical and approximate solutions to a new class of partial differential equations stemming from a version of asymmetric-stress elasticity theory appropriate for the study and prediction of the behaviour of fibre-reinforced materials containing fibres that resist bending. These new solutions are of theoretical and practical interest in the static and dynamic analysis of thin-walled, linearly elastic fibre-reinforced structures influenced by couple-stress and unsymmetric stress due to fibre bending stiffness. The static and free vibration solutions are constructed considering bending resistance fibres in a small deformation of beams and plates. Numerical results for displacements, stresses, couple-stress and natural frequencies of vibration are provided to investigate the influence of the fibres resistance in bending on the deformed beams and plates.

Acknowledgements

I would like to express my thanks and deep gratitude to my supervisor, Dr. Kostas Soldatos, for his patience, encouragement and useful advices during this research work. I would like also to thank Dr. Gareth Parry for his support in my first year. I would like to thank all my friends and colleagues in the school of Mathematical Sciences at the University of Nottingham.

I would also like to extend my thanks to Libyan government for offering me this scholarship and for their financial support during my study.

I would like to give my special thanks and acknowledgement to my mother for her love, forgiveness, prayer and support. I wish to thank my wife for her patience, help, prayer and support. My personal thanks are to my lovely sons, Mohmad and Ahmad, and pretty daughter, Fatema. I would like to thank my brothers, sisters and all relatives for their prayer and encouragement throughout my study.

Contents

Chapter 1. Introduction

1.1. Introduction

Fibre reinforced material have been used in many applications which require high strength-to-weight and stiffness-to-weight ratios. One of the applications of the composite materials is in aircraft and spacecraft which are typical weight-sensitive structures in which composite materials are cost-effective (Jones, 1998). The highly reinforced structures are being increasingly used in mechanical and civil engineering applications (Ye, 2003). Assuming that the fibres are perfectly flexible is a valid approximation in many cases of interest, but is not invariably applicable (Spencer and Soldatos, 2007). A version of asymmetric-stress elasticity, which takes into consideration that the fibres resist bending is presented by Spencer and Soldatos (2007) and developed for flat plate structure component by Soldatos (2009).

1.2. Literature review

Bending and vibration of beams and plates have been studied under considerations of two-dimensional theories and the three-dimensional symmetric elasticity theory. A review of different theories used for modelling multilayered composite plates is presented (Noor and Burton, 1989a). Reviews of refined shear deformation theories for isotropic and anisotropic laminated beams and plates were presented in (Ghugal and Shimpi, 2001, Ghugal and Shimpi, 2002), respectively. Three dimensional solutions were presented in the case of simply supported boundary conditions. The 3D elasticity solutions are difficult to obtain in the case of different boundary conditions. Therefore, several two-dimensional theories have been developed to produce accurate distributions of displacements, stresses

and frequencies. This section presents a related literature review to the present thesis and is divided into three subsections. The first subsection is for homogeneous isotropic beams and plates. Then, theories for laminated anisotropic beams and plates when fibres are perfectly flexible are reviewed in the second subsection. The third subsection is for laminated anisotropic beams and plates when fibres possess bending stiffness.

1.2.1. Homogeneous isotropic beams and plates

The Euler-Bernoulli beam theory is also called Euler beam theory, or Bernoulli beam theory, or classical beam theory or elementary theory of bending beams. Jacob Bernoulli (1654-1705) discovered that, at any point, the beam curvature is proportional to the bending moment (Han et al., 1999). Daniel Bernoulli (1700-1782) introduced the motion equation of vibrating beam (Han et al., 1999). The classical beam theory assumed that the plane sections which are normal to the neutral layer remain plane and normal to the deformed neutral layer meaning that the transverse shear and transverse normal strains are zero. The effect of the transverse shear deformation is disregarded in the Bernoulli-Euler elementary of beam bending. The classical plate theory which was developed by Kirchhoff in (Kirchhoff, 1850a, Kirchhoff, 1850b) is based on the hypothesis that straight lines normal to the undeformed middle surface are assumed to remain straight and normal to the deformed middle surface and do not undergo thickness stretching. The classical plate theory neglects the transverse shear deformation effect.

The effects of shear deformation and rotational inertia were taken into consideration in investigating transverse vibrations of prismatic bars by Stephen Timoshenko in (Timoshenko, 1921). Considering such effects, solution of transverse vibration of a beam of uniform cross section is presented in (Timoshenko, 1922).

The effect of transverse shear deformation was considered in studying the bending of elastic plates in (Reissner, 1945). It was observed there that important differences were noted between the results of such study and the results obtained by means of the classical plate theory. In the same manner that followed in Timoshenko's one-dimensional theory of bars, Mindlin includes the effects of rotatory inertia and shear deformation into a two-dimensional theory of flexural motions of isotropic elastic plates (Mindlin, 1951).

1.2.2. Laminated anisotropic beams and plates when fibres are perfectly flexible

The classical thin lamination theory is also called classical lamination plate theory or classical laminated theory. With the use of such theory, the complicated three-dimensional elasticity problems can be converted to two-dimensional problems of mechanics of elastic plates and one-dimensional problems of mechanics of elastic beams. Pister and Donng (1959) presented formulation of a system of equations governing the elastic bending of plates which consist two or more thin bounded layers. Study of bending and stretching of certain laminated plates which consist two orthotropic sheets is presented in (Reissner and Stavsky, 1961). The classical lamination theory is discussed in (Jones, 1975, Herakovich, 1997) where the reduced stiffnesses were used in the stress-strain relations. It was considered there that the laminate deformed according to the Kirchhoff hypothesis for plates and the Kirchhoff-Love Hypothesis for shells. As stated in (Jones, 1975), the derivations of the resultant forces and moments discussed there are in quite similar manner that in the classical work presented in (Pister and Dong, 1959, Reissner and Stavsky, 1961).

The exact symmetric elasticity solutions for flexure of composite laminates were in (Pagano, 1969). Pagano compared between numerical results based on this exact solution

and the corresponding results based on classical laminated plate theory solution. It was observed, there, that as the length to thickness ratio increases, the solutions obtained by the classical plate theory, for stresses and displacements converge to the exact linear elasticity solution. Moreover, for very thin structures, it was observed that the use of classical plate theory appears adequate. Pagano's exact symmetric elasticity solution, as pointed out in (Soldatos and Watson, 1997b), has been used extensively by several researchers to test the accuracy of many approximate plate theories (see, for instance, (Di Sciuva, 1986, Reddy, 1984, Lee et al., 1990, Soldatos, 1992a, Touratier, 1991, Lu and Liu, 1992, Di Sciuva, 1992, Cho and Parmerter, 1993, He et al., 1993, Liu et al., 1994, Lee et al., 1994, Li and Liu, 1995, Noor and Burton, 1989b, Savoia, 1995, Heuer, 1992)). This exact plane strain solution was extended by considering a laminate with finite boundaries constructing three-dimensional symmetric elasticity solution (Pagano, 1970a). Three further papers presented defining the exact response of composite laminates under static bending (Pagano, 1970b, Pagano and Wang, 1971, Pagano and Hatfield, 1972).

In (Srinivas et al., 1970), an exact three-dimensional linear, small deformation theory of elasticity solution is developed for the free vibration of simply-supported, homogeneous, isotropic, thick rectangular plates. Srinivas and Rao (1970) presented the three-dimensional, linear, small deformation theory of elasticity solution for the bending, vibration and buckling of simply supported thick orthotropic rectangular plates and laminates.

Different researches tried to improve accuracy of laminate beam and plate theories by assuming the form of transverse deformation through different types of functions (polynomials, trigonometric, hyperbolic, etc). A parabolic shear deformation beam theory were presented in (Levinson, 1981, Bickford, 1982). These theories satisfy the shear strain free boundary conditions at the top and bottom beam surfaces. Considering the parabolic

distribution of the transverse shear strains through the plate thickness, a higher-order shear deformation theory of laminated composite plates (HSDT) is developed in (Reddy, 1984). It was observed that the HSDT predicts the results of deflection and stresses more accurately than the aforementioned first-order theory (FSDT) (Reddy and Chao, 1981). Various laminated plate theories comparison were presented in (Idlbi et al., 1997). Those theories have proposed by Reissner, Reddy and Touratier in (Reissner, 1985), (Reddy, 1984) and (Touratier, 1991), respectively.

There are several parabolic, trigonometric and hyperbolic shear deformation beam and plate theories which exist in the literature (see, for instance Refs. (Krishna Murty, 1984, Shimpi and Ghugal, 2001, Ghugal and Sharma, 2009, Dahake and Ghugal, November 2012)). Taking into account the shear deformations, two unknown functions are involved in a plate theory for orthotropic plate analysis in (Shimpi and Patel, 2006). In such theory, bending and shear components were involved in the transverse displacement. This theory gives two uncoupled governing equations for static analysis, and inertially coupled for dynamic analysis. In addition to the use of a sinusoidal function in the in-plane displacement to include the shear deformation effect, the cosine function is used in transverse displacement to include the effect of transverse normal strain in (Ghugal and Sayyad, 2010).

All plate theories presented in (Yang et al., 1966, Whitney and Pagano, 1970, Bert, 1984, Bhimaraddi and Stevens, 1984, Reddy, 1984, Murty and Vellaichamy, 1987, Whitney and Sun, 1973, Nelson and Lorch, 1974, Lo et al., 1977, Valisetty and Rehfield, 1985, Mau, 1973, Srinivas, 1973) violate the interlaminar transverse stress continuity conditions (Soldatos, 1992b). In spite that these theories produce quite accurate predictions for transverse displacement and natural frequencies (global response characteristics of the plate), they generally do not produce accurate distributions of displacements and stresses

through the plate thickness (Soldatos, 1992b). A historical review of the Zig-Zag theories for multilayered plates and shells was presented in (Carrera, 2003). These theories are able to produce continuous distributions for displacement and transverse stress fields. In accordance with (Messina and Soldatos, 2002), the five degrees of freedom parabolic shear deformable theory (PSDPT) is developed with imposing the continuity of the transverse shear stresses at the interfaces in (Lee et al., 1990, Lee et al., 1993, Lee et al., 1994) . There are several models which appear in the literature and capable of satisfying continuity of transverse shear stresses (see, for instance Refs. (Pagano, 1970b, Soldatos, 1992b, Karama et al., 1998, Heuer, 1992, Messina and Soldatos, 2002, Soldatos and Watson, 1997b, Soldatos and Watson, 1997a, Chakrabarti and Sheikh, 2004, Singh et al., 2011)).

In (Noor and Burton, 1989a), solutions were obtained by six different modelling approaches that based on two-dimensional shear deformation theories and were compared with three-dimensional elasticity solutions presented in (Srinivas et al., 1970, Srinivas and Rao, 1970). According to (Noor and Burton, 1989a), obtaining accurate prediction of the displacements and stresses distribution through the plate thickness requires the use of three-dimensional equilibrium and constitutive relations. Two advanced plate theories have been proposed in (Soldatos and Watson, 1997b, Soldatos and Watson, 1997a) which have taken into consideration the use of three-dimensional equilibrium equations. Those plate theories are described below.

In the aforementioned two-dimensional plate theories which takes the transverse deformation effects into consideration, the shape of the shear deformation pattern is imposed by a very simple (shape) functions. In the study of the general five-degrees-of-freedom shear deformable plate theory (G5DOFPT) (Soldatos and Watson, 1997b), the equilibrium equations of three-dimensional elasticity have been used to specify general shape functions. For judging the accuracy of the method, it was applied to the solution of

the problem of cylindrical bending of simply supported elastic plate, for which the aforementioned exact elasticity solution is available in the literature (Pagano, 1969). In such study, a general three-degrees-of-freedom shear deformable beam theory (G3DOFBT) was considered as a particular one-dimensional version of (G5DOFPT). Furthermore, successful comparisons for numerical results of through-thickness displacement and stress distributions for a simply supported plate were provided. These comparisons were conducted between numerical results based on (G3DOFBT) and their counterparts based on the exact three-dimensional solution (Pagano, 1969). Moreover, stress analysis results for a two-layered plate subjected to different combination of edge boundary conditions were presented. It is worth mentioning that the exact solutions in the case of applying such different edge boundary conditions are difficult to obtain.

A general four-degrees-of-freedom beam theory (G4DOFBT) has been proposed in (Soldatos and Watson, 1997a). The difference between such theory and the G3DOFBT is that the effects of the transverse normal deformation were taken into consideration in G4DOFBT. In their study, two shape functions were involved in the assumption of the displacement field when each one of them is associated with one of the two unknown displacement components. The determination of such shape functions is based on the use of appropriate equations of three-dimensional elasticity which are presented in terms of the displacement field assumed and subsequently solved in the case of simply supported plate edges. The obtained choice of the shape functions allows the method to reproduce the exact elasticity numerical results (Pagano, 1969) for simply supported infinite strips. Therefore, it was pointed out in (Soldatos and Watson, 1997a) that there is no need to present numerical results for simply supported case. Furthermore, the theory were applied on different set of edges boundary conditions for homogeneous orthotropic and two-

layered plate when one of the edges is rigidly clamped and the other edge is either free of traction or guided.

1.2.3. Laminated anisotropic beams and plates when fibres possess bending stiffness

Although the assumption that the reinforcing fibres are perfectly flexible is a valid approximation in many cases, it is not invariable applicable (Spencer and Soldatos, 2007). The fibre bending stiffness was incorporated in a continuum theory in (Spencer and Soldatos, 2007) by assuming that the strain-energy depends on deformation, fibre direction and the gradient of the fibre direction. This leads to the theory that requires the inclusion of couple-stress and non-symmetric stress. Consequently, the theory possesses the ability to account for the size effect such as those due to fibre diameter or fibre spacing (Spencer and Soldatos, 2007). That finite elasticity theory (Spencer and Soldatos, 2007) produced, as a particular case, a version of asymmetric-stress linear elasticity theory which considers the resistance of fibres in bending effects (Soldatos, 2009). In addition, an attention has been paid to a variety of finite and infinite small elasticity problems when the fibres resist bending in (Soldatos, 2010b, Soldatos, 2010a, Dagher and Soldatos, 2011, Soldatos, 2012).

The problem of flexure of plate with a family of straight fibres resistant bending were described in (Soldatos, 2009) from the viewpoint of the linearised asymmetric-stress three dimension elasticity developed in (Spencer and Soldatos, 2007). The elastic plate was assumed to be subjected to small static or dynamic flexure. The boundary conditions and equations of motion of the asymmetric-stress elasticity theory have been proposed to be in the form that contains terms which include the anti-symmetric part of the shear stress components whom defined by the non-zero couple-stress. Furthermore, an additional elastic modulus (d^f), due to the fibre bending stiffness, has been involved in the equations

of motions. In addition, an advanced two dimensional thin-walled structures modelling has been produced taking into consideration the effects of the fibres resistance in bending. Moreover, an advanced version of classical plate theory has been proposed considering the assumption that the plates contain fibres which resist bending. Consequently, Additional terms, due to fibres stiffness, have been included in the motion equations of the advanced version of classical plate theory and the boundary conditions.

The most important references to the thesis work are the study of Spencer and Soldatos (2007) which presents the version of the asymmetric-stress elasticity and the study of Soldatos (2009) that developed the theory for the flat plate structure component. In addition, The other important reference to this work is study presented by Soldatos and Watson (1997a) which presented the G5DOFPT in the case of perfectly flexible fibres. For comparisons reason Pagano's plane strain solution (1969) and 3D elasticity solution presented by Srinivas. S and Rao, A. K (1970) is important to this work as well.

It is noted that attention should be paid to study the flexure and free vibration of fibre-reinforced beams and plates containing fibres which resist bending.

This thesis discusses these problems based on the analytical solution of relevant differential equations of asymmetric-stress theory of elasticity (Spencer and Soldatos, 2007, Soldatos, 2009). The problems are studied in the framework of the linear theory of elasticity. A summary with the problems investigated in this thesis is described in the next section.

1.3. Outline of the thesis

After the present introduction of the thesis, the main body of it is organised in four chapters. Each chapter begins with its own introduction and ends with a conclusion which

summarises the important observations and findings of the chapter. The thesis conclusion and future work are presented in the sixth chapter.

Chapter 2 presents an asymmetric-stress elasticity analysis for the plane strain statics and dynamics of a simply supported beam. The first step after the introduction of this chapter is the formulation of the problem where the plain strain version of the problem of plates with a family of straight fibres resistant to bending – 3D elasticity consideration (Soldatos, 2009) is described. Then, considering that the fibres resist bending, the equations of motion are given in terms of the displacement field presenting the Navier-type partial differential equations. The static and the free vibration solutions of the problem are discussed separately. Numerical results and discussion are provided for the static and dynamic solutions. In the numerical results section, it is shown that the obtained solution makes the plane strain symmetric elasticity solution (Pagano, 1969) a special case where the intrinsic length parameter l that due to the resistance of fibres in bending, takes value of zero. At the end of this chapter, a brief conclusion is provided and followed by the further work which shows the link of chapter 2 with chapters 3, 4, 5 and suggested future work.

Chapter 3 presents approximate solutions for small flexure and free vibration problem of beams subjected to different sets of end boundary conditions. The solutions are obtained on the basis of the one-dimensional version (G3DOFBT) of the advanced version of the approximate theory (G5DOFPT) developed in (Soldatos, 2009).The chapter follows the same notation to that described in chapter 2. Different sets of end boundary conditions are applied on the beam ends $x = 0, L_1$. The static and free vibrations solutions are obtained in the case when the fibres resist bending. The shape function when fibres resist bending is determined in similar manner to that discussed in the case of perfectly flexible fibres presented in (Soldatos and Watson, 1997b). The equilibrium equations of three-

dimensional asymmetric-stress elasticity (Soldatos, 2009) have been used to specify the shape function. Successful comparisons made between corresponding numerical results based on the advanced version of the general three-degrees-of-freedom shear deformable beam theory (Soldatos, 2009) and the exact solution found in the chapter 2. Further numerical results are provided for two-layered beams subjected to different boundary conditions based on the G3DOFBT solution. These boundary conditions are clamped-clamped (CC), clamped-free (CF) and clamped-simply (CS). The chapter is ended by a brief conclusion and further work that proposes the main aim of chapters 4 and 5.

Asymmetric-stress elasticity analysis for the three-dimensional statics and dynamics of a simply supported rectangular plate (SSSS) is considered in chapter 4. Taking into consideration the resistance of fibres in bending, the 3D static and dynamic elasticity solutions for small flexure and free vibration of a SSSS transversely isotropic elastic rectangular plate are found. This chapter provides successful comparisons between numerical results based on the obtained static and dynamic 3-D asymmetric-stress elasticity solutions (when the plate extends from $-\infty$ to $+\infty$ in the y direction) and their counterparts based on the plane strain asymmetric-stress elasticity solutions found in the chapter 2. Furthermore, an analysis of displacements, stresses distributions as well as the plate frequency values is conducted. Summary and the important findings are given in the conclusion, then, further work that illustrates the link of chapter 4 with chapters 5 and suggested future work.

Chapter 5 presents approximate solutions for flexure and free vibration problem of rectangular plate subjected to different sets of edge boundary conditions. The solutions are obtained on the basis of the advanced version of the approximate theory (G5DOFPT) developed in (Soldatos, 2009). The chapter follows the same notation to that described in chapter 4. Small flexure and dynamic solutions for a homogeneous rectangular plate

subjected to different sets of end boundary conditions (Levy-type solution) are found. The equilibrium equations of three-dimensional asymmetric-stress elasticity (Soldatos, 2009) have been used to specify the two shape functions. The new form of the shape functions obtained in this chapter and chapter 3 was explicitly dependent on the aforementioned material length parameter (l) that is related to the fibres bending stiffness; represented by the elastic modulus (d^f). Numerical results are provided for dimensionless transverse displacement, shear stresses, and fundamental frequency parameter for a homogeneous rectangular plate subjected to different sets of end boundary conditions. The final section of this chapter summarizes the discussion and brings attention to the important observations those have noted within the chapter.

Finally, chapter 6 provides a brief summary of the contributions presented in this thesis and directions for further work.

1.4. Statement of originality

This section describes the original work in the thesis. To the best of the author's knowledge the following described work has not been published by another author.

Asymmetric-stress linear elasticity solution for the plane strain statics and dynamics of a simply supported beam presented in the chapter 2 is original work. In addition, original work is presented in chapter 3 for solutions of small flexure and free vibration of transversely isotropic elastic beams subjected to different sets of end boundary conditions (SS, CS, CC and CF) when the beams contain fibres which resist bending. In the framework of the linear theory of elasticity, original work is presented in chapter 4 for asymmetric-stress elasticity analysis for the three-dimensional statics and dynamics of a simply supported rectangular plate. Considering that the fibres possess bending stiffness,

solutions for small flexure and free vibration of thin transversely isotropic rectangular homogeneous plate subjected to different sets of edge boundary conditions (SSSS, SSCC and SSCF) are constructed. This work is presented in chapter 5 and is original. Furthermore, all the numerical results provided in chapters 2, 3, 4 and 5 when fibres resist bending are new in the literature and original as well.

Chapter 2. Asymmetric-stress elasticity analysis for the plane strain statics and dynamics of a simply supported beam

2.1. Introduction

In this chapter, plane strain solutions of small flexure and free vibration of transversely isotropic elastic cross-ply laminated beam will be discussed. The considered beam contains fibres resist bending. The discussion is based on the analytical solution of relevant plane strain differential equations of asymmetric-stress elasticity theory (Spencer and Soldatos, 2007, Soldatos, 2009). The main purpose of this chapter is to solve the static and dynamic problem of transversely isotropic elastic cross-ply laminated beam and to investigate the effect of the fibres resistance in bending on the deformed beam. This investigation is made by analysing displacements, stresses, couple-stress distributions as well as the beam frequency values computed for various values of a non-dimensional parameter related to the resistance of fibres in bending.

2.2. Problem formulation

Consider a transversely isotropic, linearly elastic cross-ply laminated plate having arbitrary constant thickness h in the z direction and, horizontal constant length L_1 in the x direction. The plate is assumed to be of infinite extent in the y direction. Consider further that the plate contains fibres which are lying in parallel to the x-direction and resist bending. Moreover, the plate is assumed to be simply supported on the ends x=0 and $x = L_1$. In the static

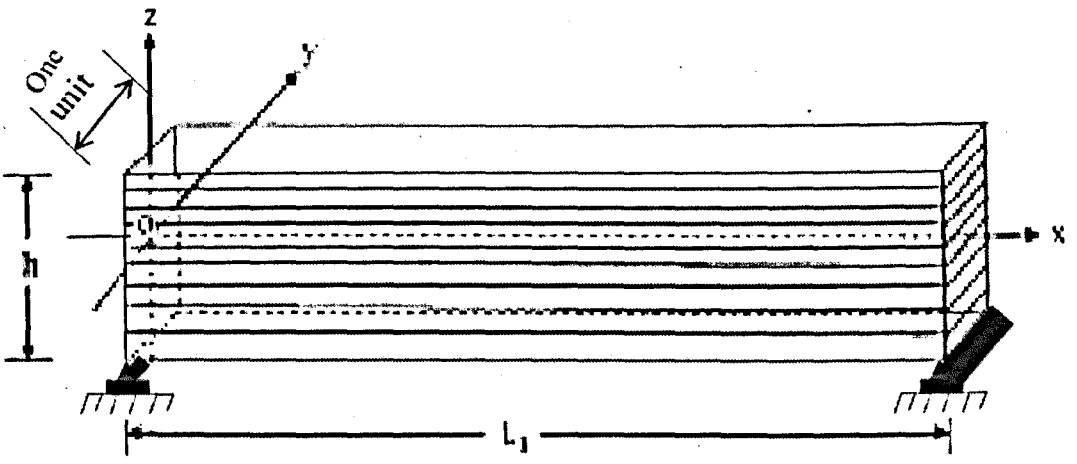

Figure 2.1 Co-ordinate system

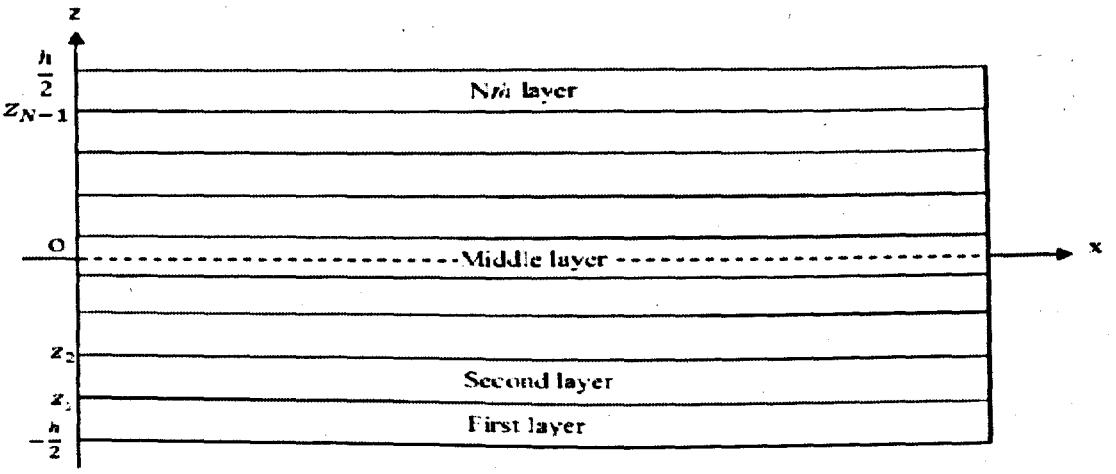

Figure 2.2 An example of the beam layer numbering

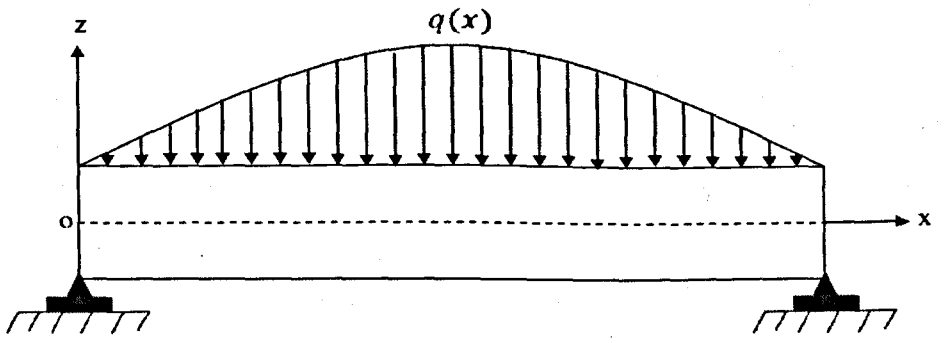

Figure 2.3 Lateral loading

The beam is subjected to small static flexure caused by the action of a given external lateral loading $q(x)$ (see Figure 2.3) or to free vibration. Due to the plane-strain symmetries involved in this problem, all quantities involved are independent of y and the displacement function in y direction is equal to zero. It can be considered that any of the plate cross-sections could alternatively be regarded as a transversely isotropic beam of thickness h, length L_1 and a unit width along the y-direction (see Figure 2.1). The standard infinitesimal strain tensor components are as follows:

$$e_{xx} = U_{,x}\,,\; e_{zz} = W_{,z}\,,\; 2e_{xz} = U_{,z} + W_{,x}, \tag{2.1}$$

where here as well as in what follows, a comma denotes partial differentiation with respect to variable(s) denoted by the associated index(ices). In addition, U and W represent the displacement functions in x and z directions, respectively.

Assume, now that the beam is composed of an arbitrary number, N, of transversely isotropic layers. For identifying the layers of the beam, an index (k) is introduced, where the bottom layer corresponds to $k = 1$ (see Figure 2.2). The symmetric part of the stress tensor in each layer is described by the form of generalized Hooke's law in the case of transversely isotropic material having the axis of transverse isotropic parallel to fibres direction. Consequently, the symmetric part of the stress tensor for each layer takes the following form (Soldatos, 2009):

$$\begin{bmatrix} \sigma_x^{(k)} \\ \sigma_z^{(k)} \\ \tau_{(xz)}^{(k)} \end{bmatrix} = \begin{bmatrix} C_{11}^{(k)} & C_{13}^{(k)} & 0 \\ C_{13}^{(k)} & C_{33}^{(k)} & 0 \\ 0 & 0 & C_{55}^{(k)} \end{bmatrix} \begin{bmatrix} e_x^{(k)} \\ e_z^{(k)} \\ 2e_{xz}^{(k)} \end{bmatrix}, \tag{2.2}$$

where $C_{ij}^{(k)}$ represent the four independent transverse isotropic elastic modules of the kth layer.

In the case when fibres resist bending, the elasticity theory requires to include the couple-stress and consequently asymmetric-stress (Spencer and Soldatos, 2007). The anti-symmetric part of the associated shear stress tensor component is denoted by symbol with indices in square brackets. This part is defined as follows:

$$\tau_{[xz]}^{(k)} = \frac{1}{2} m_{xy,x}^{(k)}, \tag{2.3}$$

where $m_{xy}^{(k)}$ represents the non-zero couple stress which is related to the fibre curvature as follows, (Soldatos, 2009):

$$m_{xy}^{(k)} = d^{f(k)} K_z^{f(k)} = -\frac{1}{2} d^{f(k)} W_{,xx}^{(k)}. \tag{2.4}$$

Here $K_z^{f(k)}$ represents the fibre curvature. It should be mentioned that the couple-stress has dimension of moment. Moreover, $d^{f(k)}$ is an elastic modulus that accounts for the fibre bending stiffness in the k-th layer. This elastic modulus has dimension of force (Soldatos, 2009). In this regard and, in order to perform an appropriate comparison between the methods in this thesis, the following notation:

$$d^{f(k)} = \frac{1}{12} C_{11} l^{(k)} L_1, \tag{2.5}$$

is employed to include a material intrinsic length parameter $l^{(k)}$, which may, for instance, be considered related to the thickness of the fibre in the k-th layer (see equation A1.3 in Appendix1).

Thus, the shear stresses take the following form:

$$\tau_{xz}^{(k)} = \tau_{(xz)}^{(k)} + \tau_{[xz]}^{(k)}, \tag{2.6.a}$$

$$\tau_{zx}^{(k)} = \tau_{(xz)}^{(k)} - \tau_{[xz]}^{(k)}, \tag{2.6.b}$$

The equations of motion (Soldatos, 2009) take the following form:

$$\sigma_{x,x}^{(k)} + \tau_{(xz),z}^{(k)} - \tau_{[xz],z}^{(k)} = \rho \ddot{U}^{(k)}, \tag{2.7.a}$$

$$\tau_{(xz),x}^{(k)} + \tau_{[xz],x}^{(k)} + \sigma_{z,z}^{(k)} = \rho \ddot{W}^{(k)}. \tag{2.7.b}$$

Here, a dot denotes partial differentiation with respect to time and ρ denotes the material density. It is worth mentioning that when the couple-stress takes zero value, the shear stresses in (2.6) and the equations of motion (2.7) reduce to their perfectly flexible fibres counterparts that are met in symmetric linear elasticity theory.

The lateral boundary conditions are assumed as follows:

$$\sigma_z\left(x, \frac{h}{2}\right) = q(x), \ \sigma_z\left(x, -\frac{h}{2}\right) = 0, \tag{2.8.a}$$

$$\tau_{zx}\left(x, \frac{h}{2}\right) = 0, \ \tau_{zx}\left(x, -\frac{h}{2}\right) = 0, \tag{2.8.b}$$

where $q(x)$ is the external lateral loading which acts normally and downwards on the top lateral plane of the beam (see figure 2.2). Such loading can be expressed in the following Fourier series:

$$q(x) = \sum_{m=1}^{\infty} q_m \sin(Mx) \ \ M = m\pi/L_1, \quad (m = 1, 2, \ldots). \tag{2.9}$$

In addition, the boundary conditions for simply supported ends are described as follows:

$$\sigma_x(0, z) = 0, \sigma_x(L_1, z) = 0, \tag{2.10.a}$$

$$W(0, z) = 0, W(L_1, z) = 0, \tag{2.10.b}$$

$$m_{xy}(0,\ z) = 0,\ m_{xy}(L_1,\ z) = 0. \tag{2.10.c}$$

Furthermore, the conditions of traction and displacement continuity at the kth material interface, $z = z_k$, of the laminate are as follows ($k = 1, \ldots, N-1$):

$$\sigma_z{}^{(k)}\big|_{z=z_k} = \sigma_z{}^{(k+1)}\big|_{z=z_k}, \tag{2.11.a}$$

$$(\tau^{(k)}{}_{(xz)} - \tau^{(k)}{}_{[xz]})\Big|_{z=z_k} = (\tau^{(k+1)}{}_{(xz)} - \tau^{(k+1)}{}_{[xz]})\Big|_{z=z_k}, \tag{2.11.b}$$

$$U^{(k)}(x,z)\big|_{z=z_k} = U^{(k+1)}(x,z)\big|_{z=z_k}, \tag{2.11.c}$$

$$W^{(k)}(x,z)\big|_{z=z_k} = W^{(k+1)}(x,z)\big|_{z=z_k}. \tag{2.11.d}$$

2.3. Navier-type partial differential equations

With the use of equations (2.1-6), the equations of motion (2.7) can be written in terms of displacements to form the following Navier-type equations:

$$C_{11}^{(k)}U_{,xx}^{(k)} + \left(C_{13}^{(k)} + C_{55}^{(k)}\right)W_{,xz}^{(k)} + C_{55}^{(k)}U_{,zz}^{(k)} + \frac{hL_1C_{11}^{(k)}}{24}\lambda^{(k)}W_{,xxxz}^{(k)} = \rho\ddot{U}^{(k)}, \tag{2.12.a}$$

$$C_{55}^{(k)}W_{,xx}^{(k)} + \left(C_{13}^{(k)} + C_{55}^{(k)}\right)U_{,xz}^{(k)} + C_{33}^{(k)}W_{,zz}^{(k)} - \frac{hL_1C_{11}^{(k)}}{24}\lambda^{(k)}W_{,xxxx}^{(k)} = \rho\ddot{W}^{(k)}, \tag{2.12.b}$$

where

$$0 \le x \le L_1,\ -\frac{h}{2} \le z \le \frac{h}{2},\ \ \lambda^{(k)} = \frac{l^{(k)}}{h}. \tag{2.13}$$

These can be re-arranged in the following matrix form:

$$\boldsymbol{A}.\boldsymbol{X} = \boldsymbol{J} \tag{2.14}$$

where

$$\boldsymbol{A} = \begin{bmatrix} C_{11}^{(k)} \frac{\partial^2}{\partial x^2} + C_{55}^{(k)} \frac{\partial^2}{\partial z^2} & \left(C_{13}^{(k)} + C_{55}^{(k)}\right) \frac{\partial^2}{\partial x \partial z} + \frac{hL_1 C_{11}^{(k)}}{24} \lambda^{(k)} \frac{\partial^4}{\partial x^3 \partial z} \\ \left(C_{13}^{(k)} + C_{55}^{(k)}\right) \frac{\partial^2}{\partial x \partial z} & C_{55}^{(k)} \frac{\partial^2}{\partial x^2} + C_{33}^{(k)} \frac{\partial^2}{\partial z^2} - \frac{hL_1 C_{11}^{(k)}}{24} \lambda^{(k)} \frac{\partial^4}{\partial x^4} \end{bmatrix}, \quad (2.15.a)$$

$$\boldsymbol{X} = [U^{(k)} \quad W^{(k)}]^T, \boldsymbol{J} = [\rho \ddot{U} \quad \rho \ddot{W}]^T, \quad (2.15.b)$$

and are admit of an exact solution, provided that the beam ends are subjected to the set of six simply supported boundary conditions (2.10).

2.4. Solution of the static problem

For the flexure problem of the described simply supported (SS) beam, the inertia terms appearing in the right-hand sides of equations (2.7), (2.12) and (2.14) are disregarded to yield:

$$\boldsymbol{A}.\boldsymbol{X} = 0. \quad (2.16)$$

The set of SS end boundary conditions (2.10) is satisfied by choosing the displacement field in the following form of trigonometric series:

$$U^{(k)} = h \sum_{m=1}^{\infty} \phi^{(k)}(Z) \cos(m\pi X), \quad (2.17.a)$$

$$W^{(k)} = h \sum_{m=1}^{\infty} \chi^{(k)}(Z) \sin(m\pi X). \quad (2.17.b)$$

Here, $X = \frac{x}{L_1}$, $Z = \frac{z}{h}$ and, therefore,

$$0 \leq X \leq 1, -\frac{1}{2} \leq Z \leq \frac{1}{2}. \quad (2.18)$$

For each m, the substitution of equations (2.17) in equations (2.16) converts them to the following set of ordinary differential equations:

$$G(D)\,.\,\boldsymbol{B} = 0, \tag{2.19}$$

where

$$G(D) = \begin{bmatrix} d_1^{(k)} + d_2^{(k)} D^2 & d_4^{(k)} D + d_{11}^{(k)} D \\ -d_4^{(k)} D & d_8^{(k)} + d_9^{(k)} D^2 + d_{12}^{(k)} \end{bmatrix}, \quad \boldsymbol{B} = \begin{bmatrix} \phi^{(k)}(Z) \\ \chi^{(k)}(Z) \end{bmatrix}, \tag{2.20}$$

and

$$D = \frac{d}{dZ}, \; d_1^{(k)} = -h^2 M^2, \; d_2^{(k)} = C_{55}^{(k)} / C_{11}^{(k)}, \tag{2.21.a}$$

$$d_4^{(k)} = h\,M\,(C_{13}^{(k)} + C_{55}^{(k)})\,/C_{11}^{(k)}, \; d_8^{(k)} = -(C_{55}^{(k)}\,h^2 M^2)/C_{11}^{(k)}, \tag{2.21.b}$$

$$d_9^{(k)} = C_{33}^{(k)} / C_{11}^{(k)}, \; d_{11}^{(k)} = -\frac{h}{24}\,M^3\,l^{(k)}\,L_1, \; d_{12}^{(k)} = -\frac{h^2}{24}\,M^4\,l^{(k)}\,L_1. \tag{2.21.c}$$

The additional terms $d_{11}^{(k)}$ and $d_{12}^{(k)}$ are due to the presence of the fiber bending stiffness those depend on the additional intrinsic parameter $l^{(k)}$ which has dimension of length and is assumed to represent the fibers thickness. and For a non-trivial solution of equation (2.19), the determinant of **G** must be zero. This condition yields the following characteristic equation:

$$det\,(\boldsymbol{G}(p)) = 0 \tag{2.22}$$

i.e.

$$d_2^{(k)} d_9^{(k)}\,p^4 + \left(d_1^{(k)} d_9^{(k)} + d_2^{(k)} d_8^{(k)} + d_2^{(k)} d_{12}^{(k)} + {d_4^{(k)}}^2 + d_4^{(k)} d_{11}^{(k)}\right) p^2 + d_1^{(k)}(d_8^{(k)} +$$

$$d_{12}^{(k)}) = 0, \tag{2.23}$$

Solution of (2.23) gives four characteristic values $p_i^{(k)} (i = 1,..,4)$. The eigenvector corresponding to a non-repeated root $p = p_i^{(k)}$ is:

$$\begin{bmatrix}\phi_i^{(k)}(Z)\\ \chi_i^{(k)}(Z)\end{bmatrix} = \begin{bmatrix}\left(d_4^{(k)} + d_{11}^{(k)}\right) p_i^{(k)}\\ -(d_1^{(k)} + d_2^{(k)} {p_i^{(k)}}^2)\end{bmatrix} A\, e^{p_i^{(k)} Z} \tag{2.24}$$

where A is an arbitrary constant. Hence, the expression of $\phi^{(k)}$ and $\chi^{(k)}$ can be given in the following form:

$$\begin{bmatrix}\phi^{(k)}(Z)\\ \chi^{(k)}(Z)\end{bmatrix} = \sum_{i=1}^{4} A_i^{(k)} \begin{bmatrix}\left(d_4^{(k)} + d_{11}^{(k)}\right) p_i^{(k)}\\ -(d_1^{(k)} + d_2^{(k)} {p_i^{(k)}}^2)\end{bmatrix} e^{p_i^{(k)} Z}, \tag{2.25}$$

i.e.

$$\phi^{(k)} = \sum_{i=1}^{4} A_i^{(k)} p_i^{(k)} h \left(M \frac{C_{13}^k + C_{55}^k}{C_{11}^k} - \frac{1}{24} l^{(k)} L_1 M^3 \right) e^{p_i^{(k)} Z}, \tag{2.26.a}$$

$$\chi^{(k)} = \sum_{i=1}^{4} A_i^{(k)} \left(h^2 M^2 - \left(\frac{C_{55}^k}{C_{11}^k}\right) {p_i^{(k)}}^2 \right) e^{p_i^{(k)} Z}, \tag{2.26.b}$$

where $A_i^{(k)}$ $(i = 1,2,3,4\,;\ k = 1, \ldots N)$ are $4N$ arbitrary constants. These will be determined in subsection 2.4.1 in similar way described (Soldatos, 2003). The only difference here is considering the additional terms due to the fiber bending stiffness.

The use of equations (2.17) and (2.26) yields the following expression of the displacement field of the present static problem:

$$U^{(K)} = h \sum_{m=1}^{\infty} \sum_{i=1}^{4} h\, A_i^{(k)} p_i^{(k)} cos(m\pi X) \left(M \frac{C_{13}^k + C_{55}^k}{C_{11}^k} - \frac{l^{(k)}}{24} L_1 M^3 \right) e^{p_i^{(k)} Z}, \tag{2.27.a}$$

$$W^{(k)} = h \sum_{m=1}^{\infty} \sum_{i=1}^{4} A_i^{(k)}\, sin(m\pi X) \left(h^2 M^2 - \left(\frac{C_{55}^k}{C_{11}^k}\right) {p_i^{(k)}}^2 \right) e^{p_i^{(k)} Z}. \tag{2.27.b}$$

The influence of the presence of the fiber bending stiffness on the displacement field (2.27) appears obvious in equation (2.27.a) which depend on the additional length intrinsic

parameter $l^{(k)}$. As a result of that, the stresses distributions will be affected by the presence of the fiber bending stiffness.

2.4.1. Expressions for Stresses, couple-stress and interface continuity conditions

The substitution of the displacement field obtained into (2.2) yields the following normal stress and the symmetric part of the shear stresses:

$$\sigma_x^{(k)} = h \sum_{m=1}^{\infty} \left(-C_{11}^{(k)} M \phi^{(k)}(Z) + C_{13}^{(k)} \frac{1}{h} D \chi^{(k)}(Z) \right) sin(m\pi X), \qquad (2.28.a)$$

$$\sigma_z^{(k)} = h \sum_{m=1}^{\infty} \left(-C_{13}^{(k)} M \phi^{(k)}(Z) + C_{33}^{(k)} \frac{1}{h} D \chi^{(k)}(Z) \right) sin(m\pi X), \qquad (2.28.b)$$

$$\tau_{(xz)}^{(k)} = h \sum_{m=1}^{\infty} \left(C_{55}^{(k)} \left(\frac{1}{h} D \phi^{(k)}(Z) + M \chi^{(k)}(Z) \right) \right) cos\ (m\pi X). \qquad (2.28.c)$$

Furthermore, the couple-stress and the anti-symmetric part of the shear stress are expressed, respectively, as follows:

$$m_{xy}^{(k)} = \frac{h\, l^{(k)}\, L_1}{12} C_{11}^{(k)} \sum_{m=1}^{\infty} M^2 \chi^{(k)}(Z) \sin(m\pi X), \qquad (2.29.a)$$

$$\tau_{[xz]}^{(k)} = \frac{h\, l^{(k)}\, L_1}{24} C_{11}^{(k)} \sum_{m=1}^{\infty} M^3 \chi^{(k)}(Z) \cos\ (m\pi X). \qquad (2.29.b)$$

The use of equations (2.28.c) and (2.29.b) yields unequal shear stresses $\tau_{xz}^{(k)}$ and $\tau_{zx}^{(k)}$ as shown below

$$\tau_{xz}^{(k)} = h\sum_{m=1}^{\infty}\left(C_{55}^{(k)}(\frac{1}{h}D\phi^{(k)} + M\chi^{(k)}) - \frac{C_{11}^{(k)}l^{(k)}L_1}{24}M^3\chi^{(k)}\right)cos(m\pi X), \qquad (2.30.a)$$

$$\tau_{zx}^{(k)} = h\sum_{m=1}^{\infty}\left(C_{55}^{(k)}(\frac{1}{h}\mathrm{D}\phi^{(k)} + \mathrm{M}\chi^{(k)}) + \frac{C_{11}^{(k)}l^{(k)}\mathrm{L}_1}{24}\mathrm{M}^3\chi^{(k)}\right)\cos(m\pi X). \qquad (2.30.\mathrm{b})$$

The difference between the two shear stresses $\tau_{xz}^{(k)}$ and $\tau_{zx}^{(k)}$ is caused by the non-zero anti-symmetric part of the shear stress, $\tau_{[xz]}^{(k)}$. It is evident that when $l^{(k)} = 0$, the couple-stress and the related anti-symmetric part of the shear stress shown in equations (2.29) will take zero value. In that case, in which the fibres are assumed perfectly flexible, the shear stresses presented in equation (2.30) become equal.

The determination of the $4N$ arbitrary constants which appear in equations (2.27) requires a same number of algebraic equations to solve. The number of 4(N-1) of these equations can be obtained from applying the continuity conditions (2.11) at (N-1) material interfaces of the laminated beam considered. Using equations (2.27), (2.28.b) and (2.30.a) and requiring satisfaction of those continuity conditions at the kth material interface, $z = z_k$, yields, for $(k = 1, \dots, N-1)$, the following set of 4(N-1) algebraic equations:

$$-C_{13}^{(k)}\,M\,\phi^{(k)}\left(\frac{z_k}{h}\right) + C_{33}^{(k)}\frac{1}{h}\,\chi^{(k)'}\left(\frac{z_k}{h}\right) + C_{13}^{(k+1)}\,M\,\phi^{(k+1)}\left(\frac{z_k}{h}\right) -$$

$$C_{33}^{(k+1)}\,\frac{1}{h}\,\chi^{(k+1)'}\left(\frac{z_k}{h}\right) = 0, \qquad (2.31.a)$$

$$C_{55}^{(k)}(\frac{1}{h}\phi^{(k)'}\left(\frac{z_k}{h}\right) + M\chi^{(k)}\left(\frac{z_k}{h}\right)) - \frac{C_{11}^{(k)}\,l^{(k)}\,L_1}{24}\,M^3\chi^{(k)}\left(\frac{z_k}{h}\right) - C_{55}^{(k+1)}(\frac{1}{h}\,\phi^{(k+1)'}\left(\frac{z_k}{h}\right)$$

$$-M\,\chi^{(k+1)}\left(\frac{z_k}{h}\right)) + C_{11}^{(k+1)}\,\frac{l^{(k+1)}\,L_1}{24}\,M^3\chi^{(k+1)}\left(\frac{z_k}{h}\right) = 0, \qquad (2.31-b)$$

$$\phi^{(k)}\left(\frac{z_k}{h}\right) - \phi^{(k+1)}\left(\frac{z_k}{h}\right) = 0, \qquad (2.31-c)$$

$$\chi^{(k)}\left(\frac{z_k}{h}\right) - \chi^{(k+1)}\left(\frac{z_k}{h}\right) = 0. \qquad (2.31-d)$$

The remaining four equations are obtained by using the stress lateral surface boundary conditions (2.8) at the upper and lower surfaces of the beam where $z = \pm h/2$.

2.5. Solution for free vibration

The present section describes the plane strain asymmetric-stress elasticity solution of free vibration of simply supported transversely isotropic beams. That solution is obtained by solving the Navier asymmetric-stress elasticity equations (2.14), the right hand-side of which contains non-zero inertia terms. It can easily be verified that the following choice of the displacement field:

$$U^{(k)} = h\sum_{m=1}^{\infty} \phi^{(k)}(Z)cos(m\pi X)\, cos(\omega t), \qquad (2.32.a)$$

$$W^{(k)} = h\sum_{m=1}^{\infty} \chi^{(k)}(Z)\, sin\,(m\pi X)\, cos(\omega t), \qquad (2.32.b)$$

satisfies exactly the set of six end boundary conditions (2.10). Here ω represents an unknown natural frequency of vibration.

Consequently, with use of the displacement field (2.32), the sixth-order set of simultaneous partial differential equations (2.14) is converted into the following sixth-order set of simultaneous homogeneous ordinary differential equations:

$$\widehat{\boldsymbol{G}}(D)\,.\boldsymbol{B} = 0, \qquad (2.33)$$

where

$$\widehat{G}(D) = \begin{bmatrix} d_1^{(k)} + d_2^{(k)} D^2 + \left(\frac{C_{55}^{(1)}}{C_{11}^{(k)}}\right)\omega^{*2} & \left(d_4^{(k)} + d_{11}^{(k)}\right) D \\ -d_4^{(k)} D & d_8^{(k)} + d_9^{(k)} D^2 + d_{12}^{(k)} + \left(\frac{C_{55}^{(1)}}{C_{11}^{(k)}}\right)\omega^{*2} \end{bmatrix}, \quad (2.34)$$

in which ω^* represent the following dimensionless frequency parameter:

$$\omega^* = \omega h \sqrt{\frac{\rho}{C_{55}^{(1)}}}. \quad (2.35)$$

A non-trivial solution of the homogeneous equation (2.33) requires the determinant of the (2 x 2) matrix $\widehat{\mathbf{G}}(\hat{p})$ to be zero, namely:

$$det(\widehat{\mathbf{G}}(\hat{p})) = 0 \quad (2.36)$$

i.e.

$$d_2^{(k)} d_9^{(k)} \hat{p}^4 + \left(d_1^{(k)} + \left(\frac{C_{55}^{(1)}}{C_{11}^{(k)}}\right)\omega^{*2}\right) d_9^{(k)} \hat{p}^2 + d_2^{(k)} \left(d_8^{(k)} + \left(\frac{C_{55}^{(1)}}{C_{11}^{(k)}}\right)\omega^{*2}\right) \hat{p}^2 + d_2^{(k)} d_{12}^{(k)} \hat{p}^2 +$$

$$\left(d_4^{(k)2} + d_4^{(k)} d_{11}^{(k)}\right) \hat{p}^2 + \left(d_1^{(k)} + \left(\frac{C_{55}^{(1)}}{C_{11}^{(k)}}\right)\omega^{*2}\right)\left(d_8^{(k)} + \left(\frac{C_{55}^{(1)}}{C_{11}^{(k)}}\right)\omega^{*2} + d_{12}^{(k)}\right) = 0. \quad (2.37)$$

This yields 4N eigenvalues, $\left(\hat{p}_i^{(k)}(\omega^*),\ i = 1,..,4,\ k = 1,..,N\right)$, which depend also on the, as yet unknown, parameter ω^*. The eigenvector corresponding to a non-repeated root $\hat{p} = \hat{p}_i^{(k)}$ is as follows:

$$\begin{bmatrix} \phi_i^{(k)}(Z) \\ \chi_i^{(k)}(Z) \end{bmatrix} = \begin{bmatrix} \left(d_4^{(k)} + d_{11}^{(k)}\right) \hat{p}_i^{(k)} \\ -\left(\left(d_1^{(k)} + \left(\frac{C_{55}^{(1)}}{C_{11}^{(k)}}\right)\omega^{*2}\right) + d_2^{(k)} \hat{p}_i^{(k)2}\right) \end{bmatrix} C\, e^{\hat{p}_i^{(k)} Z}, \quad (2.38)$$

where C is an arbitrary constant. The solution of equation (2.33) which is depending on ω^* has the following form:

$$\begin{bmatrix}\phi^{(k)}(Z)\\ \chi^{(k)}(Z)\end{bmatrix}=\sum_{i=1}^{4}C_i^{(k)}\begin{bmatrix}\left(d_4^{(k)}+d_{11}^{(k)}\right)\hat{p}_i^{(k)}\\ -(d_1^{(k)}+(C_{55}^{(1)}/C_{11}^{(k)})\omega^{*2})+d_2^{(k)}\hat{p}_i^{(k)2})\end{bmatrix}e^{\hat{p}_i^{(k)}z}. \qquad (2.39)$$

Substitution of equations (2.21) and (2.39) into equation (2.32) yields the following expression of the displacement field.

$$U^{(K)}=h\sum_{m=1}^{\infty}\sum_{i=1}^{4}C_i^{(k)}\hat{p}_i^{(k)}h\cos(m\pi X)\cos\left(\frac{\omega^*}{h}\sqrt{\frac{C_{55}^{(1)}}{\rho}}t\right)(M\frac{C_{13}^{(k)}+C_{55}^{(k)}}{C_{11}^{(k)}}$$

$$-\frac{l^{(k)}L_1}{24}M^3)e^{\hat{p}_i^{(k)}z}, \qquad (2.40.a)$$

$$W^{(K)}=h\sum_{m=1}^{\infty}\sum_{i=1}^{4}C_i^{(k)}\sin(m\pi X)\cos\left(\frac{\omega^*}{h}\sqrt{\frac{C_{55}^{(1)}}{\rho}}t\right)(h^2M^2-\left(\frac{C_{55}^{(1)}}{C_{11}^{(k)}}\right)\omega^{*2}-$$

$$\left(\frac{C_{55}^{k}}{C_{11}^{k}}\right)\hat{p}_i^{(k)2})\,e^{\hat{p}_i^{(k)}z}. \qquad (2.40.b)$$

The main reason of considering the non-repeated roots of equation (2.37) is that the material is anisotropic namely the elastic coefficients $C_{ij}^{(k)}$ have different values. In addition, if the roots are repeated or some of them are, other calculations need to be done to construct the displacement field.

2.5.1. Determination of the frequency parameter

In this problem, the lateral surfaces are stress free and therefore the loading function $q(x)=0$. Satisfaction of the lateral surface conditions (2.8) and the continuity conditions (2.11) yields 4k algebraic simultaneous homogeneous equations which can be written in the matrix form as follows:

$$\boldsymbol{H}(\omega^*).\boldsymbol{S} = 0. \tag{2.41}$$

Here, **S** is a (1 x 4N) matrix which contains the arbitrary constants $C_i^{(k)}$; (i=1, .., 4& k=1, .., N) and $\mathbf{H}(\omega^*)$ is a (4N x 4N) matrix depends on ω^*. For a non-trivial solution of the homogeneous equations (2.41), the determinant of the matrix $\mathbf{H}(\omega^*)$ must be zero yielding an algebraic equation for ω^*. A solution of that algebraic equation produces an infinite number of frequencies.

As an example of a relatively simple form of equation (2.41), the particular case of a homogeneous beam (N = 1) is considered. In this case and for a single harmonic m, the (4 x 4) and (1 x 4) matrixes which appear in that equation will take the following forms:

$$\boldsymbol{H}(\omega^*) = \begin{bmatrix} h_{11} & h_{12} & h_{13} & h_{14} \\ h_{21} & h_{22} & h_{23} & h_{24} \\ h_{31} & h_{32} & h_{33} & h_{34} \\ h_{31} & h_{32} & h_{33} & h_{34} \end{bmatrix}, \quad \boldsymbol{S} = \begin{bmatrix} C_1 \\ C_2 \\ C_3 \\ C_4 \end{bmatrix}, \tag{2.42}$$

where

$$h_{1i} = -C_{13} M\, h\, \mu_i\, e^{\frac{\hat{p}_i}{2}} + C_{33}\, \eta_i(\omega^*)\, \hat{p}_i\, e^{\frac{\hat{p}_i}{2}},$$

$$h_{2i} = -C_{13} M\, h\, \mu_i\, e^{-\frac{\hat{p}_i}{2}} + C_{33}\, \eta_i\,(\omega^*)\, \hat{p}_i\, e^{-\frac{\hat{p}_i}{2}},$$

$$h_{3i} = C_{55}\, \mu_i\, \hat{p}_i\, e^{\frac{\hat{p}_i}{2}} + \left(C_{55}\, h\, M - \frac{h}{24}\, l\, L_1 C_{11} M^3 \right) \eta_i\,(\omega^*)\, e^{\frac{\hat{p}_i}{2}}, \tag{2.43}$$

$$h_{4i} = C_{55}\, \mu_i\, \hat{p}_i\, e^{-\frac{\hat{p}_i}{2}} + \left(C_{55}\, h\, M - \frac{h}{24}\, l\, L_1 C_{11} M^3 \right) \eta_i\,(\omega^*)\, e^{-\frac{\hat{p}_i}{2}},$$

$$\mu_i = \hat{p}_i\, h \left(\frac{M(C_{13} + C_{55})}{C_{11}} - \frac{1}{24} l^{(k)}\, L_1 M^3 \right),$$

$$\eta_i\,(\omega^*) = \left(h^2\, M^2 - \left(\frac{C_{55}}{C_{11}} \right) \omega^{*2} - \left(\frac{C_{55}}{C_{11}} \right) \hat{p}_i{}^2 \right),$$

and the four eigenvalues $\hat{p}_i$ are obtained by solving equation (2.36) for N=1. The only unknown in the matrix $\mathbf{H}(\omega^*)$ shown in (2.41) is therefore the dimensionless frequency parameter ω^*. For a non-trivial solution of the problem the determination of $\mathbf{H}(\omega^*)$ must be zero and this yields the following equation:

$$det\big(\boldsymbol{H}(\omega^*)\big) = 0. \tag{2.45}$$

Solution of this equation yields an infinite sequence of roots. In the numerical results provided, the following *plot procedure,* in Maple software, is used for plotting the curve of det(**H**). Such curve cuts ω^* axis at the roots value which greater than x_1 and less than x_2.

$$> \text{plot(Determinant(H}, \omega^* = x_1..x_2); \tag{2.46}$$

Similar procedures to what employed in this example can be followed in the case of N > 1.

2.6. Numerical results and discussion

In this section, numerical results based on the outlined exact asymmetric-stress liner elasticity solutions of the statics and dynamics of a SS laminated beam are presented. Three examples are provided to investigate the influence of the resistance of fibres in bending by giving various values of the non-dimensional parameter λ. The first and second examples are for the static solution. Then, the third example will be for the dynamic solution.

Example 1

In the numerical results of the static problem, the material of the beam is assumed to be transversely isotropic and the layer material is characterized by the following properties (Soldatos and Watson, 1997b):

$$E_L/E_T = 40, \quad G_{LT}/E_T = 0.5, \quad G_{TT}/E_T = 0.2, \quad v_{LT} = v_{TT} = 0.25. \tag{2.47}$$

Here, the subscript L signifies the longitudinal fibres direction, T denotes the transverse fibre direction, and v_{LT} stands of the Poisson ratio that measure strain in the transverse direction T under uniaxial normal stress in the L-direction.

Here and in what follows, m=1 so expression (2.9) becomes:

$$q = q_1 \sin\left(\frac{\pi}{L_1}x\right). \tag{2.48}$$

For presentation of numerical results, the normalised quantities employed are defined as follows:

$$Z = z/h\,, \; X = x/L_1, \; \bar{W} = E_T W/L_1 q_1, \; \bar{U} = E_T U/L_1 q_1,$$
$$\bar{\tau}_{xz} = \tau_{xz}/q_1\,, \; \bar{\tau}_{zx} = \tau_{zx}/q_1\,, \; \bar{m}_{xy} = m_{xy}/L_1^3 q_1. \tag{2.49}$$

Numerical results for these non-dimensional displacements, stresses and the couple-stress for the flexure of thick homogeneous (single-layered) beams ($h/L_1 = 0.25$) are presented. It should be noted that because of the symmetries of the problem in the x-direction, displacement, stresses and couple-stress at $\frac{x}{L_1}$ and $1 - \frac{x}{L_1}$ have identical through-thickness distribution. Therefore, most of the results are presented for the left half of the beam.

Table 2.1 compares numerical values of normalised in-plane displacement obtained on the basis of the present static asymmetric-stress elasticity solution at different values of λ. The numerical values are computed at selected, equally spaced points throughout the thickness of a homogeneous simply supported transversely isotropic beam. It is observed that the in-plane displacement values at λ=0 are identical to their counterparts obtained on

the basis of the exact elasticity solution (Pagano, 1969) and provided in (Soldatos and Watson, 1997b). In addition, with increasing the value of λ, the value of in-plane displacement is decreasing; it becomes very small and approaches the zero value quickly.

It is observed that the magnitude of the in-plane displacement at the bottom surface in the case of perfectly flexible fibers is less that at the top surface. The difference between the magnitude of the in-plane displacement at the top and bottom surfaces decreases gradually with increasing the value of λ approaching a slight difference when $\lambda = 0.08$. In addition, there is a slight difference at $\lambda = 0.1$ where the magnitude of the in-plane displacement at the top surface in the case of perfectly flexible fibers is less that at the bottom surface. Furthermore, the in-plane displacement at $\lambda = 0.1$ becomes very small.

Table 2.1 Through-thickness in-plane displacement distributions for a SS homogeneous thick beam ($h/L_1 = 0.25$)

z/h	$\frac{E_T}{L_1 q_1} U(0,z)$, $\lambda = 0$	$\frac{E_T}{L_1 q_1} U(0,z)$, $\lambda = 0.02$	$\frac{E_T}{L_1 q_1} U(0,z)$, $\lambda = 0.04$	$\frac{E_T}{L_1 q_1} U(0,z)$, $\lambda = 0.06$	$\frac{E_T}{L_1 q_1} U(0,z)$, $\lambda = 0.08$	$\frac{E_T}{L_1 q_1} U(0,z)$, $\lambda = 0.1$
0.5	0.129524	0.083646	0.054515	0.034255	0.019264	0.007658
0.4	0.061373	0.039008	0.024896	0.015157	0.008012	0.002535
0.3	0.027746	0.017071	0.010413	0.005883	0.002614	0.000155
0.2	0.011110	0.006301	0.003371	0.001435	0.000088	-0.000882
0.1	0.002564	0.000849	-0.000127	-0.000713	-0.001071	-0.001283
0	-0.002681	-0.002420	-0.002164	-0.001912	-0.001664	-0.001421
-0.1	-0.007731	-0.005530	-0.004075	-0.003018	-0.002198	-0.001532
-0.2	-0.015588	-0.010414	-0.007127	-0.004838	-0.003144	-0.001831
-0.3	-0.030677	-0.019909	-0.013160	-0.008538	-0.005179	-0.002631
-0.4	-0.061091	-0.039190	-0.025534	-0.016242	-0.009538	-0.004493
-0.5	-0.122702	-0.078408	-0.050836	-0.032113	-0.018637	-0.008524

Table 2.2 Through-thickness deflection distributions for a SS homogeneous thick beam ($h/L_1 = 0.25$)

z/h	$\frac{E_T}{L_1 q_1} W\left(\frac{L_1}{2}, z\right)$, $\lambda = 0$	$\frac{E_T}{L_1 q_1} W\left(\frac{L_1}{2}, z\right)$, $\lambda = 0.02$	$\frac{E_T}{L_1 q_1} W\left(\frac{L_1}{2}, z\right)$, $\lambda = 0.04$	$\frac{E_T}{L_1 q_1} W\left(\frac{L_1}{2}, z\right)$, $\lambda = 0.06$	$\frac{E_T}{L_1 q_1} W\left(\frac{L_1}{2}, z\right)$, $\lambda = 0.08$	$\frac{E_T}{L_1 q_1} W\left(\frac{L_1}{2}, z\right)$, $\lambda = 0.1$
0.5	-1.209112	-0.949804	-0.786821	-0.674846	-0.593135	-0.530850
0.4	-1.188321	-0.928539	-0.765266	-0.653096	-0.571248	-0.508863
0.3	-1.167960	-0.908435	-0.745349	-0.633330	-0.551609	-0.489337
0.2	-1.149490	-0.890423	-0.727660	-0.615893	-0.534380	-0.472289
0.1	-1.133595	-0.874927	-0.712455	-0.600920	-0.519605	-0.457687
0	-1.120566	-0.862117	-0.699822	-0.588442	-0.507268	-0.445482
-0.1	-1.110468	-0.852018	-0.689761	-0.578436	-0.497329	-0.435617
-0.2	-1.103195	-0.844549	-0.682201	-0.570841	-0.489731	-0.428035
-0.3	-1.098430	-0.839497	-0.676994	-0.565548	-0.484392	-0.422676
-0.4	-1.095495	-0.836420	-0.673843	-0.562359	-0.481186	-0.419467
-0.5	-1.093010	-0.834433	-0.672170	-0.560904	-0.479891	-0.418294

Table 2.2 shows values of normalised deflection obtained on the basis of the present static asymmetric-stress elasticity solution at different values of λ. Those are computed again at selected, equally spaced points within the considered beam. It is seen that the values of the deflection at λ=0 are identical to their counterparts met in the symmetric elasticity and provided in (Soldatos and Watson, 1997b). It is of particular importance to note that the deflection of the beam decreases with increasing values of λ. This emphasises the expectation that as the fibre bending stiffness increases, the beam becomes stiffer.

Figure 2.4 displays the through thickness shear stress distributions $\bar{\tau}_{zx}$ at the left beam end for different values of λ. The lateral boundary conditions at the upper and lower surfaces (2.8), in terms of the shear stress τ_{zx}, are satisfied exactly. The shear stress $\bar{\tau}_{zx}$ values are affected by the presence of the resistance of fibres in bending. This effect can be

observed evidently by comparing the case of stiff fibres presented by red, blue and green lines with the black line presenting the case of perfectly flexible fibres. The absolute value of the shear stress $\bar{\tau}_{zx}$ is decreasing and approaching the value of zero with increasing the values of λ.

Figure 2.5 illustrates the through thickness shear stress distributions $\bar{\tau}_{xz}$ at the left beam end for different values of λ. The only shear stress distribution that obeys the lateral boundary conditions is at $\lambda = 0$. Figures 2.4 and 2.5 show that shear stresses $\bar{\tau}_{zx}$ and $\bar{\tau}_{xz}$ distributions are identical in the case of perfectly flexible fibres. In contrast, when the fibres possess bending stiffness, the non-dimensional shear stresses $\bar{\tau}_{zx}$ and $\bar{\tau}_{xz}$ distribution are unequal.

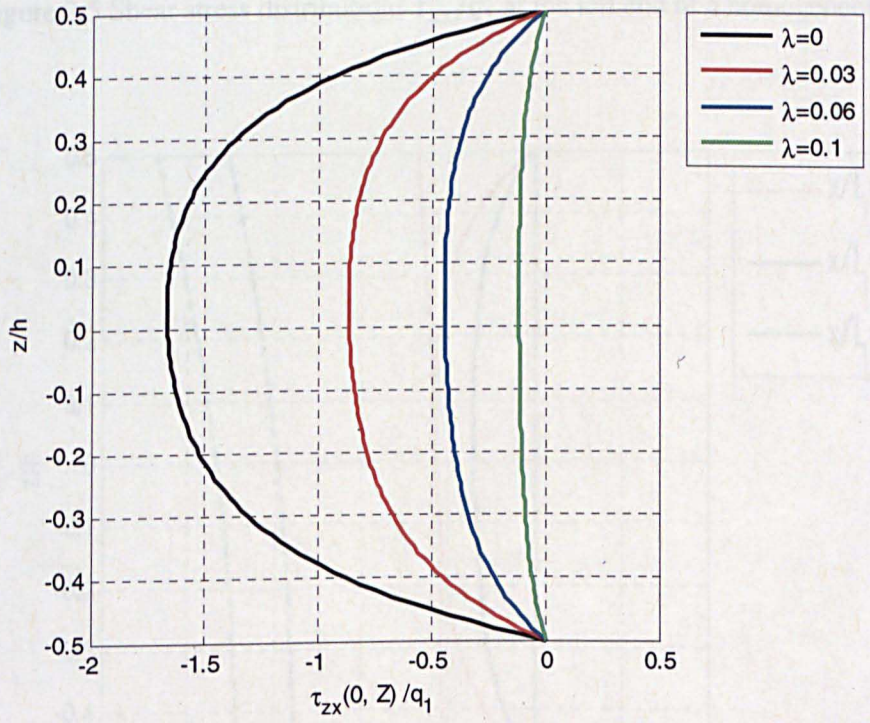

Figure 2.4 Shear stress distributions τ_{zx}/q_1 at the left end of a homogeneous beam

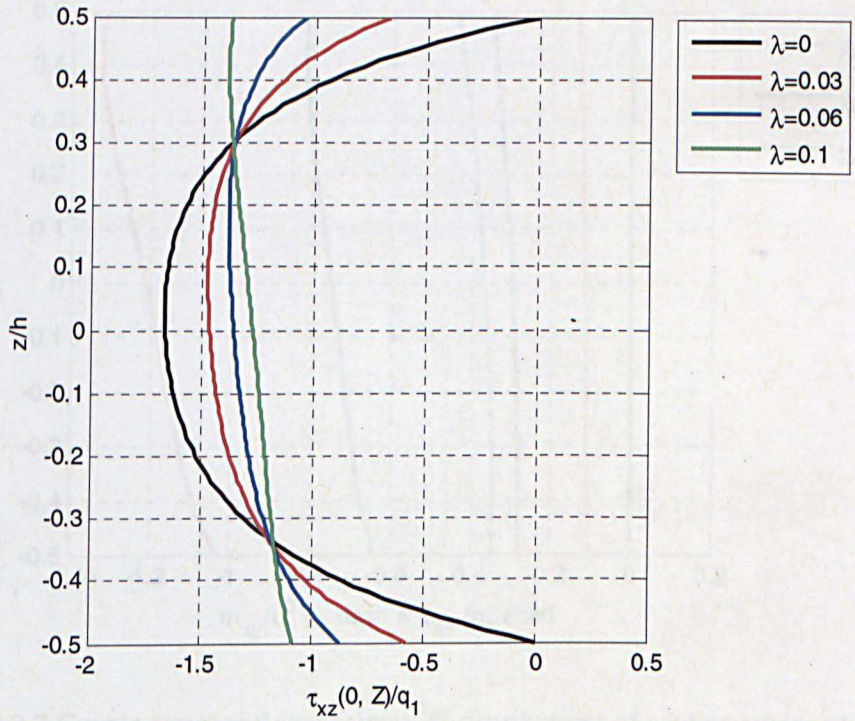

Figure 2.5 Shear stress distributions τ_{xz}/q_1 at the left end of a homogeneous beam

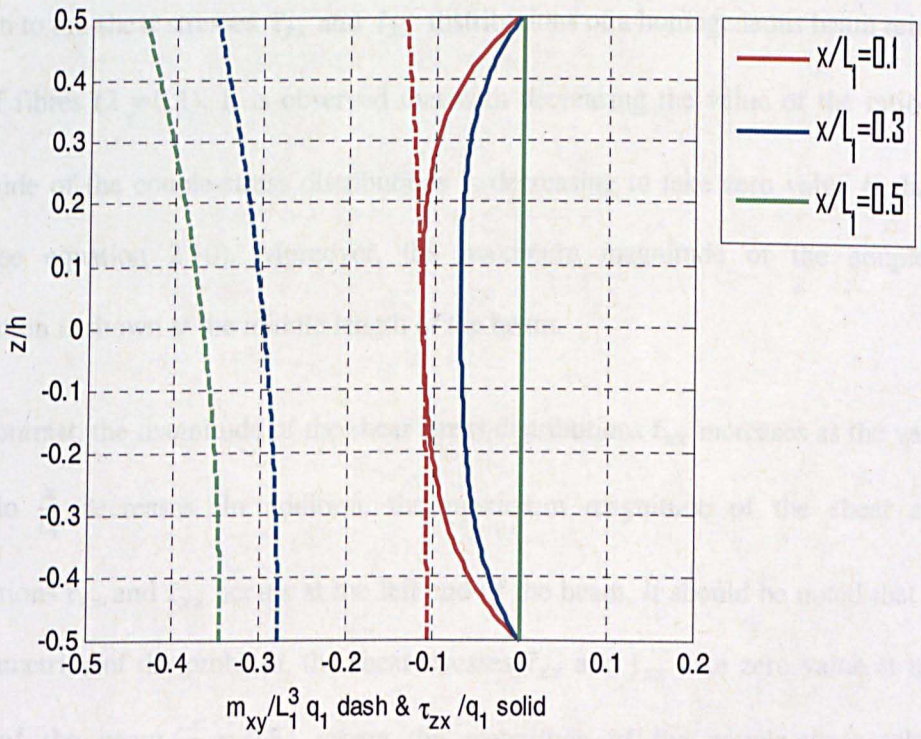

Figure 2.6 Couple-stress and shear stress $\frac{\tau_{zx}}{q_1}$ distributions of a homogeneous beam (λ=0.1)

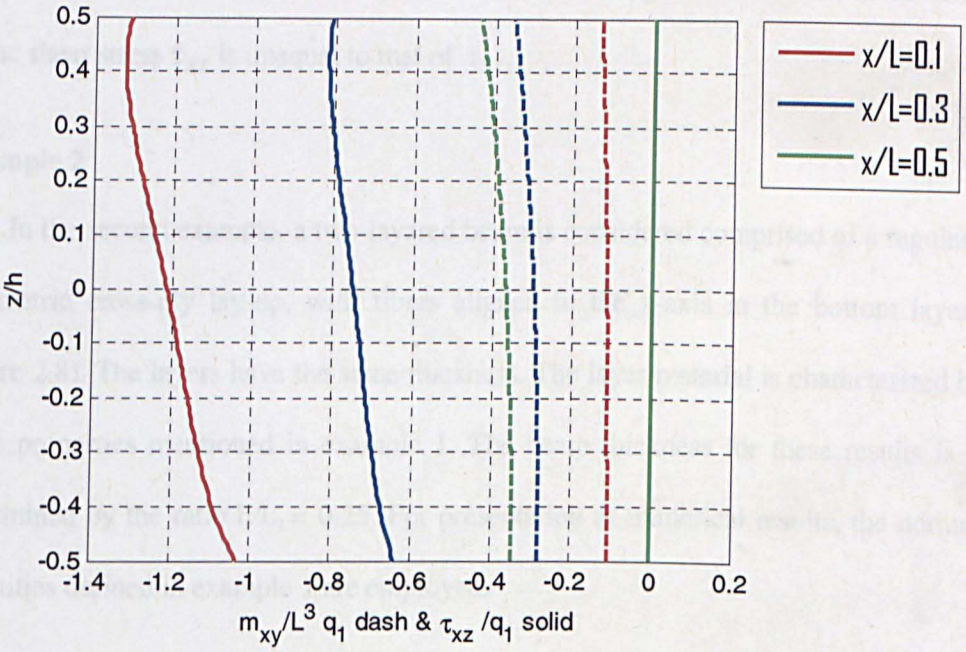

Figure 2.7 Couple-stress and shear stress $\frac{\tau_{xz}}{q_1}$ distributions of a homogeneous beam (λ=0.1)

Figures 2.6 and 2.7 present the through thickness couple-stress $\bar{m}_{xy}$ distributions in addition to the shear stresses $\bar{\tau}_{zx}$ and $\bar{\tau}_{xz}$ distributions of a homogeneous beam reinforced by stiff fibres (λ =0.1). It is observed that with decreasing the value of the ratio $\frac{x}{L_1}$, the magnitude of the couple-stress distributions is decreasing to take zero value at the beam end (see equation 2.10). Moreover, the maximum magnitude of the couple-stress distribution is shown at the middle length of the beam.

In contrast, the magnitude of the shear stress distributions $\bar{\tau}_{zx}$ increases as the values of the ratio $\frac{x}{L_1}$ decreases. In addition, the maximum magnitude of the shear stresses distributions $\bar{\tau}_{zx}$ and $\bar{\tau}_{xz}$ occurs at the left end of the beam. It should be noted that due to the symmetries of the problem, the shear stresses $\bar{\tau}_{zx}$ and $\bar{\tau}_{xz}$ take zero value at middle-length of the beam ($\frac{x}{L_1} = 0.5$) where the magnitude of the couple-stress takes the

maximum value. Furthermore, away from the middle-length of the beam, the distribution of the shear stress $\bar{\tau}_{xz}$ is unequal to that of $\bar{\tau}_{zx}$.

Example 2

In the second example, a two-layered beam is considered comprised of a regular anti-symmetric cross-ply lay-up, with fibres aligned to the x-axis in the bottom layer (see Figure 2.8). The layers have the same thickness. The layer material is characterized by the same properties mentioned in example 1. The beam thickness for these results is again determined by the ratio $h/L_1 = 0.25$. For presentation of numerical results, the normalised quantities defined in example 1 are employed.

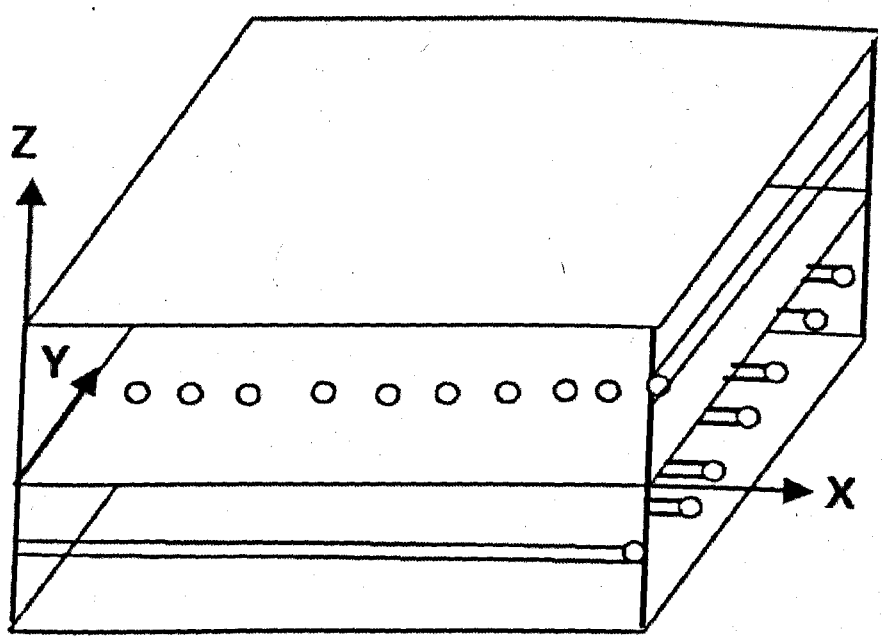

Figure 2.8 Orientation of laminations

Table 2.3 compares numerical values of normalised in-plane displacement, for two-layered beam, obtained on the basis of the present static asymmetric-stress elasticity solution at different values of λ. As previously the numerical values of the in-plane displacement at $\lambda = 0$ are identical with those obtained on the basis of exact symmetric elasticity solution and presented in (Soldatos and Watson, 1997b). It is observed that with

increasing the value of λ, the in-plane displacement value becomes smaller. In the case of λ=0.1, displacement takes very small values through the thickness of the bottom layer which is highly reinforced by stiff fibres in the x-direction.

Table 2.4 shows numerical values for the transverse displacement of a SS two-layered beam. The values of the through thickness deflection are obtained on the basis of the present asymmetric-stress elasticity solution. It should be observed that with increasing the values of λ, the beam becomes stiffer and the deflection decreases. This means that with increasing the fibre bending stiffness, the effect of the beam thickness on bending increases. The deflection values at λ=0 are again identical to the exact elasticity results presented in (Soldatos and Watson, 1997b). This emphasises that the exact elasticity solution (Pagano, 1969) is a special case of the present solution.

Table 2.3 Through-thickness in-plane displacement distributions for a SS two-layered thick beam ($h/L_1 = 0.25$)

z/h	$\frac{E_T U(0,z)}{L_1 q_1}$ at $\lambda = 0$	$\frac{E_T U(0,z)}{L_1 q_1}$ at $\lambda = .02$	$\frac{E_T U(0,z)}{L_1 q_1}$ at $\lambda = .04$	$\frac{E_T U(0,z)}{L_1 q_1}$ at $\lambda = .06$	$\frac{E_T U(0,z)}{L_1 q_1}$ at $\lambda = .08$	$\frac{E_T U(0,z)}{L_1 q_1}$ at $\lambda = 0.1$
0.5	0.961585	0.662964	0.498748	0.394872	0.323247	0.270876
0.4	0.768186	0.522300	0.387085	0.301554	0.242579	0.199458
0.3	0.601651	0.401268	0.291065	0.221350	0.173273	0.138115
0.2	0.456973	0.296223	0.207795	0.151838	0.113235	0.084992
0.1	0.329727	0.203950	0.134725	0.090889	0.060623	0.038458
0	0.215960	0.121581	0.069580	0.036605	0.013799	-0.002935
-0	0.215960	0.121581	0.069580	0.036605	0.013799	-0.002935
-0.1	0.092731	0.051221	0.028427	0.014034	0.004132	-0.003090
-0.2	0.0192490	0.009186	0.003715	0.000306	-0.002001	-0.003651
-0.3	-0.042803	-0.02666	-0.017740	-0.012064	-0.008121	-0.005214
-0.4	-0.125938	-0.075297	-0.047462	-0.029866	-0.017743	-0.008887
-0.5	-0.273368	-0.162206	-0.101178	-0.062657	-0.036164	-0.016852

Table 2.4 Through-thickness deflection distributions for a SS two-layered thick beam ($h/L_1 = 0.25$)

z/h	$\frac{E_T W(\frac{L_1}{2},z)}{L_1 q_1}$ at $\lambda = 0$	$\frac{E_T W(\frac{L_1}{2},z)}{L_1 q_1}$ at $\lambda = .02$	$\frac{E_T W(\frac{L_1}{2},z)}{L_1 q_1}$ at $\lambda = .04$	$\frac{E_T W(\frac{L_1}{2},z)}{L_1 q_1}$ at $\lambda = .06$	$\frac{E_T W(\frac{L_1}{2},z)}{L_1 q_1}$ at $\lambda = .08$	$\frac{E_T W(\frac{L_1}{2},z)}{L_1 q_1}$ at $\lambda = 0.1$
0.5	-2.656908	-1.933037	-1.534902	-1.283004	-1.109264	-0.982184
0.4	-2.650673	-1.921418	-1.520323	-1.266553	-1.091522	-0.963499
0.3	-2.641306	-1.907540	-1.503965	-1.248627	-1.072516	-0.943704
0.2	-2.629634	-1.891999	-1.486296	-1.229614	-1.052577	-0.923088
0.1	-2.616320	-1.875271	-1.467692	-1.209824	-1.031969	-0.901883
0	-2.601880	-1.857728	-1.448442	-1.189494	-1.010894	-0.880263
-0	-2.601880	-1.857728	-1.448442	-1.189494	-1.010894	-0.880263
-0.1	-2.587638	-1.841196	-1.430658	-1.170923	-0.991785	-0.860764
-0.2	-2.575068	-1.827545	-1.416427	-1.156336	-0.976964	-0.845781
-0.3	-2.565937	-1.81774	-1.406274	-1.145972	-0.966465	-0.835191
-0.4	-2.559933	-1.811568	-1.400012	-1.139666	-0.960134	-0.828849
-0.5	-2.554524	-1.807489	-1.396668	-1.136788	-0.957580	-0.826532

Table 2.4 shows numerical values for the transverse displacement of a SS two-layered beam. The values of the through thickness deflection are obtained on the basis of the present asymmetric-stress elasticity solution. It should be observed that with increasing the values of λ, the beam becomes stiffer and the deflection decreases. This means that with increasing the fibre bending stiffness, the effect of the beam thickness on bending increases. The deflection values at λ=0 are again identical to the exact elasticity results presented in (Soldatos and Watson, 1997b). This emphasises that the exact elasticity solution (Pagano, 1969) is a special case of the present solution.

Figures 2.9-12 present the distribution of the shear stresses $\bar{\tau}_{zx}$, $\bar{\tau}_{xz}$, which are an important indicator to the onset of delamination. Figure 2.9 illustrates the shear stress distributions $\bar{\tau}_{zx}$ at the left end of the two-layered beam at different values of λ. In the case of perfectly flexible fibres, a significant difference is found between the shear stress

$\bar{\tau}_{zx}$ distributions through the thickness of the top layer and that in the bottom layer. This difference decreases gradually with increasing the values of λ. The maximum value of the shear stress $\bar{\tau}_{zx}$ appears in the case of perfectly flexible fibres and it was near to the middle thickness of the bottom layer, whereas in the case of stiff fibres (λ=0.1), it appears near to the middle-plane of the beam. Furthermore, through the thickness of the beam, the absolute value of the shear stress $\bar{\tau}_{zx}$ decreases with increasing the value of λ.

Furthermore, it is observed in Figure 2.9 that the magnitude of the shear stress $\bar{\tau}_{zx}$ through the thickness of the top layer is less than that in the bottom layer. The reason of that is that the bottom layer is highly reinforced in the x-direction. Moreover, the shear stress $\bar{\tau}_{zx}$ is decreasing with increasing the value of λ and largest value of this bending parameter is associated with the most symmetrical profile. This is caused by subtracting the value of the anti-symmetric part of the shear stress from the symmetric part of it (see 2.6.b).

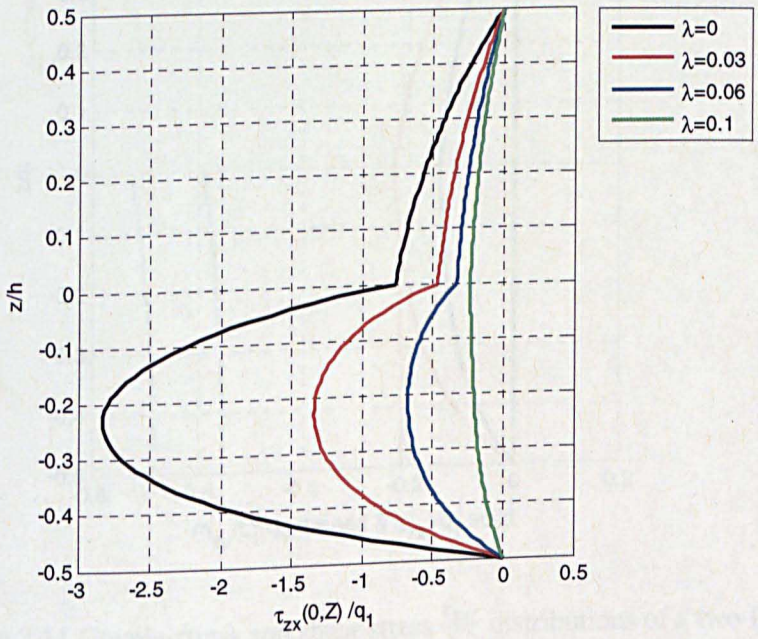

Figure 2.9 Shear stress distributions τ_{zx}/q_1 at the left end of a two-layered beam

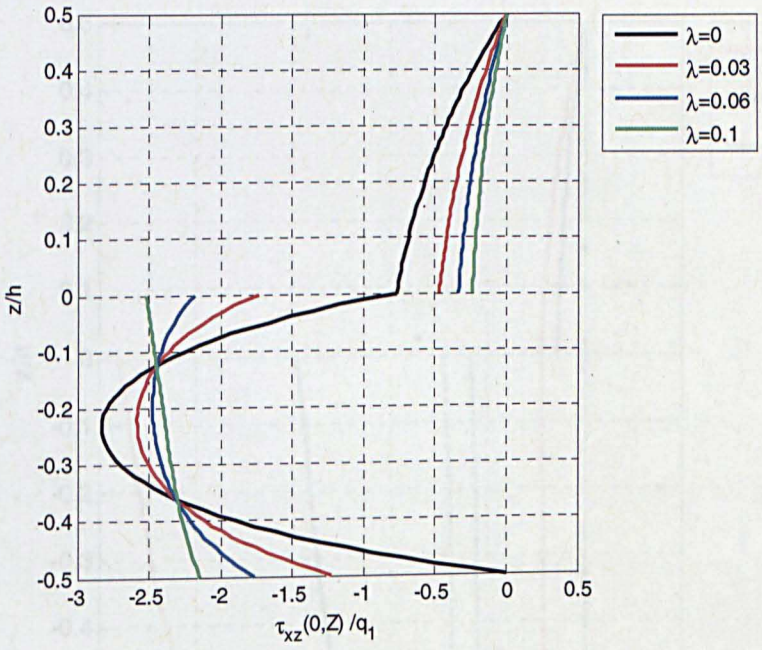

Figure 2.10 Shear stress distributions τ_{xz}/q_1 at the left end of a two-layered beam

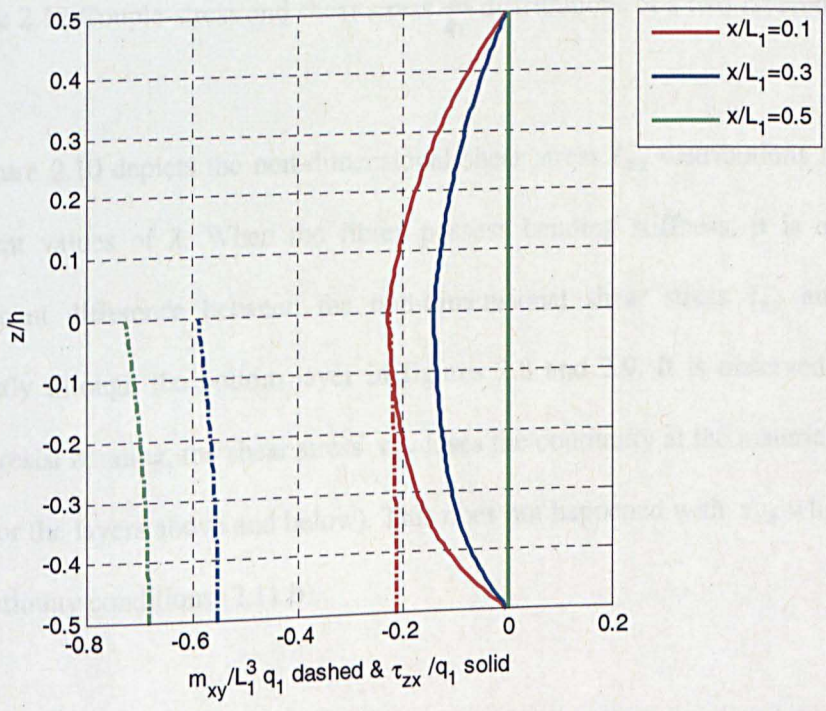

Figure 2.11 Couple-stress and shear stress $\frac{\tau_{zx}}{q_1}$ distributions of a two-layered beam (λ=0.1)

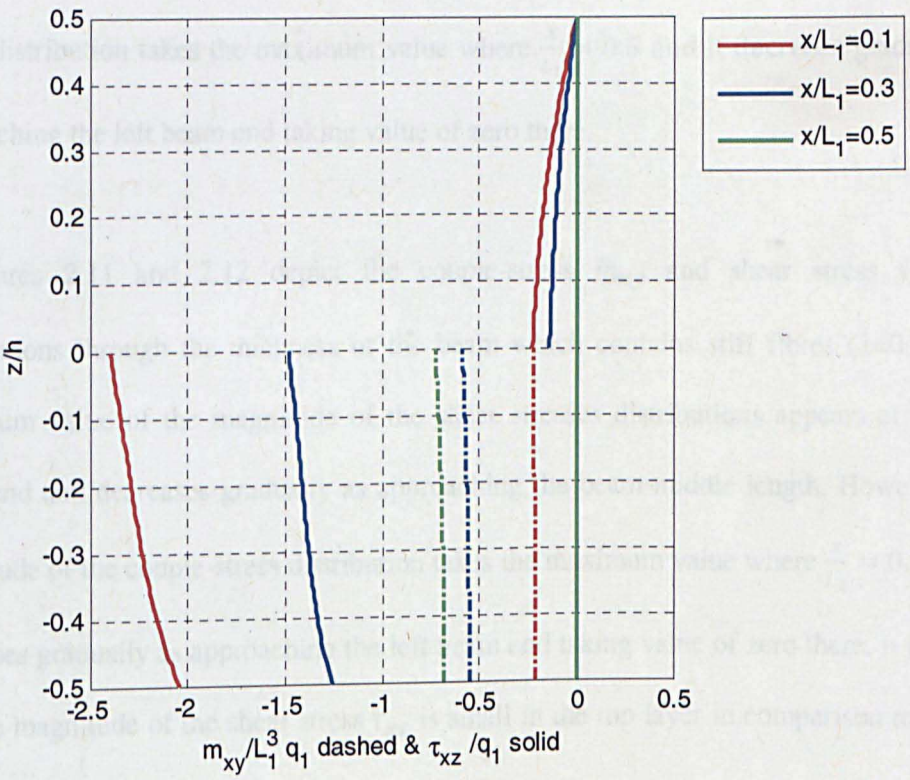

Figure 2.12 Couple-stress and shear stress $\frac{\tau_{xz}}{q_1}$ distributions of a two-layered beam (λ=0.1)

Figure 2.10 depicts the non-dimensional shear stress $\bar{\tau}_{xz}$ distributions for the beam at different values of λ. When the fibres possess bending stiffness, it is observed that a significant difference between the non-dimensional shear stress $\bar{\tau}_{zx}$ and $\bar{\tau}_{xz}$ appears evidently through the bottom layer in figures 2.8 and 2.9. It is observed that when the fibres resist bending, the shear stress τ_{xz} loses the continuity at the material interface (one each for the layers above and below). This does not happened with τ_{xz} which is governed by continuity conditions (2.11.b).

Figure 2.11 depicts the couple-stress $\bar{m}_{xy}$ and shear stress $\bar{\tau}_{zx}$ distributions through the thickness of the beam which contains stiff fibres (λ=0.1). The maximum value of the magnitude of the shear stress distributions appears at the left beam end and decreases

gradually as approaching the beam middle length. However, the magnitude of the couple-stress distribution takes the maximum value where $\frac{x}{L_1} = 0.5$ and it decrease gradually as approaching the left beam end taking value of zero there.

Figures 2.11 and 2.12 depict the couple-stress $\bar{m}_{xy}$ and shear stress $\bar{\tau}_{zx}$, $\bar{\tau}_{xz}$ distributions through the thickness of the beam which contains stiff fibres (λ=0.1). The maximum value of the magnitude of the shear stresses distributions appears at the left beam end and decreases gradually as approaching the beam middle length. However, the magnitude of the couple-stress distribution takes the maximum value where $\frac{x}{L_1} = 0.5$ and it decreases gradually as approaching the left beam end taking value of zero there. It is noted that the magnitude of the shear stress $\bar{\tau}_{xz}$ is small in the top layer in comparison to that in the bottom layer.

Example 3

In the third example, numerical results based on the present solution for free vibration of transversely isotropic beam are presented. In this example, the influence of the resistance of fibres in bending on the frequency values is investigated. Tables 2.5-7 show numerical results for different cases of the beam thickness to length ratio (h/L_1). The beam is assumed to have the following properties:

$$E_L/E_T = 25, \quad G_{LT}/E_T = 0.5, \quad G_{TT}/E_T = 0.2, \quad \nu_{LT} = \nu_{TT} = 0.25. \tag{2.50}$$

Table 2.5 presents the fundamental frequency parameter (ω^*), defined by equation (2.35), at different values of h/L_1. In each case, numerical results for different values of λ are presented. It is observed that the value of ω^* decreases with decreasing the value of the

ratio h/L_1. It is, further, of particular importance to note that in each case of the beam thickness, the value of ω^* increases with increasing the value of λ. This comparison agrees with the expectation that with increasing the fibre bending stiffness, the beam becomes stiffer. This observation makes again evident that the presence of the resistance of fibres in bending has significant effect on the beam stiffness.

Table 2.5 Fundamental frequency parameter, ω^*, of SS homogeneous beams

λ	$\frac{h}{L_1}$=0.25	$\frac{h}{L_1}$=0.20	$\frac{h}{L_1}$=0.15	$\frac{h}{L_1}$=0.10	$\frac{h}{L_1}$=0.05	$\frac{h}{L_1}$=0.01
0	0.6289	0.4698	0.3127	0.1649	0.0475	0.0020
0.02	0.6943	0.5173	0.3452	0.1850	0.0569	0.0035
0.04	0.7540	0.5609	0.3750	0.2031	0.0649	0.0045
0.06	0.8094	0.6013	0.4026	0.2197	0.0720	0.0053
0.08	0.8613	0.6392	0.4284	0.2351	0.0784	0.0061
0.1	0.9103	0.6750	0.4527	0.2496	0.0844	0.0067

Table 2.6 . First six frequency parameter, ω^*, of a SS homogeneous beam (h/L_1=0.25)

λ	*I*	*II*	*III*	*IV*	*V*	*VI*
0	0.6289	0.7854	5.5600	6.3762	8.4046	11.0004
0.02	0.6943	0.8250	5.5600	6.3761	8.4030	10.9959
0.04	0.7540	0.8629	5.5600	6.3760	8.4014	10.9914
0.06	0.8094	0.8991	5.5600	6.3759	8.3997	10.9869
0.08	0.8613	0.9400	5.5600	6.3758	8.3981	10.9822
0.1	0.9103	0.9996	5.5600	6.3756	8.3964	10.9776

Table 2.7 First six frequency parameter, ω^*, of a SS homogeneous beam ($h/L_1 = 0.1$)

λ	I	II	III	IV	V	VI
0	0.1649	0.3140	2.2230	3.8536	4.5902	6.6750
0.02	0.1850	0.3206	2.2230	3.8534	4.5914	6.6749
0.04	0.2031	0.3269	2.2230	3.8531	4.5926	6.6746
0.06	0.2197	0.3331	2.2230	3.8529	4.5938	6.6742
0.08	0.2351	0.3392	2.2230	3.8527	4.5950	6.6738
0.1	0.2496	0.3451	2.2230	3.8525	4.5962	6.6735

Table 2.6 compares the values of first six non-dimensional frequency parameter for free vibration of homogeneous thick beam (h/L_1=0.25) at different values of λ. It is noted that the values of fundamental and second frequency parameter are affected by the increase of the λ value more than that in the other shown frequencies. Moreover, the shown value of the third frequency is not affected by the increase of the value of λ. The expected cause of that is it corresponds to a predominantly in-plane displacement which has not been affected by the increasing of the value of λ as that of the flexure. Furthermore, there are a slight differences in the values of the fourth, fifth and sixth frequencies corresponding to the increase of the value of λ. In addition, with increasing the value of λ, the values of the fundamental and second frequency parameter increase whereas the values of the fourth, fifth and sixth frequency parameter decrease.

Table 2-7 shows the values of first six non-dimensional frequency parameter for free vibration of homogeneous thin beam (h/L_1=0.1) which contains unidirectional family of straight fibres that resist bending. It is noted again that the value of the shown third frequency parameter is not affected by the shown change of λ value. Moreover, with increasing the value of λ, the values of the first, second and fifth frequency parameter increase, whereas the values of the fourth and sixth frequency parameter decrease.

2.7. Conclusions

In summary, the linear static and dynamic problems of fibre-reinforced elastic beams containing fibres which resist bending are considered in this chapter. In the static problem, the discussion is limited to a particular loading condition while general loading can be treated by the use of a Fourier sine-series expansion. Plane strain asymmetric-stress elasticity solution of flexure of simply supported transversely isotropic beam is successfully found. The obtained solution makes the plane strain elasticity solution (Pagano, 1969) a special case where the intrinsic length parameter l that due to the resistance of fibres in bending, takes value of zero.

Furthermore, an exact solution of free vibration problem of a SS transversely isotropic beam is found. The solutions displacement field The discussion is based on the analytical solution of relevant plane strain differential equations of asymmetric-stress theory of elasticity (Spencer and Soldatos, 2007) and (Soldatos, 2009). Finding the static and dynamic solutions adds a new contribution to what is in the literature which pays attention to the influence of the presence of the resistance of fibres in bending.

The plane strain solutions constructed (displacement field) contain terms the due to the presence of the fibre bending stiffness. Those terms depend on the the additional length intrinsic parameter $l^{(k)}$ which is assumed to represent the fibres thickness. As a result of that, the stresses distributions and the free frequency parameter value will be affected by the change of the fiber bending stiffness.

The influence of the presence of the resistance of fibres in bending on the displacements shear stresses, couple stress, and free vibration frequency is discussed for both the static and dynamic problem. The following important findings are observed:

i) It is observed that the results at λ=0 are identical to the perfectly flexible results based on the exact elasticity solution.

ii) With increasing the value of λ, the deflection decreases.

iii) When the fibres resist bending, the shear stresses $\bar{\tau}_{zx}$, $\bar{\tau}_{xz}$ distributions are unequal.

iv) The magnitude of the shear stress $\bar{\tau}_{zx}$ through the thickness of the top layer is less than that in the bottom layer which is reinforced in the x-direction.

v) The shear stress $\bar{\tau}_{zx}$ is decreasing with increasing the value of λ. The largest value of this bending parameter is associated with the most symmetrical profile.

vi) The maximum magnitude of the couple stress at nonzero value of λ appears at the middle–length of the beam ($\frac{x}{L_1} = 0.5$).

vii) With increasing the value of λ, the fundamental frequency value increases.

2.8. Further work

The main aim of this subsection is to make a link between the present chapter and the forthcoming related chapters in the thesis.

Since the present solutions are exact, they can serve as a benchmark of the accuracy of relevant thin plate theories developed in (Soldatos, 2009), through appropriate comparisons of corresponding numerical results. One of aforementioned thin plate theories

is the general three-degrees-of-freedom shear deformable plate theory (G5DOFPT) which was applied in the case of perfectly flexible fibres in (Soldatos and Watson, 1997b).

The third chapter of this study will focus on applying the one-dimensional advanced version of (G5DOFPT) developed in (Soldatos, 2009). This one-dimensional theory is called a general three-degrees-of-freedom shear deformation beam theory (G3DOFBT). The G3DOFBT will be employed in the case when the fibres resist bending. The main propose is the ability of the one-dimensional thin theory to be applied on boundary conditions different from simply supported boundary condition. The reliability of such method will be tested by comparing its numerical results with their counterparts based on the obtained plane strain asymmetric-stress elasticity solutions of flexure and free vibration of simply supported transversely isotropic beam.

Furthermore, the obtained solutions in the present chapter will be used in the fourth chapter to compare their results with corresponding numerical results based on the three-dimensional asymmetric-stress elasticity solutions of flexure and free vibration of simply supported transversely isotropic rectangular plate. In such comparison and, in order to perform an appropriate comparison, the compared results would be for the case of rectangular plate of infinite extent in y-direction.

Chapter 3. Flexure and free vibration problem of beams subjected to different sets of end boundary conditions

3.1. Introduction

The general three-degrees-of-freedom shear deformable beam theory as introduced in (Soldatos, 2009) is considered for the solution of flexure and free vibration problem of beams subjected to different sets of end boundary conditions. Considering the fibres possess bending stiffness, the theory is initially applied to the solutions of the flexure and free vibration of thin simply supported homogeneous beam, for which the exact asymmetric-stress elasticity solutions have been obtained in the previous chapter. Then, this advanced beam theory is used to find the static and dynamic solutions in the case of different end boundary conditions.

Furthermore, analysis of numerical results based on the obtained solutions of flexure and free vibration of thin transversely isotropic beams subjected to different end boundary conditions is conducted. The main reason of studying this new generation of 2D elastic plate models is to take the advantages of applying it on the flexure and free vibration beam associated with different end boundary conditions for which explicit 3D elasticity solution is very difficult to obtain.

The advanced version of the general three-degrees-of-freedom shear deformable beam theory is used for an accurate stress analysis of two-layered composite beams having one

of their ends clamped and the other either simply supported, clamped or free of tractions. The determination of the shape function of the shear deformation is based on the use of the equilibrium and constitutive relations of three-dimensional asymmetric-stress elasticity (see subsection 3.4.1). According to study presented by Noor and Burton (1989a), the accurate prediction of the displacements and stresses distribution requires the use of three-dimensional equilibrium and constitutive relations. Therefore, the advanced version of the general three-degrees-of-freedom shear deformable beam theory is applied in this chapter.

The general three-degrees-of-freedom shear deformable beam theory was applied by Soldatos and Watson (1997b) in the case of perfectly flexible fibres, equivalently $\lambda=0$, in connection with the accurate stress analysis of homogeneous and laminated composite structural elements. The most significant difference between the employed advanced version of the general three-degrees-of-freedom shear deformable beam theory in this chapter and that presented by Soldatos and Watson (1997b) is that the beams contain fibres that have the ability to resist bending, equivalently $\lambda\neq0$.

3.2. Constitutive equations considering the resistance of fibres in bending

The considered beam notation is the same to that described in chapter 2. Different sets of end boundary conditions from simply supported are applied on the ends $x = 0, L_1$. The beam is subjected to small static flexure caused by the action of a given external lateral loading $q(x)$ or dynamic flexure. In the static problem, such loading acts normally and downwards on its top lateral plane of the beam.

The shear deformable, elastic beam model begins with the displacement approximation assumed in (Soldatos and Watson, 1997b) which has the following form:

$$U(x,z,t) = u(x,t) - zw_{,x} + \varphi(z)u_1(x,t), \tag{3.1.a}$$

$$W(x,z,t) = w(x,t), \tag{3-1.b}$$

where t denotes time. In addition, U(x, z, t) and W(x, z, t) represent displacement components along x and z directions, respectively. Moreover, $w(x,t)$ presents the deflection of the beam which is assumed to be independent of the beam thickness. Moreover, $u(x.t)$ is enforced to represent in-plane displacement of the beam middle plane. Therefore, they have evidently dimension of length. Furthermore, the other unknown displacement $u_1(x,t)$ depicts the value of transverse shear strain on the beam middle plane and is, as a result of that, assumed to be dimensionless quantity. This means that, the shape function $\varphi(z)$, which will be determined a posteriori, should have evidently dimensions of length and is imposed to have the following conditions:

$$\varphi(0) = 0, \left.\frac{d\varphi}{dz}\right|_{z=0} = 1 \tag{3.2}$$

Inserting the displacement approximation (3.1) into the following well-known linear kinematic relations:

$$\varepsilon_x = \frac{\partial U}{\partial x}, \ \gamma_{xz} = \frac{\partial U}{\partial z} + \frac{\partial W}{\partial x}, \tag{3.3}$$

yields the following approximate strain field:

$$\varepsilon_x = e_x^c + zk_x^c + \varphi(z)k_x^a, \ \gamma_{xz} = \varphi'(z)e_{xz}^a, \tag{3.4}$$

where

$$e_x^c = u_{,x}, \ k_x^c = -w_{,xx}, \ k_x^a = u_{1,x}, \ and \ e_{xz}^a = u_1. \tag{3.5}$$

Quantities denoted with a superscript "c" are identical with their classical beam theory counterparts. The components which are denoted with a superscript "a" represent the

transverse shear deformation effects. Such components, after the choice represented by equations (3.2), take the value of the transverse strain γ_{xz} , on the beam central axis. The prime stands for ordinary differentiation with respect to z.

It is considered that the beam is composed of an arbitrary number, N, of perfectly bonded transversely isotropic layers. Accordingly, the generalised Hooke's law within the kth layer of such a cross-ply laminate is given as follows:

$$\sigma_x^{(k)} = Q_{11}^{(k)}\varepsilon_x, \quad \tau_{(xz)}^{(k)} = Q_{55}^{(k)}\gamma_{xz}, \tag{3.6}$$

where $\tau_{(xz)}$ denotes to the symmetric part of the stress tensor component and the appearing $Q's$ are the reduced stiffnesses (Jones, 1975). Quantities with superscript "k" are due to the k^{th} layer of a cross-ply laminate. The anti-symmetric part of the shear stress component has the following form (Soldatos, 2009):

$$\tau_{[xz]}^{(k)} = -\tau_{[zx]}^{(k)} = \frac{1}{2}m_{xy,x}^{(k)} = \frac{1}{2}d^{f\,(k)}K_{z,x}^{f} = -\frac{1}{2}d^{f\,(k)}w_{,xxx}. \tag{3.7}$$

Furthermore, with the use of equations (2.6), (3.6.b) and (3.7), the shear stresses can be written as follows:

$$\tau_{xz}^{(k)} = Q_{55}^{(k)}\gamma_{xz} - \frac{1}{2}d^{f\,(k)}w_{,xxx}\,, \tag{3.8.a}$$

$$\tau_{zx}^{(k)} = Q_{55}^{(k)}\gamma_{xz} + \frac{1}{2}d^{f\,(k)}w_{,xxx} \tag{3.8.b}$$

In addition, the force and moment resultants are as follows:

$$N_x^c = \int_{-\frac{h}{2}}^{\frac{h}{2}}\sigma_x\,dz, \quad M_x^c = \int_{-\frac{h}{2}}^{\frac{h}{2}}\sigma_x\,z\,dz, \quad M_x^f = \frac{1}{2}\int_{-\frac{h}{2}}^{\frac{h}{2}}m_{xy}\,dz, \tag{3.9.a}$$

$$M_x^a = \int_{-\frac{h}{2}}^{\frac{h}{2}}\sigma_x\,\varphi(z)dz, \quad Q_x^a = \int_{-\frac{h}{2}}^{\frac{h}{2}}\tau_{(xz)}\,\varphi'(z)\,dz. \tag{3.9.b}$$

Determination of the three unknown degrees of freedom (u, u_1 and w) requires solution of the following relevant equations of motion (Soldatos, 2009):

$$N^c_{x,x} = \rho_0\, \ddot{u} - \rho_1\, \ddot{w}_{,x} + \hat{\rho}^{11}_0\, \ddot{u}_1\,,$$

$$M^c_{x,xx} + M^f_{x,xx} = q(x) + \rho_0\, \ddot{w} + \rho_1\, \ddot{u}_{,x} - \rho_2\, \ddot{w}_{,xx} + \hat{\rho}^{11}_1\, \ddot{u}_{1,x}\,, \tag{3.10}$$

$$M^a_{x,x} - Q^a_x = \hat{\rho}^{11}_0\, \ddot{u} - \hat{\rho}^{11}_1\, \ddot{w}_{,x} + \hat{\rho}^{12}_0\, \ddot{u}_1\,,$$

where the dots stand for ordinary differentiation with respect to time and, the appearing inertia terms are defined as follows:

$$\rho_i = \int_{-\frac{h}{2}}^{\frac{h}{2}} \rho\ z^i\, dz\,,\ \hat{\rho}^{Lm}_i = \int_{-\frac{h}{2}}^{\frac{h}{2}} \rho\ z^i\, [\varphi(z)]^m\, dz\,. \tag{3.11}$$

Here ρ denotes the material density of the elastic beam considered. The equations of motion (3.10) are associated with the following variationally consistent set of end boundary conditions at $x = 0,\ L_1$ (Soldatos, 2009):

either u or N^c_x is prescribed, (3.12.a)

either w or $M^c_{x,x} + M^f_{x,x}$ is prescribed, (3.12.b)

either w_x or $M^c_x + M^f_x$ is prescribed, (3.12.c)

either u_1 or M^a_x is prescribed. (3.12.d)

3.3. Navier-type differential equations

Introduction of equations (3.6-8) into equations (3.9) yields the following force and moment resultants in terms of the three degrees of freedom and their derivatives:

$$\begin{bmatrix} N_x^c \\ M_x^c \\ M_x^a \end{bmatrix} = \begin{bmatrix} A_{11}^c & B_{11}^c & B_{11}^a \\ B_{11}^c & D_{11} & D_{11}^a \\ B_{11}^a & D_{11}^a & D_{11}^{aa} \end{bmatrix} \begin{bmatrix} u_{,x} \\ -w_{,xx} \\ u_{1,x} \end{bmatrix}, \; M_x^f = -\frac{1}{2} h\, d^f\, w_{,xx}, \; Q_x^a = A_{55}^a u_1. \tag{3.13}$$

The rigidities can be calculated by the use of the following expressions:

$$(A_{11}^c, B_{11}^c, B_{11}^a, D_{11}^a, D_{11}^{aa}) = \int_{-\frac{h}{2}}^{\frac{h}{2}} Q_{55}^{(k)} \left(1, z, \varphi(z), z\varphi(z), \varphi^2(z)\right) dz, \tag{3.14.a}$$

$$D_{11} = \int_{-\frac{h}{2}}^{\frac{h}{2}} Q_{11}^{(k)}\, z^2\, dz, \quad A_{55}^a = \int_{-\frac{h}{2}}^{\frac{h}{2}} Q_{55}^{(k)} (\varphi'(z))^2\, dz. \tag{3.14.b,c}$$

It can be seen that four of those rigidities depend on the shape function $\varphi(z)$, which will be determined in subsection 3.4.1.

The equations of motion (3.10) can be converted into a set of three simultaneous differential equations for the same number of unknowns. With the use of equation (3.13), these differential equations can be obtained in terms of the displacement field yielding the following Navier- type differential equations system:

$$A_{11}^c u_{,xx} - B_{11}^c w_{,xxx} + B_{11}^a u_{1,xx} = \rho_0\, \ddot{u} - \rho_1\, \ddot{w}_{,x} + \hat{\rho}_0^{11}\, \ddot{u}_1, \tag{3.15.a}$$

$$B_{11}^c u_{,xxx} - \left(D_{11}^f\right) w_{,xxxx} + D_{11}^a u_{1,xxx} = q(x) + \rho_0 \ddot{w} + \rho_1 \ddot{u}_{,x} - \rho_2 \ddot{w}_{,xx} + \hat{\rho}_1^{11} \ddot{u}_{1,x}, \tag{3.15.b}$$

$$B_{11}^a u_{,xx} - D_{11}^a w_{,xxx} + D_{11}^{aa} u_{1,xx} - A_{55}^a u_1 = \hat{\rho}_0^{11}\, \ddot{u} - \hat{\rho}_1^{11}\, \ddot{w}_{,x} + \hat{\rho}_0^{12}\, \ddot{u}_1, \tag{3.15.c}$$

The rigidity, D_{11}^f, appears in equation (3.16.b) is depending on the conventional rigidity, D_{11}, and the fibre bending elastic modulus and defined according to:

$$D_{11}^f = \frac{1}{2} h\, d^f + D_{11}. \tag{3.16}$$

In accordance with the number of end boundary conditions (3.12), the equations (3.15) form an eighth order set of ordinary differential equations, with respect to the co-

ordinate parameter x. These may be solved simultaneously when a particular set of boundary conditions is specified at each end of the beam.

3.4. The static problem solution

In the present section, the 1D static solution is found for the considered flexure problem. The inertia terms appearing in the right-hand sides of the motion equations (3.15) are disregarded to yield the following equilibrium equations:

$$A_{11}^{c}u_{,xx} - B_{11}^{c}w_{,xxx} + B_{11}^{a}u_{1,xx} = 0,$$

$$B_{11}^{c}u_{,xxx} - (D_{11}^{f})w_{,xxxx} + D_{11}^{a}u_{1,xxx} = q(x), \tag{3.17}$$

$$B_{11}^{a}u_{,xx} - D_{11}^{a}w_{,xxx} + D_{11}^{aa}u_{1,xx} - A_{55}^{a}u_{1} = 0.$$

The difference between equations (3.17) and their corresponding equilibrium equations in the case of perfectly flexible fibres presented in (Soldatos and Watson, 1997b) is the expression of the rigidity D_{11}^{f}, which shown in equation (3.16). By setting the intrinsic length parameter l or the additional elastic d^f equal to zero, the equilibrium equations (3.17) reduce to the conventional perfectly flexible counterparts.

Recognizing that the lateral load function can be expressed in the form of a Fourier series, it is considered that:

$$q(x) = q_m \sin(p_m x),\ p_m = m\pi/L_1, \quad (m = 1, 2, \ldots). \tag{3.18}$$

This would be understood as being a simple harmonic in the corresponding Fourier sine-series expansion of any relevant loading distribution. The following boundary conditions can be applied on the ends $x = 0,\ L_1$:

at a simply supported end: $N_x^c = 0, w = 0,\ M_x^c + M_x^f = 0, M_x^a = 0,$ (3.19.a)

at a clamped end: $u = 0, w = 0, w_{,x} = 0, u_1 = 0,$ (3.19.b)

and at a free end: $N_x^c = 0, M_{x,x}^c + M_{x,x}^f = 0, M_x^c + M_x^f = 0, M_x^a = 0.$ (3.19.c)

The general solution of the non-homogeneous ordinary differential system (3.17) will be the three degrees of freedom u, u_1 and w and has the following form:

$$S = S_c + S_p. \tag{3.20}$$

Here S_c is the complementary solution and S_p is a particular solution of the non-homogeneous system. As presented in the case of perfectly flexible fibres (Soldatos and Watson, 1997b), the simply supported boundary conditions (3.19.a) are satisfied by the following trigonometric displacement choice of S_p:

$$u = A\cos(p_m x),\ u_1 = B\cos(p_m x), w = C\sin(p_m x). \tag{3.21}$$

Inserting equations (3.21) into Navier- type differential equations (3.17) will convert it into the following system of three simultaneous linear algebraic equations of the three unknown constants A, B and C.

$$\begin{bmatrix} p_m^2 A_{11}^c & -p_m^3 B_{11}^c & p_m^2 B_{11}^a \\ p_m^3 B_{11}^c & -p_m^4 D_{11}^f & p_m^3 D_{11}^a \\ p_m^2 B_{11}^a & -p_m^3 D_{11}^a & p_m^2 D_{11}^{aa} - A_{55}^a \end{bmatrix} \begin{bmatrix} A \\ C \\ B \end{bmatrix} = \begin{bmatrix} 0 \\ q_m \\ 0 \end{bmatrix}, \tag{3.22}$$

where, for any chosen shape function $\varphi(z)$, the rigidities in equations (3.22) can be calculated by equations (3.14) and (3.16). A corresponding set of A, B and C values will be obtained by solving algebraic equations system (3.22).

Furthermore, the general solution of the eighth-order system of equilibrium differential equations (3.17) can be written as follows:

$$u(x) = K_2 \frac{H_2}{H_3} e^{\sqrt{H_3}x} + K_3 \frac{H_2}{H_3} e^{-\sqrt{H_3}x} + K_2 H_1 e^{\sqrt{H_3}x} + K_3 H_1 e^{-\sqrt{H_3}x} +$$

$$\frac{K_1}{2} H_2 x^2 + K_7 x + K_8 + A\cos(p_m x), \tag{3.23.a}$$

$$u_1(x) = K_1 + K_2 e^{\sqrt{H_3}x} + K_3 e^{-\sqrt{H_3}x} + B\cos(p_m x), \tag{3.23.b}$$

$$w(x) = K_2 \frac{H_4}{\sqrt{H_3}} e^{\sqrt{H_3}x} - K_3 \frac{H_4}{\sqrt{H_3}} e^{-\sqrt{H_3}x} + K_2 \frac{H_5}{H_3^{(3/2)}} e^{\sqrt{H_3}x} - K_3 \frac{H_5}{H_3^{(3/2)}} e^{-\sqrt{H_3}x} +$$

$$\frac{K_1}{6} H_5 x^3 + \frac{K_4}{2} x^2 + K_5 x + K_6 + C\sin(p_m x). \tag{3.23.c}$$

In the above

$$H_1 = -\frac{F_1 B_{11}^a + B_{11}^c F_3}{F_1 A_{11}^c}, \quad H_2 = -\frac{B_{11}^c A_{55}^a}{F_1},$$

$$H_3 = \frac{-F_1 B_{11}^c A_{55}^a + F_2 A_{11}^c A_{55}^a}{F_1 F_4 - F_2 F_3}, \; H_4 = -\frac{F_3}{F_1}, \; H_5 = -\frac{A_{11}^c A_{55}^a}{F_1}, \tag{3.24}$$

$$F_1 = A_{11}^c D_{11}^a - B_{11}^c B_{11}^a, \quad F_2 = B_{11}^c D_{11}^a - B_{11}^a D_{11}^f,$$

$$F_3 = (B_{11}^a)^2 - A_{11}^c D_{11}^{aa}, \quad F_4 = B_{11}^a D_{11}^a - B_{11}^c D_{11}^{aa}.$$

Values of the arbitrary constants $(K_1, K_2, \ldots, K_8)$ can be found when a set of eight end boundary conditions is specified. As in the perfectly flexible case (Soldatos and Watson, 1997b), these arbitrary constants take value of zero when simply supported boundary conditions are applied. The general solution (3.23) reduces the complementary solution (3.21) in the case of SS end boundary conditions

This influence of the resistance of fibres in bending on $\varphi(z)$ will affect, consequently, five of the rigidities, shown in equations (3.14) and (3.16). As a result of this effect o It is worth mentioning the obtained general solution can be reduced to the perfectly flexible

fibres solution by giving value of zero to the fibre bending elastic modulus d^f, making the value of the rigidity $D_{11}^f = D_{11}$ (see equation 3.16). In the following section, it will be observed that the shape function $\varphi(z)$ will be affected by the presence of the fibre bending stiffness by showing that it depends on d^f.n the referred rigidities, equations (3.22) and (3.24) show that the values of the unknown constants A, B and C and therefore, the displacement field will also be affected by the presence of the resistance of fibres in bending (see equation 3.23). Finally, the dependence of the stresses and the couple-stress on the displacement field makes them, as well, affected by the resistance of fibres in bending.

3.4.1. Determination of the shape function $\varphi(z)$ when fibres resist bending

Determination of the shape function when fibres resist bending is similar to that followed in the case of perfectly flexible fibres presented in (Soldatos and Watson, 1997b). In this section, the shape function will be, firstly, found for the general case of an N-layered beam. Then a particular case of the shape function for a homogeneous transversely isotropic beam will be considered as an example. In the present case where the fibres resist bending, the first equilibrium equations of the three-dimensional asymmetric-stress elasticity will be used to find the shape function. This is as follows:

$$\sigma_{x,x} + \tau_{(xz),z} - \tau_{[xz],z} = 0. \tag{3.25}$$

Since the displacement W, in (3.1.b), is independent on z, the use of equation (3.7) yields that the differentiation of the anti-symmetric part of the shear stress component with respect to z equals zero. Thus, the third term in equilibrium equation (3.25) cancels and this equation reduces to its perfectly flexible fibres counterpart met in (Soldatos and Watson, 1997b). There a detailed discussion led to the shape function,

$$\varphi^{(k)} = \lambda_1 \left(C_1^{(k)} e^{\alpha_k z} + C_2^{(k)} e^{-\alpha_k z} + p_m z - \lambda_2\right), \quad {\alpha_k}^2 = \frac{Q_{11}^{(k)}}{Q_{55}^{(k)}} {p_m}^2 \tag{3.26}$$

when λ_1, λ_2, $C_1^{(k)}$, $C_2^{(k)}$ are 2*N*+2 constants, $k = 1, 2, \ldots, N$ and N is the number of the layers of *N*-layered cross-ply laminated beam. In addition, $C_1^{(k)}$, $C_2^{(k)}$ indicate the arbitrary constants related to the *k*th layer. In order to find the values of these constants, 2*N*+2 algebraic equations of them are needed. Two of those can be obtained by applying conditions (3.2) yielding the following equations:

$$C_1{}^{(mp)} + C_2{}^{(mp)} - \lambda_2 = 0, \tag{3.27.a}$$

$$\lambda_1[\alpha_{mp}(C_1{}^{(mp)} - C_2{}^{(mp)}) + p_m] = 1. \tag{3.27.b}$$

Here, $C_1^{(mp)}$, $C_2^{(mp)}$ indicate arbitrary constants associated with the layer which contains the central axis of the beam considered. Solving equations (3.27) simultaneously yields an expression of λ_1 and λ_2 in terms of $C_1^{(mp)}$ and $C_2^{(mp)}$.

In addition, 2*N* of the arbitrary constants $C_1^{(k)}$, $C_2^{(k)}$ can be determined by applying: (*i*) the two zero shear stress $\tau_{(xz)} - \tau_{[xz]}$ boundary conditions given on the top and the bottom of the beam, and (*ii*) the 2(*N*-1) continuity of the in-plane displacement $U(x, z)$ and the shear stress $\tau_{(xz)} - \tau_{[xz]}$ at the kth material surfaces, $z = z_k$; of that is the following conditions ($k = 1, 2, \ldots, N-1$):

$$U^{(k)}(x, z)\big|_{z=z_k} = U^{(k+1)}(x, z)\big|_{z=z_k}, \tag{3.28.a}$$

$$(\tau^{(k)}{}_{(xz)} - \tau^{(k)}{}_{[xz]})\Big|_{z=z_k} = (\tau^{(k+1)}{}_{(xz)} - \tau^{(k+1)}{}_{[xz]})\Big|_{z=z_k}. \tag{3.28.b}$$

It should be mentioned that the presence of $\tau^{(k)}{}_{[xz]}$ in the shear stress continuity condition (3.28.b) suggests that the final form of the shape function is affected by the presence of the

resistance of fibres in bending. This influence is caused by the non-zero couple-stress. The use of equations (3.1.a), (3.21), (3.26) and (3.28.a) yields the following *N*-1 algebraic equations ($k = 1, 2, \ldots, N-1$):

$$C_1^{(k)} e^{\alpha_k z_k} + C_2^{(k)} e^{-\alpha_k z_k} - C_1^{(k+1)} e^{\alpha_{k+1} z_k} - C_2^{(k+1)} e^{-\alpha_{k+1} z_k} = 0. \tag{3.29.a}$$

In addition, inserting equations (3.4.b), (3.5.d), (3.7), (3.6.b), (3.21) and (3.26) into equations of the shear stress continuity (3.28.b) yields the following *N-1* algebraic equations ($k = 1, 2, \ldots, N-1$):

$$C_1^{(k)} e^{\alpha_k z_k} - C_2^{(k)} e^{-\alpha_k z_k} - \frac{Q_{55}^{(k+1)} \alpha_{k+1}}{Q_{55}^{(k)} \alpha_k} \left(C_1^{(k+1)} e^{\alpha_{k+1} z_k} - C_2^{(k+1)} e^{-\alpha_{k+1} z_k} \right) -$$

$$\left(\frac{(p_m)^3 \left(d^{f^{(k)}} - d^{f^{(k+1)}} \right)}{2\, Q_{55}^{(k)} \alpha_k} \right) = \left(\frac{Q_{55}^{(k+1)}}{Q_{55}^{(k)}} - 1 \right) \frac{p_m}{\alpha_k}. \tag{3.29.b}$$

Finally, in order to determine the 2*N*+2 constants appearing in the shape function (3.26), the last required two algebraic equations can be obtained by requiring value of zero for the shear stress $\tau_{(xz)} - \tau_{[xz]}$ on the upper and lower surfaces of the beam where $z = \pm h/2$, thus leading to:

$$(\tau_{(xz)} - \tau_{[xz]})\big|_{z=\frac{h}{2}} = 0, \tag{3.30}$$

$$(\tau_{(xz)} - \tau_{[xz]})\big|_{z=\frac{-h}{2}} = 0\,. \tag{3.31}$$

Inserting of equations (3.4.b), (3.5.d), (3.12.a), (3.6.b), (3.21) and equation (3-26) into equations (3.30) and (3.31) yields the following two algebraic equations:

$$C_1^{(1)} e^{-\alpha_1 \frac{h}{2}} - C_2^{(1)} e^{\alpha_1 \frac{h}{2}} - \left(\frac{(p_m)^3 \left(d^{f^{(1)}} \right)}{2\, Q_{55}^{(1)} \alpha_1} \right) = -\frac{p_m}{\alpha_1}, \tag{3.32}$$

$$C_1^{(N)} e^{\alpha_N \frac{h}{2}} - C_2^{(N)} e^{-\alpha_N \frac{h}{2}} - \left(\frac{(p_m)^3 \left(d^{f^{(N)}} \right)}{2\, Q_{55}^{(N)} \alpha_N} \right) = -\frac{p_m}{\alpha_N}. \tag{3.33}$$

Equations (3.27.a, b), (3.29.a, b), (3.32) and (3.33) form a set of $2N+2$ simultaneous algebraic equations which will be used to determine the $2N+2$ constants involved in the shape function $\varphi(z)$.

3.4.2. Shape function of a homogeneous beam (N=1)

As an example, the particular case of a homogeneous beam (N=1) is considered. The required constants, required for determination of the shape function would be λ_1, λ_2, C_1 and C_2. The index k has been dropped, and the shape function for a homogeneous transversely isotropic beam would have the following reduced form of that expressed by equation (3.26):

$$\varphi = \lambda_1 \left(C_1\, e^{\alpha z} + C_2\, e^{-\alpha z} + p_m z - \lambda_2 \right), \tag{3.34}$$

and the aforementioned $2N+2$ equations would be the following four equations:

$$C_1 + C_2 - \lambda_2 = 0, \tag{3.35}$$

$$\lambda_1 \left(\alpha \left(C_1 - C_2 \right) + p_m \right) = 1, \quad \alpha^2 = \frac{Q_{11}}{Q_{55}}\, {p_m}^2, \tag{3.36}$$

$$C_1 e^{-\alpha \frac{h}{2}} - C_2 e^{\alpha \frac{h}{2}} = -\frac{p_m}{\alpha} + \frac{1}{2\, \alpha\, Q_{55}}\, d^f {p_m}^3, \tag{3.37}$$

$$C_1 e^{\alpha \frac{h}{2}} - C_2 e^{-\alpha \frac{h}{2}} = -\frac{p_m}{\alpha} + \frac{1}{2\, \alpha\, Q_{55}}\, d^f {p_m}^3. \tag{3.38}$$

Their solution leads to the required constants:

$$C_1 = \frac{1}{4}\frac{p_m(d^f {p_m}^2 - 2\,Q_{55})}{\alpha\, Q_{55}\cosh\left(\alpha\frac{h}{2}\right)},\quad C_2 = -\frac{1}{4}\frac{p_m(d^f {p_m}^2 - 2\,Q_{55})}{\alpha\, Q_{55}\cosh\left(\alpha\frac{h}{2}\right)},$$

$$\lambda_2 = 0, \lambda_1 = \frac{2\cosh\left(\alpha\frac{h}{2}\right)}{p_m\left[d^f {p_m}^2 - 2\,Q_{55} + 2\,Q_{55}\cosh\left(\alpha\frac{h}{2}\right)\right]}. \tag{3.39}$$

Inserting equations (3.39) into equation (3.34) yields the shape function for a homogeneous orthotropic beam as:

$$\varphi(z) = \frac{1}{2}\frac{2\,d^f {p_m}^2 \sinh(\alpha z) + 4\,\alpha z\, Q_{55}\cosh\left(\alpha\frac{h}{2}\right) - 4\,Q_{55}\sinh(\alpha z)}{\alpha\left[d^f {p_m}^2 - 2\,Q_{55} + 2\,Q_{55}\cosh\left(\alpha\frac{h}{2}\right)\right]}. \tag{3.40}$$

3.5. The dynamic problem solution

In this section, the solution of free vibration of transversely isotropic beam is found when the fibre resists bending. The beam is subjected to different sets of end boundary conditions. The solution is obtained by solving the Navier- type differential equations system (3.15), the right hand-side of which contains non-zero inertia terms and $q(x) = 0$. The effective way to test the reliability of such thin-walled structures modelling is by performing numerical comparisons with corresponding results of the dynamic plane strain asymmetric-stress elasticity solution found in the previous chapter. In this context, the solution in the case of SS boundary conditions is found first. Then, different boundary conditions are considered.

The beam theories employed in this case of the boundary conditions are associated with the following choices of the shape function appeared in the displacement field (3.1):

General 3-degree-of-freedom shear deformable beam theory described in subsection 3.4.1 in the present chapter: $\varphi(z)$ exponential;

Parabolic shear deformable theory (PSDT) (Bickford, 1982): $\varphi(z) = z(1 - \frac{4z^2}{3h^2})$;

Classical beam theory (CBT) $\varphi(z) = 0$.

It is shown in section 3.6.2, as expected, that for thin beams the vibration frequencies obtained on the basis of results of the solution of one-dimensional version of CPT are very close to their counterparts based on the developed G3DOFBT. This is not true in the static problem. As the accurate prediction of the displacements and stresses distribution requires the use of three-dimensional equilibrium and constitutive relations (Noor and Burton, 1989a). For the simplicity of CPT in comparison to G3DOFBT to employ, the dynamic solution is found for different sets of boundary conditions based on the one-dimensional version of the advanced version of CPT (Soldatos, 2009).

3.5.1. Solution for the case of simply supported ends

The simply supported end boundary conditions (3.19.a) are satisfied exactly at the ends $x = 0$ and $x = L_1$ by the following displacement field:

$$\{u, u_1, w\} = \{A^{(u)} cos(p_m x),\ A^{(u_1)} cos(p_m x),\ A^{(w)} sin(p_m x)\}\ cos\ (\omega t), \tag{3.41}$$

where ω represents an unknown natural frequency of vibration. With the use of the displacement field (3.41), the dynamic form of the Navier-type equation (3.15) can be converted to the following eigenvalue problem:

$$-A_{11}^{c}A^{(u)}{p_m}^2 + B_{11}^{c}A^{(w)}{p_m}^3 - B_{11}^{a}A^{(u_1)}{p_m}^2 + \rho_0 A^{(u)}\omega^2 - \rho_1 A^{(w)}p_m\omega^2 +$$

$$\hat{\rho}_0^{11} A^{(u_1)}\omega^2 = 0,$$

$$B_{11}^{c}A^{(u)}{p_m}^3 - (D_{11}^{f})A^{(w)}{p_m}^4 + D_{11}^{a}A^{(u_1)}{p_m}^3 + \rho_0 A^{(w)}\omega^2 - \rho_1 A^{(u)}p_m\omega^2 +$$

$$\rho_2 A^{(w)}{p_m}^2\omega^2 - \hat{\rho}_1^{11} A^{(u_1)}p_m\omega^2 = 0, \tag{3.42}$$

$$- B_{11}^{a} A^{(u)} p_m{}^2 + D_{11}^{a} A^{(w)} p_m{}^3 - D_{11}^{aa} A^{(u_1)} p_m{}^2 - A_{55}^{a} A^{(u_1)} + \hat{\rho}_0^{11} A^{(u)} \omega^2$$

$$- \hat{\rho}_1^{11} A^{(w)} p_m \omega^2 + \hat{\rho}_0^{12} A^{(u_1)} \omega^2 = 0.$$

This can be re-arranged in the following matrix form:

$$(\boldsymbol{K} - \omega^{*2}\, \boldsymbol{H})\, \boldsymbol{X} = \boldsymbol{0}, \quad \boldsymbol{X} = (A^{(u)}, A^{(w)}, A^{(u_1)})^T. \tag{3.43}$$

Here the normalised frequency parameter is considered as defined in equation (2.35) where $C_{55}^{(k)} = G_{12}^{(k)}$ and the stiffness and mass matrices are as follows:

$$\boldsymbol{K} = p_m{}^2 \begin{bmatrix} A_{11}^{c} & -B_{11}^{c} p_m & B_{11}^{a} \\ -B_{11}^{c} p_m & p_m{}^2 D_{11}^{f} & -D_{11}^{a} p_m \\ B_{11}^{a} & -D_{11}^{a} p_m & D_{11}^{aa} + \frac{A_{55}^{a}}{p_m{}^2} \end{bmatrix}, \quad \boldsymbol{H} = \frac{G_{12}}{\rho h^2} \begin{bmatrix} \rho_0 & -\rho_1 p_m & \hat{\rho}_0^{11} \\ -\rho_1 p_m & \rho_0 & -\hat{\rho}_1^{11} p_m \\ \hat{\rho}_0^{11} & -\hat{\rho}_1^{11} p_m & \hat{\rho}_0^{12} \end{bmatrix}. \tag{3.44}$$

The values of the frequency parameter ω^* can be obtained by solving the eigenvalue problem (3.43).

3.5.2. Dynamic solution for a homogeneous beam subjected to different sets of end boundary conditions

The advanced version of CBT (Soldatos, 2009), which takes into account the presence of the resistance of fibres in bending, is employed to find the dynamic solution for a free vibration of homogeneous beam subjected to different sets of end boundary conditions. As already mentioned, the shape function is chosen to be zero in the displacement field (3.1). Consequently, the Navier-type equations take the following form:

$$A_{11}^{c} u_{,xx} - \rho_0 \ddot{u} = 0, \tag{3.45.a}$$

$$(D_{11}^{f}) w_{,xxxx} - \rho_0 \ddot{w} - \rho_2 \ddot{w}_{,xx} = 0. \tag{3.45.b}$$

In this case, the end boundary conditions (3.19) are reduced to the following:

at a simply supported end: $N_x^c = 0, w = 0,\ M_x^c + M_x^f = 0,$ (3.46.a)

at a clamped end: $u = 0, w = 0, w_{,x} = 0\ ,$ (3.46.b)

and at a free end: $N_x^c = 0, M_{x,x}^c + M_{x,x}^f = 0, M_x^c + M_x^f = 0.$ (3.46.c)

Equations (3.45.a) and (3.45.b) are uncoupled. Therefore, the solution of flexure vibration can be obtained by the solution of (3.45.b). The solution of equations (3.45.b) is assumed in the following form:

$$w(x) = w^*(x)\, cos(\omega t). \tag{3.47}$$

Inserting equations (3.47) into equations (3.45.b) yields the following ordinary differential equations:

$$\left(-D_{11}^f\right) w^*{}_{,xxxx} + \frac{G_{12}\rho_0}{h^2\rho}\, \omega^{*^2} w^* - \frac{G_{12}\rho_2}{h^2\rho}\, \omega^{*^2}\, w^*{}_{,xx} = 0, \tag{3.48}$$

The solution of this equation is as follows:

$$w^* = c_1 e^{\alpha_1 x} + c_2 e^{-\alpha_1 x} + c_3 e^{\alpha_2 x} + c_4 e^{-\alpha_2 x}, \tag{3.49}$$

where $c_i\ , i = 1, 2, \ldots, 4$ are four arbitrary constants which can be obtained, for each value the frequency parameter, when set of four end boundary conditions is specified at $x = 0, L_1$ and,

$$\alpha_1 = \frac{1}{2g_1}\sqrt{-2g_1(g_3 + \sqrt{g_3{}^2 - 4g_1g_2})},$$

$$\alpha_2 = \frac{\sqrt{2}}{2g_1}\sqrt{g_1(-g_3 + \sqrt{g_3{}^2 - 4g_1g_2})}, \tag{3.50}$$

$$g_1 = -D_{11}^f,\ g_2 = \frac{G_{12}\rho_0}{h^2\rho}\, \omega^{*^2},\ g_3 = -\frac{G_{12}\rho_2}{h^2\rho}\, \omega^{*^2}.$$

Using equation (3.49), (3.47) and (3.1), with the shape function equals to zero, one can write the following:

$$W(x,z,t) = [c_3 e^{\alpha_2 x} + c_4 e^{-\alpha_2 x} + c_5 e^{\alpha_3 x} + c_6 e^{-\alpha_3 x}] cos(\omega t). \quad (3.51)$$

Appling a specified set of four boundary conditions that, due to W(x, z, t), (see equations 3.46) on the deflection (3.51) yields the following four algebraic simultaneous homogeneous equations:

$$\boldsymbol{R}(\omega^*) . \boldsymbol{C} = 0, \quad (3.52)$$

where $\mathbf{C} = (c_1, c_2, c_3, c_4, c_5, c_6)^T$ and $\mathbf{R}(\omega^*)$ is a (4 x 4) matrix that depends on ω^*. For a non-trivial solution of the homogeneous equations (3.52), the determinant of the matrix $\mathbf{R}(\omega^*)$ must be zero yielding the following algebraic equation, of ω^*:

$$det\,(\boldsymbol{R}(\omega^*)) = 0. \quad (3.53)$$

Here, Maple software is used to find numerical values of ω^* in similar manner described for finding the roots of equation (2.45).

3.6. Numerical results and discussion

G3DOFBT is initially applied to the stress analysis of beams deformed in cylindrical bending having both of their ends simply supported. The reason of beginning with this case of the end boundary conditions is to test the reliability of the 1D beam model. This is conducted by comparing its results against corresponding numerical results based on the plane strain asymmetric-stress elasticity solutions introduced in the previous chapter. After the reliability of the method is successfully checked, three other sets of end boundary conditions are considered. The obtained displacements, stresses, couple-stress and frequency results when fibres resist bending are new. The numerical results are presented

in two subsections: first, numerical results referring to the static solution; and then, the free vibration numerical results.

3.6.1. Static solution numerical results

In order to make appropriate comparisons between the results based on the G3DOBT and the exact asymmetric-stress solution results, the fibre bending stiffness elastic modulus d^f is considered in that same notation that employed in chapter two (see equation 2.5). For the same reason, the non-dimensional parameter λ defined in equation (2.13) is also considered.

It is found that numerical results based on the employed 1-D models for thick beam ($h/L_1 = 0.25$) at λ=0 are identical to their counterparts presented in the case of perfectly flexible fibres (Soldatos and Watson, 1997b). In the following results, the beam is considered to be thin; its thickness is determined by the ratio $h/L_1 = 0.01$. The material of the beam is assumed to be transversely isotropic and has the following elastic properties:

$$E_L/E_T = 40, \quad G_{LT}/E_T = 0.5, \quad G_{TT}/E_T = 0.2, \quad v_{LT} = v_{LT} = 0.25, \tag{3.54}$$

where the subscripts L and T denote properties associated with the longitudinal and transverse fibre direction, respectively

For testing the reliability of the employed method, a homogeneous beam with fibres aligned to the x-axis is firstly considered. Then, two-layered beams are considered comprised of a regular anti-symmetric cross-ply lay-up with fibres aligned to the x-axis in the bottom layer. For presenting the numerical results, the following normalised quantities are used:

$$Z = z/h\,,\ X = x/L_1, \tag{3.55.a}$$

$$\bar{W} = E_T W 10^2 h^3/{L_1}^4 q_1\,,\ \bar{U} = E_T U h/{L_1}^2 q_1\,, \tag{3.55.b}$$

$$\bar{m}_{xy} = m_{xy}/L_1^3 q_1,\ \bar{\tau}_{xz} = \tau_{xz} h/L_1 q_1\,,\ \bar{\tau}_{zx} = \tau_{zx} h/L_1 q_1\,. \tag{3.55.c}$$

Figures 3.1-3.4 depict normalised numerical results for a SS homogenous beam at different values of λ and, based on two different methods. The solid lines represent results obtained by the plane strain asymmetric-stress elasticity solution outlined in chapter 2 while the results of the G3DOFBT solution are represented by dashed lines. For the comparison reason of the results of the considered deformed thin elastic beam ($h/L_1 = 0.01$), the values of the λ have begun with small values in comparison to those taken in chapter two. It should be mentioned that for different thickness and elastic properties shown in (3.54), different values of λ can be given.

Figure 3.1 shows normalised deflection distributions at the top of the beam. It is observed that the two models give results of good agreement at λ=0. However, with increasing the value of λ, the difference between the deflection values of the two methods increases. Figure 3.2 shows the through-thickness in-plane displacement distributions of the beam. In the case of stiff fibres (λ=0.001), G3DOFBT provides results of displacement distributions that are close to those predicted by the plane strain asymmetric-stress elasticity solution.

Figures 3.3 and 3.4 present the through-thickness shear stress distributions $\bar{\tau}_{zx}$and $\bar{\tau}_{xz}$ at the left end of the beam, respectively. It can be seen that the two models give results of a good agreement in the case of perfectly flexible fibres when λ =0. In the cases when the fibres resist bending ($\lambda \neq 0$), they become different. Both models employed provide results of the shear stress $\bar{\tau}_{zx}$ which are identical to each other near the top and the bottom

of the beam. The cause of that is the effect of the lateral surface boundary conditions applied on the top and bottom surfaces of the beam ($z = \mp\frac{h}{2}$).

In addition, the two models provide results of good agreement in the case of λ=0.001 whereas they do not in the case of λ=0.005. It should be noted that with increasing the value of λ, the difference between the values of the shear stresses $\bar{\tau}_{zx}$ and $\bar{\tau}_{xz}$ obtained by the two methods increases. This is apparently due to the limitations of the three-degrees-of-freedom beam theory which seem to become more pronouncing in the when the fibres possess bending stiffness; which seems to increase the effective beam thickness.

Despite this observation, it is believed that for thin beams, the displacement and stress distributions are considerably accurate when $\lambda \leq 0.001$. Nevertheless, improvement and probably elimination of this drawback (which might be more pronounced for big values of fibre bending stiffness elastic modulus) can be achieved by replacing the G3DOFBT with the general four-degrees-of freedom beam theory (G4DOFBT) (Soldatos and Watson, 1997a). In that case, transverse normal deflection effects will also be taken into consideration.

Figures 3.5-3.16 present results for two-layered beams subjected to different boundary conditions based on the G3DOFBT solution. These boundary conditions are clamped-clamped (CC), clamped-free (CF) and clamped-simply (CS). Figures 3.5-3.8 depict results for CC two-layered beam. For different values of λ, Figures 3.5 and 3.6 show the deflection and couple-stress distributions of the beam, respectively. It is noted again that the magnitude of the deflection decreases with increasing the value of λ.

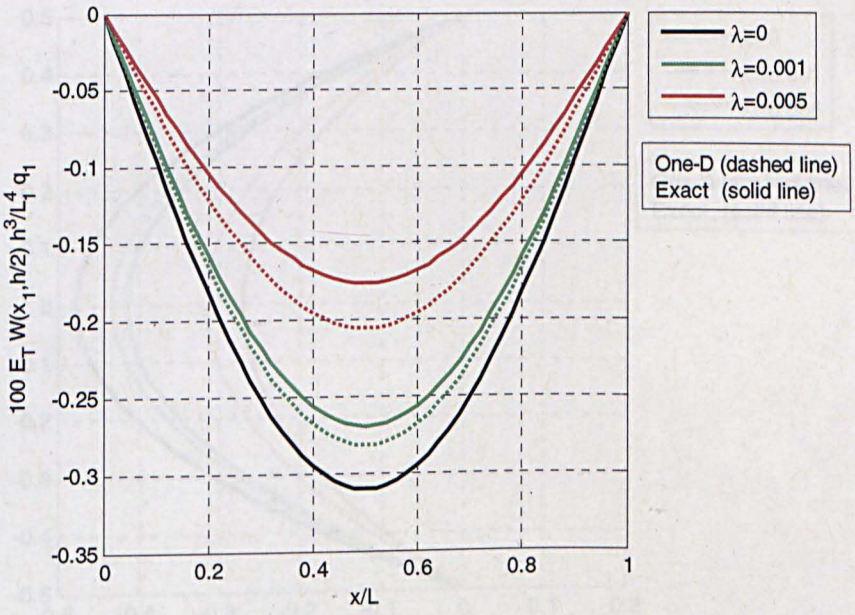

Figure 3.1 Deflection of a thin SS homogeneous beam ($h/L_1 = 0.01$)

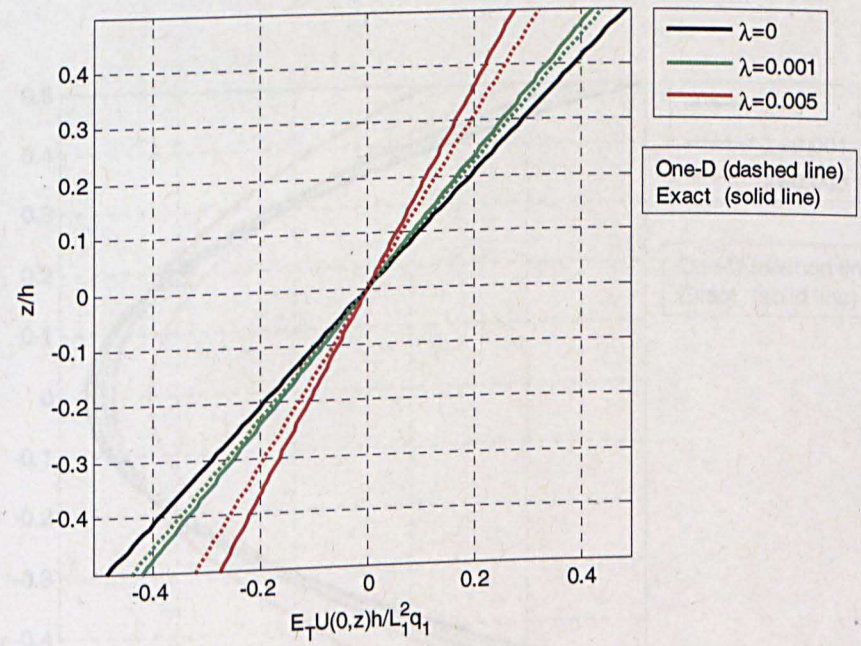

Figure 3.2 Through-thickness in-plane displacement distributions for a thin SS homogeneous beam ($h/L_1 = 0.01$)

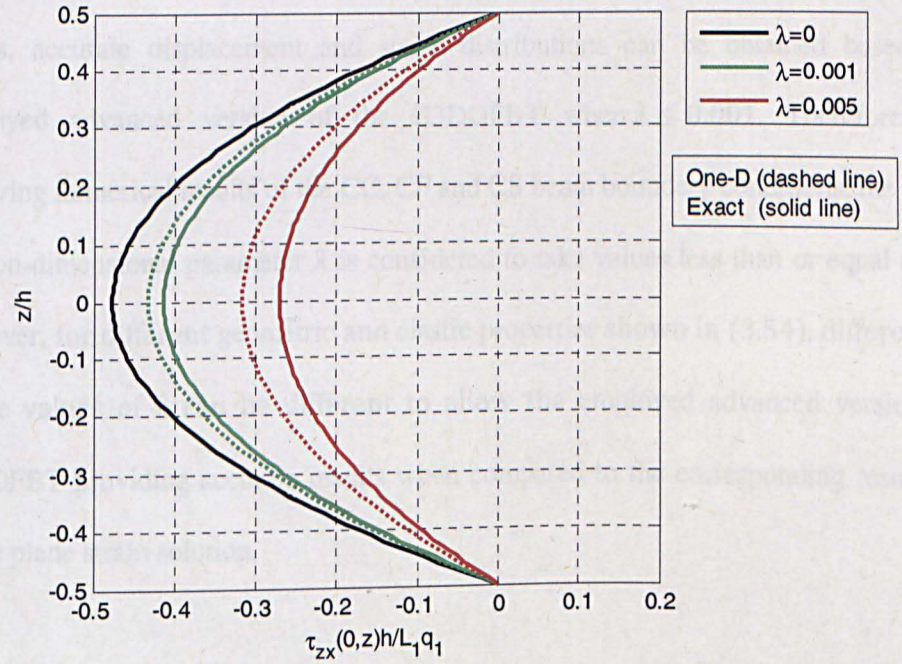

Figure 3.3 Shear stress $\frac{\tau_{zx}h}{q_1L_1}$ distributions for a SS thin homogeneous beam $(h/L_1 = 0.01)$

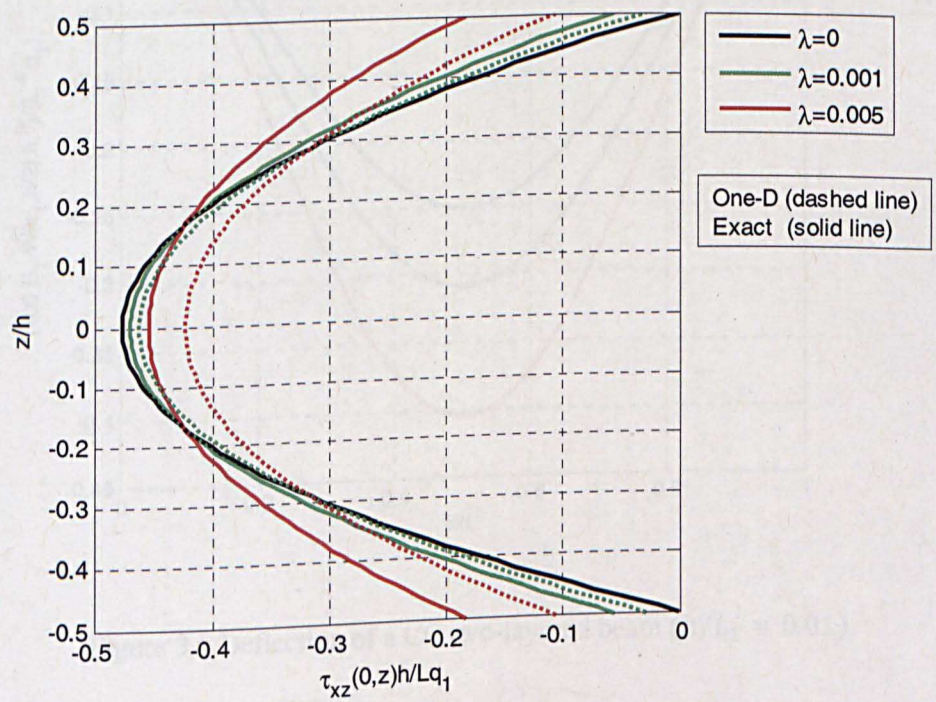

Figure 3.4 Shear stress $\frac{\tau_{xz}h}{q_1L_1}$ distributions for a SS thin homogeneous beam $(h/L_1 = 0.01)$

As aforementioned above, for the considered geometric and elastic properties of the beams, accurate displacement and stress distributions can be obtained based on the employed advanced version of the G3DOFBT when $\lambda \leq 0.001$. Therefore, in the following numerical results of the CC, CF and CS beam boundary conditions, the values of the non-dimensional parameter λ is considered to take values less than or equal to 0.001. However, for different geometric and elastic properties shown in (3.54), different range of the values of λ can be different to allow the employed advanced version of the G3DOFBT providing accurate results when compared to the corresponding results based on the plane strain solution.

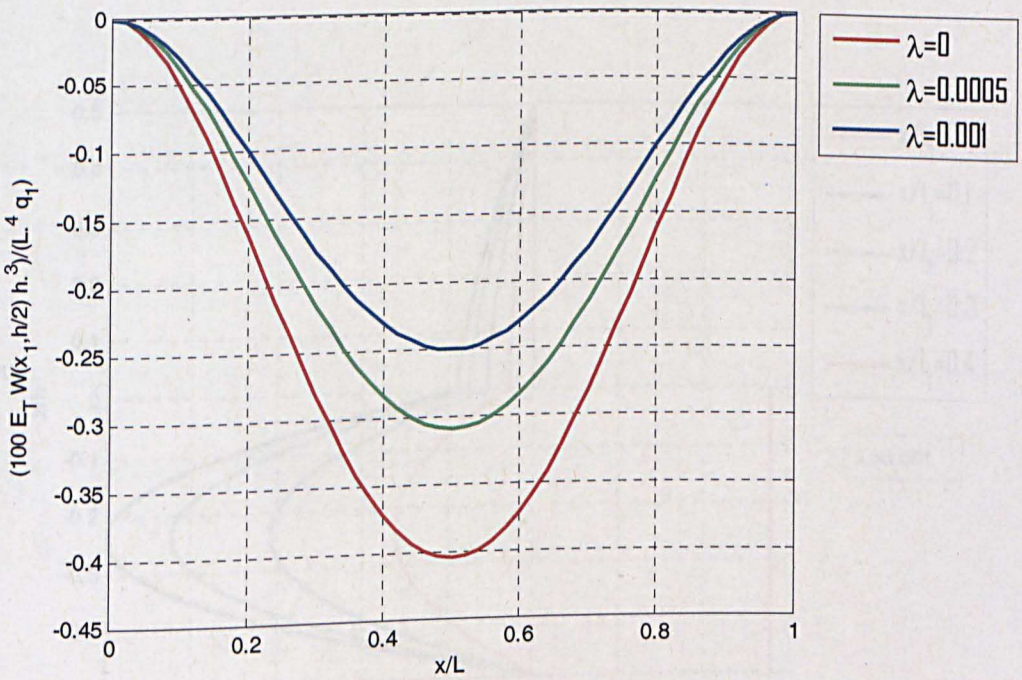

Figure 3.5 Deflection of a CC two-layered beam ($h/L_1 = 0.01$)

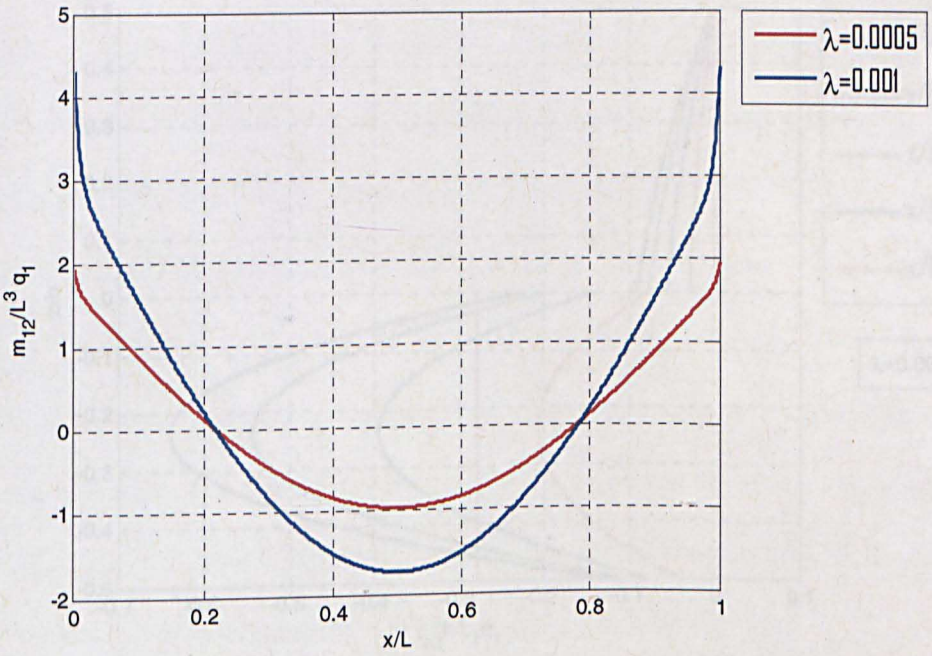

Figure 3.6 Couple-stress m_{xy} for a CC two-layered stiff beam $(h/L_1 = 0.01)$

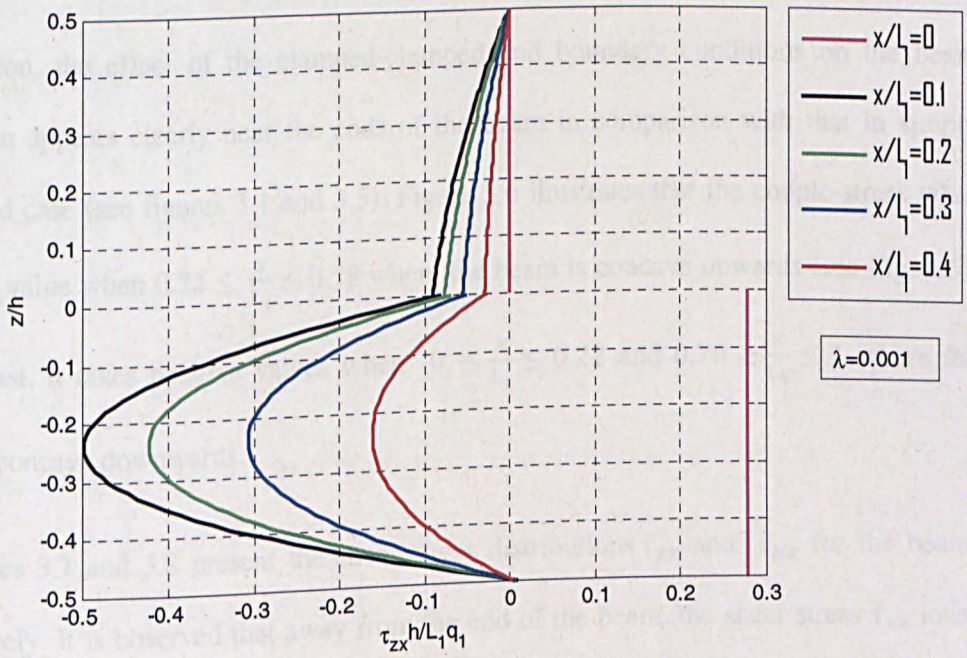

Figure 3.7 Through-thickness shear stress $\frac{\tau_{zx}h}{q_1 L_1}$ distributions for a CC two-layered stiff beam$(h/L_1 = 0.01)$

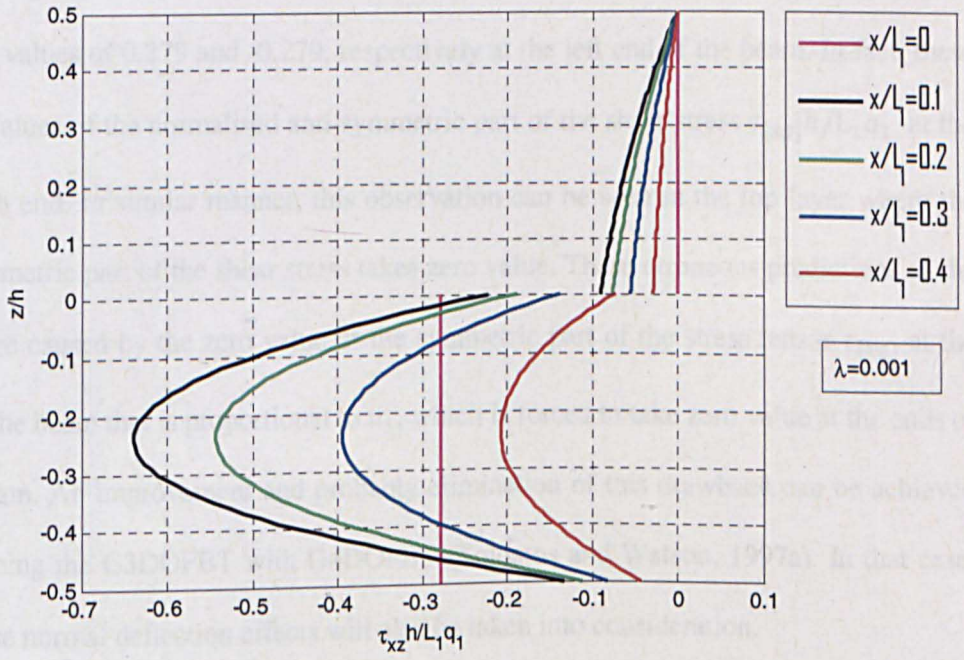

Figure 3.8 Through-thickness shear stress $\frac{\tau_{xz}h}{q_1 L_1}$ distributions for a CC two-layered stiff beam($h/L_1 = 0.01$)

In addition, the effect of the clamped-clamped end boundary conditions on the beam deflection appears clearly near the ends of the beam in comparison with that in simply supported case (see figures 3.1 and 3.5). Figure 3.6 illustrates that the couple-stress takes negative value when $0.22 \leq \frac{x}{L_1} \leq 0.78$ where the beam is concave upwards (see Fig. 3.5). In contrast, it takes positive values when $0 \leq \frac{x}{L_1} \leq 0.22$ and $0.78 \geq \frac{x}{L_1} \leq 1$ where the beam is concave downwards.

Figures 3.7 and 3.8 present the shear stress distributions $\bar{\tau}_{zx}$ and $\bar{\tau}_{xz}$ for the beam, respectively. It is observed that away from the end of the beam, the shear stress $\bar{\tau}_{xz}$ loses the continuity at the material interface ($z = 0$); the cause is when fibres resist bending $\bar{\tau}_{zx}$ and $\bar{\tau}_{xz}$ are unequal. It is of particular interest to note that in the bottom layer, although the magnitude of the shear stress $\bar{\tau}_{zx}$ and $\bar{\tau}_{xz}$ distributions is naturally increasing when

approaching the clamped end, the theory erroneously predicts that the shear stresses take abruptly values of 0.279 and -0.279, respectively at the left end of the beam. In fact, these are the values of the normalised anti-symmetric part of the shear stress $\tau_{[xz]}h/\mathrm{L}_1 q_1$ at the left beam end. In similar manner, this observation can be seen in the top layer where the anti-symmetric part of the shear stress takes zero value. These erroneous predictions of the theory are caused by the zero value of the symmetric part of the stress tensor $\tau_{(xz)}$ at the ends of the beam that is proportional to u_1, which is forced to take zero value at the ends of a CC beam. An improvement and probably elimination of this drawback can be achieved by replacing the G3DOFBT with G4DOFBT (Soldatos and Watson, 1997a). In that case, transverse normal deflection effects will also be taken into consideration.

Figures 3.9 and 3.12 show results for CF two-layered beam. For different values of λ, figures 3.9 and 3.10 present the deflection and couple-stress distributions of a CF two layered beam, respectively. Figure 3.9 emphasises again that with increasing the value of λ, the magnitude of the deflection decreases and the beam becomes stiffer. It is observed that the magnitude of the couple stress takes the maximum value at the clamped end and it decreases with increasing the value of the ratio x/L_1. It is noted further that the couple-stress takes positive values along the beam where the beam is concave downwards.

Figures 3.11 and 3.12 show the normalised transverse shear stresses distributions $\bar{\tau}_{zx}$ and $\bar{\tau}_{xz}$ of the beam, respectively. It is observed that due to the presence of couple stress, the shear stress $\bar{\tau}_{xz}$ loses the continuity that it satisfies in the case of perfectly flexible fibres. In addition, the magnitude of the two shear stresses in the top layer is much smaller than that in the bottom layer which is highly reinforced by stiff fibres ($\lambda = 0.001$) in the x-

direction. It can be seen in the bottom layer that the magnitude of the shear stress $\bar{\tau}_{xz}$ is bigger than that of $\bar{\tau}_{zx}$.

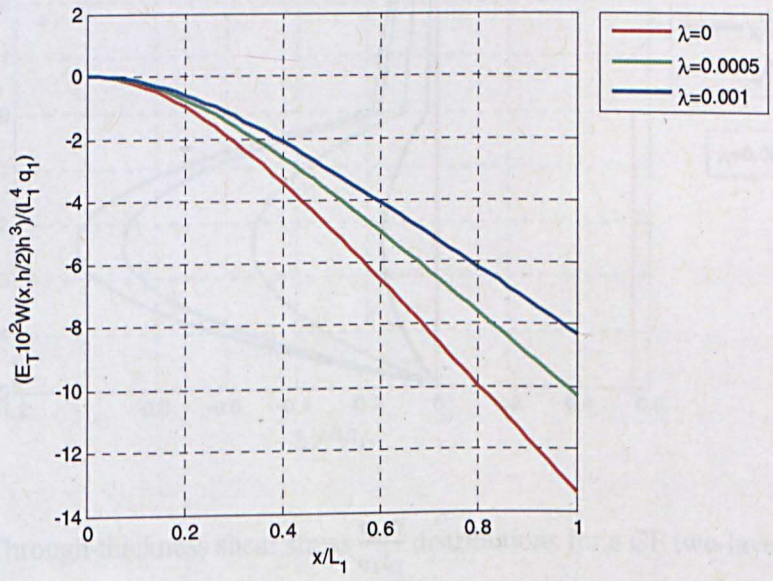

Figure 3.9 Deflection of a CF two-layered beam ($h/L_1 = 0.01$)

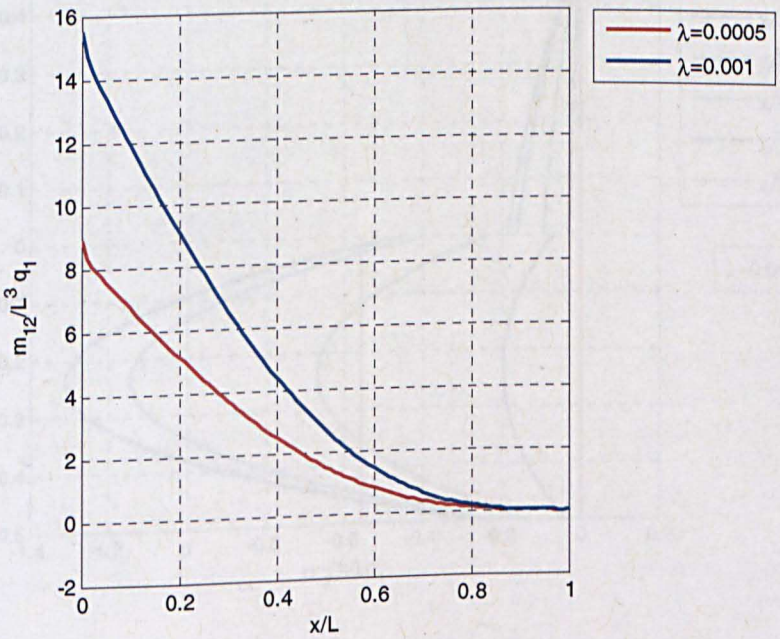

Figure 3.10 Couple-stress m_{xy} for a CF two-layered stiff beam ($h/L_1 = 0.01$)

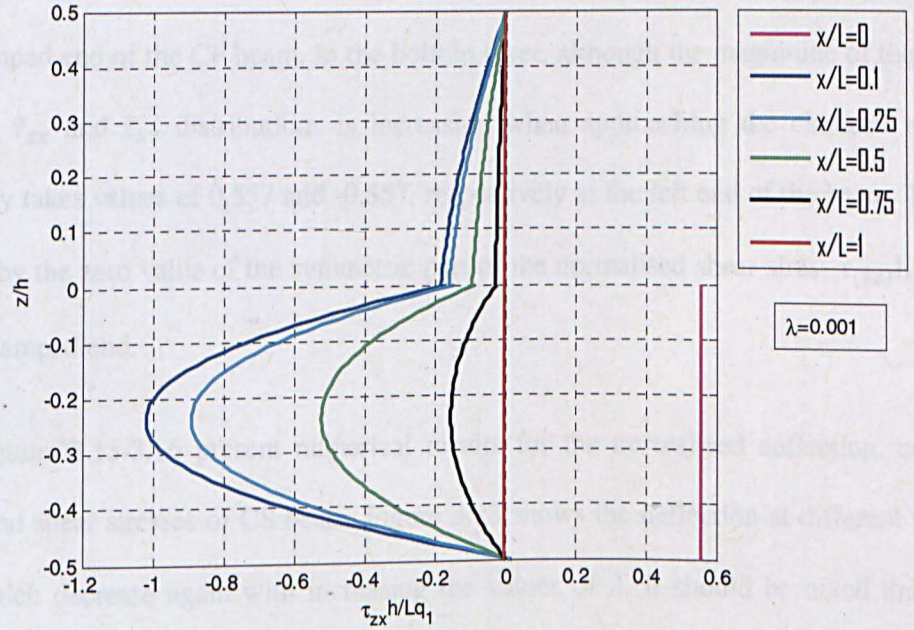

Figure 3.11 Through-thickness shear stress $\frac{\tau_{zx}h}{q_1L_1}$ distributions for a CF two-layered beam

$(h/L_1 = 0.01)$

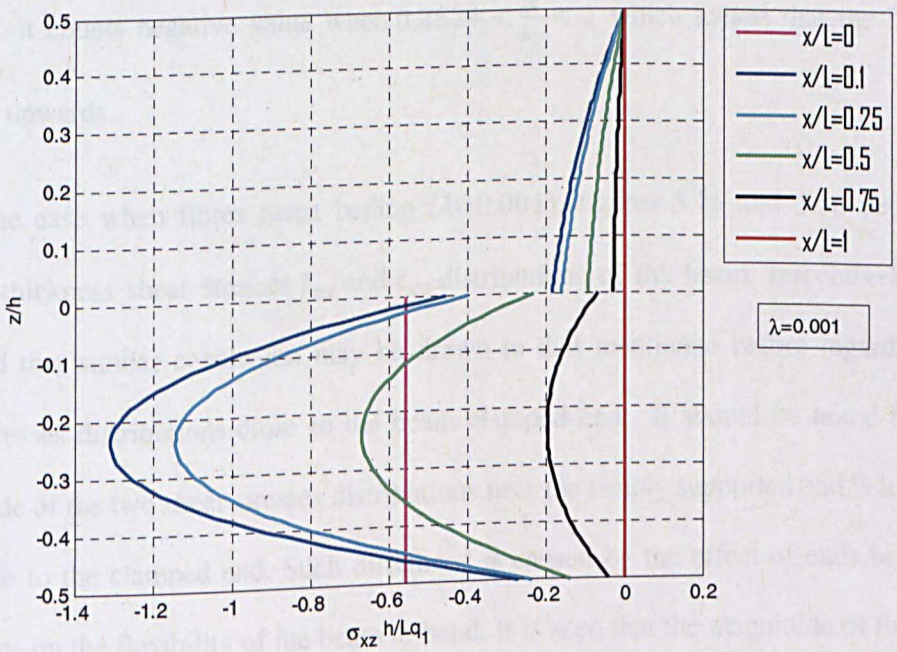

Figure 3.12 Through-thickness shear stress $\frac{\tau_{xz}h}{q_1L_1}$ distributions for a CF two-layered beam

$(h/L_1 = 0.01)$

Similar observation to that has been discussed in the clamped-clamped case is noted at the clamped end of the CF beam. In the bottom layer, although the magnitude of the shear stresses $\bar{\tau}_{zx}$ and $\bar{\tau}_{xz}$ distributions is increasing when approaching the clamped end, it suddenly takes values of 0.557 and -0.557, respectively at the left end of the beam. This is caused by the zero value of the symmetric part of the normalised shear stress $\tau_{(xz)}h/L_1q_1$ at the clamped end.

Figures 3.13-3.16 present numerical results for the normalised deflection, couple-stress and shear stresses of CS beam. Figure 3.13 shows the deflection at different values of λ which decrease again with increasing the values of λ. It should be noted that as a result of the end boundary conditions effect on the deflection lines, they behave differently at the left end from that at the right one. Figure 3.14 illustrates the couple-stress distribution for the beam which independent on the beam thickness. The positive couple-stress value, close to the clamped end, shows that the beam is concave downwards whereas, it counts negative value when $0.2524 < \frac{x}{L_1} < 1$ which means that the beam is concave upwards.

In the case when fibres resist beding (λ=0.001), figures 3.15 and 3.16 depict the through-thickness shear stresses $\bar{\tau}_{zx}$ and $\bar{\tau}_{xz}$ distributions of the beam, respectively. It is observed that similar conclusion may be drawn to that mentioned before regarding the shear stresses distributions close to the beam clamped end. It should be noted that the magnitude of the two shear stresses distributions near the simply supported end is less than that close to the clamped end. Such difference is caused by the effect of ends boundary conditions on the flexibility of the beam to bend. It is seen that the magnitude of the shear stress $\bar{\tau}_{zx}$ whithin the thickness of the bottom layer is less than that for $\bar{\tau}_{xz}$.

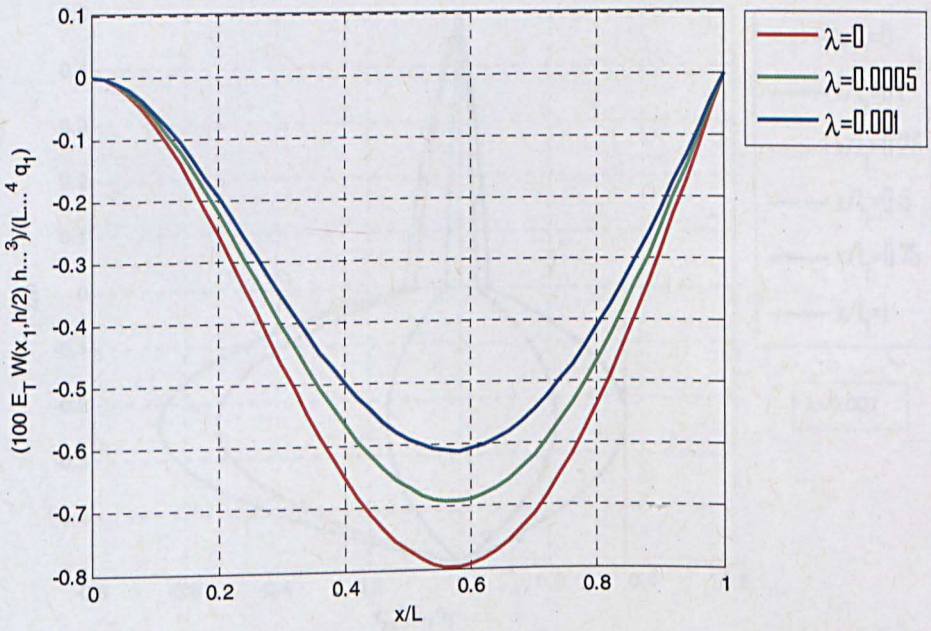

Figure 3.13 Deflection of a CS two-layered beam ($h/L_1 = 0.01$)

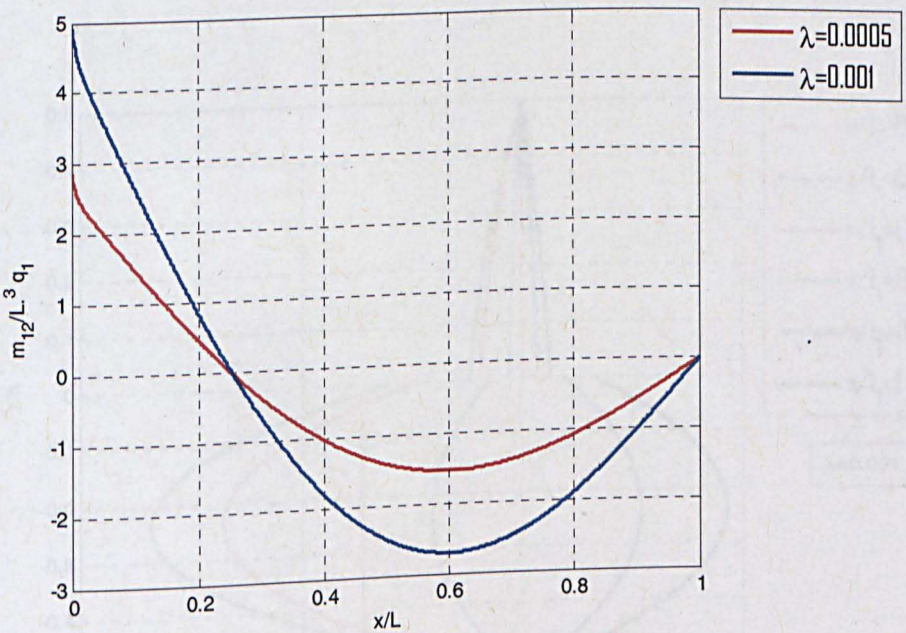

Figure 3.14 Couple-stress for a CS two-layered beam ($h/L_1 = 0.01$)

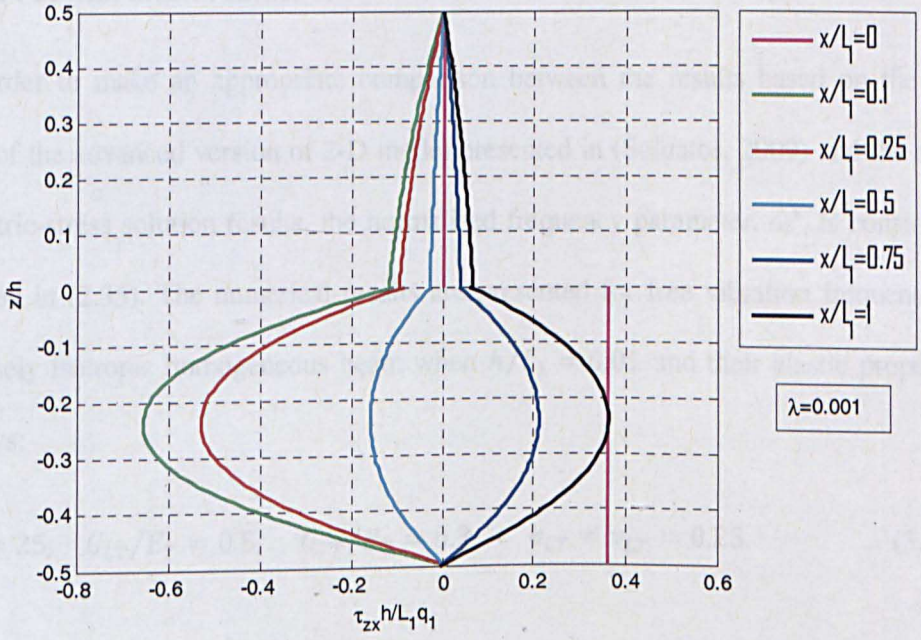

Figure 3.15 Through-thickness shear stress $\frac{\tau_{zx}h}{q_1 L_1}$ distributions for a CF two-layered stiff beam ($h/L_1 = 0.01$)

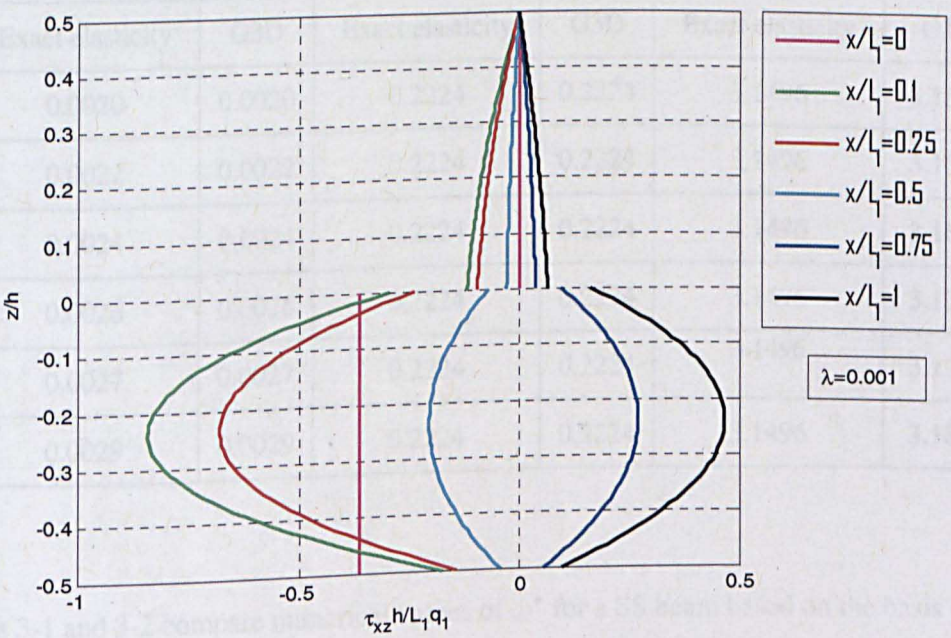

Figure 3.16 Through-thickness shear stress $\frac{\tau_{xz}h}{q_1 L_1}$ distributions for a CF two-layered stiff beam ($h/L_1 = 0.01$)

3.6.2. *Free vibration results*

In order to make an appropriate comparison between the results based on the 1-D version of the advanced version of 2-D model presented in (Soldatos, 2009) and the exact asymmetric-stress solution results, the normalised frequency parameter, ω^*, is considered as defined in (2.35). The numerical results are presented for free vibration frequency of transversely isotropic homogeneous beam when $h/L_1 = 0.01$ and their elastic properties as follows:

$$E_L/E_T = 25, \quad G_{LT}/E_T = 0.5, \quad G_{TT}/E_T = 0.2, \quad v_{LT} = v_{LT} = 0.25. \tag{3.56}$$

Table 3-1 Frequency parameter, ω^*, obtained by exact elasticity and G3D solutions of a SS beam ($h/L_1 = 0.01$)

$\lambda=\frac{l}{h}$	Fundamental frequency parameter, ω^*,		Third frequency parameter, ω^*,		Fourth frequency parameter, ω^*,	
	Exact elasticity	G3D	Exact elasticity	G3D	Exact elasticity	G3D
0	0.0020	0.0020	0.2224	0.2224	3.1496	3.1516
0.002	0.0022	0.0022	0.2224	0.2224	3.1496	3.1563
0.004	0.0024	0.0024	0.2224	0.2224	3.1496	3.1631
0.006	0.0026	0.0026	0.2224	0.2224	3.1496	3.1711
0.008	0.0027	0.0027	0.2224	0.2224	3.1496	3.1797
0.01	0.0029	0.0029	0.2224	0.2224	3.1496	3.1885

Tables 3-1 and 3-2 compare numerical values of ω^* for a SS beam based on the basis of exact asymmetric-stress elasticity solution found in chapter 2 and the present solution based on the advanced version of G3DOFBT. All comparisons shown that the general

one-dimensional beam theory employed provides an accurate normalised frequency parameter values regardless of the fibre thickness; represented by the value of λ.

Table 3-2 Frequency parameter, ω^*, obtained by exact elasticity and G3D solutions of a SS beam ($h/L_1 = 0.01$)

$\lambda=\frac{l}{h}$	Fundamental frequency parameter, ω^*,		Third frequency parameter, ω^*,		Fourth frequency parameter, ω^*,	
	Exact elasticity	G3D	Exact elasticity	G3D	Exact elasticity	G3D
0	0.0020	0.0020	0.2224	0.2224	3.1496	3.1516
0.02	0.0035	0.0035	0.2224	0.2224	3.1496	3.2301
0.04	0.0045	0.0045	0.2224	0.2224	3.1496	3.2901
0.06	0.0053	0.0053	0.2224	0.2224	3.1496	3.3277
0.08	0.0061	0.0061	0.2224	0.2224	3.1496	3.3528
0.1	0.0067	0.0067	0.2224	0.2224	3.1496	3.3707

Table 3-3 Fundamental frequency parameter, ω^*, of a SS beam ($h/L_1 = 0.01$)

$\lambda = l/h$	Exact elasticity	G3D	PSDT	CPT
0	0.0020124	0.0020121	0.0020121	0.0020171
0.002	0.0022054	0.0022058	0.0022058	0.0022104
0.004	0.0023823	0.0023839	0.0023839	0.0023881
0.006	0.0025492	0.0025495	0.0025495	0.0025534
0.008	0.0027037	0.0027050	0.0027050	0.0027087
0.01	0.0028510	0.0028521	0.0028520	0.0028556

Table 3-4 Fundamental frequency parameter, ω^*, of a SS beam ($h/L_1 = 0.01$)

$\lambda = l/h$	Exact elasticity	G3D	PSDT	CPT
0	0.0020124	0.0020121	0.0020121	0.0020171
0.02	0.0034940	0.0034958	0.0034957	0.0034985
0.04	0.0045116	0.0045158	0.0045156	0.0045179
0.06	0.0053395	0.0053445	0.0053444	0.0053462
0.08	0.0060554	0.0060610	0.0060608	0.0060625
0.1	0.0066950	0.0067013	0.0067011	0.0067026

Table 3-5 Fundamental frequency , ω^*, for a beam subjected to different boundary conditions ($h/L_1 = 0.01$)

$\lambda = l/h$	CF beam	SS beam	CS beam	CC beam
0	0.000719	0.002017	0.003151	0.004572
0.02	0.001246	0.003499	0.005465	0.007931
0.04	0.001610	0.004518	0.007058	0.010241
0.06	0.001905	0.005346	0.008352	0.012119
0.08	0.002160	0.006062	0.009471	0.013743
0.1	0.002388	0.006703	0.010471	0.015194

Tables 3-3 and 3-4 compare frequency values of ω^* obtained on the basis of advanced version of three beam theories with their counterparts obtained on the basis of aforementioned exact asymmetric-stress elasticity solution (chapter 2). The beam theories employed here are those detailed in section 3.5, namely G3DOFBT, PSDT and CPT. Regardless of the fibre thickness, represented by the values of λ, the advanced version of such one-dimensional beam theories provide values of fundamental frequency parameters

that are of good agreement with their counterparts predicted by the exact asymmetric-stress elasticity solution. Therefore, the advanced CPT is employed further for predictions only of natural frequencies of beam subjected to several sets of boundary conditions.

Table 3-5 shows frequency parameter values for ω^* of SS, CS, CC and CF beams at different values of λ. The maximum frequencies appear in the case of clamped-clamped beam while the minimum are shown when the beam is clamped-free where the beam is more flexible. Furthermore, the normalised fundamental frequency parameter values for the simply-simply supported beam are less than their counterparts of clamped-simply supported beam where the beam is less flexible. It is of particular interest to see that all the shown boundary condition cases make it immediately clear that with increasing the values of λ, the fundamental frequency values of ω^* increases. This emphasizes that with increasing the value of λ the beam becomes stiffer.

3.7. Conclusion

A new application of one-dimensional higher-order models of homogeneous and laminated composite beams has been studied in this chapter. Taking into account that the beam contains fibres which resist bending, solutions for the flexure and free vibration of a beam subjected to different end boundary conditions have been obtained on the basis of an advanced version of general three-degrees-of-freedom beam theory. The single shape function was determined by combining the appropriate equilibrium equation of asymmetric-stress three-dimensional elasticity and the one-dimensional solution for simply supported beam as discussed in (Soldatos and Watson, 1997b).

The form of the shape function obtained was explicitly dependent on a material length parameter (l) which is related to the fibres bending stiffness; represented by the elastic modulus (d^f). The flexure and free vibration problems of a simply supported thin beam were initially considered, for which exact asymmetric-stress elasticity solutions were obtained and discussed in the second chapter of this study. In order to test the reliability of the employed method, comparisons were made between corresponding numerical results based on the general three-degrees-of-freedom shear deformable beam theory and the exact asymmetric-stress elasticity solutions.

For the static solution of the small flexure of thin elastic beam having elastic properties given in (3.54), the range is estimated of the non-dimensional parameter $\lambda = l/h$, allows the G3DOFBT providing displacement and stress distributions that of good agreement with the exact asymmetric-stress elasticity solution results. Furthermore, the accuracy of the employed theory decreases with increasing the values of λ which is equivalent to increasing the effective thickness of the beam. Despite this observation, it is believed that for the thin beam having elastic properties given in (3.54),, the displacement and stress distributions, in the static problem, are still very accurate, particularly when $\lambda \leq 0.001$. However, for different geometric and elastic properties from those in this chapter, different range of the values of λ can be different to allow the employed model providing accurate results when compared to the corresponding results based on the plane strain solution.

The one-dimensional advanced beam theory is applied dealing with beams subjected to different end boundary conditions providing new stress analysis results. Results for transverse displacement and couple-stress and shear stresses distributions were obtained for a two-layered beam having (i) both of its ends clamped, and (ii) one end clamped and the other free, and (iii) one end clamped and the other simply supported. The effects of the

fibre bending stiffness on the shear stresses were shown by presenting $\bar{\tau}_{xz}$ and $\bar{\tau}_{zx}$ for each case of the end boundary conditions. It is worth mentioning that τ_{xz} and τ_{zx} are identical in the case of perfectly flexible fibres (λ=0). On the contrary, when fibres resist bending ($\lambda \neq 0$), $\tau_{xz} \neq \tau_{zx}$.

It was observed that suddenly change was counted for the magnitude of two shear stresses τ_{xz} and τ_{zx} at the beams clamped end. This is apparently due to the limitation of the G3DOFBT. Neglecting the transverse normal deformation has erroneously been assumed for simplification in G3DOFBT making $\tau_{(xz)}$ proportional to u_1, which is forced by the end boundary conditions to take zero values at the beams clamped end. The way to avoid this drawback is to replace the G3DOFBT with the G4DOFBT which takes transverse normal deformation into account. This observation was seen in the case of perfectly flexible fibres (Soldatos and Watson, 1997b).

In the dynamic case, no limitation has been seen for the values of λ to allow the G3DOFBT providing accurate results when compared with their counterparts that based on the exact asymmetric-stress elasticity solution when the beam is simply supported at the ends $x = 0$ and $x = L_1$. An advanced version of three general one-dimensional beam theories was employed and gave results of good agreement of the fundamental frequency parameter with their counterparts of the exact solution. The fundamental frequency parameter of SS, CS, CC and CF homogeneous beams were provided based on one of aforementioned one-dimensional beam theories which is CPT presented in (Soldatos, 2009). It is of particular interest to observe that the obtained numerical results in the shown boundary condition cases emphasise that the values of ω^* increases with increasing the value of λ.

3.8. Further work

In a similar manner, an application of the new version of the general five-degrees-of-freedom plate theory (Soldatos, 2009) for flexure and free vibration of rectangular plate subjected to different sets of end boundary conditions is proposed to be studied in the fifth chapter. The three-dimensional asymmetric-stress elasticity solution will be obtained for simply supported boundary conditions in chapter four which will serve as a benchmark to assess the accuracy of the five-degrees-of-freedom plate theory.

Chapter 4. Asymmetric-stress elasticity analysis for the three-dimensional statics and dynamics of a simply supported rectangular plate

4.1. Introduction

In this chapter, three-dimensional asymmetric-stress elasticity solutions of small flexure and free vibration of transversely isotropic elastic cross-ply laminated rectangular plate will be discussed. It is considered that the plate contains fibres which posses bending stiffness. The discussion is based on the analytical solution of relevant differential equations of asymmetric-stress elasticity theory (Spencer and Soldatos, 2007, Soldatos, 2009). when the fibres possess bending stiffness.

The main purposes of this chapter are to solve the static and dynamic problem and to investigate the effect of fibre bending stiffness on the deformed plate. In this investigation, the analyses of displacements, stresses distributions as well as the plate frequency values will be conducted. Numerical results are provided based on the obtained solutions for rectangular plates those have different values of the ratio L_2/L_1. In order to show the relation between those solutions and the plane strain solutions constructed in chapter two, numerical results for the case of a rectangular plat that has a large value of the ratio L_2/L_1 are computed. This chapter is provided with comparisons between numerical results based on the obtained static and dynamic 3-D asymmetric-stress elasticity solutions (when the

plate extends from $-\infty$ to $+\infty$ in the y direction) and their counterparts based on the plane strain asymmetric-stress elasticity solutions found in the second chapter.

4.2. Problem formulation

Consider a transversely isotropic, linearly elastic cross-ply laminated rectangular plate having arbitrary constant thickness h in the z direction, horizontal constant length L_1 in the x direction and width L_2 in the y direction. Moreover, the plate is assumed to be simply supported on the four edges x=0, $x = L_1$, y=0 and $y = L_2$ (SSSS).

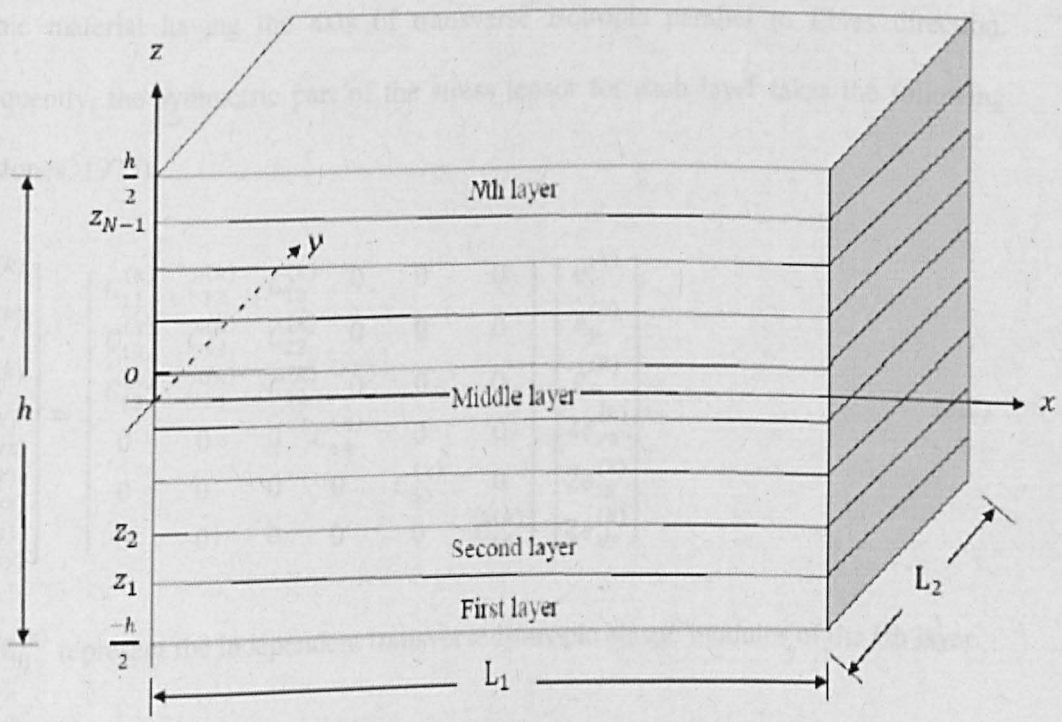

Figure 4.1 An example of N-layer elastic plate

The plate is subjected to small static flexure caused by the action of a given external lateral loading $q(x,y)$ or to dynamic flexure. The additional standard infinitesimal strain tensor components to that met in the second chapter (see equation 2.1) are as follows:

$$e_{yy} = V_{,y},\ 2e_{xy} = U_{,y} + V_{,x},\ 2e_{yz} = V_{,z} + W_{,y}, \tag{4.1}$$

where V is the additional displacement function in y direction to the displacement function U and W seen in the second chapter.

Assume, now that the plate is composed of an arbitrary number, N, of transversely isotropic layers. For identifying the layers of the plate, an index (k) is introduced, where the bottom layer corresponds to $k = 1$ (see figure 4.1). The symmetric part of the stress tensor in each layer obeys the form of generalized Hooke's law in the case of transversely isotropic material having the axis of transverse isotropic parallel to fibres direction. Consequently, the symmetric part of the stress tensor for each layer takes the following form (Jones, 1975):

$$\begin{bmatrix} \sigma_x^{(k)} \\ \sigma_y^{(k)} \\ \sigma_z^{(k)} \\ \tau_{(yz)}^{(k)} \\ \tau_{(xz)}^{(k)} \\ \tau_{(xy)}^{(k)} \end{bmatrix} = \begin{bmatrix} C_{11}^{(k)} & C_{13}^{(k)} & C_{13}^{(k)} & 0 & 0 & 0 \\ C_{13}^{(k)} & C_{33}^{(k)} & C_{23}^{(k)} & 0 & 0 & 0 \\ C_{13}^{(k)} & C_{23}^{(k)} & C_{33}^{(k)} & 0 & 0 & 0 \\ 0 & 0 & 0 & C_{44}^{(k)} & 0 & 0 \\ 0 & 0 & 0 & 0 & C_{55}^{(k)} & 0 \\ 0 & 0 & 0 & 0 & 0 & C_{66}^{(k)} \end{bmatrix} \begin{bmatrix} e_x^{(k)} \\ e_y^{(k)} \\ e_z^{(k)} \\ 2e_{yz}^{(k)} \\ 2e_{xz}^{(k)} \\ 2e_{xy}^{(k)} \end{bmatrix}, \tag{4.2}$$

where $C_{ij}^{(k)}$ represent the independent transverse isotropic elastic modules of the kth layer.

The anti-symmetric part of the associated shear stress tensor component $\tau_{[xz]}$ is defined in equation (2.3) and the other one $\tau_{[xy]}$ is defined as follows:

$$\tau_{[xy]}^{(k)} = -\frac{1}{2} m_{xz,x}^{(k)}, \tag{4.3}$$

where m_{xz} represents the non-zero couple stress which is related to the fibre curvature as follows, (Soldatos, 2009):

$$m_{xz}^{(k)} = d^{f^{(k)}} K_y^{f^{(k)}} = \frac{1}{2} d^{f^{(k)}} V_{,xx}^{(k)}. \tag{4.4}$$

Here $K_y^{f^{(k)}}$ represents the fibre curvature in y direction.

In addition to shear stresses mentioned in equation (2.6), the other shear stresses take the following form:

$$\tau_{xy}^{(k)} = \tau_{(xy)}^{(k)} + \tau_{[xy]}^{(k)}, \tag{4.5.a}$$

$$\tau_{yx}^{(k)} = \tau_{(xy)}^{(k)} - \tau_{[xy]}^{(k)}. \tag{4.5.b}$$

Accordingly, the equations of motion of three-dimensional asymmetric-stress elasticity (Soldatos, 2009) take the following form:

$$\begin{aligned}
&\sigma_{x,x}^{(k)} + \tau_{(xy),y}^{(k)} - \tau_{[xy],y}^{(k)} + \tau_{(xz),z}^{(k)} - \tau_{[xz],z}^{(k)} = \rho \ddot{U}^{(k)}, \\
&\tau_{(xy),x}^{(k)} + \tau_{[xy],x}^{(k)} + \sigma_{y,y}^{(k)} + \tau_{(yz),z}^{(k)} = \rho \ddot{V}^{(k)}, \\
&\tau_{(xz),x}^{(k)} + \tau_{[xz],x}^{(k)} + \tau_{(yz),y}^{(k)} + \sigma_{z,z}^{(k)} = \rho \ddot{W}^{(k)}.
\end{aligned} \tag{4.6}$$

It is worth mentioning that when the stress couples defined in equations (2.4) and (4.4) take zero value, the shear stresses ((2.6) & (4.5)) and the equations of motion (4.6) will be reduced to their counterparts met in linear symmetric elasticity theory and discussed for orthotropic rectangular plate in (Srinivas and Rao, 1970).

The lateral boundary conditions are formed as follows:

$$\sigma_z\left(x, y, \frac{h}{2}\right) = q(x, y), \ \sigma_z\left(x, y, \frac{-h}{2}\right) = 0,$$

$$\tau_{yz}\left(x,y,\frac{h}{2}\right)=0,\ \tau_{yz}\left(x,y,\frac{-h}{2}\right)=0, \tag{4.7}$$

$$\tau_{zx}\left(x,y,\frac{h}{2}\right)=0,\ \tau_{zx}\left(x,y,\frac{-h}{2}\right)=0,$$

where $q(x,y)$ is the external lateral loading which acts normally and downwards on its top lateral plane of the plate. Such loading can be expressed in the following Fourier series:

$$q(x,y)=\sum_{m=1}^{\infty}\sum_{n=1}^{\infty}q_{mn}\,sin(Mx)\ sin(Ny), \tag{4.8}$$

where $M=m\pi/\mathrm{L}_1$, $N=n\pi/\mathrm{L}_2$ and $(m=1,2,\ldots\,\&\,n=1,2,\ldots)$.

In addition, the simply supported edge boundary conditions on straight edges $x=0$ and $x=\mathrm{L}_1$ are described as follows:

$$\sigma_x(0,y,z)=0,\ \sigma_x(L_1,y,z)=0, \tag{4.9.a.1}$$

$$V(0,y,z)=0,\ V(L_1,y,z)=0, \tag{4.9.a.2}$$

$$W(0,y,z)=0,\ W(L_1,y,z)=0, \tag{4.9.a.3}$$

$$m_{xy}(0,y,z)=0,\ m_{xy}(L_1,y,z)=0, \tag{4.9.a.4}$$

$$m_{xz}(0,x,z)=0,\ m_{xz}(L_1,y,z)=0, \tag{4.9.a.5}$$

At edges $y=0$ and $y=\mathrm{L}_2$, they are specified as follows:

$$\sigma_y(x,0,z)=0,\ \sigma_y(x,L_2,z)=0, \tag{4.9.b.1}$$

$$U(x,0,z)=0,\ U(x,L_2,z)=0, \tag{4.9.b.2}$$

$$W(x,0,z)=0,\ W(x,L_2,z)=0. \tag{4.9.b.3}$$

Furthermore, at the interface $z = z_k (k = 1,2,\dots,N-1)$, the equilibrium conditions are:

$$\sigma_z{}^{(k)}\big|_{z=z_k} = \sigma_z{}^{(k+1)}\big|_{z=z_k}, \tag{4.10.a}$$

$$(\tau^{(k)}{}_{(xz)} - \tau^{(k)}{}_{[xz]})\big|_{z=z_k} = (\tau^{(k+1)}{}_{(xz)} - \tau^{(k+1)}{}_{[xz]})\big|_{z=z_k}, \tag{4.10.b}$$

$$(\tau^{(k)}{}_{(yz)})\big|_{z=z_k} = (\tau^{(k+1)}{}_{(yz)})\big|_{z=z_k}. \tag{4.10.c}$$

While the continuity conditions of displacements take the following form:

$$\begin{aligned} U^{(k)}(x,z)\big|_{z=z_k} &= U^{(k+1)}(x,z)\big|_{z=z_k}, \\ V^{(k)}(x,z)\big|_{z=z_k} &= V^{(k+1)}(x,z)\big|_{z=z_k}, \\ W^{(k)}(x,z)\big|_{z=z_k} &= W^{(k+1)}(x,z)\big|_{z=z_k}. \end{aligned} \tag{4.11}$$

4.3. Navier-type partial differential equations

With use of the equations (2.1-6) and (4.1-5), one can write the equations of motion (4.6) in terms of displacements yielding the following Navier-type equations:

$$\begin{aligned} &C_{11}^{(k)}U_{,xx}^{(k)} + C_{55}^{(k)}U_{,yy}^{(k)} + C_{55}^{(k)}U_{,zz}^{(k)} + \left(C_{13}^{(k)} + C_{55}^{(k)}\right)V_{,xy}^{(k)} + \frac{hL_1C_{11}^{(k)}}{24}\lambda^{(k)}W_{,xxxy}^{(k)} + (C_{13}^{(k)} + \\ &C_{55}^{(k)})\,W_{,xz}^{(k)} + \frac{hL_1C_{11}^{(k)}}{24}\lambda^{(k)}W_{,xxxz}^{(k)} = \rho\ddot{U}, \\ &\left(C_{13}^{(k)} + C_{55}^{(k)}\right)U_{,xy}^{(k)} + C_{55}^{(k)}V_{,xx}^{(k)} + C_{33}^{(k)}V_{,yy}^{(k)} + C_{44}^{(k)}V_{,zz}^{(k)} - \frac{hL_1C_{11}^{(k)}}{24}\lambda^{(k)}V_{,xxxx}^{(k)} + (C_{23}^{(k)} + \\ &C_{44}^{(k)})\,W_{,yz}^{(k)} = \rho\ddot{V}, \end{aligned} \tag{4.12}$$

$$\left(C_{13}^{(k)}+C_{55}^{(k)}\right)U_{,xz}^{(k)}+\left(C_{23}^{(k)}+C_{44}^{(k)}\right)V_{,yz}^{(k)}+C_{55}^{(k)}W_{,xx}^{(k)}+C_{44}^{(k)}W_{,yy}^{(k)}+C_{33}^{(k)}W_{,zz}^{(k)}-$$

$$\frac{hL_1C_{11}^{(k)}}{24}\lambda^{(k)}W_{,xxxx}^{(k)}=\rho\ddot{W}$$

where $0\le x\le L_1$, $0\le y\le L_2$, $-\frac{h}{2}\le z\le\frac{h}{2}$, $\lambda^{(k)}=\frac{l^{(k)}}{h}$. (4.13)

These can be re-arranged in the following matrix form:

$$\boldsymbol{A}.\boldsymbol{X}=\boldsymbol{J}, \tag{4.14}$$

where

$$\boldsymbol{A}=\begin{bmatrix}a_{11} & a_{12} & a_{13}\\ a_{21} & a_{22} & a_{23}\\ a_{31} & a_{32} & a_{33}\end{bmatrix},\ =[U^{(k)}\quad V^{(k)}\quad W^{(k)}]^T,\ \boldsymbol{J}=[\rho\ddot{U}\quad \rho\ddot{V}\quad \rho\ddot{W}]^T, \tag{4.15}$$

$$a_{11}=C_{11}^{(k)}\frac{\partial^2}{\partial x^2}+C_{55}^{(k)}\frac{\partial^2}{\partial y^2}+C_{55}^{(k)}\frac{\partial^2}{\partial z^2},\ a_{12}=\left(C_{13}^{(k)}+C_{55}^{(k)}\right)\frac{\partial^2}{\partial x\partial y}+\frac{hL_1C_{11}^{(k)}}{24}\lambda^{(k)}\frac{\partial^4}{\partial x^3\partial y},$$

$$a_{13}=\left(C_{13}^{(k)}+C_{55}^{(k)}\right)\frac{\partial^2}{\partial x\partial z}+\frac{hL_1C_{11}^{(k)}}{24}\lambda^{(k)}\frac{\partial^4}{\partial x^3\partial z},\ a_{21}=\left(C_{13}^{(k)}+C_{55}^{(k)}\right)\frac{\partial^2}{\partial x\partial y},$$

$$a_{22}=C_{55}^{(k)}\frac{\partial^2}{\partial x^2}+C_{33}^{(k)}\frac{\partial^2}{\partial y^2}+C_{44}^{(k)}\frac{\partial^2}{\partial z^2}-\frac{hL_1C_{11}^{(k)}}{24}\lambda^{(k)}\frac{\partial^4}{\partial x^4},\ a_{23}=\left(C_{23}^{(k)}+C_{44}^{(k)}\right)\frac{\partial^2}{\partial y\partial z}, \tag{4.16}$$

$$a_{31}=\left(C_{13}^{(k)}+C_{55}^{(k)}\right)\frac{\partial^2}{\partial x\partial z},\ a_{32}=\left(C_{23}^{(k)}+C_{44}^{(k)}\right)\frac{\partial^2}{\partial y\partial z},$$

$$a_{33}=C_{55}^{(k)}\frac{\partial^2}{\partial x^2}+C_{44}^{(k)}\frac{\partial^2}{\partial y^2}+C_{33}^{(k)}\frac{\partial^2}{\partial z^2}-\frac{hL_1C_{11}^{(k)}}{24}\lambda^{(k)}\frac{\partial^4}{\partial x^4}.$$

The Navier-type equations (4.14) are susceptible of an exact solution, provided that the plate edges are subjected to the set of sixteen simply supported boundary conditions (4.9).

The static and dynamic solutions of equations (4.14) will be discussed in sections 4.4 and 4.5, respectively.

4.4. Static solution

For the flexure problem of the described SSSS rectangular plate, the inertia terms appearing in the right-hand sides of equations (4.6), (4.12) and (4.14) are disregarded yielding the following equilibrium equations:

$$\boldsymbol{A}.\boldsymbol{X} = 0. \tag{4.17}$$

It is observed that when the stress couples defined in equations (2.4) and (4.4) take zero value, the equations of motion (4.17) will be reduced to their counterparts met in linear elasticity theory and discussed for orthotropic rectangular plate in (Pagano, 1970a).

The set of SSSS edge boundary conditions (4.9) are identically satisfied by choosing the displacement field in the following form of trigonometric series:

$$U^{(k)} = h\sum_{m=1}^{\infty}\sum_{n=1}^{\infty} \phi^{(k)}(Z)\cos(m\pi X)\sin(n\pi Y), \tag{4.18.a}$$

$$V^{(k)} = h\sum_{m=1}^{\infty}\sum_{n=1}^{\infty} \psi^{(k)}(Z)\sin(m\pi X)\cos(n\pi Y), \tag{4.18.b}$$

$$W^{(k)} = h\sum_{m=1}^{\infty}\sum_{n=1}^{\infty} \chi^{(k)}(Z)\sin(m\pi X)\sin(n\pi Y). \tag{4.18.c}$$

Here, $X = \frac{x}{L_1}$, $Y = \frac{y}{L_2}$, $Z = \frac{z}{h}$ and, therefore,

$$0 \le X \le 1,\ 0 \le Y \le 1,\ -\frac{1}{2} \le Z \le \frac{1}{2}. \tag{4.19}$$

For each combination of m and n, the substitution of equations (4.18) in the equilibrium equations (4.17) converts them to the following set of ordinary differential equations:

$$\boldsymbol{G}(D)\,.\,\boldsymbol{B}=0, \tag{4.20}$$

where

$$\boldsymbol{G}(D)=\begin{bmatrix} d_1^{(k)}+d_2^{(k)}D^2 & d_3^{(k)}+d_{10}^{(k)} & d_4^{(k)}D+d_{11}^{(k)}D \\ d_3^{(k)} & d_5^{(k)}+d_6^{(k)}D^2+d_{12}^{(k)} & d_7^{(k)}D \\ -d_4^{(k)}D & -d_7^{(k)}D & d_8^{(k)}+d_9^{(k)}D^2+d_{12}^{(k)} \end{bmatrix}, \tag{4.21.a}$$

$$\boldsymbol{B}=\begin{bmatrix} \phi^{(k)}(Z) \\ \psi^{(k)}(Z) \\ \chi^{(k)}(Z) \end{bmatrix}, \tag{4.21.b}$$

and

$$D=\frac{d}{dZ},\ d_1^{(k)}=-h^2(M^2+N^2(C_{55}^{(k)}/C_{11}^{(k)})),\ d_2^{(k)}=C_{55}^{(k)}/C_{11}^{(k)},$$

$$d_3^{(k)}=h^2MN(C_{13}^{(k)}+C_{55}^{(k)})/C_{11}^{(k)},\ d_4^{(k)}=h\,M\,(C_{13}^{(k)}+C_{55}^{(k)})/C_{11}^{(k)},$$

$$d_5^{(k)}=-h^2(M^2C_{55}^{(k)}+N^2C_{33}^{(k)})/C_{11}^{(k)},\ d_6^{(k)}=C_{44}^{(k)}/C_{11}^{(k)}, \tag{4.22}$$

$$d_7^{(k)}=hN(C_{23}^{(k)}+C_{44}^{(k)})/C_{11}^{(k)},\ d_8^{(k)}=-h^2(C_{55}^{(k)}M^2+C_{44}^{(k)}N^2)/C_{11}^{(k)},$$

$$d_9^{(k)}=C_{33}^{(k)}/C_{11}^{(k)},\ d_{10}^{(k)}=\frac{h^2}{24}M^3N\,l^{(k)}L_1,\ d_{11}^{(k)}=-\frac{h}{24}M^3\,l^{(k)}L_1,$$

$$d_{12}^{(k)}=-\frac{h^2}{24}M^4\,l^{(k)}L_1.$$

For a non-trivial solution of equation (4.20), the determinant of $\boldsymbol{G}$ must be zero. This condition yields the following characteristic equation:

$$det\,(\boldsymbol{G}(p))=0 \tag{4.23}$$

or

$$d_2^{(k)}d_6^{(k)}d_9^{(k)}\,p^6+(d_2^{(k)}d_7^{(k)^2}+d_2^{(k)}d_5^{(k)}d_9^{(k)}+d_2^{(k)}d_6^{(k)}d_8^{(k)}+d_2^{(k)}d_6^{(k)}d_{12}^{(k)}+$$

$$d_2^{(k)}d_9^{(k)}d_{12}^{(k)}+d_1^{(k)}d_6^{(k)}d_9^{(k)}+d_4^{(k)}d_6^{(k)}d_{11}^{(k)}+d_4^{(k)^2}d_6^{(k)})p^4+(d_2^{(k)}d_{12}^{(k)^2}+d_3^{(k)^2}d_9^{(k)}$$

$$+d_1^{(k)}d_7^{(k)^2}+d_2^{(k)}d_5^{(k)}d_8^{(k)}+d_2^{(k)}d_5^{(k)}d_{12}^{(k)}+d_2^{(k)}d_8^{(k)}d_{12}^{(k)}+d_1^{(k)}d_5^{(k)}d_9^{(k)}+d_1^{(k)}d_6^{(k)}d_8^{(k)}$$

$$+d_1^{(k)}d_6^{(k)}d_{12}^{(k)}+d_1^{(k)}d_9^{(k)}d_{12}^{(k)}-2d_3^{(k)}d_4^{(k)}d_7^{(k)}-d_3^{(k)}d_7^{(k)}d_{11}^{(k)}-d_3^{(k)}d_9^{(k)}d_{10}^{(k)}+$$

$$-d_4^{(k)}d_7^{(k)}d_{10}^{(k)}+d_4^{(k)}d_5^{(k)}d_{11}^{(k)}+d_4^{(k)}d_{11}^{(k)}d_{12}^{(k)}+d_4^{(k)^2}d_5^{(k)}+d_4^{(k)^2}d_{12}^{(k)})\,p^2+$$

$$(d_1^{(k)}d_5^{(k)}d_8^{(k)}+d_1^{(k)}d_5^{(k)}d_{12}^{(k)}+d_1^{(k)}d_8^{(k)}d_{12}^{(k)}+d_1^{(k)}d_{12}^{(k)^2}-d_3^{(k)^2}d_8^{(k)}-d_3^{(k)^2}d_{12}^{(k)}-$$

$$d_3^{(k)}d_8^{(k)}d_{10}^{(k)}-d_3^{(k)}d_{10}^{(k)}d_{12}^{(k)})=0, \tag{4.24}$$

solution of which gives six characteristic values $p_i^{(k)}$ $(i=1,\dots,6)$. The eigenvector corresponding to a non-repeated root $p=p_i^{(k)}$ is as follows:

$$\begin{bmatrix}\phi_i^{(k)}\\ \psi_i^{(k)}\\ \chi_i^{(k)}\end{bmatrix}=$$

$$\begin{bmatrix}((d_4^{(k)}+d_{11}^{(k)})(d_5^{(k)}+d_6^{(k)}p_i^{(k)^2}+d_{12}^{(k)})-d_7^{(k)}(d_3^{(k)}+d_{10}^{(k)}))p_i^{(k)}\\ (d_7^{(k)}(d_1^{(k)}+d_2^{(k)}p_i^{(k)^2})-d_3^{(k)}(d_4^{(k)}+d_{11}^{(k)}))p_i^{(k)}\\ -(d_1^{(k)}+d_2^{(k)}p_i^{(k)^2})(d_5^{(k)}+d_6^{(k)}p_i^{(k)^2}+d_{12}^{(k)})+d_3^{(k)}(d_3^{(k)}+d_{10}^{(k)})\end{bmatrix}A\,e^{p_i^{(k)}z}, \tag{4.25}$$

where A is an arbitrary constant. The main reason of considering the non-repeated roots of equation (4.24) is that the material is anisotropic namely the elastic coefficients $C_{ij}^{(k)}$ have different values. In addition, if the roots are repeated or some of them are, other

calculations need to be done to construct the displacement field. The expression of $\phi^{(k)}$, $\psi^{(k)}$ and $\chi^{(k)}$ can be given in the following form:

$$\begin{bmatrix}\phi^{(k)}\\ \psi^{(k)}\\ \chi^{(k)}\end{bmatrix} =$$

$$\sum_{m=1}^{6} A_i^{(k)} \begin{bmatrix} ((d_4^{(k)} + d_{11}^{(k)})(d_5^{(k)} + d_6^{(k)} p_i^{(k)^2} + d_{12}^{(k)}) - d_7^{(k)}(d_3^{(k)} + d_{10}^{(k)}))p_i^{(k)} \\ (d_7^{(k)}(d_1^{(k)} + d_2^{(k)} p_i^{(k)^2}) - d_3^{(k)}(d_4^{(k)} + d_{11}^{(k)}))p_i^{(k)} \\ -(d_1^{(k)} + d_2^{(k)} p_i^{(k)^2})(d_5^{(k)} + d_6^{(k)} p_i^{(k)^2} + d_{12}^{(k)}) + d_3^{(k)}(d_3^{(k)} + d_{10}^{(k)}) \end{bmatrix} e^{p_i^{(k)} Z}, \quad (4.26)$$

where $A_i^{(k)}$ $(i = 1,2,\dots,6\,;\, k = 1,\dots N)$ are $6N$ arbitrary constants which will be determined in subsection 4.4.1 in similar way followed in the subsection 2.4.1. Inserting equations (4.22), (4.26) into equations (4.18) yields the expression of the displacement field of the present static problem.

4.4.1. Expressions of stresses, couple-stress and interface continuity conditions

Inserting of equations (4.18), (4.22) and (4.26) into the stress-strain relationships (4.2) yields the following normal and the symmetric part of the shear stresses:

$$\sigma_x^{(k)} = h \sum_{m=1}^{\infty}\sum_{n=1}^{\infty} (-C_{11}^{(k)} M\, \phi^{(k)}(Z) - C_{13}^{(k)} N\, \psi^{(k)}(Z) +$$

$$+ \frac{C_{13}^{(k)}}{h} D\, \chi^{(k)}(Z)\,)\, sin(m\pi X)\, sin(n\pi Y), \quad (4.27.a)$$

$$\sigma_y^{(k)} = h \sum_{m=1}^{\infty}\sum_{n=1}^{\infty} (-C_{12}^{(k)} M\, \phi^{(k)}(Z) - C_{33}^{(k)} N\, \psi^{(k)}(Z) +$$

$$\frac{C_{23}^{(k)}}{h} D\ \chi^{(k)}(Z))\ sin(m\pi X)\, sin(n\pi Y), \tag{4.27.b}$$

$$\sigma_z^{(k)} = h \sum_{m=1}^{\infty}\sum_{n=1}^{\infty} (-C_{12}^{(k)} M\ \phi^{(k)}(Z) - C_{23}^{(k)} N\ \psi^{(k)}(Z) +$$

$$\frac{C_{33}^{(k)}}{h} D\ \chi^{(k)}(Z))\, sin(m\pi X)\, sin(n\pi Y), \tag{4.27.c}$$

$$\tau_{(yz)}^{(k)} = h \sum_{m=1}^{\infty}\sum_{n=1}^{\infty} \left(C_{44}^{(k)}(\frac{1}{h} D\ \psi^{(k)}(Z) + N\ \chi^{(k)}(Z))\right) sin(m\pi X)\, cos(n\pi Y), \tag{4.27.d}$$

$$\tau_{(xz)}^{(k)} = h \sum_{m=1}^{\infty}\sum_{n=1}^{\infty} \left(C_{55}^{(k)}(\frac{1}{h} D\ \phi^{(k)}(Z) + M\ \chi^{(k)}(Z))\right) cos(m\pi X)\, sin(n\pi Y), \tag{4.27.e}$$

$$\tau_{(xy)}^{(k)} = h \sum_{m=1}^{\infty}\sum_{n=1}^{\infty} \left(C_{55}^{(k)}(N\, \phi^{(k)}(Z) + M\, \psi^{(k)}(Z))\right) cos(m\pi X)\, cos(n\pi Y). \tag{4.27.f}$$

Furthermore, the two non-zero couple-stress and the anti-symmetric part of the shear stress can be presented, respectively, as follows:

$$m_{xy}^{(k)} = \frac{h\, l^{(k)}\, L_1}{12} C_{11}^{(k)} \sum_{m=1}^{\infty}\sum_{n=1}^{\infty} M^2\ \chi^{(k)}(Z)\ sin(m\pi X)\, sin(n\pi Y), \tag{4.28.a}$$

$$m_{xz}^{(k)} = \frac{h\, l^{(k)}\, L_1}{12} C_{11}^{(k)} \sum_{m=1}^{\infty}\sum_{n=1}^{\infty} M^2\ \psi^{(k)}(Z)\ sin(m\pi X)\, cos(n\pi Y), \tag{4.28.b}$$

$$\tau_{[xz]}^{(k)} = \frac{h\, l^{(k)}\, L_1}{24} C_{11}^{(k)} \sum_{m=1}^{\infty}\sum_{n=1}^{\infty} M^3\, \chi^{(k)}(Z)\ cos\ (m\pi X)\, sin(n\pi Y), \tag{4.28.c}$$

$$\tau_{[xy]}^{(k)} = \frac{h\, l^{(k)}\, L_1}{24} C_{11}^{(k)} \sum_{m=1}^{\infty}\sum_{n=1}^{\infty} M^3\, \psi^{(k)}(Z)\ cos\ (m\pi X)\, cos(n\pi Y). \tag{4.28.d}$$

Introduction equations (4.27.e,f) and (4.28.c,d) into equation (4.5) yields unequal shear stresses $\tau_{xz}^{(k)}$ and $\tau_{zx}^{(k)}$ as shown in the following expressions:

$$\tau_{zx}^{(k)} = h \sum_{m=1}^{\infty}\sum_{n=1}^{\infty} (C_{55}^{(k)} (\frac{1}{h} D\ \phi^{(k)}(Z) + M\ \chi^{(k)}(Z)) -$$

$$C_{11}^{(k)} \frac{l^{(k)} L_1}{24} M^3\ \chi^{(k)}(Z))\ cos(m\pi X)\, sin(n\pi Y), \qquad (4.29.a)$$

$$\tau_{xz}^{(k)} = h \sum_{m=1}^{\infty}\sum_{n=1}^{\infty} \left(C_{55}^{(k)} (\frac{1}{h} D\ \phi^{(k)}(Z) + M\ \chi^{(k)}(Z)\right) +$$

$$C_{11}^{(k)} \frac{l^{(k)} L_1}{24} M^3\ \chi^{(k)}(Z))\ cos(m\pi X)\, sin(n\pi Y), \qquad (4.29.b)$$

$$\tau_{yx}^{(k)} = h \sum_{m=1}^{\infty}\sum_{n=1}^{\infty} (C_{55}^{(k)} (N\ \phi^{(k)}(Z) + M\ \psi^{(k)}(Z)) -$$

$$C_{11}^{(k)} \frac{l^{(k)} L_1}{24} M^3\ \psi^{(k)}(Z))\ cos(m\pi X)\, cos(n\pi Y), \qquad (4.29.c)$$

$$\tau_{xy}^{(k)} = h \sum_{m=1}^{\infty}\sum_{n=1}^{\infty} (C_{55}^{(k)} (N\ \phi^{(k)}(Z) + M\ \psi^{(k)}(Z)) +$$

$$C_{11}^{(k)} \frac{l^{(k)} L_1}{24} M^3\ \psi^{(k)}(Z))\ cos(m\pi X)\, cos(n\pi Y). \qquad (4.29.d)$$

Similar to second chapter, the two shear stresses $\tau_{xz}^{(k)}$ and $\tau_{xy}^{(k)}$ are different from the other shear stresses $\tau_{zx}^{(k)}$ and $\tau_{yx}^{(k)}$, respectively. This difference is attributed to the non-zero stress couples $m_{xz}^{(k)}$, $m_{xy}^{(k)}$ appeared as a result of the presence of the fibre bending stiffness. It is of particular importance to note that when $l = 0$, the stress couples $m_{xy}^{(k)}$ and

$m_{xz}^{(k)}$ take value of zero. Consequently, the shear stresses $\tau_{xz}^{(k)}$ and $\tau_{zx}^{(k)}$ will be the equal as will be the shear stresses $\tau_{xy}^{(k)}$ and $\tau_{yx}^{(k)}$. This case ($l = 0$), meets the perfectly flexible fibres counterparts studied in linear symmetric elasticity in (Srinivas and Rao, 1970) for an orthotropic rectangular plate.

The equilibrium and continuity conditions (4.10) and (4.11) are used for the determination of the $6N$ arbitrary constants appeared in equations (4.26). Employing such conditions in connection with equations (4.18), (4.27.c, d) and (4.29.a) at the kth material interface, $z = z_k$, yields, for $(k = 1, \dots, N-1)$, the following $6(N-1)$ algebraic equations:

$$-C_{12}^{(k)} M\, \phi^{(k)}\left(\frac{z_k}{h}\right) - C_{23}^{(k)} N \psi^{(k)}\left(\frac{z_k}{h}\right) + C_{33}^{(k)} \frac{1}{h}\, \chi^{(k)'}\left(\frac{z_k}{h}\right) + C_{12}^{(k+1)} M\, \phi^{(k+1)}\left(\frac{z_k}{h}\right) +$$

$$C_{23}^{(k+1)} N \psi^{(k+1)}\left(\frac{z_k}{h}\right) - C_{33}^{(k+1)} \frac{1}{h}\, \chi^{(k+1)'}\left(\frac{z_k}{h}\right) = 0, \qquad (4.30.a)$$

$$C_{55}^{(k)}\left(\frac{1}{h}\, \phi^{(k)'}\left(\frac{z_k}{h}\right) + M\, \chi^{(k)}\left(\frac{z_k}{h}\right)\right) - C_{11}^{(k)} \frac{l^{(k)} L_1}{24} M^3\, \chi^{(k)}\left(\frac{z_k}{h}\right) - C_{55}^{(k+1)}\left(\frac{1}{h}\, \phi^{(k+1)'}\left(\frac{z_k}{h}\right)\right.$$

$$\left. M\, \chi^{(k+1)}\left(\frac{z_k}{h}\right)\right) + C_{11}^{(k+1)} \frac{l^{(k+1)} L_1}{24} M^3\, \chi^{(k+1)}\left(\frac{z_k}{h}\right) = 0, \qquad (4.30.b)$$

$$C_{44}^{(k)}\left(\frac{1}{h}\, \psi^{(k)'}\left(\frac{z_k}{h}\right) + N \chi^{(k)}\left(\frac{z_k}{h}\right)\right) = C_{44}^{(k+1)}\left(\frac{1}{h}\, \psi^{(k+1)'}\left(\frac{z_k}{h}\right) + N \chi^{(k+1)}\left(\frac{z_k}{h}\right)\right), \qquad (4.30.c)$$

$$\phi^{(k)}\left(\frac{z_k}{h}\right) - \phi^{(k+1)}\left(\frac{z_k}{h}\right) = 0, \qquad (4.30.d)$$

$$\psi^{(k)}\left(\frac{z_k}{h}\right) - \psi^{(k+1)}\left(\frac{z_k}{h}\right) = 0, \qquad (4.30.e)$$

$$\chi^{(k)}\left(\frac{z_k}{h}\right) - \chi^{(k+1)}\left(\frac{z_k}{h}\right) = 0. \qquad (4.30.f)$$

In order to determine the aforementioned $6N$ arbitrary constants, another six algebraic equations in addition to equations (4.30) are required. Remaining equations can be obtained by applying the stress lateral surface boundary conditions (4.7) at the upper and lower surfaces of the plate where $z = \pm h/2$.

4.5. Dynamic solution

The dynamic three-dimensional asymmetric-stress elasticity solution of harmonic free vibration of simply supported transversely isotropic plate is found in the present section. The solution is obtained by solving the Navier asymmetric-stress elasticity equations (4.14), the right hand-side of which contains non-zero inertia terms. The set of sixteen simply supported boundary conditions (4.9) is identically satisfied by the following choice of the displacement field:

$$U^{(k)} = h\sum_{m=1}^{\infty}\sum_{n=1}^{\infty} \phi^{(k)}(Z)\, cos(m\pi X)\, sin\,(m\pi Y)\, cos(\omega t),$$

$$V^{(k)} = h\sum_{m=1}^{\infty}\sum_{n=1}^{\infty} \psi^{(k)}(Z)\, sin(m\pi X)\, cos\,(m\pi Y)\, cos(\omega t), \qquad (4.31)$$

$$W^{(k)} = h\sum_{m=1}^{\infty}\sum_{n=1}^{\infty} \chi^{(k)}(Z)\, sin(m\pi X)\, sin\,(m\pi Y)\, cos(\omega t).$$

Inserting equations (4.31) into the set of simultaneous partial differential equations (4.14) converts it to a corresponding following set of simultaneous homogeneous ordinary differential equations:

$$\widehat{\boldsymbol{G}}(D)\,.\,\boldsymbol{B} = 0 \qquad (4.32)$$

where

$$\widehat{\boldsymbol{G}}(D)=\begin{bmatrix} \hat{d}_1^{(k)}+d_2^{(k)}D^2 & d_3^{(k)}+d_{10}^{(k)} & (d_4^{(k)}+d_{11}^{(k)})D \\ d_3^{(k)} & \hat{d}_5^{(k)}+d_6^{(k)}D^2+d_{12}^{(k)} & d_7^{(k)}D \\ -d_4^{(k)}D & -d_7^{(k)}D & \hat{d}_8^{(k)}+d_9^{(k)}D^2+d_{12}^{(k)} \end{bmatrix}, \qquad (4.33.a)$$

$$\boldsymbol{B}=\begin{bmatrix} \phi^{(k)}(Z) \\ \psi^{(k)}(Z) \\ \chi^{(k)}(Z) \end{bmatrix}, \qquad (4.33.b)$$

and

$$\hat{d}_i^{(k)}=d_i^{(k)}+\frac{c_{55}^{(k)}\omega^{*2}}{c_{11}^{(k)}}\,;i=1,5,8. \qquad (4.34)$$

Here, ω^* represents the dimensionless frequency parameter given in equation (2.35).

For each combination of m and n, a non-trivial solution of the homogeneous equation (2.33) requires the determinant of the (3 x 3) matrix $\widehat{\mathbf{G}}(\hat{p})$ to be zero, namely:

$$det(\widehat{\boldsymbol{G}}(\hat{p}))=0 \qquad (4.35)$$

i.e.

$$d_2^{(k)}\,d_6^{(k)}\,d_9^{(k)}\,p^6+(d_2^{(k)}\,d_7^{(k)^2}+d_2^{(k)}\,\hat{d}_5^{(k)}\,d_9^{(k)}+d_2^{(k)}\,d_6^{(k)}\,\hat{d}_8^{(k)}+d_2^{(k)}\,d_6^{(k)}\,d_{12}^{(k)}+$$

$$+d_2^{(k)}\,d_9^{(k)}\,d_{12}^{(k)}+\hat{d}_1^{(k)}\,d_6^{(k)}\,d_9^{(k)}+d_4^{(k)}\,d_6^{(k)}\,d_{11}^{(k)}+d_4^{(k)^2}d_6^{(k)})\,p^4+(d_2^{(k)}\,d_{12}^{(k)^2}+$$

$$d_3^{(k)^2}d_9^{(k)}+\hat{d}_1^{(k)}d_7^{(k)^2}+d_2^{(k)}\hat{d}_5^{(k)}\hat{d}_8^{(k)}+d_2^{(k)}\hat{d}_5^{(k)}d_{12}^{(k)}+d_2^{(k)}\hat{d}_8^{(k)}d_{12}^{(k)}+\hat{d}_1^{(k)}\hat{d}_5^{(k)}d_9^{(k)}$$

$$+\hat{d}_1^{(k)}\,d_6^{(k)}\,\hat{d}_8^{(k)}+\hat{d}_1^{(k)}\,d_6^{(k)}\,d_{12}^{(k)}+\hat{d}_1^{(k)}\,d_9^{(k)}d_{12}^{(k)}-2d_3^{(k)}\,d_4^{(k)}d_7^{(k)}-d_3^{(k)}d_7^{(k)}d_{11}^{(k)}-$$

$$-d_3^{(k)}\,d_9^{(k)}\,d_{10}^{(k)}-d_4^{(k)}\,d_7^{(k)}\,d_{10}^{(k)}+d_4^{(k)}\,\hat{d}_5^{(k)}\,d_{11}^{(k)}+d_4^{(k)}\,d_{11}^{(k)}\,d_{12}^{(k)}+d_4^{(k)^2}\,\hat{d}_5^{(k)}+$$

$$d_4^{(k)^2}\,d_{12}^{(k)})\,p^2+(\hat{d}_1^{(k)}\,\hat{d}_5^{(k)}\,\hat{d}_8^{(k)}+\hat{d}_1^{(k)}\,\hat{d}_5^{(k)}\,d_{12}^{(k)}+\hat{d}_1^{(k)}\,\hat{d}_8^{(k)}\,d_{12}^{(k)}+\hat{d}_1^{(k)}\,d_{12}^{(k)^2}-$$

$$d_3^{(k)^2}\hat{d}_8^{(k)} - d_3^{(k)^2}d_{12}^{(k)} - d_3^{(k)}\hat{d}_8^{(k)}d_{10}^{(k)} - d_3^{(k)}d_{10}^{(k)}d_{12}^{(k)}) = 0. \tag{4.36}$$

This, for the kth layer, yields six eigenvalues $\left(\hat{p}_i^{(k)}(\omega^*),\ i = 1, 2, \ldots, 6\right)$ which depend also on, the as yet unknown parameter, ω^*. The eigenvector corresponding to a non-repeated root $\hat{p} = \hat{p}_i^{(k)}$ is as follows:

$$\begin{bmatrix} \phi_i^{(k)} \\ \psi_i^{(k)} \\ \chi_i^{(k)} \end{bmatrix} =$$

$$\begin{bmatrix} ((d_4^{(k)} + d_{11}^{(k)})(\hat{d}_5^{(k)} + d_6^{(k)}p_i^{(k)^2} + d_{12}^{(k)}) - d_7^{(k)}(d_3^{(k)} + d_{10}^{(k)}))p_i^{(k)} \\ (d_7^{(k)}(\hat{d}_1^{(k)} + d_2^{(k)}p_i^{(k)^2}) - d_3^{(k)}(d_4^{(k)} + d_{11}^{(k)}))p_i^{(k)} \\ -(\hat{d}_1^{(k)} + d_2^{(k)}p_i^{(k)^2})(\hat{d}_5^{(k)} + d_6^{(k)}p_i^{(k)^2} + d_{12}^{(k)}) + d_3^{(k)}(d_3^{(k)} + d_{10}^{(k)}) \end{bmatrix} Ce^{p_i^{(k)}z}, \tag{4.37}$$

where C is an arbitrary constant. The solution of equation (4.32) which is depending on ω^* has the following form:

$$\begin{bmatrix} \phi^{(k)} \\ \psi^{(k)} \\ \chi^{(k)} \end{bmatrix} =$$

$$\sum_{m=1}^{6} C_i^{(k)} \begin{bmatrix} ((d_4^{(k)} + d_{11}^{(k)})(\hat{d}_5^{(k)} + d_6^{(k)}p_i^{(k)^2} + d_{12}^{(k)}) - d_7^{(k)}(d_3^{(k)} + d_{10}^{(k)}))p_i^{(k)} \\ (d_7^{(k)}(\hat{d}_1^{(k)} + d_2^{(k)}p_i^{(k)^2}) - d_3^{(k)}(d_4^{(k)} + d_{11}^{(k)}))p_i^{(k)} \\ -(\hat{d}_1^{(k)} + d_2^{(k)}p_i^{(k)^2})(\hat{d}_5^{(k)} + d_6^{(k)}p_i^{(k)^2} + d_{12}^{(k)}) + d_3^{(k)}(d_3^{(k)} + d_{10}^{(k)}) \end{bmatrix} e^{p_i^{(k)}z}. \tag{4.38}$$

Introduction of equations (4.22), (4.34) and (4.38) into equation (4.31) yields the expression of the displacement field.

4.5.1. Determination of the frequency parameter

The way of finding the frequency parameter values of the free vibration of a SSSS N-layered plate is described in. This will be very similar to the manner followed in free vibration of a SS N-layered beam shown in the subsection (2.5.1). Then, the case of the free vibration of a SSSS homogeneous plate ($N = 1$) is given as an example.

The lateral surfaces are stress free and therefore the loading function $q(x, y) = 0$. For each combination of m and n, satisfaction of the lateral surface conditions (4.7), the conditions of equilibrium (4.10) and continuity conditions (4.11) yields the following $6N$ algebraic simultaneous homogeneous equations:

$$\boldsymbol{H}(\omega^*) \,.\, \boldsymbol{S} = 0. \tag{4.39}$$

Here, $\boldsymbol{S}$ is a (1 x 6N) matrix which contains the arbitrary constants $C_i^{(k)}$; (i=1,..,6 & k=1,...,N) and $\mathbf{H}(\omega^*)$ is a (6N x 6N) matrix depends on ω^*. For a non-trivial solution of the homogeneous equations (4.39), the determinant of the matrix $\mathbf{H}(\omega^*)$ must be zero yielding an algebraic equation of ω^*. A solution of that algebraic equation produces an infinite number of frequencies.

As an example of a relatively simple form of equation (4.39), a particular case of a homogeneous plate (N = 1) is considered. In this case of a single harmonic, the (6 x 6) and (1 x 6) matrixes which appear in equation (4.39) will take the following form:

$$\boldsymbol{H}(\omega^*) = \begin{bmatrix} h_{11} & h_{12} & h_{13} & h_{14} & h_{15} & h_{16} \\ h_{21} & h_{22} & h_{23} & h_{24} & h_{25} & h_{26} \\ h_{31} & h_{32} & h_{33} & h_{34} & h_{35} & h_{36} \\ h_{41} & h_{42} & h_{43} & h_{44} & h_{45} & h_{46} \\ h_{51} & h_{52} & h_{53} & h_{54} & h_{55} & h_{56} \\ h_{61} & h_{62} & h_{63} & h_{64} & h_{65} & h_{66} \end{bmatrix}, \quad \boldsymbol{S} = \begin{bmatrix} C_1 \\ C_2 \\ C_3 \\ C_4 \\ C_5 \\ C_6 \end{bmatrix}, \tag{4.40}$$

where

$$h_{1i} = (-C_{13}M\,h\,\alpha_i(\omega^*) - C_{23}N\,h\,\beta_i + C_{33}\,\gamma_i(\omega^*)\,\hat{p}_i)e^{\frac{\hat{p}_i}{2}}, \tag{4.41.a}$$

$$h_{2i} = (-C_{13}M\,h\,\alpha_i(\omega^*) - C_{23}N\,h\,\beta_i + C_{33}\,\gamma_i(\omega^*)\,\hat{p}_i)e^{\frac{-\hat{p}_i}{2}}, \tag{4.41.b}$$

$$h_{3i} = (\beta_i\,\hat{p}_i + N\,h\,\gamma_i(\omega^*))e^{\frac{\hat{p}_i}{2}}, \tag{4.41.c}$$

$$h_{4i} = (\beta_i\,\hat{p}_i + N\,h\,\gamma_i(\omega^*))e^{\frac{-\hat{p}_i}{2}}, \tag{4.41.d}$$

$$h_{5i} = \left(C_{55}\,\alpha_i(\omega^*)\,\hat{p}_i + \left(C_{55}\,M\,h - \frac{h}{24}\,l\,L_1C_{11}M^3\right)\gamma_i(\omega^*)\right)e^{\frac{\hat{p}_i}{2}}, \tag{4.41.e}$$

$$h_{5i} = \left(C_{55}\,\alpha_i(\omega^*)\,\hat{p}_i + \left(C_{55}\,M\,h - \frac{h}{24}\,l\,L_1C_{11}M^3\right)\gamma_i(\omega^*)\right)e^{\frac{-\hat{p}_i}{2}}. \tag{4.41.c}$$

Also

$$\alpha_i(\omega^*) = ((d_4 + d_{11})(\hat{d}_5 + d_6\hat{p}_i^2 + d_{12}) - d_7(d_3 + d_{10}))\hat{p}_i,$$

$$\beta_i = (d_7(\hat{d}_1 + d_2\hat{p}_i^2) - d_3(d_4 + d_{11}))\,\hat{p}_i,$$

$$\gamma_i(\omega^*) = -(\hat{d}_1 + d_2\hat{p}_i^2)(\hat{d}_5 + d_6\hat{p}_i^2 + d_{12}) + d_3(d_3 + d_{10}),$$

$$d_1 = -h^2(M^2 + N^2(C_{55}/C_{11})) + \frac{C_{55}\omega^{*2}}{C_{11}},\quad d_2 = C_{55}/C_{11},$$

$$d_3 = h^2MN(C_{13} + C_{55})/C_{11},\quad d_4 = h\,M\,(C_{13} + C_{55})/C_{11}, \tag{4.42}$$

$$d_5 = (-h^2(M^2C_{55} + N^2C_{33})/C_{11}) + \frac{C_{55}\omega^{*2}}{C_{11}},\quad d_6 = C_{44}/C_{11},$$

$$d_7 = hN(C_{23} + C_{44})/C_{11},\quad d_8 = \frac{C_{55}\omega^{*2}}{C_{11}} + (-h^2(C_{55}\,M^2 + C_{44}\,N^2)/C_{11}),$$

$d_9 = C_{33}/C_{11}$, $d_{10} = \frac{h^2}{24} M^3 N\, l\, L_1$, $d_{11} = -\frac{h}{24} M^3\, l\, L_1$,

$d_{12} = -\frac{h^2}{24} M^4\, l\, L_1$.

The six eigenvalues $\hat{p}_i$, $(i = 1, \ldots, 6)$ are obtained by solving equation (4.36) in the case of (N=1). The only unknown in the matrix $\mathbf{H}(\omega^*)$ shown in (4.40) is ω^*. For a non-trivial solution of the problem the determination of $\mathbf{H}(\omega^*)$ must be zero and this yields the following equation:

$$det\big(\boldsymbol{H}(\omega^*)\big) = 0. \tag{4.43}$$

Solution of this equation yields an infinite sequence of roots. A computer program can be used to obtain roots of equation (2.45) as in the second chapter. Similar procedures to this example can be followed in the case of N > 1.

4.6. Numerical results and discussion

Numerical results for the static and dynamic solutions for a SSSS homogonous rectangular plate are presented in this section. In the case of a rectangular plat that has a large value of the ratio L_2/L_1, results based on the present solutions are compared with their counterparts based on the asymmetric-stress plane strain solution. In addition, this section provides results based on the present solutions and computed at different values of the ratio L_2/L_1. Those, results are presented at different values of λ.

4.6.1. Static solution results

In the numerical results of the static problem, the material of the homogeneous plate is assumed to be transversely isotropic and the single- layered plate material is characterized

by the properties that are given in equations (2.47). We take, $m = n = 1$, therefore, equation (4.8) will be:

$$q(x,y) = q_{11}\, sin\left(\frac{\pi}{L_1}x\right) sin\left(\frac{\pi}{L_2}y\right). \tag{4.44}$$

For presentation of numerical results, the normalised quantities employed are defined as follows:

$$X = x/L_1,\ Y = y/L_2, Z = z/h, \bar{U} = E_T U/L_1 q_{11}, \bar{V} = E_T V/L_1 q_{11}, \bar{W} = E_T W/L_1 q_{11},$$

$$\bar{\tau}_{yz} = \tau_{yz}/q_{11}, \bar{\tau}_{xy} = \tau_{xy}/q_{11},\ \bar{\tau}_{zx} = \tau_{yx}/q_{11}, \bar{\tau}_{xz} = \tau_{xz}/q_{11},\ \bar{\tau}_{zx} = \tau_{zx}/q_{11}. \tag{4.45}$$

Numerical results for these non-dimensional displacements and shear stresses for the flexure of thick homogeneous (single-layered) plate ($h/L_1 = 0.25$) are presented.

Table 4-1 Through-thickness distributions of $\bar{U}\left(0, \frac{L_2}{2}, Z\right)$ for a SSSS homogeneous plate ($h/L_1 = 0.25, \lambda = 0$)

$\frac{Z}{h}$	3D $L_2/L_1 = 1$	3D $L_2/L_1 = 1.5$	3D $L_2/L_1 = 2$	3D $L_2/L_1 = 100$	Plane strain $\bar{U}(0,Z)$
0.5	0.102445	0.118650	0.123841	0.129522	0.129524
0.4	0.046636	0.055299	0.058162	0.061372	0.061373
0.3	0.019766	0.024386	0.025958	0.027745	0.027746
0.2	0.007060	0.009399	0.010207	0.011110	0.011110
0.1	0.001065	0.001980	0.002281	0.002564	0.002564
0	-0.002193	-0.002353	-0.002453	-0.002681	-0.002681
-0.1	-0.005263	-0.006491	-0.006991	-0.007731	-0.007731
-0.2	-0.010581	-0.013219	-0.014223	-0.015587	-0.015588
-0.3	-0.021739	-0.026641	-0.028411	-0.030676	-0.030677
-0.4	-0.045333	-0.054277	-0.057352	-0.061090	-0.061091
-0.5	-0.094368	-0.110910	-0.116361	-0.122610	-0.122702

Table 4-2 Through-thickness distributions of $\bar{U}\left(0,\frac{L_2}{2},Z\right)$ for a SSSS homogeneous plate ($h/L_1 = 0.25, \lambda = 0.04$)

$\frac{Z}{h}$	3D $L_2/L_1 = 1$	3D $L_2/L_1 = 1.5$	3D $L_2/L_1 = 2$	3D $L_2/L_1 = 100$	Plane strain $\bar{U}(0,Z)$
0.5	0.045796	0.051032	0.052685	0.054514	0.054515
0.4	0.019929	0.022855	0.0238124	0.024896	0.024896
0.3	0.007630	0.009251	0.0097948	0.010413	0.010413
0.2	0.001961	0.002792	0.0030699	0.003371	0.003371
0.1	-0.000570	-0.000272	-0.0001860	-0.000127	-0.000127
0	-0.001811	-0.001940	-0.0020137	-0.002164	-0.002164
-0.1	-0.002933	-0.003483	-0.0037161	-0.004075	-0.004075
-0.2	-0.005032	-0.006103	-0.0065257	-0.007126	-0.007127
-0.3	-0.009703	-0.011549	-0.0122363	-0.013160	-0.013160
-0.4	-0.019867	-0.023015	-0.0241218	-0.025533	-0.025534
-0.5	-0.041287	-0.046780	-0.0486111	-0.050835	-0.050836

Tables 4-1 and 4-2 show the normalised through-thickness distributions of $\bar{U}\left(0,\frac{L_2}{2},Z\right)$ for the cases of perfectly flexible and stiff fibres, respectively. It is observed that the magnitude of the numerical values obtained at λ=0 are higher than that of their counterparts presented for λ=0.04. In the both cases of λ, this magnitude increases gradually with increasing the value of L_2/L_1. Furthermore, a successful comparison is shown between the present 3D elasticity results at $L_2/L_1 = 100$ and the results based the static plane strain solution presented in the second chapter of the present study.

Tables 4-3 and 4-4 show normalised through-thickness distributions of $\bar{V}\left(\frac{L_1}{2},0,Z\right)$ for the cases of perfectly flexible and stiff fibres, respectively. The magnitude of the through-thickness distributions at λ=0.04 is lower than that at λ=0. In addition, it decreases with increasing the value of L_2/L_1. The values at $L_2/L_1 = 100$ are remarkably small and, practically negligible, whereas it takes zero value in the plane strain solution.

Tables 4-5 and 4-6 compare numerical values of the through-thickness of the normalised deflection $\bar{W}\left(\frac{L_1}{2},\frac{L_2}{2},Z\right)$ for the cases of perfectly flexible and stiff fibres, respectively. It is noted that when the fibres possess bending stiffness, the magnitude of the through thickness deflection distributions is lower than the corresponding values of the case of perfectly flexible fibres. This observation emphasise that in the presence of the resistance of fibres in bending, the plate becomes stiffer. In addition, the magnitude of the deflection distributions decreases with decreasing the value of L_2/L_1 which means that the plate becomes stiffer. It is observed that the numerical results of the deflection at $L_2/L_1 = 100$ are very close to their counterparts based on the plane strain solution. It should be mentioned that the numerical values that based on the plane strain solution in the case of λ=0 and shown in tables 4-1 and 4-5 are identical to that presented in (Soldatos and Watson, 1997b).

Table 4-3 Through-thickness distributions of $\bar{V}\left(\frac{L_1}{2},0,Z\right)$ for a SSSS homogeneous plate ($h/L_1 = 0.25, \lambda = 0$)

$\frac{Z}{h}$	3D $L_2/L_1 = 1$	3D $L_2/L_1 = 1.5$	3D $L_2/L_1 = 2$	3D $L_2/L_1 = 100$	Plane strain $V\left(\frac{L_1}{2},Z\right)$
0.5	0.279031	0.216831	0.167917	0.003355	0
0.4	0.205331	0.160471	0.123923	0.002437	0
0.3	0.139491	0.108673	0.083079	0.001574	0
0.2	0.079542	0.060327	0.044628	0.000752	0
0.1	0.023702	0.014421	0.007881	-0.000040	0
0	-0.029694	-0.029992	-0.027809	-0.000812	0
-0.1	-0.082245	-0.073831	-0.063066	-0.001576	0
-0.2	-0.135523	-0.117998	-0.098508	-0.002342	0
-0.3	-0.191121	-0.163409	-0.134758	-0.003121	0
-0.4	-0.250693	-0.211010	-0.172464	-0.003922	0
-0.5	-0.316024	-0.261824	-0.212324	-0.004759	0

Table 4-4 Through-thickness distributions of $\bar{V}\left(\frac{L_1}{2}, 0, Z\right)$ for a SSSS homogeneous plate

$(h/L_1 = 0.25, \lambda = 0.04)$

$\frac{Z}{h}$	3D $L_2/L_1 = 1$	3D $L_2/L_1 = 1.5$	3D $L_2/L_1 = 2$	3D $L_2/L_1 = 100$	Plane strain $V\left(\frac{L_1}{2}, Z\right)$
0.5	0.180015	0.132699	0.101108	0.001993	0
0.4	0.129221	0.0954698	0.072398	0.001402	0
0.3	0.084598	0.0618527	0.046217	0.000855	0
0.2	0.044639	0.030999	0.021980	0.000343	0
0.1	0.007980	0.002131	-0.000848	-0.000142	0
0	-0.026649	-0.025481	-0.022771	-0.000612	0
-0.1	-0.060458	-0.052532	-0.044274	-0.001072	0
-0.2	-0.094631	-0.079714	-0.065835	-0.001533	0
-0.3	-0.130356	-0.107712	-0.087928	-0.002002	0
-0.4	-0.168859	-0.137233	-0.111044	-0.002488	0
-0.5	-0.211444	-0.169022	-0.135698	-0.003000	0

Table 4-5 Through-thickness distributions of $\bar{W}\left(\frac{L_1}{2}, \frac{L_2}{2}, Z\right)$ for a SSSS homogeneous plate

$(h/L_1 = 0.25, \lambda = 0)$

$\frac{Z}{h}$	3D $L_2/L_1 = 1$	3D $L_2/L_1 = 1.5$	3D $L_2/L_1 = 2$	3D $L_2/L_1 = 100$	Plane strain $W\left(\frac{L_1}{2}, Z\right)$
0.5	-0.997631	-1.127779	-1.167499	-1.209098	-1.209112
0.4	-0.981106	-1.109264	-1.148040	-1.188307	-1.188321
0.3	-0.963823	-1.090542	-1.128632	-1.167947	-1.167960
0.2	-0.947297	-1.073098	-1.110748	-1.149477	-1.149490
0.1	-0.932304	-1.057650	-1.095091	-1.133582	-1.133595
0	-0.919205	-1.044518	-1.081965	-1.120553	-1.120566
-0.1	-0.908097	-1.033779	-1.071443	-1.110455	-1.110468
-0.2	-0.898867	-1.025326	-1.063418	-1.103182	-1.103195
-0.3	-0.891152	-1.018826	-1.057566	-1.098416	-1.098430
-0.4	-0.884220	-1.013581	-1.053198	-1.095480	-1.095495
-0.5	-0.876681	-1.008210	-1.048935	-1.092994	-1.093010

Table 4-6 Through-thickness distributions of $\bar{W}\left(\frac{L_1}{2},\frac{L_2}{2},Z\right)$ for a SSSS homogeneous plate

$(\mathrm{h}/L_1 = 0.25, \lambda = 0.04)$

$\frac{Z}{h}$	3D $L_2/L_1 = 1$	3D $L_2/L_1 = 1.5$	3D $L_2/L_1 = 2$	3D $L_2/L_1 = 100$	Plane strain $W(L_1/2, Z)$
0.5	-0.693023	-0.751391	-0.768682	-0.786815	-0.786821
0.4	-0.674278	-0.731243	-0.747934	-0.765260	-0.765266
0.3	-0.656217	-0.712263	-0.728552	-0.745344	-0.745349
0.2	-0.639588	-0.695103	-0.711158	-0.727655	-0.727660
0.1	-0.624772	-0.680069	-0.696035	-0.712450	-0.712455
0	-0.611941	-0.667282	-0.683287	-0.699817	-0.699822
-0.1	-0.601125	-0.656753	-0.672921	-0.689755	-0.689761
-0.2	-0.592244	-0.648411	-0.664865	-0.682195	-0.682201
-0.3	-0.585093	-0.642084	-0.658961	-0.676987	-0.676994
-0.4	-0.579284	-0.637442	-0.654894	-0.673836	-0.673843
-0.5	-0.574118	-0.633862	-0.652061	-0.672163	-0.672170

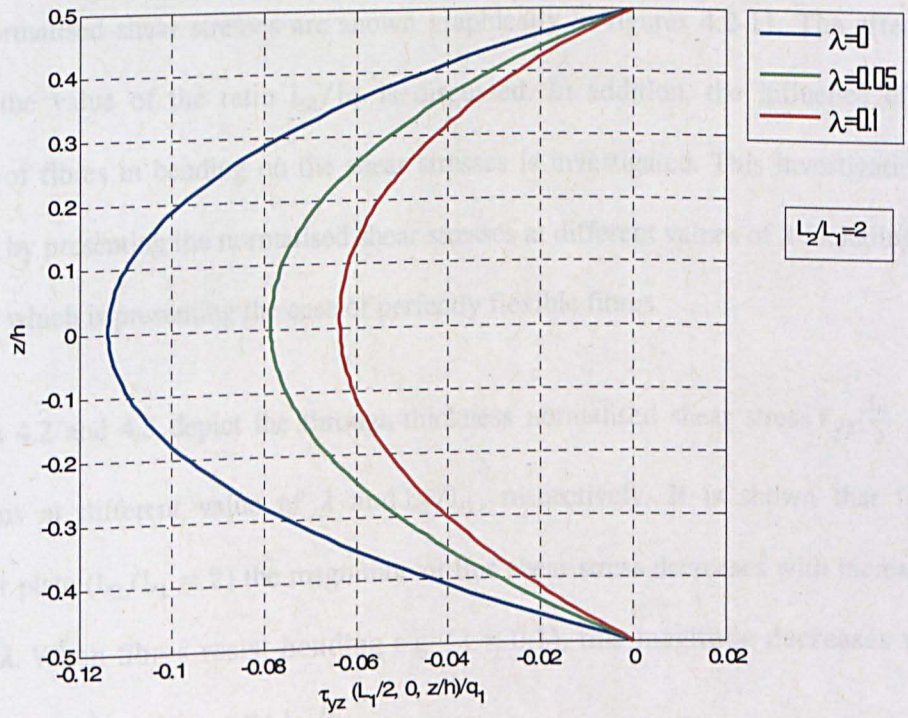

Figure 4.2 Through-thickness shear stress $\tau_{yz}(\frac{L_1}{2}, 0, \frac{z}{h})/q_1$ at different value of λ

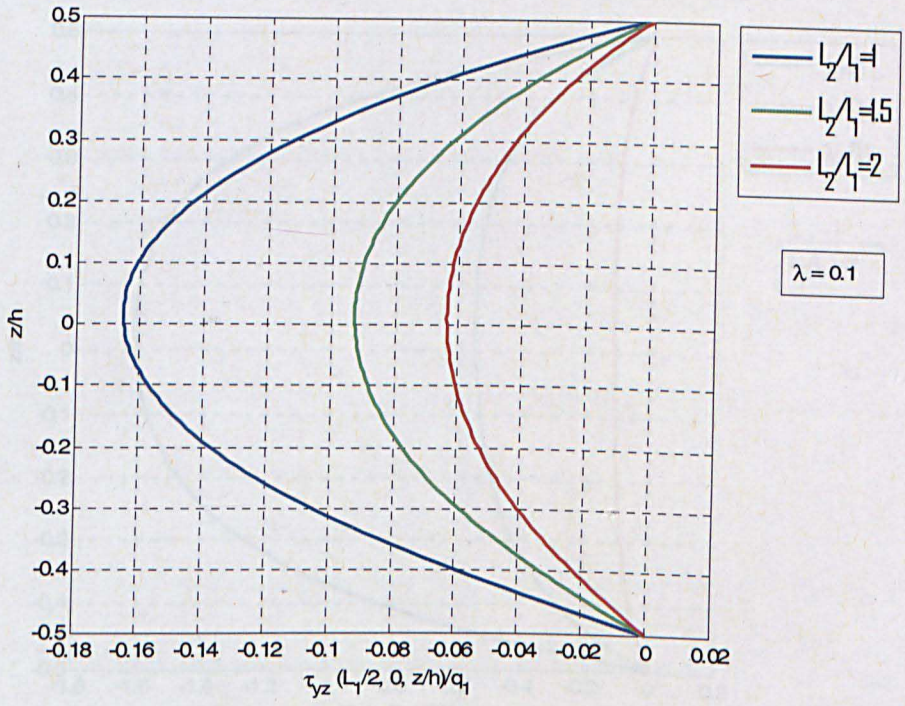

Figure 4.3 Through-thickness shear stress $\tau_{yz}(\frac{L_1}{2}, 0, \frac{z}{h})/q_1$ at different value of L_2/L_1

The normalised shear stresses are shown graphically in figures 4.2-11. The effect of changing the value of the ratio L_2/L_1 is discussed. In addition, the influence of the resistance of fibres in bending on the shear stresses is investigated. This investigation is conducted by presenting the normalised shear stresses at different values of λ including the zero value which is presenting the case of perfectly flexible fibres.

Figures 4.2 and 4.3 depict the through-thickness normalised shear stress $\bar{\tau}_{yz}(\frac{L_1}{2}, 0, \frac{z}{h})$ distributions at different value of λ and L_2/L_1, respectively. It is shown that for a rectangular plate ($L_2/L_1 = 2$) the magnitude of this shear stress decreases with increasing values of λ. When fibres resist bending e.g. ($\lambda = 0.1$), this magitude decreases with increasing the value of the ratio L_2/L_1.

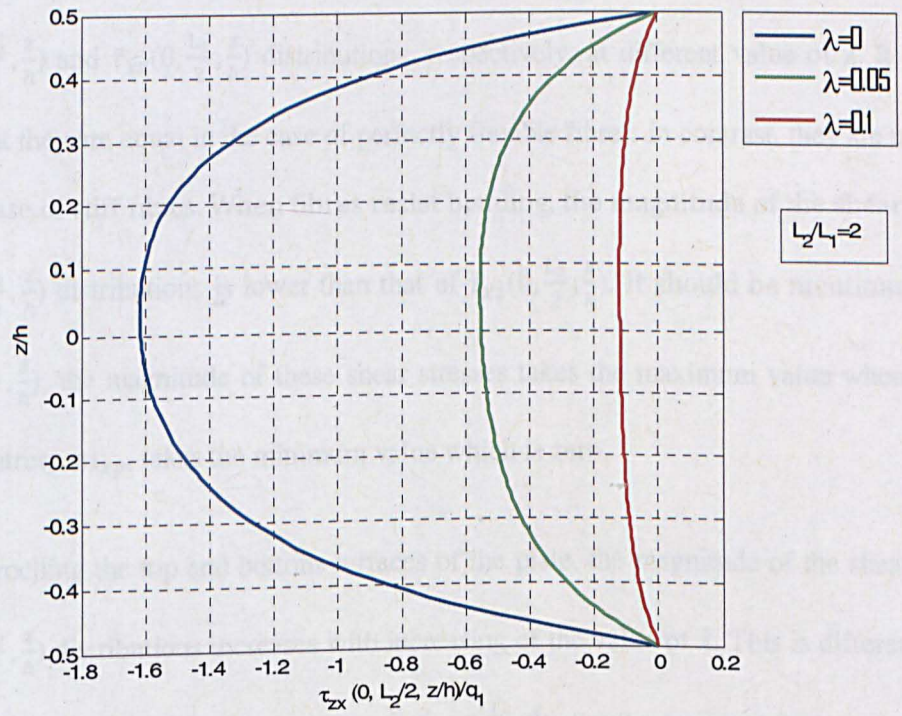

Figure 4.4 Through-thickness shear stress $\frac{\tau_{zx}\left(0,\frac{L_2}{2},\frac{z}{h}\right)}{q_1}$ distributions at different value of λ

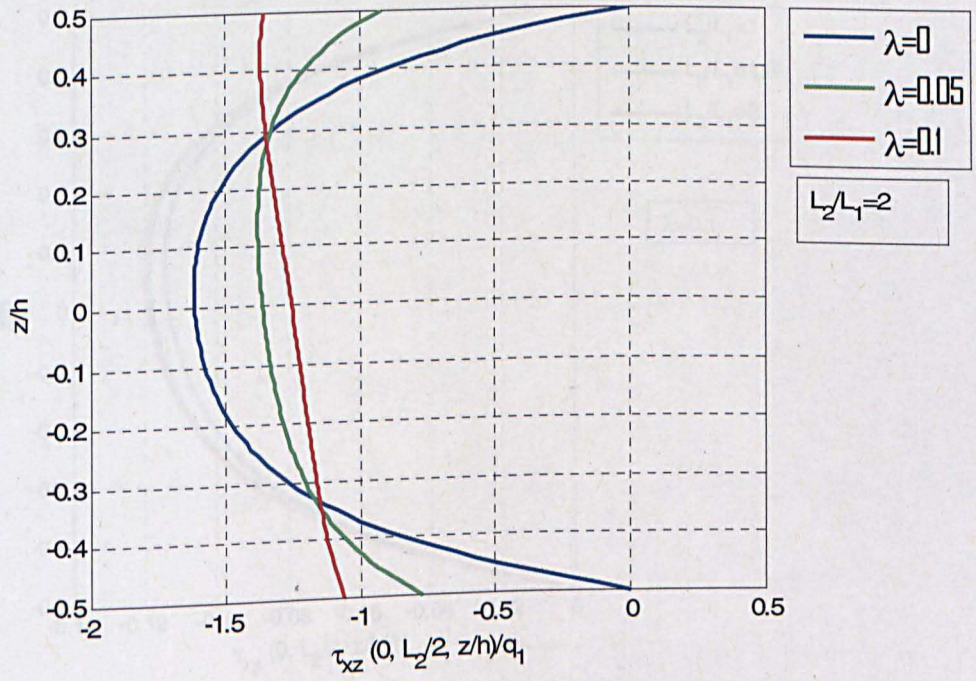

Figure 4.5 Through-thickness shear stress $\frac{\tau_{xz}\left(0,\frac{L_2}{2},\frac{z}{h}\right)}{q_1}$ distributions at different value of λ

For $L_2/L_1 = 2$, figures 4.4 and 4.5 present the through-thickness shear stresses $\bar{\tau}_{zx}(0,\frac{L_2}{2},\frac{z}{h})$ and $\bar{\tau}_{xz}(0,\frac{L_2}{2},\frac{z}{h})$ distributions, respectively, at different value of λ. It can be seen that they are equal in the case of perfectly flexible fibres. In contrast, they are unequal in the case of stiff fibres. When fibres resist bending, the magnitude of the shear stress $\bar{\tau}_{zx}(0,\frac{L_2}{2},\frac{z}{h})$ distributions is lower than that of $\bar{\tau}_{xz}(0,\frac{L_2}{2},\frac{z}{h})$. It should be mentioned that at $(0,\frac{L_2}{2},\frac{z}{h})$, the magnitude of these shear stresses takes the maximum value whereas the couple-stress, m_{xy}, takes the minimum value which is zero.

Approching the top and bottom surfaces of the plate, the magnitude of the shear stress $\bar{\tau}_{xz}(0,\frac{L_2}{2},\frac{z}{h})$ distributions increases with increasing of the value of λ. This is different from that of the through thickness shear stress $\bar{\tau}_{zx}(0,\frac{L_2}{2},\frac{z}{h})$ distributions which decreased with the increasing of the value of λ.

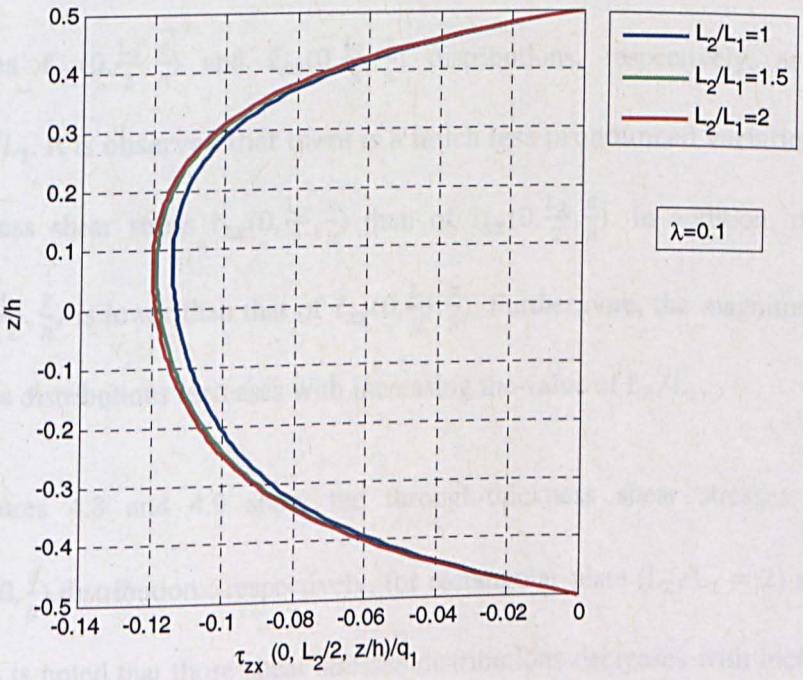

Figure 4.6 Through-thickness shear stress $\frac{\tau_{zx}\left(0,\frac{L_2}{2},\frac{z}{h}\right)}{q_1}$ at different value of L_2/L_1

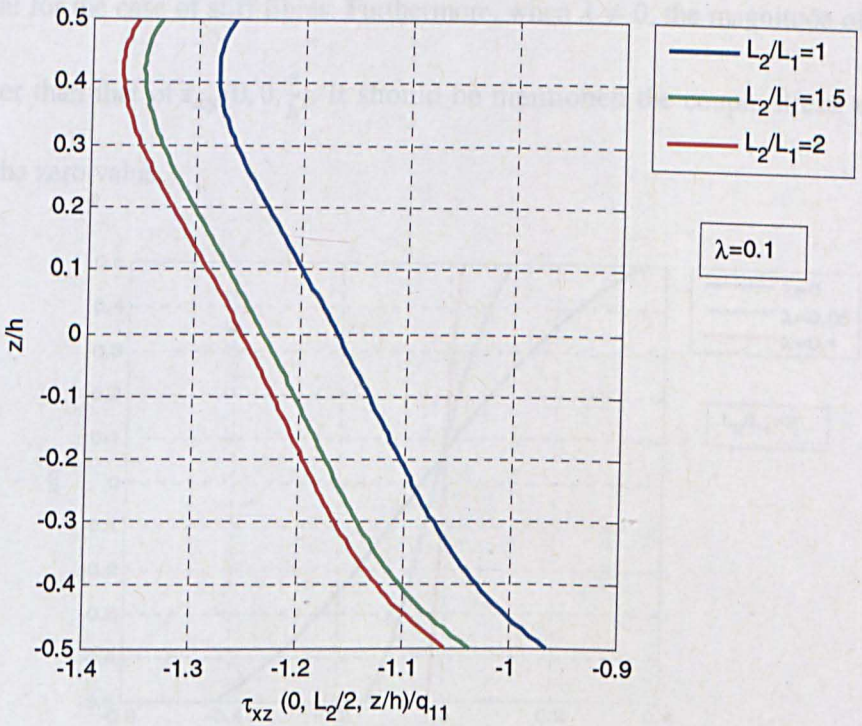

Figure 4.7 Through-thickness shear stress $\frac{\tau_{zx}\left(0,\frac{L_2}{2},\frac{z}{h}\right)}{q_1}$ at different value of L_2/L_1

For the case stiff fibres ($\lambda = 0.1$), figures 4.6 and 4.7 depict the through-thickness shear stresses $\bar{\tau}_{zx}(0,\frac{L_2}{2},\frac{z}{h})$ and $\bar{\tau}_{xz}(0,\frac{L_2}{2},\frac{z}{h})$ distributions, respectively, at different value of L_2/L_1. It is observed that there is a much less pronounced variation of the through-thickness shear stress $\bar{\tau}_{zx}(0,\frac{L_2}{2},\frac{z}{h})$ than of $\bar{\tau}_{xz}(0,\frac{L_2}{2},\frac{z}{h})$. In addition, the magnitude of $\bar{\tau}_{zx}(0,\frac{L_2}{2},\frac{z}{h})$ is lower than that of $\bar{\tau}_{xz}(0,\frac{L_2}{2},\frac{z}{h})$. Furthermore, the magnitude of those shear stresses distributions increases with increasing the value of L_2/L_1.

Figures 4.8 and 4.9 show the through-thickness shear stresses $\bar{\tau}_{yx}(0,0,\frac{z}{h})$ and $\bar{\tau}_{xy}(0,0,\frac{z}{h})$ distributions, respectively, for rectangular plate ($L_2/L_1 = 2$) at different value of λ. It is noted that those shear stresses distributions decreases with increasing the value of λ. In the case of $\lambda = 0$, the shear stresses $\bar{\tau}_{yx}$ and $\bar{\tau}_{xy}$ are equal. In contrast, they are

unequal for the case of stiff fibres. Furthermore, when $\lambda \neq 0$, the magnitude of $\bar{\tau}_{yx}(0,0,\frac{z}{h})$ is lower than that of $\bar{\tau}_{xy}(0,0,\frac{z}{h})$. It should be mentioned the couple-stress, $m_{xz}(0,0,\frac{z}{h})$, takes the zero value.

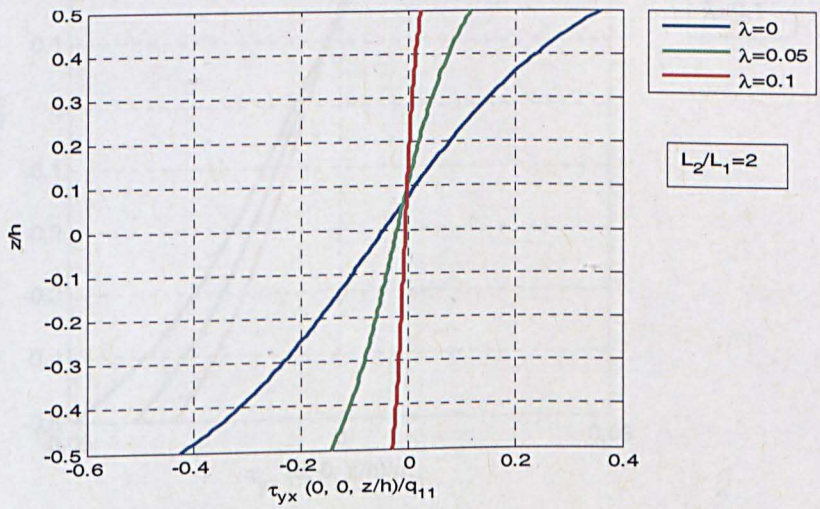

Figure 4.8 Through-thickness shear stress $\frac{\tau_{yx}(0,0,\frac{z}{h})}{q_{11}}$ distributions at different value of λ

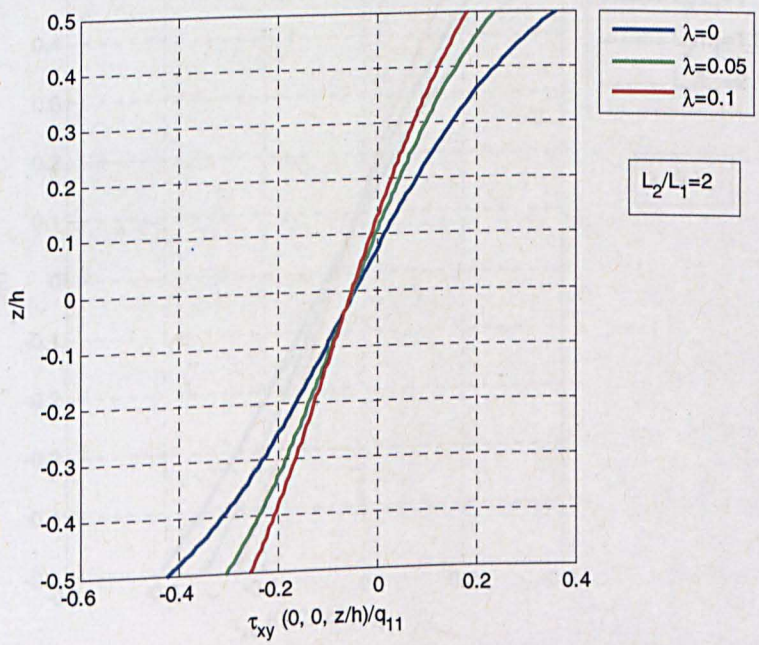

Figure 4.9 Through-thickness shear stress $\frac{\tau_{xy}(0,0,\frac{z}{h})}{q_{11}}$ at different value of λ

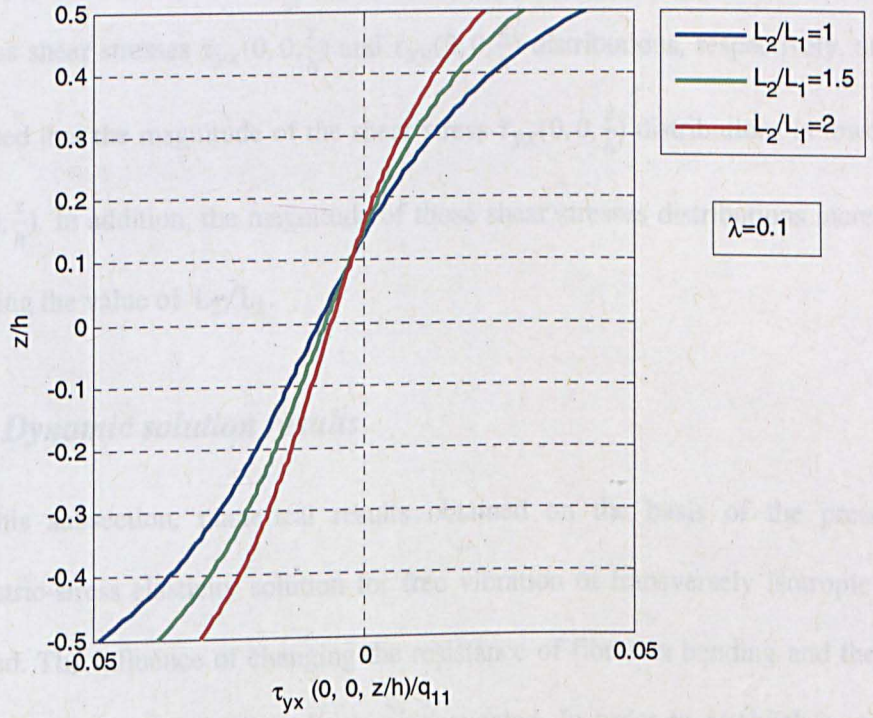

Figure 4.10 Through-thickness shear stress $\frac{\tau_{yx}(0,0,\frac{z}{h})}{q_{11}}$ at different value of L_2/L_1

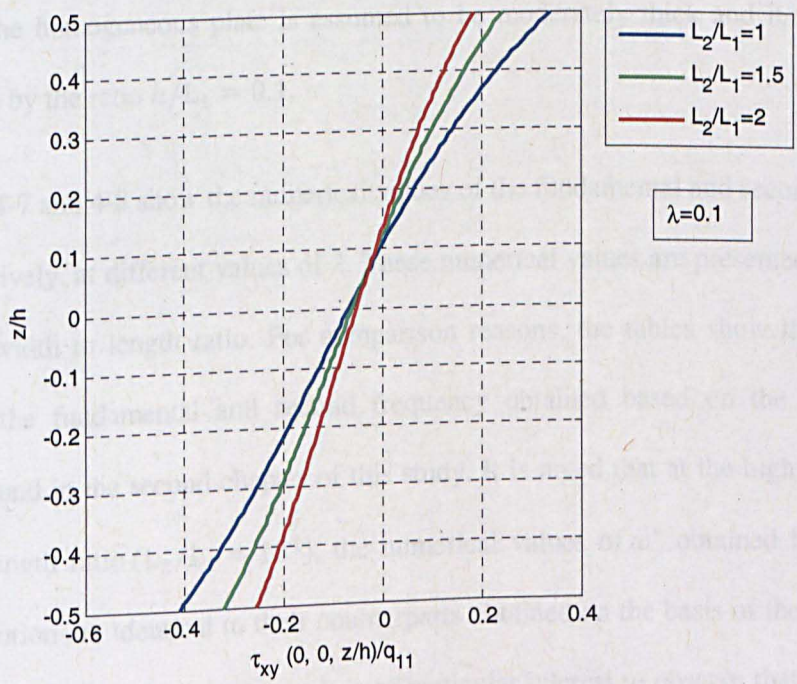

Figure 4.11 Through-thickness shear stress $\frac{\tau_{xy}(0,0,\frac{z}{h})}{q_{11}}$ at different value of L_2/L_1

For different values of the ratio L_2/L_1, figures 4.10 and 4.11 show the through-thickness shear stresses $\bar{\tau}_{yx}(0,0,\frac{z}{h})$ and $\bar{\tau}_{xy}(0,0,\frac{z}{h})$ distributions, respectively, at $\lambda = 0.1$. It is noted that the magnitude of the shear stress $\bar{\tau}_{yx}(0,0,\frac{z}{h})$ distributions is lower than of $\bar{\tau}_{xy}(0,0,\frac{z}{h})$. In addition, the magnitude of those shear stresses distributions increases with decreasing the value of L_2/L_1.

4.6.2. Dynamic solution results

In this subsection, numerical results obtained on the basis of the present exact asymmetric-stress elasticity solution for free vibration of transversely isotropic plate are presented. The influence of changing the resistance of fibres in bending and the width to length ratio on the frequency values is investigated. In order to establish a more direct correlation with our previous findings in the second chapter of the present study, the material of the plate is assumed to have the properties given in equations (2.50). As an example, the homogeneous plate is assumed to be moderately thick and its thickness is determined by the ratio $h/L_1 = 0.1$.

Tables 4-7 and 4-8 show the numerical values of the fundamental and second frequency ω^*, respectively, at different values of λ. These numerical values are presented at different values of width to length ratio. For comparison reasons, the tables show the numerical values of the fundamental and second frequency obtained based on the plane strain solution found in the second chapter of this study. It is noted that at the high value of the width to length ratio ($L_2/L_1 = 10^4$), the numerical values of ω^* obtained based on the present solution are identical to their counterparts obtained on the basis of the plane strain solution found in the second chapter. It is of particular interest to observe that the value of

ω^* increases with increasing the value of λ which emphasise again that with increasing the fibre bending stiffness, the plate becomes stiffer.

Table 4-7 Fundamental frequency, ω^*, for a moderately thick homogeneous plate $(h/L_1 = 0.1)$

$\lambda=\frac{l}{h}$	3D asymmetric-stress elasticity					Plane strain
	$\frac{L_2}{L_1}=0.5$	$\frac{L_2}{L_1}=1$	$\frac{L_2}{L_1}=5$	$\frac{L_2}{L_1}=10$	$\frac{L_2}{L_1}=10^4$	
0	0.2433	0.1767	0.1652	0.1650	0.1649	0.1649
0.002	0.2453	0.1787	0.1673	0.1671	0.1670	0.1670
0.004	0.2470	0.1806	0.1694	0.1692	0.1691	0.1691
0.006	0.2487	0.1825	0.1715	0.1713	0.1712	0.1712
0.008	0.2502	0.1844	0.1735	0.1733	0.7132	0.1732
0.01	0.2512	0.1862	0.1755	0.1753	0.1752	0.1752

Table 4-8 second frequency, ω^*, for a moderately thick homogeneous plate $(h/L_1 = 0.1)$

$\lambda=\frac{l}{h}$	3D asymmetric-stress elasticity					Plane strain
	$\frac{L_2}{L_1}=0.5$	$\frac{L_2}{L_1}=1$	$\frac{L_2}{L_1}=5$	$\frac{L_2}{L_1}=10$	$\frac{L_2}{L_1}=10^4$	
0	0.3160	0.3150	0.3145	0.3143	0.3142	0.3142
0.002	0.3173	0.3163	0.3152	0.3150	0.3148	0.3148
0.004	0.3183	0.3171	0.3158	0.3156	0.3155	0.3155
0.006	0.3193	0.3182	0.3164	0.3162	0.3161	0.3161
0.008	0.3203	0.3192	0.3170	0.3168	0.3167	0.3167
0.01	0.3213	0.3203	0.3176	0.3174	0.3173	0.3174

Furthermore, it is noted that the value of ω^* increases with decreasing the value of L_2/L_1. This observation emphasise again that the plate becomes stiffer with decreasing the value of L_2/L_1. In addition, with changing the value of this ratio, there is a much less pronounced variation of the second frequency values than that of the corresponding fundamental frequency counterparts.

4.7. Conclusion

In summary, exact three-dimensional asymmetric-stress elasticity solutions are constructed for the statics and dynamics of a simply supported rectangular plate. The obtained exact solutions are discussed in the framework of the linear theory of elasticity. Comparisons are shown between the present three dimensional asymmetric-stress elasticity solutions results at high values of L_2/L_1 and the corresponding plane strain solution counterparts. Comparisons of the through-thickness displacements distributions between the case of perfectly flexible fibres and the stiff fibres are conducted at different values of L_2/L_1. The effect of giving different values of λ and L_2/L_1 on the shear stresses is discussed. Furthermore, the influence of having different value of these ratios on the values of the fundamental and second frequency is also discussed.

It has been observed that the magnitude of the shear stress τ_{yz} decreases with increasing values of λ. When fibres resist bending e.g. (λ=0.1) this magnitude decreases with increasing the value of the ratio L_2/L_1. In addition, when fibres resist bending, the magnitude of the shear stress τ_{xz} takes the maximum value at the left plate edge ($x = 0$ and $y = \frac{L_2}{2}$) whereas the couple stress, m_{xy}, takes the minimum value which is zero. Furthermore, approching the top and bottom surfaces of the plate, the

magnitude of the shear stress $\bar{\tau}_{xz}(0,\frac{L_2}{2},\frac{z}{h})$ distributions increases with increasing of the value of λ. However, the magnitude of the through thickness shear stress $\bar{\tau}_{zx}(0,\frac{L_2}{2},\frac{z}{h})$ distributions decreases, there, with the increasing of the value of λ. It is noted that the through-thickness shear stresses $\bar{\tau}_{yx}(0,0,\frac{z}{h})$ and $\bar{\tau}_{xy}(0,0,\frac{z}{h})$ distributions decreases with increasing the value of λ. Furthermore, when $\lambda \neq 0$, the magnitude of $\bar{\tau}_{yx}(0,0,\frac{z}{h})$ is lower than that of $\bar{\tau}_{xy}(0,0,\frac{z}{h})$.

It is of particular interest to conclude that the magnitude of the deflection decreases with increasing the value of λ and it does also with decreasing the value of the width to length ratio. Furthermore, when the fibres resist bending, the shear stresses τ_{zx} and τ_{xz} are unequal and so are the shear stresses τ_{yx} and τ_{xy}. In addition, the value of the fundamental and second frequency increases with the increasing of the value of λ and, it does as well with decreasing the value of L_2/L_1.

4.8. Further work

Since the obtained three-dimensional asymmetric-stress elasticity solutions are exact, they can serve as a benchmark of the accuracy of relevant thin plate theories developed in (Soldatos, 2009), through an appropriate comparisons of corresponding numerical results. The general five-degrees-of-freedom shear deformable plate theory (G5DOFPT) is one of aforementioned thin plate theories which was applied in the case of perfectly flexible fibres in (Soldatos and Watson, 1997b).

In the fifth chapter, considering the fibres possess bending stiffness, the G5DOFPT will be employed to solve the flexure and free vibration problem of rectangular plate subjected to different sets of edge boundary conditions. The reliability of such method will

be tested by comparing its numerical results with their counterparts based on the present three-dimensional asymmetric-stress elasticity solutions of flexure and free vibration of SSSS transversely isotropic rectangular plate.

Chapter 5. Flexure and free vibration problem of rectangular plate subjected to different sets of edge boundary conditions

5.1. Introduction

This chapter presents solutions for flexure and free vibration of thin transversely isotropic rectangular plate subjected to different sets of edge boundary conditions. Considering the fibres possess bending stiffness, the advanced version of two-dimensional thin-walled structure modelling, developed in (Soldatos, 2009), has been employed. This two-dimensional theory is initially applied to the solutions of the small flexure and free vibration of thin simply supported homogeneous plate at the four edges, for which the exact asymmetric-stress elasticity solutions have been obtained in the fourth chapter. Then, the method is used for stress analysis of rectangular plates subjected to different sets of edge boundary conditions.

In the case of perfectly flexible fibres, the one-dimensional of G5DOFPT was employed in (Soldatos and Watson, 1997b) for cylindrical bending of plates subjected to different sets of edge boundary conditions. In addition, considering the resistance of fibres in bending, the advanced version of G3DOFBT (Soldatos, 2009) has been employed in the third chapter of the this thesis for flexure and free vibration of thin transversely isotropic beams subjected to different end boundary conditions.

The main reason of studying the considered version of 2D elastic plate theory is its ability to be applied on the flexure and free vibration plates associated with different edge

boundary conditions for which explicit 3D elasticity solution is very difficult to obtain. An analysis of numerical results based on the obtained static and dynamic solutions is conducted. The effect of the presence of the resistance of fibres in bending on the deformed plates which subjected to different sets of edge boundary conditions from simply supported boundary conditions is investigated. This is discussed at different values of the width to length ratio (L_2/L_1).

5.2. Basic equations considering the resistance of fibres in bending

In this chapter, the plate is subjected to small static flexure caused by the action of a given external lateral loading $q(x,y)$ or to dynamic flexure. In the static problem, such loading acts normally and downwards on the top lateral plane of the plate. The plate is subjected to three different sets of edge boundary conditions that applied on the edges $x = 0, L_1$ and simply supported at $y = 0, L_2$.

The implied shear deformable, elastic plate model begins with the displacement field approximation assumed in (Soldatos and Watson, 1997b) of the following form:

$$U(x,y,z,t) = u(x,y,t) - zw_{,x} + \varphi_1(z)u_1(x,y,t), \tag{5.1.a}$$

$$V(x,y,z,t) = v(x,y,t) - zw_{,y} + \varphi_2(z)v_1(x,y,t), \tag{5.1.b}$$

$$W(x,y,z,t) = w(x,y,t), \tag{5.1.c}$$

where $U(\mathrm{x,y,z,t})$, $V(\mathrm{x,y,z,t})$ and $W(\mathrm{x,y,z,t})$ represent displacement components along x, y and z directions, respectively. In addition, $u(\mathrm{x,y,t})$, $v(\mathrm{x,y,t})$ and $w(\mathrm{x,y,t})$ represent the unknown in-plane displacements of the plate middle plane. Therefore, they have evidently dimension of length. The later three and $u_1(\mathrm{x,y,t})$ and $v_1(\mathrm{x,y,t})$, which

represent the unknown values of the transverse strains on the plane middle plane, are the five main unknowns (degrees of freedom) of the employed theory. Since the aforementioned values of the transverse are dimensionless quantity, then, the shape functions $\varphi_1(z)$ and $\varphi_2(z)$ are assumed to have dimensions of length. Such shape functions are imposed to have the following conditions:

$$\varphi_1(0) = 0, \varphi_2(0) = 0, \tag{5.2.a}$$

$$\left.\frac{d\varphi_1}{dz}\right|_{z=0} = 1, \left.\frac{d\varphi_2}{dz}\right|_{z=0} = 1. \tag{5.2.b}$$

By inserting the displacement approximation (5.1) into the linear kinematic relations of three-dimensional elasticity:

$$\varepsilon_x = \frac{\partial U}{\partial x}, \varepsilon_y = \frac{\partial V}{\partial y}, \varepsilon_z = \frac{\partial W}{\partial z}, \tag{5.3.a}$$

$$\gamma_{xz} = \frac{\partial U}{\partial z} + \frac{\partial W}{\partial x}, \gamma_{yz} = \frac{\partial V}{\partial z} + \frac{\partial W}{\partial y}, \gamma_{xy} = \frac{\partial U}{\partial z} + \frac{\partial V}{\partial y}, \tag{5.3.b}$$

one obtains the following approximate strain field (Soldatos, 2009):

$$\varepsilon_x = e_x^c + zk_x^c + \varphi_1(z)k_x^a, \varepsilon_y = e_y^c + zk_y^c + \varphi_2(z)k_y^a, \varepsilon_z = o \tag{5.4.a}$$

$$\gamma_{xy} = e_{xy}^c + zk_{xy}^c + \varphi_1(z)k_{xy}^a + \varphi_2(z)k_{yx}^a, \gamma_{xz} = \varphi_1'(z)e_{xz}^a, \gamma_{yz} = \varphi_2'(z)e_{yz}^a, \tag{5.4.b}$$

$$k_z^f = k_x^c, k_y^f = \hat{k}_x^c + zk_{x,y}^c - \varphi_2(z)k_{yx,x}^a, \tag{5.4.c}$$

where

$$e_x^c = u_{,x}, e_y^c = v_{,y}, e_{xy}^c = u_{,y} + v_{,x}, \tag{5.5.a}$$

$$k_x^c = -w_{,xx}, k_y^c = -w_{,yy}, k_{xy}^c = -2w_{,xy}, \tag{5.5.b}$$

$$k_x^a = u_{1,x}\,, k_y^a = v_{1,y}\,, k_{xy}^a = u_{1,y}\,, k_{yx}^a = v_{1,x} \tag{5.5.c}$$

$$e_{xz}^a = u_1\,, e_{yz}^a = v_1\,, \tag{5.5.d}$$

$$\hat{k}_x^c = v_{,xx}\,. \tag{5.5.e}$$

Here the quantities denoted with a superscript $^{(c)}$ are identical with their classical beam theory counterparts. The components which are denoted with a superscript $^{(a)}$ represent the transverse shear deformation effects. Furthermore, the additional kinematic relations k_z^f and k_y^f represent the fibres curvature in the z-and y-directions.

It is considered that the plate is composed of an arbitrary number, N, of perfectly bonded transversely isotropic layers. Accordingly, the generalised Hooke's law within the kth layer of such a cross-ply laminate is given as:

$$\begin{bmatrix} \sigma_x^{(k)} \\ \sigma_y^{(k)} \\ \sigma_z^{(k)} \\ \tau_{(yz)}^{(k)} \\ \tau_{(xz)}^{(k)} \\ \tau_{(xy)}^{(k)} \end{bmatrix} = \begin{bmatrix} Q_{11}^{(k)} & Q_{13}^{(k)} & Q_{13}^{(k)} & 0 & 0 & 0 \\ Q_{13}^{(k)} & Q_{33}^{(k)} & Q_{23}^{(k)} & 0 & 0 & 0 \\ Q_{13}^{(k)} & Q_{23}^{(k)} & Q_{33}^{(k)} & 0 & 0 & 0 \\ 0 & 0 & 0 & Q_{44}^{(k)} & 0 & 0 \\ 0 & 0 & 0 & 0 & Q_{55}^{(k)} & 0 \\ 0 & 0 & 0 & 0 & 0 & Q_{66}^{(k)} \end{bmatrix} \begin{bmatrix} \varepsilon_x^{(k)} \\ \varepsilon_y^{(k)} \\ 0 \\ \gamma_{yz}^{(k)} \\ \gamma_{xz}^{(k)} \\ \gamma_{xy}^{(k)} \end{bmatrix}, \tag{5.6}$$

where a symbol with indices enclosed in parentheses denotes the symmetric part of the associated shear stress component (Soldatos, 2009) and the appearing $Q^{,s}$ are the reduced elastic stiffnesses (Jones, 1975). The anti-symmetric part of the shear stress component has the form (Soldatos, 2009):

$$\tau_{[xz]}^{(k)} = -\tau_{[zx]}^{(k)} = \frac{1}{2} m_{xy,x}^{(k)} = \frac{1}{2} d^{f(k)} K_{z,x}^f = -\frac{1}{2} d^{f(k)} w_{,xxx}\,, \tag{5.7.a}$$

$$\tau_{[xy]}^{(k)} = -\tau_{[yx]}^{(k)} = -\frac{1}{2} m_{xz,x}^{(k)} = -\frac{1}{2} d^{f(k)} K_{y,x}^{f} = -\frac{1}{2} d^{f(k)} (v_{,xxx} - z\, w_{,yxxx}$$

$$+\varphi_2(z)\, v_{1,xxx}) . \qquad (5.7.b)$$

Furthermore, with the use of equations (2.6), (4.5) and (5.4-7) the shear stresses can be written as:

$$\tau_{xz}^{(k)} = Q_{55}^{(k)} \varphi_1{}'(z)\, u_1 - \frac{1}{2} d^{f(k)} w_{,xxx} , \qquad (5.8.a)$$

$$\tau_{zx}^{(k)} = Q_{55}^{(k)} \varphi_1{}'(z)\, u_1 + \frac{1}{2} d^{f(k)} w_{,xxx} , \qquad (5.8.b)$$

$$\tau_{xy}^{(k)} = Q_{66}^{(k)} (u_{,y} + v_{,x} - 2z\, w_{,xy} + \varphi_1(z)\, u_{1,y} + \varphi_2(z)\, v_{1,x}) - \frac{1}{2} d^{f(k)} (v_{,xxx} -$$

$$z\, w_{,yxxx} + \varphi_2(z)\, v_{1,xxx}) , \qquad (5.8.c)$$

$$\tau_{yx}^{(k)} = Q_{66}^{(k)} (u_{,y} + v_{,x} - 2z\, w_{,xy} + \varphi_1(z)\, u_{1,y} + \varphi_2(z)\, v_{1,x}) + \frac{1}{2} d^{f(k)} (v_{,xxx} -$$

$$z\, w_{,yxxx} + \varphi_2(z)\, v_{1,xxx}) . \qquad (5.8.d)$$

In addition, the force and moment resultants (Soldatos, 2009) are:

$$(N_x^c, N_y^c, N_{xy}^c) = \int_{-\frac{h}{2}}^{\frac{h}{2}} (\sigma_x, \sigma_y, \tau_{xy})\, dz, \qquad (5.9.a)$$

$$(M_x^c, M_y^c, M_{xy}^c) = \int_{-\frac{h}{2}}^{\frac{h}{2}} (\sigma_x, \sigma_y, \tau_{xy})\, z\, dz, \qquad (5.9.b)$$

$$(M_x^a, M_y^a, M_{xy}^a, M_{yx}^a) = \int_{-\frac{h}{2}}^{\frac{h}{2}} (\varphi_1\sigma_x, \varphi_2\sigma_y, \varphi_1\tau_{xy}, \varphi_2\tau_{xy})\, dz, \qquad (5.9.c)$$

$$(Q_x^a, Q_y^a) = \int_{-\frac{h}{2}}^{\frac{h}{2}} (\varphi_1{}' \tau_{xz},\ \varphi_2{}' \tau_{xz})\, dz, \tag{5.9.d}$$

$$(M_x^f, \hat{M}_x^f, \hat{L}_x^f, \tilde{L}_x^f) = \frac{1}{2}\int_{-\frac{h}{2}}^{\frac{h}{2}} \left(m_{xy}, m_{xz}, m_{xz}\frac{z}{h}, m_{xz}\frac{\varphi_2}{h}\right) dz. \tag{5.9.e}$$

Considering the fibres possess bending stiffness, the five equations of motion of G5DOFPT (Soldatos, 2009), in terms of force and moment resultants, are, in convenient notation, as follows:

$$N_{x,x}^c + N_{xy,y}^c = \rho_0\, \ddot{u} - \rho_1\, \ddot{w}_{,x} + \hat{\rho}_0^{11}\, \ddot{u}_1\,, \tag{5.9.a}$$

$$N_{yx,x}^c + N_{y,y}^c - \hat{M}_{x,xx}^f = \rho_0\, \ddot{v} - \rho_1\, \ddot{w}_{,y} + \hat{\rho}_0^{21}\, \ddot{v}_1\,, \tag{5.9.b}$$

$$M_{x,xx}^c + M_{x,xx}^f - h\, \hat{L}_{x,xxy}^f + 2\, M_{xy,xy}^c + M_{y,yy}^c = q(x,y) + \rho_0\, \ddot{w} + \rho_1\left(\ddot{u}_{,x} + \ddot{v}_{,y}\right) -$$

$$\rho_2\left(\ddot{w}_{,xx} + \ddot{w}_{,yy}\right) + \hat{\rho}_1^{11}\, \ddot{u}_{1,x} + \hat{\rho}_1^{21}\, \ddot{v}_{1,y}\,, \tag{5.9.c}$$

$$M_{x,x}^a + M_{xy,y}^a - Q_x^a = \hat{\rho}_0^{11}\, \ddot{u} - \hat{\rho}_1^{11}\, \ddot{w}_{,x} + \hat{\rho}_0^{12}\, \ddot{u}_1\,, \tag{5.9.d}$$

$$M_{yx,x}^a + M_{y,y}^a - Q_y^a - h\, \tilde{L}_{x,xx}^f = \hat{\rho}_0^{21}\, \ddot{v} - \hat{\rho}_1^{21}\, \ddot{w}_{,y} + \hat{\rho}_0^{22}\, \ddot{v}_1\,. \tag{5.9.e}$$

Here, the coefficients that appears in the inertia terms are defined as:

$$\rho_i = \int_{-\frac{h}{2}}^{\frac{h}{2}} \rho\, z^i dz, \hat{\rho}_i^{Lm} = \int_{-\frac{h}{2}}^{\frac{h}{2}} \rho\, z^i [\varphi_L(z)]^m dz\,, \quad (i = 0,1,2; L,m = 1,2). \tag{5.10.a,b}$$

The two-dimensional equations of motion (5.9) are associated with the following sets of edge boundary conditions at $x = 0,\ L_1$ (Soldatos, 2009):

either u or N_x^c is prescribed, (5.11.a)

either v or $N_{xy}^{c} - \widehat{M}_{x,x}^{f}$ is prescribed, (5.11.b)

either v_x or $\widehat{M}_{x}^{f}$ is prescribed, (5.11.c)

either w or $M_{x,x}^{c} + M_{xy,y}^{c} + M_{x,x}^{f} - \mathrm{h}\widehat{\mathrm{L}}_{\mathrm{x,yx}}^{\mathrm{f}} - \mathrm{h}\,\widehat{\mathrm{L}}_{\mathrm{x,xy}}^{\mathrm{f}}$ is prescribed, (5.11.d)

either w_x or $M_{x}^{c} + M_{x}^{f} + h\,\widehat{L}_{x,y}^{f}$ is prescribed, (5.11.e)

either u_1 or M_{x}^{a} is prescribed, (5.11.f)

either v_1 or $M_{xy}^{a} + \tilde{L}_{x,x}^{f}$ is prescribed, (5.11.g)

either $v_{1,x}$ or $\tilde{L}_{x}^{f}$ is prescribed. (5.11.h)

In addition, considering that the fibres aligned to the x-axis and the plate is simply supported at $y = 0$, L_2, the following edge boundary conditions are applied:

$$N_{y}^{c} = 0, \quad u = 0, \quad \mathrm{w} = 0, \quad M_{y}^{c} = 0, \quad M_{y}^{a} = 0, \quad u_1 = 0. \tag{5.12}$$

5.3. Equations of motion in terms of the five-degrees-of-freedom

Introduction of equations (5.6-8) into equations (5.9) yields the following force and moment resultants in terms of the five degrees of freedom and their derivatives:

$$\begin{bmatrix} N_x^c \\ N_y^c \\ N_{xy}^c \\ M_x^c \\ M_y^c \\ M_{xy}^c \\ M_x^a \\ M_y^a \\ M_{xy}^a \\ M_{yx}^a \end{bmatrix} =$$

$$\begin{bmatrix} A_{11} & A_{12} & 0 & B_{11} & B_{12} & 0 & B_{111} & B_{122} & 0 & 0 \\ A_{12} & A_{22} & 0 & B_{12} & B_{22} & 0 & B_{121} & B_{222} & 0 & 0 \\ 0 & 0 & A_{66} & 0 & 0 & B_{66} & 0 & 0 & B_{661} & B_{662} \\ B_{11} & B_{12} & 0 & D_{11} & D_{12} & 0 & D_{111} & D_{122} & 0 & 0 \\ B_{12} & B_{22} & 0 & D_{12} & D_{22} & 0 & D_{121} & D_{222} & 0 & 0 \\ 0 & 0 & B_{66} & 0 & 0 & D_{66} & 0 & 0 & D_{661} & D_{662} \\ B_{111} & B_{121} & 0 & D_{111} & D_{121} & 0 & D_{1111} & D_{1221} & 0 & 0 \\ B_{122} & B_{222} & 0 & D_{122} & D_{222} & 0 & D_{1221} & D_{2222} & 0 & 0 \\ 0 & 0 & B_{661} & 0 & 0 & D_{661} & 0 & 0 & D_{6611} & D_{6621} \\ 0 & 0 & B_{662} & 0 & 0 & D_{662} & 0 & 0 & D_{6621} & D_{6622} \end{bmatrix} \begin{bmatrix} u_{,x} \\ v_{,y} \\ u_{,y} + v_{,x} \\ -w_{,xx} \\ -w_{,yy} \\ -2w_{,xy} \\ u_{1,x} \\ v_{1,y} \\ u_{1,y} \\ v_{1,x} \end{bmatrix},$$

$$\begin{bmatrix} Q_x^a \\ Q_y^a \end{bmatrix} = \begin{bmatrix} A_{5511} \\ A_{4422}^a \end{bmatrix} [u_1 \quad v_1], \tag{5.13}$$

$$M_x^f = -S_0 w_{,xx}, \tag{5.14}$$

$$\widehat{M}_x^f = S_0 v_{,xx} - S_1 w_{,yxx} + S_{02} v_{1,xx}, \tag{5.15}$$

$$\hat{L}_x^f = \frac{1}{h}(S_1 v_{,xx} - S_2 w_{,yxx} + \frac{1}{h} S_{12} v_{1,xx}), \tag{5.16}$$

$$\tilde{L}_x^f = \frac{1}{h}(S_{02} v_{,xx} - S_{12} w_{,yxx} + \frac{1}{h} S_{022} v_{1,xx}). \tag{5.17}$$

The rigidities in the case of perfectly flexible fibres (Messina and Soldatos, 2002) are defined according to:

$$A_{ij} = \int_{-\frac{h}{2}}^{\frac{h}{2}} Q_{ij}^{(k)} dz, \quad B_{ij} = \int_{-\frac{h}{2}}^{\frac{h}{2}} Q_{ij}^{(k)} z \, dz, \quad D_{ij} = \int_{-\frac{h}{2}}^{\frac{h}{2}} Q_{ij}^{(k)} z^2 \, dz, \tag{5.18}$$

$$B_{ijn} = \int_{-\frac{h}{2}}^{\frac{h}{2}} Q_{ij}^{(k)} \varphi_n(z) \, dz, \quad D_{ijn} = \int_{-\frac{h}{2}}^{\frac{h}{2}} Q_{ij}^{(k)} z \, \varphi_n(z) \, dz, \tag{5.19}$$

$$A_{ijnm} = \int_{-\frac{h}{2}}^{\frac{h}{2}} Q_{ij}^{(k)} \varphi_n'(z) \, \varphi_m'(z) dz, \quad D_{ijnm} = \int_{-\frac{h}{2}}^{\frac{h}{2}} Q_{ij}^{(k)} \varphi_n(z) \, \varphi_m(z) \, dz, \tag{5.20}$$

Additional rigidities that appear in the presence of the resistance of fibres in bending are defined according to:

$$S_i = \frac{1}{2}\int_{-\frac{h}{2}}^{\frac{h}{2}} d^f z^i dz \;,\; S_{i2} = \frac{1}{2}\int_{-\frac{h}{2}}^{\frac{h}{2}} d^f z^i \,\varphi_2(z) dz,\; S_{022} = \frac{1}{2}\int_{-\frac{h}{2}}^{\frac{h}{2}} d^f \left(\varphi_2(z)\right)^2 dz\,. \qquad (5.21)$$

Upon the use of the two-dimensional constitutive equations (5.13-17), the equations of motions (5.9) can be converted into the following set of five simultaneous differential equations that has a same number of main unknowns.

$$A_{11}u_{,xx} + (A_{12} + A_{66})v_{,xy} + A_{66}u_{,yy} - B_{11}w_{,xxx} - (B_{12} + 2B_{66})w_{,xyy} + B_{111}u_{1,xx}$$

$$+(B_{122} + B_{662})v_{1,xy} + B_{661}u_{1,yy} = \rho_0\, u_{,tt} - \rho_1\, w_{,xtt} + \hat{\rho}_0^{11}\, u_{1,tt}, \qquad (5.22.a)$$

$$(A_{12} + A_{66})u_{,xy} + A_{22}v_{,yy} + A_{66}v_{,xx} - (B_{12} + 2B_{66})w_{,xxy} - B_{22}w_{,yyy} + B_{222}v_{1,yy}$$

$$+(B_{121} + B_{661})u_{1,xy} + B_{662}v_{1,xx} + S_0 v_{,xxxx} + S_1 w_{,yxxxx} + S_{02}v_{1,xxxx} = \rho_0\, v_{,tt} -$$

$$\rho_1\, w_{,ytt} + \hat{\rho}_0^{21}\, v_{1,tt}, \qquad (5.22.b)$$

$$B_{11}u_{,xxx} + (B_{12} + 2B_{66})v_{,xxy} + B_{22}v_{,yyy} + (B_{12} + 2B_{66})u_{,xyy} - (D_{11} + S_0)w_{,xxxx}$$

$$-(2D_{12} + 4D_{66})w_{,xxyy} - D_{22}w_{,yyyy} + D_{111}u_{1,xxx} - (D_{122} + 2D_{662})v_{1,xxy} + (D_{121}$$

$$+2D_{661})u_{1,xyy} + D_{222}v_{1,yyy} - S_1 v_{,xxxxy} + S_2 w_{,xxxxyy} - S_{12}v_{1,xxxxy} = q(x,y) +$$

$$\rho_0\, w_{,tt} + \rho_1\left(u_{,xtt} + v_{,ytt}\right) - \rho_2\left(w_{,xxtt} + w_{,yytt}\right) + \hat{\rho}_1^{11}\, u_{1,xtt} + \hat{\rho}_1^{21}\, v_{1,ytt}, \qquad (5.22.c)$$

$$-A_{5511}\, u_1 + B_{111}\, u_{,xx} + (B_{121} + B_{661})\, v_{,xy} + B_{661}\, u_{,yy} - D_{111}\, w_{,xxx} - (D_{121} +$$

$$2D_{661})\, w_{,xyy} + D_{1111}\, u_{1,xx} + (D_{1221} + D_{6612})\, v_{1,xy} + D_{6611}\, u_{1,yy} = \hat{\rho}_0^{11}\, u_{,tt} -$$

$$\hat{\rho}_1^{11}\, w_{,xtt} + \hat{\rho}_0^{12}\, u_{1,tt}\,, \qquad (5.22.d)$$

$$-A_{4411}\, v_1 + (B_{122} + B_{662})\, u_{,xy} + B_{222}\, v_{,yy} + B_{662}\, v_{,xx} - (D_{122} + 2D_{662})\, w_{,xxy} -$$

$$D_{222}\, w_{,yyy} + (D_{1221} + D_{6621})\, u_{1,xy} + D_{2222}\, v_{1,yy} + D_{6622}\, v_{1,xx} - S_{02}\, v_{,xxxx} +$$

$$S_{12} w_{,xxxxy} - S_{022} v_{1,xxxx} = \hat{\rho}_0^{21}\, v_{,tt} - \hat{\rho}_1^{21}\, w_{,ytt} + \hat{\rho}_0^{22}\, v_{1,tt}\,. \qquad (5.22.e)$$

These Navier- type differential equations may be solved simultaneously when a particular set of boundary conditions is specified at each edge of the plate. In the following two sections the static and dynamic problems are discussed.

5.4. Rectangular plate under normal static load applied on its top surface

For the flexure problem of the rectangular plate, the inertia terms appearing in the right-hand sides of equations (5.9) and (5.22) are disregarded. In this section, the case of simply supported plate at the four edges $x = 0,\ L_1$ and $y = 0,\ L_2$ (SSSS) is considered. The case of different sets of edge boundary conditions that applied on the edges $x = 0, L_1$ is discussed.

5.4.1. Static solution for SSSS rectangular plates

The effective way to test the reliability of the employed 2D model is by performing numerical comparison with corresponding results of an exact three dimensional asymmetric-stress elasticity solution presented in the fourth chapter. A reasonable simply testing situation could be conducted after applying the 2D model on the case where the plate edges $x = 0,$ and $x = L_1$ are simply supported. In this particular case, equations (5.11) will take the following form:

$$N_x^c = 0,\ v = 0,\ \widehat{M}_x^f = 0,\ w = 0,$$

$$M_x^c + M_x^f + h\,\hat{L}_{x,y}^f = 0, \tag{5.23}$$

$$M_x^a = 0, \quad v_1 = 0, \quad \tilde{L}_x^f = 0.$$

It can be verified that the following choice of the displacement field:

$$u(x,y) = A_1\, cos(p_m x)\, sin(p_n y),$$

$$u_1(x,y) = B_1\, cos(p_m x)\, sin(p_n y),$$

$$v(x,y) = A_2\, sin(p_m x)\, cos(p_n y), \tag{5.24}$$

$$v_1(x,y) = B_2\, sin(p_m x)\, cos(p_n y),$$

$$w(x,y) = C\, sin(p_m x)\, sin(p_n y),\ p_m = \frac{m\pi}{L_1}, p_n = \frac{n\pi}{L_2},\ m,n = 1,2,\dots .$$

satisfies the simply supported boundary conditions described by equations (5.12) and (5.23). It is assumed that the applied external loading can be expressed as described in equations (4.8) and (4.44). Moreover, with the use of the displacement field (5.24), the set of partial differential equation (5.22) is converted into a corresponding set of linear algebraic equations that can be expressed in the following matrix form:

$$\boldsymbol{F}.\boldsymbol{X} = \boldsymbol{P}, \tag{5.25}$$

where

$$\boldsymbol{F} = \begin{bmatrix} F_{11} & F_{12} & F_{13} & F_{14} & F_{15} \\ F_{21} & F_{22} & F_{23} & F_{24} & F_{25} \\ F_{31} & F_{32} & F_{33} & F_{34} & F_{35} \\ F_{41} & F_{42} & F_{43} & F_{44} & F_{45} \\ F_{51} & F_{52} & F_{53} & F_{54} & F_{55} \end{bmatrix},\ \boldsymbol{X} = \begin{bmatrix} A_1 \\ A_2 \\ C \\ B_1 \\ B_2 \end{bmatrix},\ \boldsymbol{P} = \begin{bmatrix} 0 \\ 0 \\ q_{mn} \\ 0 \\ 0 \end{bmatrix}, \tag{5.26.a}$$

and $F_{11} = -A_{11}\, p_m{}^2 - A_{66}\, p_n{}^2,\ F_{12} = -(A_{12} + A_{66})\, p_m\, p_n,$

$$F_{13} = B_{11}{p_m}^3 + (B_{12} + 2B_{66})\, p_m\, {p_n}^2, F_{14} = -B_{111}{p_m}^2 - B_{661}{p_n}^2,$$

$$F_{15} = -(B_{122} + B_{662})p_m p_n, F_{22} = -A_{22}{p_n}^2 - A_{66}{p_m}^2 + S_0{p_m}^4,$$

$$F_{23} = (B_{12} + 2B_{66}){p_m}^2 p_n + B_{22}{p_n}^3 + S_1\, {p_m}^4 p_n, F_{24} = -(B_{121} + B_{661})p_m p_n,$$

$$F_{25} = -B_{222}{p_n}^2 - B_{662}{p_m}^2 + S_{02}{p_m}^4, F_{33} = -(D_{11} + S_0){p_m}^4 - D_{22}{p_n}^2 \qquad (5.26.b)$$

$$-(2D_{12} + 4D_{66}){p_m}^2{p_n}^2 - S_2\, {p_m}^4{p_n}^2, F_{34} = D_{111}{p_m}^3 + (D_{121} + 2D_{661})p_m{p_n}^2,$$

$$F_{35} = (D_{122} + 2D_{662}){p_m}^2 p_n + D_{222}{p_n}^3 + S_{12}\, {p_m}^4 p_n, F_{44} = -A_{5511} - D_{1111}{p_m}^2$$

$$-D_{6611}{p_n}^2, F_{45} = -(D_{1221} + D_{6621})p_m p_n, F_{55} = -A_{4422} - D_{2222}{p_n}^2 - D_{6622}{p_m}^2$$

$$-S_{022}\, {p_m}^4, F_{ij} = F_{ji}.$$

Here, for chosen shape functions $\varphi_1(z)$ and $\varphi_2(z)$, the rigidities in equations (5.26.b) can be calculated by the use of equations (5.18-21). A corresponding set of A_1, A_2, B_1, B_2 and C values will be obtained by solving algebraic equations system (5.25). By inserting the obtained values in equations (5.25), one can write the two-dimensional solution of the problem.

5.4.2. Flexure of a homogeneous rectangular plate subjected to different sets of edge boundary condition-Levy-type solutions

In this subsection, the plate is taken as simply supported at the edges $y = 0$, L_2 and subjected to different sets of edge boundary conditions at the edges $x = 0$, L_1. For a homogeneous rectangular ($N = 1$) plate, Eqs. (5.18.b), (5.19.a) and (5.21.a, b) give:

$$B_{ij} = B_{ijn} = S_1 = S_{02} = 0. \qquad (5.27)$$

The Navier- type differential equations (5.26) reduce to the uncoupled sets of simultaneous differential equations:

$$A_{11}u_{,xx} + (A_{12} + A_{66})v_{,xy} + A_{66}u_{,yy} = 0, \tag{5.28.a}$$

$$(A_{12} + A_{66})u_{,xy} + A_{22}v_{,yy} + A_{66}v_{,xx} + S_0 v_{,xxxx} = 0, \tag{5.28.b}$$

and

$$-(D_{11} + S_0)\, w_{,xxxx} - (2\,D_{12} + 4\,D_{66})\, w_{,xxyy} - D_{22}\, w_{,yyyy} + D_{111}\, u_{1,xxx} -$$

$$(D_{122} + 2D_{662})v_{1,xxy} + (D_{121}+2D_{661})u_{1,xyy} + D_{222}v_{1,yyy} + S_2 w_{,xxxxyy} -$$

$$S_{12}v_{1,xxxxy} = q(x,y)\,, \tag{5.29.a}$$

$$-A_{5511}u_1 - D_{111}w_{,xxx} - (D_{121} + 2D_{661})w_{,xyy} + D_{1111}u_{1,xx} + (D_{1221} +$$

$$D_{6612})v_{1,xy} + D_{6611}u_{1,yy} = 0, \tag{5.29.b}$$

$$-A_{4411}v_1 - (D_{122} + 2D_{662})w_{,xxy} - D_{222}w_{,yyy} + (D_{1221} + D_{6621})u_{1,xy} +$$

$$D_{2222}v_{1,yy} + D_{6622}v_{1,xx} + S_{12}w_{,xxxxy} - S_{022}v_{1,xxxx} = 0. \tag{5.29.c}$$

These two sets are associated with the simply supported edge conditions (5.12) at the edges $y = 0,\ L_2$. In addition, the following edge boundary conditions can be applied on the edges $x = 0,\ L_1$:

For equations (5.28) conditions are:

at a simply supported edges:

$$N_x^c = v = \widehat{M}_x^f = 0, \tag{5.30}$$

at a clamped edges:

$$u = v = v_{,x} = 0, \tag{5.31}$$

at a free edges:

$$N_x^c = N_{xy}^c - \widehat{M}_{x,x}^f = \widehat{M}_x^f = 0, \tag{5.32}$$

For equations (5.29) conditions are:

at a simply supported edges:

$$w = M_x^c + M_x^f + h\,\hat{L}_{x,y}^f = M_x^a = v_1 = \tilde{L}_x^f = 0. \tag{5.33}$$

at a clamped edges:

$$w = w_{,x} = u_1 = v_1 = v_{1,x} = 0. \tag{5.34}$$

at a free edges:

$$M_x^c + M_x^f + h\,\hat{L}_{x,y}^f = 0,. \tag{5.35.a}$$

$$M_{x,x}^c + M_{xy,y}^c + M_{x,x}^f - h\hat{L}_{x,yx}^f - h\,\hat{L}_{x,xy}^f = 0. \tag{5.35.b}$$

$$M_x^a = M_{xy}^a + \tilde{L}_{x,x}^f = \tilde{L}_x^f = 0. \tag{5.35.c}$$

To find the general solution of equations (5.28) and (5.29), the particular and complementary solutions are sought. The particular solution is identical to the solution of simply supported plate and obtained in the same manner described in subsection (5.4.1). In addition, the complementary solution of equations (5.28) and (5.29) is:

$$u(x,y) = \tilde{u}(x)\,sin(p_n y), \tag{5.36.a}$$

$$v(x,y) = \tilde{v}(x)\,cos(p_n y), \tag{5.36.b}$$

$$u_1(x,y) = \tilde{u}_1(x)\,sin(p_n y), \tag{5.37.a}$$

$$v_1(x,y) = \tilde{v}_1(x)\,cos(p_n y), \tag{5.37.b}$$

$$w(x,y,t) = \tilde{w}(x)\,sin(p_n y). \tag{5.37.c}$$

and satisfies the edges boundary conditions (5.12). With the use of the displacement field (5.36) and (5.37) the homogeneous equation form of (5.28) and (5.29) will be:

$$A_{11}\tilde{u}_{,xx} + (A_{12} + A_{66})p_n\tilde{v}_{,x} + A_{66}{p_n}^2\tilde{u} = 0, \tag{5.38.a}$$

$$(A_{12} + A_{66})\tilde{u}_{,x} + A_{22}{p_n}^2\,\tilde{v} + A_{66}\tilde{v}_{,xx} + S_0\tilde{v}_{,xxxx} = 0, \tag{5.38.b}$$

and

$$-(D_{11} + S_0)\tilde{w}_{,xxxx} + (2D_{12} + 4D_{66}){p_n}^2\,w_{,xx} - D_{22}{p_n}^4\,\tilde{w} + D_{111}\tilde{u}_{1,xxx} -$$

$$(D_{122} + 2D_{662})\;p_n\,\tilde{v}_{1,xx} - (D_{121} + 2\,D_{661})\,{p_n}^2\,\tilde{u}_{1,x} + D_{222}\,{p_n}^3\,\tilde{v}_1 - S_2{p_n}^2\tilde{w}_{,xxxx}$$

$$+S_{12}\;p_n\,\tilde{v}_{1,xxxx} = 0, \tag{5.39.a}$$

$$-A_{5511}\,\tilde{u}_1 - D_{111}\,\tilde{w}_{,xxx} + (D_{121} + 2D_{661})\;{p_n}^2\,\tilde{w}_{,x} + D_{1111}\,\tilde{u}_{1,xx} - (D_{1221} +$$

$$D_{6612})\;p_n\tilde{v}_{1,x} - D_{6611}{p_n}^2\,\tilde{u}_1 = 0, \tag{5.39.b}$$

$$-A_{4411}\tilde{v}_1 - (D_{122} + 2D_{662})\;p_n\,\tilde{w}_{,xx} + D_{222}{p_n}^3\,\tilde{w} + (D_{1221} + D_{6621})\;p_n\tilde{u}_{1,x}$$

$$-D_{2222}\,{p_n}^2\,\tilde{v}_1 + D_{6622}\tilde{v}_{1,xx} + S_{12}\;p_n\,\tilde{w}_{,xxxx} - S_{022}\tilde{v}_{1,xxxx} = 0. \tag{5.39.c}$$

These two sets of fourth and twelfth-order ordinary differential equations can be written in the matrix form that will be shown in equations (A2.1, 2) in the Appendix. The solutions of equations (5.38) and (5.39) which are $\tilde{u}, \tilde{v}$ and $\tilde{u}_1, \tilde{v}_1\,\tilde{w}$, respectively, will be provided in equations (A2.3) and (A2.4) in the Appendix. By inserting that solution into equations (5.36) and (5.37) gives the required complementary solution. The general solution will contain sixteen arbitrary constants which will be determined be applying the same number of boundary conditions at the edges $x = 0,\ L_1$ shown in equations (5.30-5.35).

5.4.3. *Determination of the shape functions $\varphi_1(z)$and $\varphi_2(z)$ when fibres resist bending*

Considering the fibres possess bending stiffness, the determination of the shape functions is in similar manner to that followed in the case of perfectly flexible fibres presented in (Soldatos and Watson, 1997b). This manner has been employed in the new version of the one-dimensional models in the third chapter of this study (see subsection (3.4.1)). In the present case when the fibres resist bending, the following two equilibrium equations (Soldatos, 2009)of the three-dimensional asymmetric-stress elasticity will be used to find the shape function:

$$\sigma_{x,x}^{(k)} + \tau_{(xy),y}^{(k)} - \tau_{[xy],y}^{(k)} + \tau_{(xz),z}^{(k)} - \tau_{[xz],z}^{(k)} = 0, \tag{5.40.a}$$

$$\tau_{(xy),x}^{(k)} + \tau_{[xy],x}^{(k)} + \sigma_{y,y}^{(k)} + \tau_{(yz),z}^{(k)} = 0. \tag{5.40.b}$$

Since the displacement *W,* in (5.1.c), is independent on *z,* the use of equation (5.7.a) yields that the differentiation of the anti-symmetric part of the shear stress component $\tau_{[xz]}^{(k)}$ with respect to z equals zero. Thus, the fifth term in equilibrium equation (5.40) cancels. Furthermore, the displacement *V,* in (5.1.b), is dependent on *x* and *y*. Therefore, equations (5.40.a) and (5.40.b) will be affected by the derivative of the anti-symmetric part of the shear stress component $\tau_{[xy]}^{(k)}$. This was not as in the case of that in the beams case explained in subsection 3.4.1

With the use of equations (5.3)-(5.8) and the choice of the displacement field (5.24), one can write the two equilibrium equations (5.40) as follows:

$$\propto_{11}^{(k)} + \propto_{12}^{(k)} \varphi_1^{(k)} + \propto_{13}^{(k)} \varphi_2^{(k)} + \propto_{14}^{(k)} \varphi_1''^{(k)} = 0, \tag{5.41.c}$$

$$\propto_{21}^{(k)} + \propto_{22}^{(k)} \varphi_1^{(k)} + \propto_{23}^{(k)} \varphi_2^{(k)} + \propto_{24}^{(k)} \varphi_2''^{(k)} = 0, \tag{5.41.d}$$

where

$$\propto_{11}^{(k)} = -Q_{11}^{(k)} p_m{}^2 \lambda_1 - Q_{12}^{(k)} p_m p_n \lambda_3 + Q_{11}^{(k)} p_m{}^3 z + Q_{22}^{(k)} p_m p_n{}^2 z - Q_{55}^{(k)} p_n{}^2 \lambda_1 -$$

$$Q_{55}^{(k)} p_m p_n \lambda_3 + 2Q_{55}^{(k)} p_m p_n{}^2 z + \frac{1}{2} d^f p_n p_m{}^3 \lambda_3 - \frac{1}{2} d^f p_m{}^3 p_n{}^2 z, \propto_{14}^{(k)} = Q_{55}^{(k)} \lambda_2,$$

$$\propto_{12}^{(k)} = \left(-Q_{11}^{(k)} p_m{}^2 + Q_{55}^{(k)} p_n{}^2\right) \lambda_2, \propto_{13}^{(k)} = (-Q_{12}^{(k)} - Q_{55}^{(k)} + \tfrac{1}{2} d^f p_m{}^2) p_m p_n \lambda_4,$$

$$\propto_{21}^{(k)} = -Q_{55}^{(k)} p_m p_n \lambda_1 - Q_{55}^{(k)} p_m{}^3 \lambda_3 + 2Q_{55}^{(k)} p_m{}^3 p_n z - Q_{12}^{(k)} p_m p_n \lambda_1 - Q_{22}^{(k)} p_n{}^2 \lambda_3$$

$$-Q_{12}^{(k)} p_m{}^2 p_n z + Q_{22}^{(k)} p_n{}^3 z - \frac{1}{2} d^f p_m{}^4 \lambda_3 + \frac{1}{2} d^f p_m{}^4 p_n z, \propto_{24}^{(k)} = Q_{44}^{(k)} \lambda_4,$$

$$\propto_{22}^{(k)} = -(Q_{55}^{(k)} + Q_{12}^{(k)}) p_m p_n \lambda_2, \propto_{23}^{(k)} = -\left(Q_{55}^{(k)} p_m{}^2 + Q_{22}^{(k)} p_n{}^2 + \tfrac{1}{2} d^f p_m{}^4\right) \lambda_4,$$

$$\lambda_1 = \frac{A_1}{C}, \lambda_2 = \frac{B_1}{C}, \lambda_3 = \frac{A_2}{C}, \lambda_4 = \frac{B_2}{C}. \tag{5.42}$$

A particular solution of equations (5.41) that depends on four arbitrary constants $\lambda_1, \lambda_2, \lambda_3$, and λ_4 can be written in the following form:

$$\varphi_{1\,p}^{(k)} = \frac{\propto_{23}^{(k)} \propto_{11}^{(k)} - \propto_{13}^{(k)} \propto_{21}^{(k)}}{\propto_{23}^{(k)} \propto_{12}^{(k)} - \propto_{13}^{(k)} \propto_{22}^{(k)}}, \tag{5.43.a}$$

$$\varphi_{2\,p}^{(k)} = \frac{\propto_{22}^{(k)} \propto_{11}^{(k)} - \propto_{21}^{(k)} \propto_{12}^{(k)}}{\propto_{23}^{(k)} \propto_{12}^{(k)} - \propto_{13}^{(k)} \propto_{22}^{(k)}}, \tag{5.43.b}$$

while the complementary solution of it is as follows:

$$\varphi_{1\,c}^{(k)} = (-c_1^{(k)} e^{\frac{\delta_5^{(k)}}{2} z} + c_2^{(k)} e^{-\frac{\delta_5^{(k)}}{2} z}) \frac{\delta_2^{(k)}}{\delta_5^{(k)} (\delta_3^{(k)} + \delta_4^{(k)})} - (c_3^{(k)} e^{\frac{\delta_8^{(k)}}{2} z} +$$

$$c_4^{(k)} e^{-\frac{\delta_8^{(k)}}{2} z}) \frac{\delta_6^{(k)}}{\delta_8^{(k)} (\delta_3^{(k)} + \delta_7^{(k)})}, \tag{5.44}$$

$$\varphi_{2\,c}^{(k)} = (c_1^{(k)} e^{\frac{\delta_5^{(k)}}{2}z} - c_2^{(k)} e^{-\frac{\delta_5^{(k)}}{2}z}) \frac{2\beta_{24}^{(k)}}{\delta_5^{(k)}} + \left(c_3^{(k)} e^{\frac{\delta_8^{(k)}}{2}z} - c_4^{(k)} e^{-\frac{\delta_8^{(k)}}{2}z} \right) \frac{2\beta_{24}^{(k)}}{\delta_8^{(k)}},$$

with $c_1^{(k)}, c_2^{(k)}, c_3^{(k)}$ and $c_4^{(k)}$ being the appropriately modified $2N$ constants of integration. The expressions of $\beta_{24}^{(k)}, \delta_2^{(k)}, \delta_3^{(k)}, \ldots, \delta_8^{(k)}$ are shown in (A2.5) in the Appendix. The general solution of the two equilibrium equations (5.41) forms the following shape functions:

$$\varphi_1^{(k)} = \varphi_{1\,c}^{(k)} + \varphi_{1\,p}^{(k)}, \qquad \varphi_2^{(k)} = \varphi_{2\,c}^{(k)} + \varphi_{2\,p}^{(k)}. \tag{5.45.a}$$

For N-layered plate, these shape functions contain $4(N+1)$ unknown constants to be determined. The $4N$ arbitrary constants of integration, $c_1^{(k)}, c_2^{(k)}, c_3^{(k)}$ and $c_4^{(k)}$, will be determined by the four zero shear traction boundary conditions specified on the plate lateral planes and applying the $4(N-1)$ continuity conditions on the $N-1$ material interfaces of the laminated plate considered. These $4N$ conditions can be detailed as follows:

(i) The zero shear traction boundary conditions are:

$$(\tau_{(xz)} - \tau_{[xz]})\big|_{z=\frac{h}{2}} = 0,\ (\tau_{(xz)} - \tau_{[xz]})\big|_{z=\frac{-h}{2}} = 0,\ \tau_{(yz)}\big|_{z=\frac{h}{2}} = 0,\ \tau_{(yz)}\big|_{z=\frac{-h}{2}} = 0, \tag{5.46}$$

which yield the following four of the required algebraic equations:

$$Q_{55}^{(k)} \left(\varphi_{1,z\,c}^{(k)} + \varphi_{1,z\,p}^{(k)} \right)\Big|_{z=\frac{h}{2}} \lambda_2 + \frac{1}{2} d^{f^{(k)}} p_m^3 = 0, \tag{5.47.a}$$

$$Q_{55}^{(k)} \left(\varphi_{1,z\,c}^{(k)} + \varphi_{1,z\,p}^{(k)} \right)\Big|_{z=-\frac{h}{2}} \lambda_2 + \frac{1}{2} d^{f^{(k)}} p_m^3 = 0, \tag{5.47.b}$$

$$\left(\varphi_{2,z\,c}^{(k)}+\varphi_{2,z\,p}^{(k)}\right)\Big|_{z=\frac{h}{2}}=0, \tag{5.47.c}$$

$$\left(\varphi_{2,z\,c}^{(k)}+\varphi_{2,z\,p}^{(k)}\right)\Big|_{z=-\frac{h}{2}}=0, \tag{5.47.d}$$

(ii) The continuity of the displacements $U(x,y,z)$ and $V(x,y,z)$ conditions at the kth material surfaces, $z=z_k$, of the plate $(k=1,2,\dots,N-1)$ are:

$$U^{(k)}(x,y,z)\big|_{z=z_k}=U^{(k+1)}(x,y,z)\big|_{z=z_k}, V^{(k)}(x,y,z)\big|_{z=z_k}=V^{(k+1)}(x,y,z)\big|_{z=z_k}. \tag{5.48}$$

With the use of equations (5.1), (5.24) and (5.42), one can obtain the following $2(N-1)$ algebraic equations:

$$\varphi_{1\,c}^{(k)}(z_k)+\varphi_{1\,p}^{(k)}(z_k)-\varphi_{1\,c}^{(k+1)}(z_k)-\varphi_{1\,p}^{(k+1)}(z_k)=0;(k=1,2,\dots,N-1), \tag{5.49.a}$$

$$\varphi_{2\,c}^{(k)}(z_k)+\varphi_{2\,p}^{(k)}(z_k)-\varphi_{2\,c}^{(k+1)}(z_k)-\varphi_{2\,p}^{(k+1)}(z_k)=0;(k=1,2,\dots,N-1). \tag{5.49.b}$$

(iii) The continuity of the interlaminar shear stresses $\tau_{xz}^{(k)}$ and $\tau_{zx}^{(k)}$ conditions at the kth material surfaces, $z=z_k$, of the plate $(k=1,2,\dots,N-1)$ are:

$$\left(\tau^{(k)}{}_{(xz)}-\tau^{(k)}{}_{[xz]}\right)\Big|_{z=z_k}=\left(\tau^{(k+1)}{}_{(xz)}-\tau^{(k+1)}{}_{[xz]}\right)\Big|_{z=z_k}, \tag{5.50.a}$$

$$\tau^{(k)}{}_{(yz)})\big|_{z=z_k}=\tau^{(k+1)}{}_{(yz)}\big|_{z=z_k}. \tag{5.50.b}$$

With the use of equations (5.5), (5.6), (5.7.a) and (5.50), one can obtain the following $2(N-1)$ algebraic equations:

$$Q_{55}^{(k)}\left(\varphi_{1,z\,c}^{(k)}(z_k)+\varphi_{1,z\,p}^{(k)}(z_k)\right)-Q_{55}^{(k+1)}\left(\varphi_{1,z\,c}^{(k+1)}(z_k)+\varphi_{1,z\,p}^{(k+1)}(z_k)\right)=0, \tag{5.51.a}$$

$$Q_{44}^{(k)}\left(\varphi_{2,z\,c}^{(k)}(z_k)+\varphi_{2,z\,p}^{(k)}(z_k)\right)-Q_{44}^{(k+1)}\left(\varphi_{2,z\,c}^{(k+1)}(z_k)+\varphi_{2,z\,p}^{(k+1)}(z_k)\right)=0. \tag{5.51.b}$$

Finally, by making use of the constraint equations (5.2), one can obtain the following four algebraic equations:

$$\varphi_{1\,c}^{(k)}(0) + \varphi_{1\,p}^{(k)}(0) = 0, \tag{5.52.a}$$

$$\varphi_{2\,c}^{(k)}(0) + \varphi_{2\,p}^{(k)}(0) = 0, \tag{5.52.b}$$

$$\varphi_{1,z\,c}^{(k)}\Big|_{z=0} + \varphi_{1,z\,p}^{(k)}\Big|_{z=0} = 0, \tag{5.52.c}$$

$$\varphi_{2,z\,c}^{(k)}\Big|_{z=0} + \varphi_{2,z\,p}^{(k)}\Big|_{z=0} = 0. \tag{5.52.d}$$

Equations (5.47), (5.49), (5.51) and (5.52) form a set of $4(N+1)$ linear algebraic equations, the solution of which will provide numerical values to the same number of unknowns $\lambda_1, \lambda_2, \lambda_3, \lambda_4, c_1^{(k)}, c_2^{(k)}, c_3^{(k)}$ and $c_4^{(k)}$. It should be noted that the shape functions are evidently affected by the presence of the resistance of fibres in bending.

5.5. Dynamic solution for a homogeneous rectangular plate subjected to different sets of end boundary conditions

In this section, considering that fibres resist bending, the solution of free vibration of transversely isotropic plate is constructed based on 2D plate models developed in (Soldatos, 2009). The plate is subjected to different sets of end boundary conditions. The effective way to test the reliability of such thin-walled structures modelling is by performing numerical comparisons with corresponding results of the dynamic three-dimensional asymmetric-stress elasticity solution found in the fourth chapter of this thesis. In this context, the dynamic solution of free vibration of SSSS plate is found first. Then, different boundary conditions are considered. In this problem, the lateral surfaces are stress

free and therefore the loading function $q(x,y) = 0$. Moreover, considering the equations (5.10.a) and (5.27), the solution of flexure vibration can be obtained by solving equations (5.22.c-e) which will be in the following form:

$$-(D_{11} + S_0)\, w_{,xxxx} - (2\,D_{12} + 4\,D_{66})\, w_{,xxyy} - D_{22}\, w_{,yyyy} + D_{111}\, u_{1,xxx} -$$

$$(D_{122} + 2D_{662})v_{1,xxy} + (D_{121}+2D_{661})u_{1,xyy} + D_{222}v_{1,yyy} + S_2 w_{,xxxxyy} -$$

$$S_{12}v_{1,xxxxy} = \rho_0\, w_{,tt} - \rho_2\big(w_{,xxtt} + w_{,yytt}\big) + \hat{\rho}_1^{11}\, u_{1,xtt} + \hat{\rho}_1^{21}\, v_{1,ytt}\,, \qquad (5.53.a)$$

$$-A_{5511}u_1 - D_{111}w_{,xxx} - (D_{121} + 2D_{661})w_{,xyy} + D_{1111}u_{1,xx} + (D_{1221} +$$

$$D_{6612})v_{1,xy} + D_{6611}u_{1,yy} = \hat{\rho}_0^{11}\, u_{,tt} - \hat{\rho}_1^{11}\, w_{,xtt} + \hat{\rho}_0^{12}\, u_{1,tt}\,, \qquad (5.53.b)$$

$$-A_{4411}v_1 - (D_{122} + 2D_{662})w_{,xxy} - D_{222}w_{,yyy} + (D_{1221} + D_{6621})u_{1,xy} + D_{2222}v_{1,yy}$$

$$+D_{6622}v_{1,xx} + S_{12}w_{,xxxxy} - S_{022}v_{1,xxxx} = \hat{\rho}_0^{21}\, v_{,tt} - \hat{\rho}_1^{21}\, w_{,ytt} + \hat{\rho}_0^{22}\, v_{1,tt}\,. \qquad (5.53.c)$$

5.5.1. Dynamic solution for SSSS rectangular plate

The SSSS edge boundary conditions (5.12) and (5.33) are exactly satisfied by a displacement field of the form,

$$u_1(x,y,t) = A^{(u_1)}\, cos(p_m x)\, sin(p_n y)\, cos(\omega t), \qquad (5.54.a)$$

$$v_1(x,y,t) = A^{(v_1)}\, sin(p_m x)\, cos(p_n y)\, cos(\omega t), \qquad (5.54.b)$$

$$w(x,y,t) = A^{(w)}\, sin(p_m x)\, sin(p_n y)\, cos(\omega t), \qquad (5.54.c)$$

where $A^{(u_1)}, A^{(v_1)}$ and $A^{(w)}$ are unknown constants. With the use of this displacement field, the set of partial differential equations (5.53) is converted into the following corresponding eigenvalue problem:

$$(\boldsymbol{K} - (\omega^*)^2\, \boldsymbol{H})\, \boldsymbol{X} = 0,\ \boldsymbol{X} = (A^{(w)} \quad A^{(u_1)} \quad A^{(v_1)})^T. \tag{5.55}$$

Here the normalised frequency parameter is considered as defined in equation (2.35) where $C_{55}^{(1)} = G_{12}^{(1)}$ and the mass and stiffness matrices are as follows:

$$\boldsymbol{H} = \frac{G_{12}}{\rho h^2}\begin{bmatrix} \rho_0 + \rho_2(p_m^2 + p_n^2) & -\hat{\rho}_1^{11} p_m & -\hat{\rho}_1^{21} p_n \\ sym & \hat{\rho}_0^{12} & 0 \\ & & \hat{\rho}_0^{22} \end{bmatrix}, \boldsymbol{K} = \begin{bmatrix} k_{11} & k_{12} & k_{13} \\ sym & k_{22} & k_{23} \\ & & k_{33} \end{bmatrix}, \tag{5.56}$$

where

$$k_{11} = -(D_{11} + S_0)p_m^4 - D_{22}p_n^4 - (2D_{12} + 4D_{66})p_m^2 p_n^2 - S_2 p_m^4 p_n^2,$$

$$k_{12} = D_{111}p_m^3 + (D_{121} + 2D_{661})p_m p_n^2,\ \ k_{13} = (D_{122} + 2D_{662})p_n p_m^2 + D_{222}p_n^3 \tag{5.57}$$

$$+S_{12}p_m^4 p_n,\ \ k_{22} = -A_{5511} - D_{1111}p_m^2 - D_{6611}p_n^2,\ \ k_{23} = -(D_{1221} + D_{6621})p_m p_n,$$

$$k_{33} = -A_{4422} - D_{2222}p_n^2 - D_{6622}p_m^2 - S_{022}p_m^4 .$$

The values of the frequency parameter ω^* can be obtained by solving the eigenvalue problem (5.55).

5.5.2. Free vibration of a homogeneous rectangular plates subjected to different sets of end boundary conditions

The dynamic solution for a free vibration of homogeneous rectangular plate subjected to different sets of end boundary conditions is found based on the advanced version of CPT (Soldatos, 2009), which takes into account that the fibres resist bending. The shape

functions take zero value in the displacement field (5.1) and therefore equations (5.53) are reduced to the following equation:

$$-(D_{11} + S_0)\, w_{,xxxx} - (2\,D_{12} + 4\,D_{66})\, w_{,xxyy} - D_{22}\, w_{,yyyy} + S_2 w_{,xxxxyy}$$

$$= \rho_0\, w_{,tt} - \rho_2\left(w_{,xxtt} + w_{,yytt}\right). \tag{5.58}$$

This partial differential equation is associated with the following simply supported boundary conditions that applied on $y = 0,\ L_2$:

$$N_y^c = 0,\quad u = 0,\quad w = 0,\quad M_y^c = 0, \tag{5.59}$$

and at the edges $x = 0,\ L_1$, the following sets of edge boundary conditions can be applied:

at a simply supported edges: $w = M_x^c + M_x^f + h\,\hat{L}_{x,y}^f = 0.$ (5.60)

at a clamped edges: $w = w_{,x} = 0.$ (5.61)

at a free edges: $M_x^c + M_x^f + h\,\hat{L}_{x,y}^f = 0,$ (5.62.a)

$$M_{x,x}^c + M_{xy,y}^c + M_{x,x}^f - h\hat{L}_{x,yx}^f - h\,\hat{L}_{x,xy}^f = 0. \tag{5.62.b}$$

The solution of equations (5.58) is assumed in the following form:

$$w(x) = w^*(x) sin\,(p_n y)\, cos(\omega t). \tag{5.63}$$

Inserting equations (5.63) into equations (5.58) yields the following ordinary differential equations:

$$-(D_{11} + S_0 + S_2\, p_n^2) w_{,xxxx}^* + \left((2\,D_{12} + 4\,D_{66})\, p_n^2 - \rho_2\,\omega^2\right) w_{,xx}^* + (-D_{22}\, p_n^4 +$$

$$(\rho_0 + \rho_2 p_n^2)\,\omega^2)\, w^* = 0. \tag{5.64}$$

The solution of this ordinary differential equation is as follows:

$$w^*(x) = \sum_{i=1}^{4} k_i \, e^{\alpha_i x}, \tag{5.65}$$

where k_1, k_2, k_3, k_4 are arbitrary constants. The expressions of $\alpha_i \, ; i = 1, .., 4$ are given in the equations (A2.6) in the Appendix. By inserting equation (5.65) into equations (5.63), one can obtain the following solution of equation (5.58):

$$w(x) = sin\,(p_n y)\, cos(\omega t) \sum_{i=1}^{4} k_i \, e^{\alpha_i x}. \tag{5.66}$$

The case of SSCC rectangular plate is considered as example to find the frequency parameter. In such case, inserting the solution (5.66) into the set of edge boundary conditions (5.61) at $x = 0,\ L_1$ yields the following:

$$\mathbf{J} \times \mathbf{K} = \mathbf{0}, \tag{5.67}$$

where

$$\boldsymbol{K} = [k_1 \quad k_2 \quad k_3 \quad k_4]^T, \tag{5.68}$$

$$\boldsymbol{J} = \begin{bmatrix} k_1 & k_2 & k_3 & k_4 \\ k_1 \propto_1 & k_2 \propto_2 & k_3 \propto_3 & k_4 \propto_4 \\ k_1 e^{\propto_1 L_1} & k_2 e^{\propto_2 L_1} & k_3 e^{\propto_3 L_1} & k_4 e^{\propto_4 L_1} \\ k_1 \propto_1 e^{\propto_1 L_1} & k_2 \propto_2 e^{\propto_2 L_1} & k_3 \propto_3 e^{\propto_3 L_1} & k_4 \propto_4 e^{\propto_4 L_1} \end{bmatrix}. \tag{5.69}$$

For a non-trivial solution of equation (5.67), the determinant of $\mathbf{J}$ must be zero. This condition yields the following characteristic equation:

$$det\,(\boldsymbol{J}(\omega^*)) = 0. \tag{5.70}$$

where ω^* represent the dimensionless frequency parameter that expressed by equation (2.35). Equations (5.70) can be solved by similar manner that followed to solve equation (2.45). The roots of such algebraic equations produce the value of frequencies.

5.6. Numerical results and discussion

The following numerical results are divided into two parts. In the first part, numerical results for the static problem are presented. Then, results for the dynamic solution are provided. Considering the fibre bending stiffness, the shape function which is used in this section is the same one that used in the third chapter.

5.6.1. Flexure numerical results

In this subsection, the employed method is initially applied for the solution of rectangular plate deformed in cylindrical bending and has the four edges simply supported (SSSS plates). This case of SSSS is used to test the reliability of the employed thin plate theory, by comparing its results against corresponding numerical results based on the exact asymmetric-stress three-dimensional solution presented in the fourth chapter. Furthermore, different sets of edge boundary conditions are considered as further applications of the method.

The material of the plate is assumed to be transversely isotropic and the layer material is characterized as described in (3.54). For presenting the numerical results of thin rectangular plate, the following normalised quantities are used (Soldatos and Shu, 2001):

$$X = x/L_1,\ Y = y/L_2,\ Z = z/h, \tag{3.71}$$

$$\bar{W} = E_T W 10^2 h^3/{L_1}^4 q_{11},\ \bar{\tau}_{xz} = \tau_{xz} h/L_1 q_{11},\ \bar{\tau}_{zx} = \tau_{zx} h/L_1 q_{11}. \tag{3.72}$$

As example of numerical results, this subsection focuses on studying the affect the presence of the resistance of fibres in bending on the deflection and shear stresses (τ_{zx} & τ_{zx}) distributions.

Table 5.1 Through-thickness deflection distributions for a SSSS homogeneous plate

Z/h	$E_T W(L_1/2, L_2/2, Z)/L_1 q_1 ; (h/L_1 = 0.25,\ L_2/L_1 = 10000)$					
	$\lambda = 0$		$\lambda = 0.001$		$\lambda = 0.005$	
	2-D theory	3-D elasticity	2-D theory	3-D elasticity	2-D theory	3-D elasticity
0.5	-1.132048	-1.209112	-1.119139	-1.192557	-1.070003	-1.130897
0.4	-1.132048	-1.188321	-1.119139	-1.171735	-1.070003	-1.109962
0.3	-1.132048	-1.167960	-1.119139	-1.151390	-1.070003	-1.089675
0.2	-1.132048	-1.149490	-1.119139	-1.132947	-1.070003	-1.071337
0.1	-1.132048	-1.133595	-1.119139	-1.117077	-1.070003	-1.055557
0	-1.132048	-1.120566	-1.119139	-1.104060	-1.070003	-1.042589
-0.1	-1.132048	-1.110468	-1.119139	-1.093961	-1.070003	-1.032485
-0.2	-1.132048	-1.103195	-1.119139	-1.086674	-1.070003	-1.025149
-0.3	-1.132048	-1.098430	-1.119139	-1.081890	-1.070003	-1.020294
-0.4	-1.132048	-1.095495	-1.119139	-1.078945	-1.070003	-1.017314
-0.5	-1.132048	-1.093010	-1.119139	-1.076491	-1.070003	-1.014978

Table 5.2 Through-thickness deflection distributions for a SSSS homogeneous plate

Z/h	$E_T W(L_1/2, L_2/2, Z)10^2 h^3/{L_1}^4 q_1 ; (h/L_1 = 0.01,\ L_2/L_1 = 2)$					
	$\lambda = 0$		$\lambda = 0.001$		$\lambda = 0.005$	
	2-D theory	3-D elasticity	2-D theory	3-D elasticity	2-D theory	3-D elasticity
0.5	-0.304978	-0.304675	-0.290532	-0.277225	-0.244246	-0.203783
0.4	-0.304978	-0.304680	-0.290532	-0.277230	-0.244246	-0.203786
0.3	-0.304978	-0.304684	-0.290532	-0.277233	-0.244246	-0.203789
0.2	-0.304978	-0.304687	-0.290532	-0.277236	-0.244246	-0.203791
0.1	-0.304978	-0.304688	-0.290532	-0.277237	-0.244246	-0.203792
0	-0.304978	-0.304689	-0.290532	-0.277237	-0.244246	-0.203792
-0.1	-0.304978	-0.304688	-0.290532	-0.277237	-0.244246	-0.203792
-0.2	-0.304978	-0.304687	-0.290532	-0.277235	-0.244246	-0.203790
-0.3	-0.304978	-0.304684	-0.290532	-0.277233	-0.244246	-0.203788
-0.4	-0.304978	-0.304680	-0.290532	-0.277229	-0.244246	-0.203786
-0.5	-0.304978	-0.304675	-0.290532	-0.277225	-0.244246	-0.203782

Table 5.3 Through-thickness shear stress, $\bar{\tau}_{zx}$, distributions for a SSSS homogeneous plate

Z/h	$\tau_{zx}(0, L_2/2, Z)/q_1; (h/L_1 = 0.25,\ L_2/L_1 = 10000)$					
	$\lambda = 0$		$\lambda = 0.001$		$\lambda = 0.005$	
	2-D theory	3-D elasticity	2-D theory	3-D elasticity	2-D theory	3-D elasticity
0.5	0	0	0	0	0	0
0.4	-0.895456	-0.928471	-0.870726	-0.907833	-0.803782	-0.830907
0.3	-1.336337	-1.372025	-1.306579	-1.341342	-1.199822	-1.227002
0.2	-1.549672	-1.574516	-1.517482	-1.539083	-1.391461	-1.407081
0.1	-1.645319	-1.654684	-1.612038	-1.617219	-1.477380	-1.477683
0	-1.672531	-1.666482	-1.638940	-1.628535	-1.501824	-1.487239
-0.1	-1.645319	-1.626493	-1.612038	-1.589272	-1.477380	-1.450707
-0.2	-1.549672	-1.522382	-1.517482	-1.487400	-1.391461	-1.357192
-0.3	-1.336337	-1.306658	-1.306579	-1.276538	-1.199822	-1.164445
-0.4	-0.895456	-0.872582	-0.870726	-0.852425	-0.803782	-0.777415
-0.5	0	0	0	0	0	0

Table 5.4 Through-thickness shear stress, $\bar{\tau}_{zx}$, distributions for a SSSS homogeneous plate

Z/h	$\tau_{zx}(0, L_2/2, Z)/q_1; (h/L_1 = 0.01,\ L_2/L_1 = 2)$					
	$\lambda = 0$		$\lambda = 0.001$		$\lambda = 0.005$	
	2-D theory	3-D elasticity	2-D theory	3-D elasticity	2-D theory	3-D elasticity
0.5	0	0	0	0	0	0
0.4	-0.170579	-0.170421	-0.155384	-0.155016	-0.101284	-0.113800
0.3	-0.303113	-0.302832	-0.276496	-0.275458	-0.188415	-0.202219
0.2	-0.397705	-0.397337	-0.362937	-0.361420	-0.250602	-0.265325
0.1	-0.454430	-0.454011	-0.414774	-0.412970	-0.287894	-0.303169
0	-0.473333	-0.472897	-0.432049	-0.430149	-0.300322	-0.315780
-0.1	-0.454430	-0.454011	-0.414774	-0.412970	-0.287894	-0.303169
-0.2	-0.397705	-0.397337	-0.362937	-0.361420	-0.250602	-0.265325
-0.3	-0.303113	-0.302832	-0.276496	-0.275458	-0.188415	-0.202219
-0.4	-0.170579	-0.170421	-0.155384	-0.155016	-0.101284	-0.113800
-0.5	0	0	0	0	0	0

Table 5.5 Through-thickness shear stress, $\bar{\tau}_{xz}$, distributions for a SSSS homogeneous plate

Z/h	$\tau_{xz}(0, L_2/2, Z)/q_1 ; (h/L_1 = 0.25,\ L_2/L_1 = 10000)$					
	$\lambda = 0$		$\lambda = 0.001$		$\lambda = 0.005$	
	2-D theory	3-D elasticity	2-D theory	3-D elasticity	2-D theory	3-D elasticity
0.5	0	0	-0.014519	-0.030943	-0.138213	0.146715
0.4	-0.895456	-0.928471	-0.899764	-0.938236	-0.942597	-0.974906
0.3	-1.336337	-1.372025	-1.335617	-1.371217	-1.338638	-1.368369
0.2	-1.549672	-1.574516	-1.546520	-1.568479	-1.530276	-1.546069
0.1	-1.645319	-1.654684	-1.641076	-1.646204	-1.616195	-1.614624
0	-1.672531	-1.666482	-1.667977	-1.657182	-1.640639	-1.622498
-0.1	-1.645319	-1.626493	-1.641076	-1.617656	-1.616195	-1.584655
-0.2	-1.549672	-1.522382	-1.546520	-1.515595	-1.530276	-1.490188
-0.3	-1.336337	-1.306658	-1.335617	-1.304609	-1.338638	-1.296811
-0.4	-0.895456	-0.872582	-0.899764	-0.880420	-0.942597	-0.909394
-0.5	0	0	-0.014519	-0.027931	-0.138213	-0.131677

Table 5.6 Through-thickness shear stress, $\bar{\tau}_{xz}$, distributions for a SSSS homogeneous plate

Z/h	$\tau_{xz}(0, L_2/2, Z)\mathrm{h}/q_1 L_1 ; (h/L_1 = 0.01,\ L_2/L_1 = 2)$					
	$\lambda = 0$		$\lambda = 0.001$		$\lambda = 0.005$	
	2-D theory	3-D elasticity	2-D theory	3-D elasticity	2-D theory	3-D elasticity
0.5	0	0	-0.029657	-0.028772	-0.115888	-0.105750
0.4	-0.170579	-0.170421	-0.185537	-0.183789	-0.228031	-0.219552
0.3	-0.303113	-0.302832	-0.306650	-0.304231	-0.315162	-0.307971
0.2	-0.397705	-0.397337	-0.393091	-0.390194	-0.377349	-0.371080
0.1	-0.454430	-0.454011	-0.444928	-0.441744	-0.414642	-0.408923
0	-0.473333	-0.472897	-0.462202	-0.458923	-0.427069	-0.421535
-0.1	-0.454430	-0.454011	-0.444928	-0.441744	-0.414642	-0.408923
-0.2	-0.397705	-0.397337	-0.393091	-0.390193	-0.377349	-0.371079
-0.3	-0.303113	-0.302832	-0.306650	-0.304231	-0.315162	-0.307971
-0.4	-0.170579	-0.170421	-0.185537	-0.183789	-0.228031	-0.219551
-0.5	0	0	-0.029657	-0.028772	-0.115888	-0.105749

Tables 5.1 and 5.2 compare numerical values of normalised deflection distributions for thick and thin SSSS homogeneous plates, respectively, at different values of λ. Such numerical values are obtained on the basis of the exact asymmetric-stress elasticity solution and employed two-dimensional plate theory. It is shown that the value of the deflection which obtained based on the 2D theory does not change through the plate thickness. This happened because such theory does not take the transverse normal deformation effects into account and the deflection is independent on z (see equation 5.1.c).

Table 5.1 shows that numerical values of the deflection at $\lambda = 0$ are identical to that presented in the case perfectly flexible fibres (Soldatos and Watson, 1997b). It is observed that the two-dimensional plate theory employed provides deflection distributions that are close to those predicted by the exact asymmetric-stress three-dimensional solution for thick plates. Table 5.2 shows that the numerical values obtained on the basis of the two-dimensional plate theory employed are close to their counterparts of the exact asymmetric-stress three-dimensional solution for thin plate at $\lambda = 0$ and $\lambda = 0.001$. However, they are not for the case of $\lambda = 0.005$.

Table 5.3 depicts numerical values of normalised through-thickness shear stress, $\bar{\tau}_{zx}$, distributions for a SSSS thick homogeneous rectangular plate $(h/L_1 = 0.25)$ obtained on the basis of the exact asymmetric-stress solution and the employed two-dimensional theory at different values of λ. It is noted that the two-dimensional theory provides close results to the exact three-dimensional solution. It should be mentioned that for the case perfectly flexible fibres ($\lambda = 0$), the numerical values are identical to those presented in (Soldatos and Watson, 1997b).Table 5.4 compares numerical values of normalised through-thickness shear stress, $\bar{\tau}_{zx}$, distributions for a SSSS thin homogeneous rectangular plate $(h/L_1 = 0.01)$ obtained based on the exact asymmetric-stress solution and the

employed five degrees-of-freedom plate theory at different values of λ. It is observed that the results of the two solutions are very close to each other.

Tables 5.5 and 5.6 present numerical values of normalised through-thickness shear stress, $\bar{\tau}_{xz}$, distributions for a SSSS thick plate $(h/L_1 = 0.25)$ and thin plate $(h/L_1 = 0.01)$, respectively. It is observed that results based on the 2-D theory are close to their counterparts obtained on the basis of the 3-D asymmetric-stress solution. Furthermore, the results of the thin plate are closer than that of the thick plate. In the case of stiff fibres $(\lambda = 0.001 \ \& \ \lambda = 0.005)$, it should be observed that $\bar{\tau}_{xz} \neq \bar{\tau}_{zx}$.

Figures 5.1 and 5.2 show the normalised deflection distributions of a homogeneous plate that is simply supported on the edges $y = 0, L_2$, clamped at the edge $x = 0$ and free at the edge $x = L_1$ (SSCF plate) for $\lambda = 0$ and $\lambda = 0.001$, respectively. It is shown that the magnitude of the normalised deflection at $\lambda = 0.001$ is less than that of $\lambda = 0$. This emphasise that when fibres resist bending, the plate becomes stiffer.

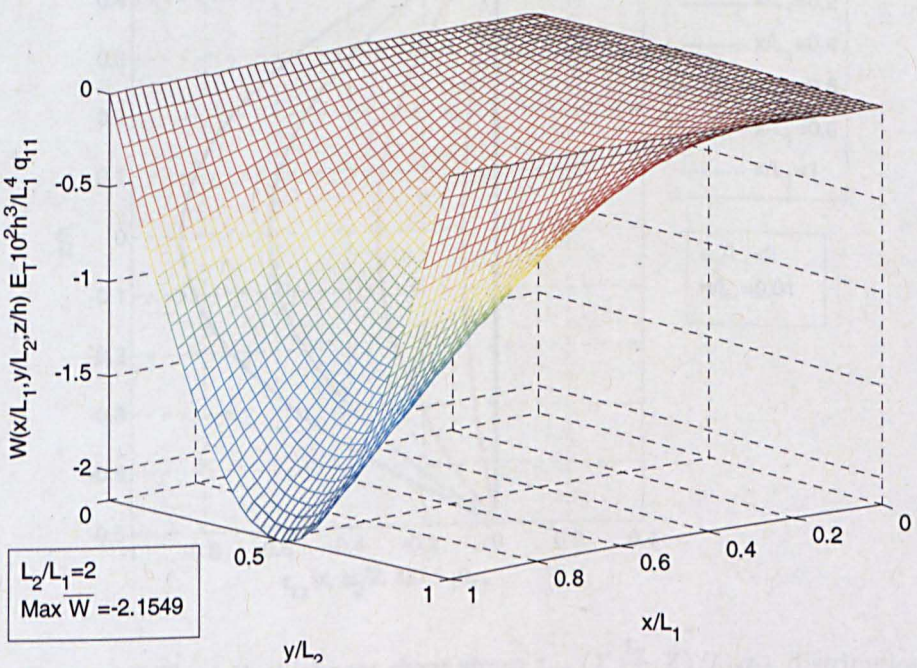

Figure 5.1 Deflection distributions of a SSCF homogeneous plate $(h/L_1 = 0.01, \lambda = 0)$

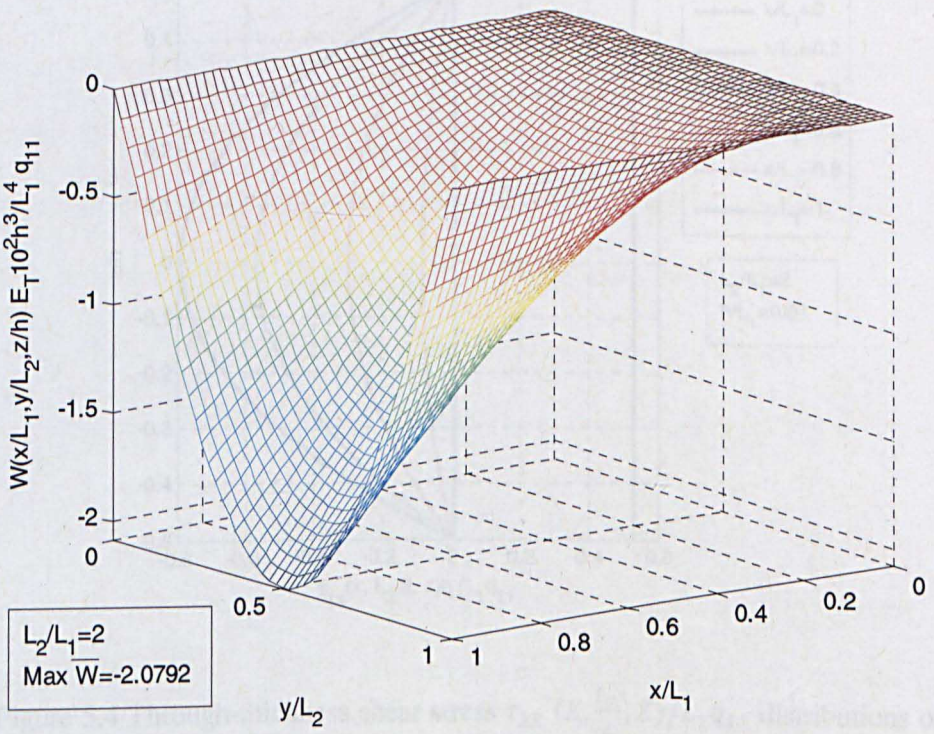

Figure 5.2 Deflection distributions of a SSCF homogeneous plate ($h/L_1 = 0.01, \lambda = 0.001$)

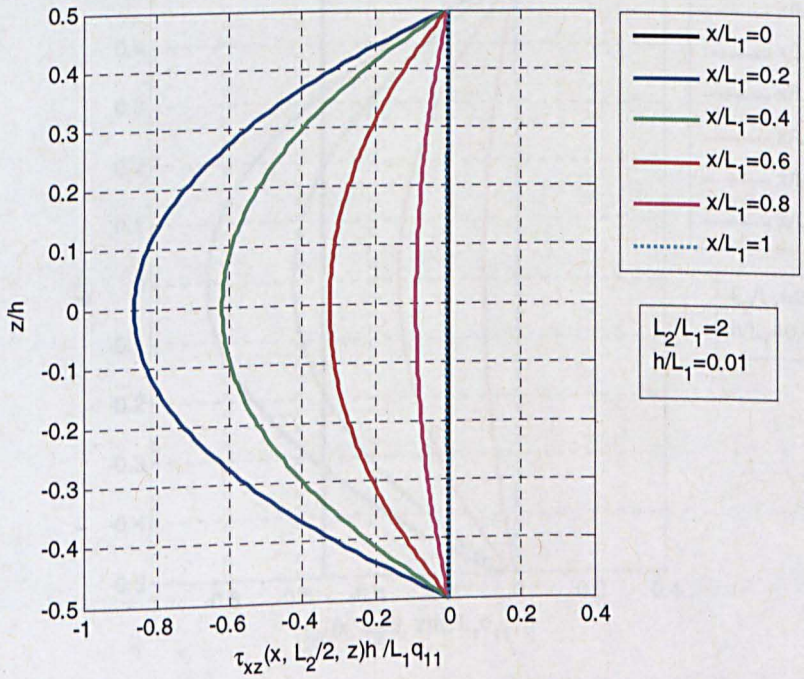

Figure 5.3 Through-thickness shear stress $\tau_{xz}\ (X, \frac{L_2}{2}, Z)/L_1 q_{11}$ distributions of a SSCF thin homogeneous plate ($h/L_1 = 0.01, \lambda = 0$)

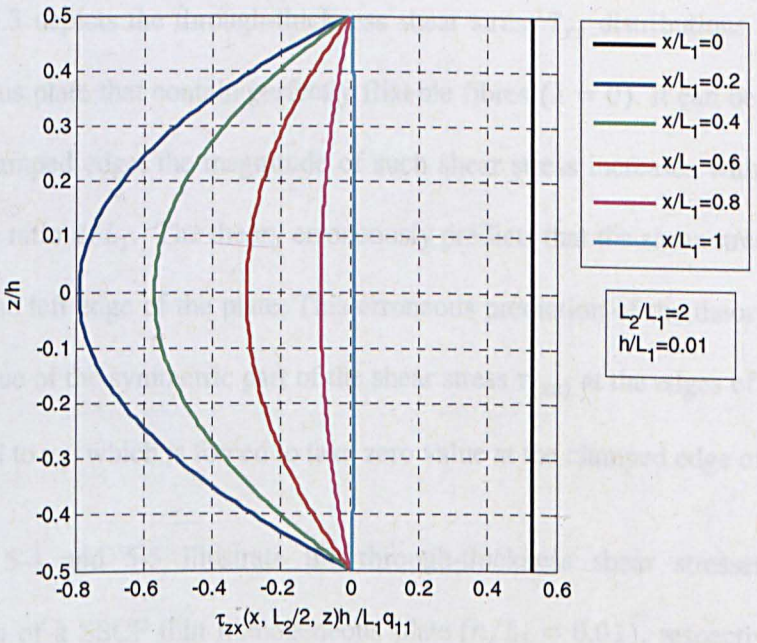

Figure 5.4 Through-thickness shear stress $\tau_{zx}\ (X, \frac{L_2}{2}, Z)/L_1 q_{11}$ distributions of a SSCF thin homogeneous plate $(h/L_1 = 0.01, \lambda = 0.001)$

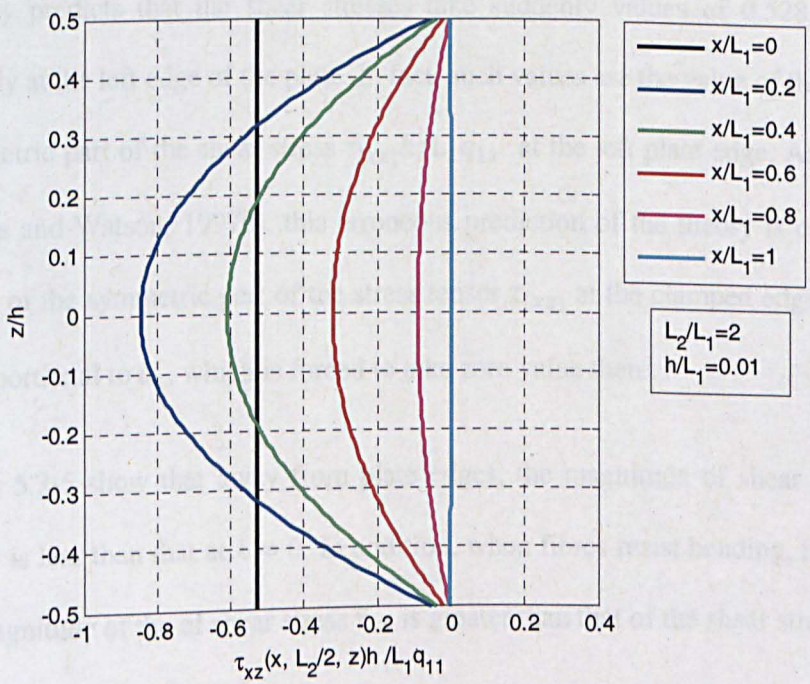

Figure 5.5 Through-thickness shear stress $\tau_{xz}\ (X, \frac{L_2}{2}, z)/L_1 q_{11}$ distributions of a SSCF thin homogeneous plate $(h/L_1 = 0.01, \lambda = 0.001)$

Figure 5.3 depicts the through-thickness shear stress $\bar{\tau}_{xz}$ distributions of a SSCF thin homogeneous plate that contain perfectly flixeble fibres ($\lambda = 0$). It can be seen that away from the clamped edge, the magnitude of such shear stress increases with decreasing the value of the ratio x/L_1. The theory erroneously predicts that the shear stresses take values of zero at the left edge of the plate. This erroneous prediction of the theory are caused by the zero value of the symmetric part of the shear stress $\tau_{(xz)}$ at the edges of the plate that is proportional to u_1, which is forced to take zero value at the clamped edge of the plate.

Figures 5-4 and 5-5 illustrate the through-thickness shear stresses $\bar{\tau}_{zx}$ and $\bar{\tau}_{xz}$ distributions of a SSCF thin homogeneous plate ($h/L_1 = 0.01$), respectively. This plate contains stiff fibres ($\lambda = 0.001$). Away from the free edge, it can be seen that $\bar{\tau}_{zx} \neq \bar{\tau}_{xz}$. It is of particle interest to note that although the magnitude of the shear stress $\bar{\tau}_{zx}$ and $\bar{\tau}_{xz}$ distributions is naturally increasing when approaching the clamped edge, the theory erroneously predicts that the shear stresses take suddenly values of 0.528 and -0.528, respectively at the left edge of the plate. In fact, such values are the value of the normalised anti-symmetric part of the shear stress $\tau_{[xz]}h/\mathrm{L}_1 q_{11}$ at the left plate edge. As pointed out in(Soldatos and Watson, 1997b), this erroneous prediction of the theory is caused by the zero value of the symmetric part of the stress tensor $\tau_{(xz)}$ at the clamped edge of the plate that is proportional to u_1, which is forced to take zero value there.

Figures 5.3-5 show that away from plate edges, the magnitude of shear stress $\bar{\tau}_{zx}$ at $\lambda = 0.001$ is less than that at $\lambda = 0$. In addition, when fibres resist bending, it is observed that the magnitude of the of shear stress $\bar{\tau}_{xz}$ is greater than that of the shear stress $\bar{\tau}_{zx}$.

Based on the employed version of the G5DOFPT, figures 5.6 and 5.7 show the normalised deflection distributions of a homogeneous plate that is simply supported on the edges $y = 0, L_2$, clamped at the edges $x = 0, L_1$ (SSCC plate) for $\lambda = 0$ and $\lambda = 0.001$,

respectively. It is shown that the magnitude of the normalised deflection at $\lambda = 0$ is greater than that of $\lambda = 0.001$. This emphasise again that when fibres resist bending, the plate becomes stiffer. Such figures show that there is a considerable difference between the deflection distributions in corresponding SSCC and SSSS plates presented in table 5-2. This shows that the two clamped edges make the plate less flexible.

It should be taken into account that, due to the symmetric of the problem for SSCC case, the shear stresses at x/L_1 and $1-(x/L_1)$ have identical through thickness distributions. Therefore, figures 5.8, 5.9 and 5.10 present shear stresses distributions a only for the left half of the SSCC thin homogeneous plate ($h/L_1 = 0.01$).

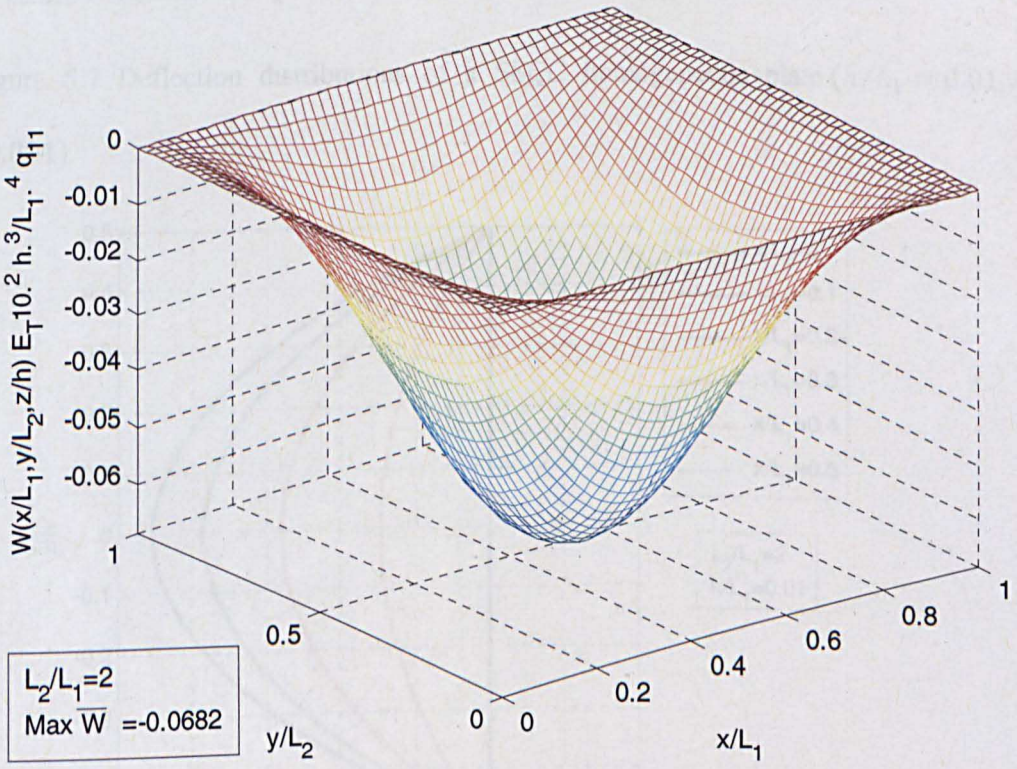

Figure 5.6 Deflection distributions of a SSCC homogeneous plate ($h/L_1 = 0.01, \lambda = 0$)

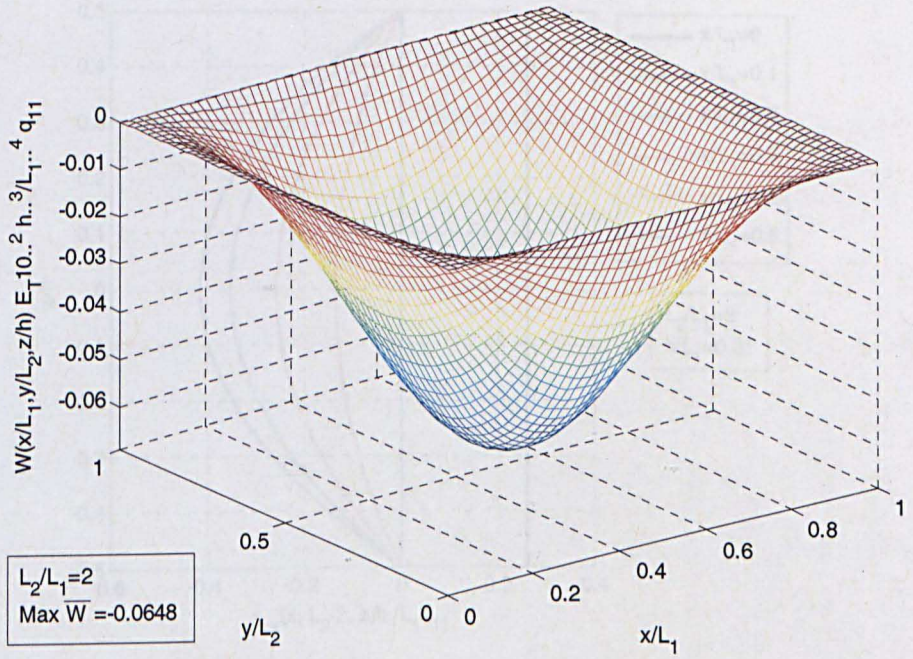

Figure 5.7 Deflection distributions of a SSCC homogeneous plate ($h/L_1 = 0.01, \lambda =$ 00.001)

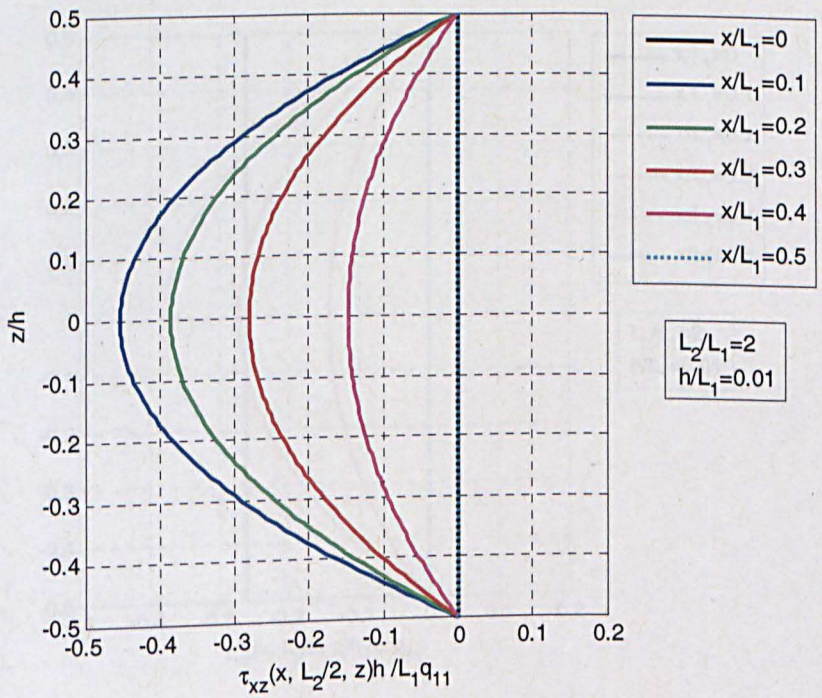

Figure 5.8 Through-thickness shear stress $\tau_{zx}(\frac{x}{L_1}, \frac{L_2}{2}, \frac{z}{h})/L_1 q_{11}$ or $\tau_{xz}(\frac{x}{L_1}, \frac{L_2}{2}, \frac{z}{h})/$ $L_1 q_{11}$ distributions of a SSCC thin homogeneous plate ($h/L_1 = 0.01, \lambda = 0$)

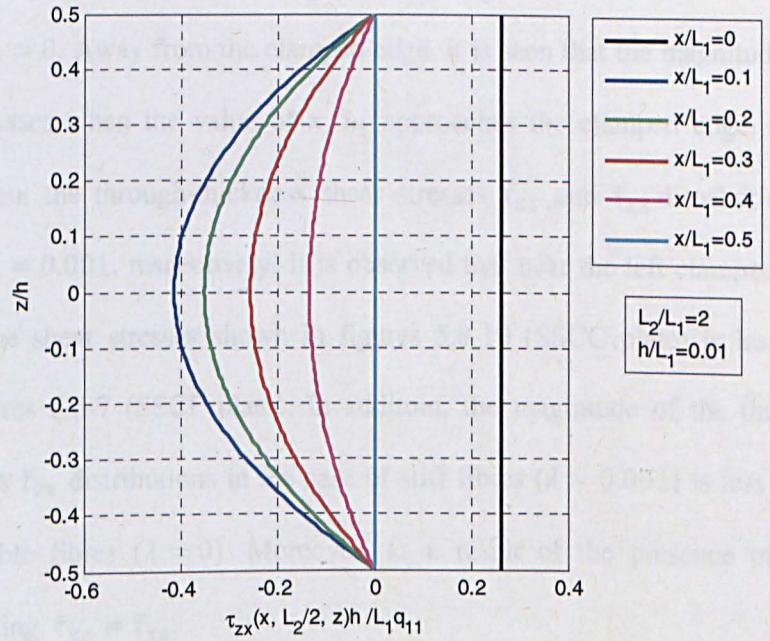

Figure 5.9 Through-thickness shear stress $\tau_{zx}(\frac{x}{L_1}, \frac{L_2}{2}, \frac{z}{h})/L_1 q_{11}$ distributions of a SSCC thin homogeneous plate $(h/L_1 = 0.01, \lambda = 0.001)$

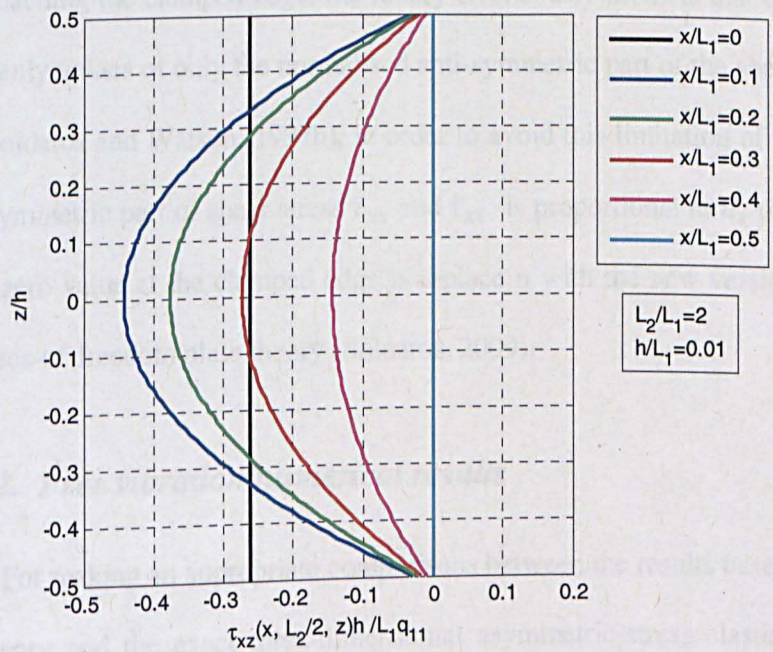

Figure 5.10 Through-thickness shear stress $\tau_{xz}(\frac{x}{L_1}, \frac{L_2}{2}, \frac{z}{h})/L_1 q_{11}$ distributions of a SSCC thin homogeneous plate $(h/L_1 = 0.01, \lambda = 0.001)$

Figure 5.8 depicts the through-thickness shear stress $\bar{\tau}_{xz}$ distributions of a SSCC plate for $\lambda = 0$. Away from the clamped edge, it is seen that the magnitude of such shear stress increases when the value of x/L_1 approaches the clamped edge. Figures 5.9 and 5.10 present the through-thickness shear stresses $\bar{\tau}_{zx}$ and $\bar{\tau}_{xz}$ distributions of a SSCC plate for $\lambda = 0.001$, respectively. It is observed that near the left clamped egde, the magnitude of the shear stresses shown in figures 5.8-10 (SSCC plate) is less than that shown in figurres 5.5-7 (SSCF plate). In additoin, the magintude of the through-thickness shear stress $\bar{\tau}_{zx}$ distributions in the case of stiff fibres ($\lambda = 0.001$) is less than that of perfectly flexible fibres ($\lambda = 0$). Moreover, as a result of the presence of fibres resistance in bending, $\bar{\tau}_{zx} \neq \bar{\tau}_{xz}$.

Furthermore, as seen at the clamped edge in the case of SSCF plate, although the magnitude of the shear stress $\bar{\tau}_{zx}$ and $\bar{\tau}_{xz}$ distributions is naturally increasing when approaching the clamped edge, the theory erroneously predicts that the shear stresses take suddenly values of only the normalised anti-symmetric part of the shear stress. As sugested in (Soldatos and Watson, 1997b), in order to avoid this limitation of the G5DOFPT where the symmetric part of shear stress $\bar{\tau}_{zx}$ and $\bar{\tau}_{xz}$ is proportional to u_1 that has been forced to take zero value at the clamped edge is replace it with the new version of the general six-degrees-of-freedom plate theory (Soldatos, 2009).

5.6.2. Free vibration numerical results

For making an appropriate comparisons between the results based on the employed 2-D theory and the exact three-dimensional asymmetric-stress elasticity solution and the exact pane strain solution, the normalised frequency parameter, (ω^*), is considered as defined in (2.35). The numerical results are presented for free vibration frequency of

transversely isotropic homogeneous thin plate ($h/L_1 = 0.01$) and their elastic properties as follows:

$$E_L/E_T = 25, \quad G_{LT}/E_T = 0.5, \quad G_{TT}/E_T = 0.2, \quad v_{LT} = v_{LT} = 0.25. \tag{5.68}$$

Table 5-7 compares numerical values of the normalised fundamental frequency parameter, ω^*, obtained on the basis of the three-dimensional asymmetric-stress elasticity solution, exact plane strain asymmetric-stress elasticity solution and three kinds of Two-dimensional mathematical modelling of fibre-reinforced thin-walled structures. The two-dimensional thin-walled structures modelling are the G5DOFPT, G3DOFBT and the classical plate theory (CPT) developed in (Soldatos, 2009). It is observed that the thin-walled theories provide very close results to those predicted on the basis of the exact plane strain and three-dimensional asymmetric-stress elasticity solutions at different value of λ. This makes it confident to employ the advanced version of CPT (Soldatos, 2009) on different sets of edge boundary conditions.

Table 5-7 Fundamental frequency parameter, ω^*, obtained by different theories for free vibration of a SSSS thin homogeneous plate ($h/L_1 = 0.01$)

$\lambda = \frac{l}{h}$	3D-asymmetric-stress elasticity $L_2/L_1 = 10^4$	Plane strain asymmetric-stress elasticity	G5DOFPT $L_2/L_1 = 10^4$	G3DOFBT	CPT $L_2/L_1 = 10^4$
0	0.002013	0.002011	0.002012	0.002017	0.002013
0.0002	0.002032	0.002033	0.002022	0.002037	0.002027
0.0004	0.002051	0.002050	0.002032	0.002057	0.002037
0.0006	0.002073	0.002073	0.002042	0.002076	0.002047
0.0008	0.002093	0.002092	0.002052	0.002097	0.002057
0.001	0.002111	0.002112	0.002062	0.002115	0.002067

Table 5-8 Fundamental frequency parameter, ω^*, obtained by classical plate theory solution for free vibration of a SSSS thin homogeneous plate ($h/L_1 = 0.01$)

$\lambda = \frac{l}{h}$	$L_2/L_1 = 10^4$	$L_2/L_1 = 2$	$L_2/L_1 = 1.5$	$L_2/L_1 = 1$
0	0.002013	0.002045	0.002069	0.002154
0.0002	0.002027	0.002055	0.002079	0.002163
0.0004	0.002037	0.002064	0.002089	0.002172
0.0006	0.002047	0.002074	0.002099	0.002182
0.0008	0.002057	0.002084	0.002108	0.002191
0.001	0.002067	0.002094	0.002118	0.002200

Table 5-9 Fundamental frequency parameter, ω^*, obtained by classical plate theory solution for free vibration of a SSCC thin homogeneous plate ($h/L_1 = 0.01$)

$\lambda = \frac{l}{h}$	$L_2/L_1 = 10^4$	$L_2/L_1 = 2$	$L_2/L_1 = 1.5$	$L_2/L_1 = 1$
0	0.004572	0.004587	0.004600	0.004645
0.0002	0.004595	0.004610	0.004623	0.004667
0.0004	0.004618	0.004633	0.004646	0.004690
0.0006	0.004641	0.004655	0.004668	0.004712
0.0008	0.004663	0.004678	0.004691	0.004734
0.001	0.004686	0.004700	0.004713	0.004756

Table 5-8 presents numerical values of the normalised fundamental frequency obtained on the basis of the advanced version of CPT at different values of λ for SSSS thin homogeneous plate having different value of L_2/L_1. It is observed that the value of the fundamental frequency increases with decreasing the value of L_2/L_1. In addition, it increases with increasing the value of λ. This makes immediately clear that the stiffness the plate increases with increasing the value of λ and decreasing the value of L_2/L_1.

Table 5-9 shows numerical values of the normalised fundamental frequency obtained on the basis of the advanced version of CPT at different values of λ for SSCC thin homogeneous plate having different value of L_2/L_1. It is noted again that the value of the fundamental frequency increases with increasing the value of λ and decreasing the value of L_2/L_1. Furthermore, the numerical values of the fundamental frequency shown in table 5-8 of the SSSS plate are less than their counterparts appear in table 5-9 of the SSCC plate.

Table 5-10 Fundamental frequency parameter, ω^*, obtained by classical plate theory solution for free vibration of a SSCF thin homogeneous plate ($h/L_1 = 0.01$,)

$\lambda = \frac{l}{h}$	$L_2/L_1 = 10^4$	$L_2/L_1 = 2$	$L_2/L_1 = 1.5$	$L_2/L_1 = 1$
0	0.000719	0.000720	0.000730	0.000803
0.0002	0.000722	0.000723	0.000734	0.000806
0.0004	0.000726	0.000727	0.000737	0.000810
0.0006	0.000729	0.000730	0.000741	0.000813
0.0008	0.000733	0.000734	0.000744	0.000816
0.001	0.000736	0.000737	0.000748	0.000819

Table 5-10 illustrates numerical values of the normalised fundamental frequency at different values of λ for SSCF thin homogeneous plate having different value of L_2/L_1. The same effect of increasing the value of λ and decreasing the value of L_2/L_1 on the value of the normalised fundamental frequency that shown in the cases of SSSS and SSCC plates is appears in SSCF plate case. It is observed that the lowest values of the normalised fundamental frequency of the three cases of edge boundary conditions shown in tables 5-8, 5-9 and 5-10 is that for the SSCF plate. Whereas, the highest values the normalised fundamental frequency are presented in the case of SSCC plate.

5.7. Conclusion

A new application of two-dimensional higher-order plate theory of homogeneous and laminated composite plates (Soldatos, 2009) has been studied in this chapter. Considering the fibres possess bending stiffness, solutions for the flexure and free vibration of a plate subjected to different sets of edge boundary conditions have been obtained on the basis of an advanced version of general five-degrees-of-freedom beam theory (Soldatos, 2009). The two shape functions were determined by combining the appropriate equilibrium equations of asymmetric-stress three-dimensional elasticity and the two-dimensional solution for simply supported plate. The forms of such shape functions obtained were explicitly dependent on a material length parameter (l) that related to the fibres bending stiffness elastic modulus (d^f).

The flexure and free vibration problems of a simply supported thin plate were initially considered, for which a three-dimensional asymmetric-stress elasticity solutions were obtained and discussed in the fourth chapter of this study. In order to test the reliability of the employed version of G5DOFPT theory, comparisons were made between its and the corresponding numerical results based on the three-dimensional asymmetric-stress elasticity solutions. For the static solution for the flexure of thin plate, an observation is drawn for the range of the non-dimensional parameter λ, to allow the G5DOFPT providing results close to the three-dimensional asymmetric-stress elasticity solution results. Furthermore, the accuracy of the employed version of G5DOFPT theory decreases with increasing the values of λ. Despite this observation, it is believed that for the thin plate considered, the displacement and stress distributions, in the static problem, are still considerably accurate when $\lambda \leq 0.001$.

Taking into account the resistance of fibres in bending, the two-dimensional plate theory is applied for flexure of plate subjected to different edge boundary conditions. It is observed, in each case of the applied edge boundary conditions that the magnitude of the deflection decreases with increasing the value of λ. Furthermore, it is observed that in the presence of fibres bending stiffness ($\lambda \neq 0$), $\tau_{xz} \neq \tau_{zx}$. This has been existed as an effect of the non-zero couple-stresses.

Similar observation that drawn in the third chapter is noted here for the suddenly change was in the magnitude of two shear stresses τ_{xz} and τ_{zx} at the plate clamped edge. This is apparently due to the limitation of the G5DOFPT. Neglecting the transverse normal deformation has erroneously been assumed in G5DOFPT making $\tau_{(xz)}$ proportional to u_1, which is forced by the end boundary conditions to take zero values at the plate clamped edge. The way to avoid this drawback is to replace the G5DOFPT with the G6DOFPT which takes transverse normal deformation into account. This observation was seen in the case of perfectly flexible fibres (Soldatos and Watson, 1997b).

In the dynamic solution, no limitation has been seen for the values of λ to allow the G5DOFPT, CPT providing accurate results when compared with their counterparts that based on the three-dimensional asymmetric-stress elasticity solution. These two-dimensional thin-walled structures modelling produce numerical values of the fundamental frequency which are in a good agreement with their counterparts of the three-dimensional asymmetric-stress elasticity solution. Numerical values for the fundamental frequency parameter of SSSS, SSCC and SSCF homogeneous plates were provided based on the advanced version of CPT. It is of particular interest to observe that the obtained numerical results in the shown boundary condition cases emphasise that the values of the normalised fundamental frequency increases with increasing the value of λ and decreasing the value of L_2/L_1.

Chapter 6. Conclusion and Future Work

In this chapter, the writer concludes this thesis by summarizing the contributions and discussing directions for future work. This is organised to be in two sections which are relevant to those met at the end of chapters 2-5 of the thesis.

6.1. Conclusion

Based on the relevant equations of asymmetric-stress theory of elasticity (Spencer and Soldatos, 2007, Soldatos, 2009), plane strain asymmetric-stress elasticity solutions of small flexure and free vibration of simply supported transversely isotropic beam have been constructed in chapter 2. In the framework of the linear theory of elasticity, exact three-dimensional asymmetric-stress elasticity solutions are constructed for the statics and dynamics of a simply supported rectangular plate in chapter 4. Numerical results based on these solutions have been computed for small flexure and free vibrations of simply supported transversely isotropic thick beam and plate. Those numerical results have been computed at different values of the non-dimensional parameter λ which is related to the fibres bending stiffness, represented by the elastic modulus (d^f). The influence of the resistance of fibres in bending on the deformed beam and plate displacement, shear stresses and couple-stress distributions and frequency values has been also discussed. It has been observed that the results where fibres are perfectly flexible (λ=0) are identical to the results based on the symmetric elasticity solution. Thus, the obtained plane strain solution contains the symmetric elasticity solution presented in (Pagano, 1969) as a special case.

The exact and approximate solutions constructed (displacement field) contain terms which due to the fibre bending stiffness. Those terms depend on the additional length intrinsic parameter $l^{(k)}$ which is assumed to represent the fibres thickness. As a result of that, the stresses and couple stress distributions and the free frequency parameter value will be affected by the change of the fiber bending stiffness. Comparisons have been shown between the present three dimensional asymmetric-stress elasticity solutions results at high values of plate aspect ratio (width to length ratio) L_2/L_1 and the corresponding plane strain solution counterparts. It has been observed that when the fibres resist bending, the shear stresses τ_{zx} and τ_{xz} are unequal and so are the shear stresses τ_{yx} and τ_{xy} in the plate case. Moreover, the shear stress τ_{zx} is decreasing with increasing the value of λ and largest value of this bending parameter is associated with the most symmetrical profile. It is of particular interest to note that the magnitude of the deflection decreases with increasing the value of λ and it does also with decreasing the value of L_2/L_1. Furthermore, the value of the fundamental frequency increases with the increasing of the value of λ and, it does so with decreasing the value of L_2/L_1 as well. Therefore, it can be concluded that with increasing the resistance of fibres in bending or decreasing the width to length ratio, the simply supported plate becomes less flexible.

Since the solutions presented in chapters 2 and 4 are exact, they can serve as a benchmark of the accuracy of relevant thin plate theories developed in (Soldatos, 2009), through appropriate comparisons of corresponding numerical results. Accordingly, such solutions have been, for first time, used to test the reliability of the advanced version of general five-degrees-of-freedom shear deformable plate theory (G5DOFPT) presented in (Soldatos, 2009) which has been employed in chapters 3 and 5.

Small flexure and free vibration of transversely isotropic elastic beams and plates subjected to different sets of end boundary conditions when the beams and plates contain fibres which resist bending have been studied in chapters 3 and 5, respectively. Relevant solutions have been constructed on the basis of the advanced version of (G5DOFPT) presented in (Soldatos, 2009). The forms of the shape functions obtained were explicitly dependent on a material length parameter ($l = \lambda h$) which is related to the fibres bending stiffness; represented by the elastic modulus (d^f). Comparisons have been made between corresponding numerical results based on the general five-degrees-of-freedom shear deformable plate theory and the exact asymmetric-stress elasticity solutions which have been found in chapters 2 and 4. According to those comparisons, the static results are good for flexure. In addition, stress results are believed good and can be improved by considering transverse normal deformation considered in the advanced version of the general six-degrees-of-freedom shear deformable plate theory presented in (Soldatos, 2009).

It is observed that the value of the deflection which obtained based on the 2D theory does not change through the plate thickness. This happened because such theory does not take the transverse normal deformation effects into account. For the static solutions and considered geometric and elastic beams and plates properties, an observation has been drawn for the range of the non-dimensional parameter λ, to allow the G5DOFPT providing results that in a good agreement with the asymmetric-stress elasticity solution results. However, for different geometric and elastic properties from those in this chapter, different range of the values of λ can be different to allow the employed model providing accurate results when compared to the corresponding results based on the plane strain solution.

On the basis of the one-dimensional advanced version of G5DOFPT, results for transverse displacement, couple-stress and shear stresses distributions have been obtained for a two-layered beam having its ends CC, CF and CS. Considering the resistance of fibres in bending, the advanced version of G5DOFPT is applied for flexure of plate subjected to different edge boundary conditions which are SSCC and SSCF.

In the dynamic solutions, no limitation has been seen for the values of λ to allow the G5DOFPT, CPT providing accurate results when compared with their counterparts that based on the three-dimensional asymmetric-stress elasticity solution in the case of simply supported beam and plate. Numerical values for the fundamental frequency parameter of SSSS, SSCC and SSCF homogeneous plates were provided based on the advanced version of CPT. It is of particular interest to observe that the obtained numerical results in the shown boundary condition cases have shown that the values of the normalised fundamental frequency increases with increasing the value of λ and decreasing the value of L_2/L_1 for the plate. This emphasizes again that with increasing the resistance of fibres in bending or decreasing the width to length ratio of the considered plates, the beams and plate become stiffer.

6.2. Future Work

Future work should extend the presented solutions for flexure and free vibration of beams subjected to different combinations of edge boundary conditions on the basis of the advanced version of the one dimensional version of the advanced version of the general six-degrees-of-freedom plate theory (G6DOFPT) (Soldatos, 2009) proposed in (Soldatos, 2009). This model takes the transverse normal deformation effects into account. In the specification of the shape functions, the equations of three-dimensional asymmetric-stress elasticity will be used. The case of SS beam will be used to test the accuracy of the model,

by comparing its results against corresponding numerical results based on the exact plain strain solution found in chapter 2.

The writer aims to replace the plates approach of the advanced version of G5DOFPT (Soldatos, 2009), employed in chapter 5, with an advanced version of G6DOFPT (Soldatos, 2009) which takes transverse normal deformation effects into account. In the specification of the shape functions, the equations of three-dimensional asymmetric-stress elasticity will be used. In order to test the accuracy of the model, the case of SSSS plate will be used to compare its results against corresponding numerical results based on the exact three-dimensional solution found in chapter 4.

Further work will focus on several applications of the advanced version of the G5DOFPT, and G6DOFPT presented in (Soldatos, 2009) and associated with the different choices of the shape functions such as parabolic, trigonometric and hyperbolic ones to solve problems presented in chapters 3 and 5.

References

BERT, W. C. (1984) A critical evaluation of few plate theories applied to laminated composites. *Composite Structures,* 2, 329-347.

BHIMARADDI, A. & STEVENS, L. K. (1984) A higher order theory for free vibration of orthotropic, homogeneous, and laminated rectangular plates. *Journal of Applied Mechanics,* 51, 195-198.

BICKFORD, W. B. (1982) A consistent higher order beam theory. *Development in Theoretical and Applied Mechanics,* 11, 137-150.

CARRERA, E. (2003) Historical review of Zig-Zag theories for multilayered plates and shells. *Applied Mechanics Reviews,* 56, 287-308.

CHAKRABARTI, A. & SHEIKH, A. H. (2004) A new triangular element to model inter-laminar shear stress continuous plate theory. *International Journal for Numerical Methods in Engineering* 60, 1237-1257.

CHO, M. & PARMERTER, R. (1993) Efficient higher order composite plate theory for general lamination configurations. *AIAA Journal,* 31, 1299-1306.

DAGHER, M. A. & SOLDATOS, K. P. (2011) On small azimuthal shear deformation of fibre-reinforced cylindrical tubes. *Journal of Mechanics of Materials and Structures* 6, 141-168.

DAHAKE, A. G. & GHUGAL, Y. M. (November 2012) Flexure of thick beams using trigonometric shear deformation theory. *International Journal of Scientific and Research Publications,* 2, 2250-3153.

DI SCIUVA, M. (1986) Bending, vibration and buckling of simply supported thick multilayered orthotropic plates: An evaluation of a new displacement model. *Journal of Sound and Vibration,* 105, 425-442.

DI SCIUVA, M. (1992) Multilayered anisotropic plate models with continuous interlaminar stresses. *Composite Structures,* 22, 149-167.

GHUGAL, Y. M. & SAYYAD, A. S. (2010) A static flexure of thick isotropic plates using trigonometric shear deformation theory. *Journal of Solid Mechanics,* 2, 79-90.

GHUGAL, Y. M. & SHARMA, R. (2009) Hyperbolic shear deformation theory for flexure and vibration of thick isotropic beams. *International Journal of Computational Methods,* 06, 585-604.

GHUGAL, Y. M. & SHIMPI, R. P. (2001) A Review of Refined Shear Deformation Theories for Isotropic and Anisotropic Laminated Beams. *Journal of Reinforced Plastics and Composites,* 20, 255-272.

GHUGAL, Y. M. & SHIMPI, R. P. (2002) A Review of Refined Shear Deformation Theories of Isotropic and Anisotropic Laminated Plates. *Journal of Reinforced Plastics and Composites,* 21, 775-813.

HAN, S. M., BENAROYA, H. & WEI, T. (1999) Dynamics of transversely vibrating beams using four engineering theories. *Journal of Sound and Vibration,* 225, 935-988.

HE, J.-F., CHOU, M. & ZHANG, X. (1993) Bending analysis of laminated plates using a refined shear deformation theory. *Composite Structures,* 24, 125-138.

HERAKOVICH, C. T. (1997) *Mechanics of Fibrous Composites*, Wiley.

HEUER, R. (1992) Static and dynamic analysis of transversely isotropic, moderately thick sandwich beams by analogy. *Acta Mechanica,* 91, 1-9.

IDLBI, A., KARAMA, M. & TOURATIER, M. (1997) Comparison of various laminated plate theories. *Composite Structures,* 37, 173-184.

JONES, R. M. (1975) Mechanics of composite materials. *Hemisphere, New York.*

JONES, R. M. (1998) Mechanics of composite materials. *Taylor & Francis, Washington, D.C.,*.

KARAMA, M., ABOU HARB, B., MISTOU, S. & CAPERAA, S. (1998) Bending, buckling and free vibration of laminated composite with a transverse shear stress continuity model. *Composites Part B: Engineering,* 29, 223-234.

KIRCHHOFF, G. R. (1850a) Uber das gleichgewicht und die bewegung einer elastischen scheibe. *Journal of Reine Angew. Math. (Crelle),,* 40, 51-88

KIRCHHOFF, G. R. (1850b) Uber die schwingungen einer kriesformigen elastischen scheibe. *Poggendorffs Annalen,* 81, 258–264.

KRISHNA MURTY, A. V. (1984) Toward a consistent beam theory. *AIAA Journal,* 22, 811-816.

LEE, K. H., LIN, W. Z. & CHOW, S. T. (1994) Bidirectional bending of laminated composite plates using an improved zig-zag model. *Composite Structures,* 28, 283-294.

LEE, K. H., SENTHILNATHAN, N. R., LIM, S. P. & CHOW, S. T. (1990) An improved zig-zag model for the bending of laminated composite plates. *Composite Structures,* 15, 137-148.

LEE, K. H., XAVIER, P. B. & CHEW, C. H. (1993) Static response of unsymmetric sandwich beams using an improved zig-zag model. *Composites Engineering,* 3, 235-248.

LEVINSON, M. (1981) A new rectangular beam theory. *Journal of Sound and Vibration,* 74, 81-87.

LI, X. & LIU, D. (1995) Zigzag theory for composite laminates. *AIAA Journal,* 33, 1163-1165.

LIU, P., ZHANG, Y. & ZHANG, K. (1994) Bending solution of high-order refined shear deformation theory for rectangular composite plates. *International Journal of Solids and Structures,* 31, 2491-2507.

LO, K. H., CHRISTENSEN, R. M. & WU, E. M. (1977) A high-order theory of plate deformation---part 2: laminated plates. *Journal of Applied Mechanics,* 44, 669-676.

LU, X. & LIU, D. (1992) Interlayer shear slip theory for cross-ply laminates with nonrigid interfaces. *AIAA Journal,* 30, 1063-1073.

MAU, S. T. (1973) A Refined Laminated Plate Theory. *Journal of applied mechanics,* 40, 606-607.

MESSINA, A. & SOLDATOS, K. P. (2002) A general vibration model of angle-ply laminated plates that accounts for the continuity of interlaminar stresses. *International Journal of Solids and Structures,* 39, 617-635.

MINDLIN, R. D. (1951) Influence of rotatory inertia and shear on flexural motions of isotropic, elastic plates. *Journal of Applied Mechanics,* 18, 31-38.

MURTY, A. V. K. & VELLAICHAMY, S. (1987) On higher order shear deformation theory of laminated composite panels *Composite Structures,* 8, 247-270.

NELSON, R. B. & LORCH, D. R. (1974) A Refined Theory for Laminated Orthotropic Plates. *Journal of applied mechanics,* 41, 177-183.

NOOR, A. K. & BURTON, W. S. (1989a) Assessment of Shear Deformation Theories for Multilayered Composite Plates. *Applied Mechanics Reviews,* 42, 1-13.

NOOR, A. K. & BURTON, W. S. (1989b) Stress and free vibration analyses of multilayered composite plates. *Composite Structures,* 11, 183-204.

PAGANO, N. J. (1969) Exact solutions for composite laminates in cylindrical bending. *Journal of Composite Materials,* 3, 398-411.

PAGANO, N. J. (1970a) Exact solutions for rectangular bidirectional composites and sandwich plates. *Journal of composite materials,* 4, 20-34.

PAGANO, N. J. (1970b) Influence of shear coupling in cylindrical bending of anisotropic laminates *Journal of Composite Materials* 4, 330-343.

PAGANO, N. J. & HATFIELD, H. J. (1972) Elastic Behaviour of Multilayered Bidirectional Composites. *AIAA Journal,* 10, 931-933.

PAGANO, N. J. & WANG, A. S. D. (1971) Further study of composite laminates under cylindrical bending *Journal of composite materials,* 5, 521-528.

PISTER, K. S. & DONG, S. B. (1959) Elastic bending of layered plates. *Journal of Engineering Mechanics Division, ASCE,* 1-10.

REDDY, J. N. (1984) A simple higher-order theory for laminated composite plates. *Journal of Applied Mechanics,* 51, 745-752.

REDDY, J. N. & CHAO, W. C. (1981) A comparison of closed-form and finite-element solutions of thick laminated anisotropic rectangular plates. *Nuclear Engineering and Design,* 64, 153-167.

REISSNER, E. (1945) The effect of transverse shear deformation on the bending of elastic plates *Journal of Applied Mechanics,* 12, A69-A77.

REISSNER, E. (1985) Reflection on the theory of elastic plates. *Applied Mechanics Reviews,* 38, 1453-1464.

REISSNER, E. & STAVSKY, Y. (1961) Bending and stretching of certain types of heterogeneous aeolotropic elastic plates. *Journal of applied mechanics,* 402-408.

SAVOIA, M. (1995) On the accuracy of one-dimensional models for multilayered composite beams. *International Journal of Solids and Structures,* 33, 521-544.

SHIMPI, R. P. & GHUGAL, Y. M. (2001) A new layerwise trigonometric shear deformation theory for two-layered cross-ply beams. *Composites Science and Technology,* 61, 1271-1283.

SHIMPI, R. P. & PATEL, H. G. (2006) A two variable refined plate theory for orthotropic plate analysis. *International Journal of Solids and Structures,* 43, 6783-6799.

SINGH, S. K., CHAKRABARTI, A., BERA, P. & SONY, J. S. D. (2011) An efficient C0 FE model for the analysis of composites and sandwich laminates with general layup. *Latin American Journal of Solids and Structures,* 8, 197-212.

SOLDATOS, K. (1992a) A transverse shear deformation theory for homogeneous monoclinic plates. *Acta Mechanica,* 94, 195-220.

SOLDATOS, K. (2010a) Second-gradient plane deformations of ideal fibre-reinforced materials II: forming flows of fibre–resin systems when fibres resist bending. *Journal of Engineering Mathematics,* 68, 179-196.

SOLDATOS, K. (2010b) Second-gradient plane deformations of ideal fibre-reinforced materials: implications of hyper-elasticity theory. *Journal of Engineering Mathematics,* 68, 99-127.

SOLDATOS, K. P. (1992b) A general laminated plate theory accounting for continuity of displacements and transverse shear stresses at material interfaces. *Composite Structures,* 20, 195-211.

SOLDATOS, K. P. (2003) Accurate stress analysis of laminated composite structures. *in "Modern Trends in Composite Mechanics", pp. 69-132, A. Altenbach and W. Becker, eds, Springer Verlag, CISM Courses and Lectures no 448 (ISBN 3-211-20302-8)*

SOLDATOS, K. P. (2009) Towards a new generation of 2D mathematical models in the mechanics of thin-walled fibre-reinforced structural components. *International Journal of Engineering Science,* 47, 1346-1356.

SOLDATOS, K. P. (2012) On loss of ellipticity in second-gradient hyper-elasticity of fibre-reinforced materials. *International Journal of Non-Linear Mechanics,* 47, 117-127.

SOLDATOS, K. P. & SHU, X. (2001) Modelling of perfectly and weakly bonded laminated plates and shallow shells. *Composites Science and Technology,* 61, 247-260.

SOLDATOS, K. P. & WATSON, P. (1997a) A general theory for the accurate stress analysis of homogeneous and laminated composite beams. *International Journal of Solids and Structures,* 34, 2857-2885.

SOLDATOS, K. P. & WATSON, P. (1997b) A method for improving the stress analysis performance of one- and two-dimensional theories for laminated composites. *Acta Mechanica,* 123, 163-186.

SPENCER, A. J. M. & SOLDATOS, K. P. (2007) Finite deformations of fibre-reinforced elastic solids with fibre bending stiffness. *International Journal of Non-Linear Mechanics,* 42, 355-368.

SRINIVAS, S. (1973) A refined analysis of composite laminates. *Journal of Sound and Vibration,* 30, 495-507.

SRINIVAS, S., JOGA RAO, C. V. & RAO, A. K. (1970) An exact analysis for vibration of simply-supported homogeneous and laminated thick rectangular plates. *Journal of Sound and Vibration,* 12, 187-199.

SRINIVAS, S. & RAO, A. K. (1970) Bending, vibration and buckling of simply supported thick orthotropic rectangular plates and laminates. *International Journal of Solids and Structures,* 6, 1463-1481.

TIMOSHENKO, S. P. (1921) On the correction for shear of the differential equation for transverse vibrations of prismatic bars. *Philosophical Magazine* 41, 744-746.

TIMOSHENKO, S. P. (1922) On the transverse vibration of bars of uniform cross-section. *Philosophical Magazine,* 43, 125-131.

TOURATIER, M. (1991) An efficient standard plate theory. *International Journal of Engineering Science,* 29, 901-916.

VALISETTY, R. R. & REHFIELD, L. W. (1985) A theory of stress analysis of composite laminates. *AIAA Journal,* 23, 1111-1117.

WHITNEY, J. M. & PAGANO, N. J. (1970) Shear deformation in heterogeneous anisotropic plates. *Journal of applied mechanics,* 37, 1031-1036.

WHITNEY, J. M. & SUN, C. T. (1973) A higher order theory for extensional motion of laminated composites. *Journal of Sound and Vibration,* 30, 85-97.

YANG, P. C., NORRIS, C. H. & STAVSKY, Y. (1966) Elastic wave propagation in heterogeneous plates. *International Journal of Solids and Structures,* 2, 665-684.

YE, J. (2003) *Laminated composite plates and shells: 3D modelling*, Springer.

Appendix

Appendix 1

Equation (3.16) can be written in the following form:

$$D_{11}^{f} = \frac{1}{2} h\, d^{f} + Q_{11}^{(k)} \frac{h^3}{12} = \frac{C_{11} h^3}{12} \left(\frac{1}{2}\, d^{f} \frac{12}{C_{11} h^2} + \frac{Q_{11}^{(k)}}{C_{11}} \right), \tag{A1.1}$$

or

$$D_{11}^{f} = \frac{C_{11} h^3}{12} \left(\frac{1}{2} \frac{l^{(k)} L_1}{h^2} + \frac{Q_{11}^{(k)}}{C_{11}} \right);\ l^{(k)} L_1 = \frac{12 d^{f}}{C_{11}}, \tag{A1.2}$$

where

$$l^{(k)} L_1 = \frac{12 d^{f}}{C_{11}}, \tag{A1.3}$$

or

$$d^{f} = \frac{1}{12} C_{11} l^{(k)} L_1. \tag{A1.4}$$

Appendix 2

The matrix form of the set of fourth and twelfth -order ordinary differential equations (5.38) and (5.39) is as follows:

$$\begin{bmatrix} \tilde{u} \\ \tilde{u}_a \\ \tilde{v} \\ \tilde{v}_a \\ \tilde{v}_b \\ \tilde{v}_c \end{bmatrix}' = \begin{bmatrix} 0 & 1 & 0 & 0 & 0 & 0 \\ k_{21} & 0 & 0 & k_{24} & 0 & 0 \\ 0 & 0 & 0 & 1 & 0 & 0 \\ 0 & 0 & 0 & 0 & 1 & 0 \\ 0 & 0 & 0 & 0 & 0 & 1 \\ 0 & k_{62} & k_{63} & 0 & k_{65} & 0 \end{bmatrix} \times \begin{bmatrix} \tilde{u} \\ \tilde{u}_a \\ \tilde{v} \\ \tilde{v}_a \\ \tilde{v}_b \\ \tilde{v}_c \end{bmatrix}, \tag{A2.1}$$

and

$$\begin{bmatrix} \tilde{u}_1 \\ \tilde{u}_{1a} \\ \tilde{u}_{1b} \\ \tilde{v}_1 \\ \tilde{v}_{1a} \\ \tilde{v}_{1b} \\ \tilde{v}_{1c} \\ \tilde{w} \\ \tilde{w}_a \\ \tilde{w}_b \end{bmatrix}' = \begin{bmatrix} 0 & 1 & 0 & 0 & 0 & 0 & 0 & 0 & 0 & 0 \\ 0 & 0 & 1 & 0 & 0 & 0 & 0 & 0 & 0 & 0 \\ 0 & g_{32} & 0 & g_{34} & 0 & g_{36} & 0 & g_{38} & 0 & g_{310} \\ 0 & 0 & 0 & 0 & 1 & 0 & 0 & 0 & 0 & 0 \\ 0 & 0 & 0 & 0 & 0 & 1 & 0 & 0 & 0 & 0 \\ 0 & 0 & 0 & 0 & 0 & 0 & 1 & 0 & 0 & 0 \\ 0 & g_{72} & 0 & g_{74} & 0 & g_{76} & 0 & g_{78} & 0 & g_{710} \\ 0 & 0 & 0 & 0 & 0 & 0 & 0 & 0 & 1 & 0 \\ 0 & 0 & 0 & 0 & 0 & 0 & 0 & 0 & 0 & 1 \\ g_{101} & 0 & g_{103} & 0 & g_{105} & 0 & 0 & 0 & g_{109} & 0 \end{bmatrix} \times \begin{bmatrix} \tilde{u}_1 \\ \tilde{u}_{1a} \\ \tilde{u}_{1b} \\ \tilde{v}_1 \\ \tilde{v}_{1a} \\ \tilde{v}_{1b} \\ \tilde{v}_{1c} \\ \tilde{w} \\ \tilde{w}_a \\ \tilde{w}_b \end{bmatrix}, \quad \text{(A2.2)}$$

where

$$k_{21} = -\frac{R_{13}}{R_{11}}, k_{24} = -\frac{R_{12}}{R_{11}}, k_{62} = -\frac{R_{21}}{R_{24}}, k_{63} = -\frac{R_{22}}{R_{24}}, k_{65} = -\frac{R_{23}}{R_{24}},$$

$$g_{32} = -\frac{R_{34}}{R_{36}}, g_{34} = -\frac{R_{31}}{R_{36}}, g_{36} = -\frac{R_{35}}{R_{36}}, g_{38} = -\frac{R_{33}}{R_{36}}, g_{310} = -\frac{R_{32}}{R_{36}},$$

$$g_{72} = -\frac{R_{54}}{R_{56}}, g_{74} = -\frac{R_{51}}{R_{56}}, g_{76} = -\frac{R_{55}}{R_{56}}, g_{78} = -\frac{R_{53}}{R_{56}}, g_{710} = -\frac{R_{52}}{R_{56}},$$

$$g_{101} = -\frac{R_{41}}{R_{42}}, g_{103} = -\frac{R_{44}}{R_{42}}, g_{105} = -\frac{R_{45}}{R_{42}}, g_{109} = -\frac{R_{43}}{R_{42}},$$

$$R_{11} = A_{11}, R_{12} = -(A_{12} + A_{66})p_n, R_{13} = A_{66}\, {p_n}^2,$$

$$R_{21} = (A_{12} + A_{66})\, p_n, R_{22} = -A_{22}\, {p_n}^2, R_{23} = A_{66}, R_{24} = S_0,$$

$$R_{31} = F_{56}F_{36} - F_{37}F_{51}, R_{32} = F_{56}F_{31} - F_{37}F_{52}, R_{33} = F_{56}F_{32} - F_{37}F_{53},$$

$$R_{34} = F_{56}F_{35} - F_{37}F_{54}, R_{35} = F_{56}F_{34} - F_{37}F_{55}, R_{36} = F_{56}F_{33} - F_{37}F_{57},$$

$$R_{51} = F_{57}E_{31} - E_{36}F_{51}, R_{52} = F_{57}E_{32} - E_{36}F_{52}, R_{53} = F_{57}E_{33} - E_{36}F_{53},$$

$$R_{54} = F_{57}E_{34} - E_{36}F_{54}, R_{55} = F_{57}E_{35} - E_{36}F_{55}, R_{56} = -E_{35}F_{55}, R_{4i} = F_{4i},$$

$$F_{31} = [D_{111}(2D_{12} + 4D_{66}) - (D_{11} + S_0 + S_2 p_n{}^2)(D_{121} + 2D_{661})]p_n{}^2,$$

$$F_{32} = -D_{111}D_{22}p_n{}^4, F_{33} = D_{111}{}^2 - (D_{11} + S_0 + S_2 p_n{}^2)D_{1111},$$

$$F_{34} = -[D_{111}(D_{122} + 2D_{662}) - (D_{11} + S_0 + S_2 p_n{}^2)(D_{1221} + D_{6621})]p_n$$

$$F_{35} = -[D_{111}(D_{121} + 2D_{661})p_n{}^2 - (D_{11} + S_0 + S_2 p_n{}^2)(D_{661}p_n{}^2 + A_{5511})],$$

$$F_{36} = D_{111}D_{222}p_n{}^3, F_{37} = D_{111}S_{12}\, p_n, F_{41} = -(A_{5511} + D_{6611}p_n{}^2),$$

$$F_{42} = -D_{111}, F_{43} = (D_{121} + 2D_{661})p_n{}^2, F_{44} = D_{1111}, F_{45} = -(D_{1221} + D_{6621})\, p_n,$$

$$F_{51} = -D_{111}(A_{4422} + D_{2222}p_n{}^2), F_{53} = D_{111}D_{222}p_n{}^3,$$

$$F_{52} = -D_{111}(D_{122} + 2D_{662})\, p_n - S_{12}(D_{121} + 2D_{661})p_n{}^3,$$

$$F_{54} = [D_{111}(D_{1221} + D_{6621}) - S_{12}(A_{5511} + D_{6611}p_n{}^2)]\, p_n, F_{56} = -D_{111}S_{022}$$

$$F_{54} = D_{111}D_{6622} - S_{12}p_n{}^2(D_{1221} + D_{6611}),\ F_{57} = S_{12}D_{111}\, p_n.$$

The solutions of equations (5.38) and (5.39) which are $\tilde{u}, \tilde{v}$ and $\tilde{u}_1, \tilde{v}_1, \tilde{w}$ can be written as follows:

$$\tilde{u} = \sum_{i=1}^{6} c_i\, X_{i1}\ e^{\alpha_i x}, \qquad \text{(A2.3.a)}$$

$$\tilde{v} = \sum_{i=1}^{6} c_i\, X_{i3}\ e^{\alpha_i x}, \qquad \text{(A2.3.b)}$$

and

$$\tilde{u}_1 = \sum_{i=7}^{16} c_i X_{i7}\ e^{\alpha_i x}, \qquad \text{(A2.4.c)}$$

$$\tilde{v}_1 = \sum_{i=7}^{16} c_i X_{i10}\ e^{\alpha_i x}, \qquad \text{(A2.4.d)}$$

$$\tilde{w} = \sum_{i=7}^{16} c_i X_{i14}\ e^{\alpha_i x}, \qquad \text{(A2.4.e)}$$

where $c_1, c_2, \dots, c_{16}$ are arbitrary constants and, $\alpha_i, i = 1, \dots, 6$ are the non-repeating eigenvalues of the 6×6 matrix appears in equation (A2.1). The $\alpha_i, i = 7, \dots, 16$ are the non-repeating eigenvalues of the 10×10 matrix appears in equation (A2.2). The eigenvectors which are corresponding to the eigenvalues $\alpha_i, i = 1, \dots, 6$ is as follows:

$$\mu_i = [X_{i1} \quad X_{i2} \quad X_{i3} \quad X_{i4} \quad X_{i5} \quad X_{i5}]^T,$$

and the eigenvectors which are corresponding to the eigenvalues $\alpha_i, i = 7, \dots, 16$ is as follows:

$$\mu_i = [X_{i7} \quad X_{i8} \quad X_{i9} \quad X_{i10} \quad X_{i11} \quad X_{i12} \quad X_{i13} \quad X_{i14} \quad X_{i15}]^T.$$

The expressions of $\beta_{24}^{(k)}, \delta_2^{(k)}, \delta_3^{(k)}, \dots, \delta_8^{(k)}$ which appear in equations (5.44) are as follows:

$$\delta_2^{(k)} = \left(\alpha_{23}^{(k)} \beta_{24}^{(k)} + \alpha_{12}^{(k)} \beta_{13}^{(k)} - \eta \right) \alpha_{13}^{(k)} \beta_{24}^{(k)},$$

$$\delta_3^{(k)} = \beta_{24}^{(k)} \alpha_{22}^{(k)} \alpha_{13}^{(k)},$$

$$\delta_4^{(k)} = -(\frac{1}{2}\alpha_{23}^{(k)}\beta_{24}^{(k)} + \frac{1}{2}\alpha_{12}^{(k)}\beta_{13}^{(k)} + \frac{1}{2}\eta)\alpha_{12}^{(k)} + \propto_{12}^{(k)^2} \beta_{13}^{(k)},$$

$$\delta_5^{(k)} = (\,2\alpha_{23}^{(k)}\beta_{24}^{(k)} + 2\alpha_{12}^{(k)}\beta_{13}^{(k)} + 2\,\eta\,)^{\frac{1}{2}},$$

$$\delta_6^{(k)} = \left(\,\alpha_{23}^{(k)}\beta_{24}^{(k)} + \alpha_{12}^{(k)}\beta_{13}^{(k)} + \eta\right)\alpha_{13}^{(k)}\beta_{24}^{(k)},$$

$$\delta_7^{(k)} = -(\frac{1}{2}\alpha_{23}^{(k)}\beta_{24}^{(k)} + \frac{1}{2}\alpha_{12}^{(k)}\beta_{13}^{(k)} - \frac{1}{2}\eta)\alpha_{12}^{(k)} + \propto_{12}^{(k)^2} \beta_{13}^{(k)},$$

$$\delta_8^{(k)} = (\,2\alpha_{23}^{(k)}\beta_{24}^{(k)} + 2\alpha_{12}^{(k)}\beta_{13}^{(k)} - 2\,\eta\,)^{\frac{1}{2}},$$

$$\eta = (\propto_{23}^{(k)^2} \beta_{24}^{(k)^2} - 2\alpha_{23}^{(k)}\beta_{24}^{(k)}\alpha_{12}^{(k)}\beta_{13}^{(k)} + \propto_{12}^{(k)^2} \beta_{13}^{(k)^2} + 4\alpha_{22}^{(k)}\beta_{13}^{(k)}\alpha_{13}^{(k)}\beta_{24}^{(k)}\,)^{\frac{1}{2}},$$

$$\beta_{13}^{(k)} = -\frac{1}{\alpha_{14}^{(k)}},\ \beta_{24}^{(k)} = -\frac{1}{\alpha_{24}^{(k)}}. \qquad \text{(A2.5)}$$

The expressions of $\alpha_i\,; i = 1,..,4$ appear in (5.65) are as follows:

$$\alpha_1 = \left(\frac{1}{2a}(-b + \sqrt{b^2 - 4ac})\right)^{\frac{1}{2}}, \alpha_2 = -\left(\frac{1}{2a}(-b + \sqrt{b^2 - 4ac})\right)^{\frac{1}{2}}, \qquad (A2.6.\,a, b)$$

$$\alpha_3 = \left(\frac{1}{2a}(-b - \sqrt{b^2 - 4ac})\right)^{\frac{1}{2}}, \alpha_4 = -\left(\frac{1}{2a}(-b + \sqrt{b^2 - 4ac})\right)^{\frac{1}{2}}, \qquad (A2.6.\,c, d)$$

$$\mathrm{a} = -\mathrm{D}_{11} - \mathrm{S}_0 - \mathrm{S}_2\mathrm{p}_\mathrm{n}^2, \mathrm{b} = (2\mathrm{D}_{12} + 4\mathrm{D}_{66})\mathrm{p}_\mathrm{n}^2 - \rho_2\omega^2, \mathrm{c} = -D_{22}p_n^4 + (\rho_0 + \rho_2 p_n^2)\omega^2.$$